Titre: Title:	Experimental and numerical investigations of higher mode effects on seismic response of reinforced concrete shear walls
Auteur: Author:	Iman Ghorbanirenani
Date:	2010
Type:	Mémoire ou thèse / Dissertation or Thesis
Référence: Citation:	Ghorbanirenani, I. (2010). Experimental and numerical investigations of higher mode effects on seismic response of reinforced concrete shear walls [Ph.D. thesis, École Polytechnique de Montréal]. PolyPublie. https://publications.polymtl.ca/429/

URL de PolyPublie: PolyPublie URL:	https://publications.polymtl.ca/429/
Directeurs de recherche: Advisors:	Robert Tremblay, & Pierre Léger
Programme: Program:	Génie civil

UNIVERSITÉ DE MONTRÉAL

EXPERIMENTAL AND NUMERICAL INVESTIGATIONS OF HIGHER MODE EFFECTS ON SEISMIC INELASTIC RESPONSE OF REINFORCED CONCRETE SHEAR WALLS

IMAN GHORBANIRENANI

DÉPARTEMENT DES GÉNIES CIVIL, GÉOLOGIQUE ET DES MINES
ÉCOLE POLYTECHNIQUE DE MONTRÉAL

THÈSE PRÉSENTÉE EN VUE DE L'OBTENTION
DU DIPLÔME DE PHILOSOPHIAE DOCTOR (Ph.D.)
(GÉNIE CIVIL)
DÉCEMBRE 2010

UNIVERSITÉ DE MONTRÉAL

ÉCOLE POLYTECHNIQUE DE MONTRÉAL

Cette thèse intitulée:

EXPERIMENTAL AND NUMERICAL INVESTIGATIONS OF HIGHER MODE EFFECTS ON SEISMIC INELASTIC RESPONSE OF REINFORCED CONCRETE SHEAR WALLS

présentée par: GHORBANIRENANI Iman

en vue de l'obtention du diplôme de : Philosophiae Doctor

a été dûment acceptée par le jury d'examen constitué de :

M. BOUAANANI Najib, Ph.D., président

M. TREMBLAY Robert, Ph.D., membre et directeur de recherche

M. LÉGER Pierre, Ph.D., membre et codirecteur de recherche

M. CHAALLAL Omar, Ph.D., membre

Mme KOBOEVIC Sanda, Ph.D., membre

ACKNOWLEDGEMENT

This research, carried out in the Department of Civil, Geological and Mining Engineering at École Polytechnique of Montréal, was completed with the help and support of many people whom I would like to thank.

First, I would like to express my deepest gratitude to my supervisors Professor Robert Tremblay and Professor Pierre Léger for their continued encouragement and their expert guidance.
I also would like to thank Professors Dan Palermo, Najib Bouaanani and Sanda Koboevic who gave me valuable advices on analyses and design of the specimens.

I would like to present my special thanks to Martin Leclerc who was involved directly on preparation of test setups and helped me in fabrication of test specimens, and also my sincere appreciation to Denis Fortier, Patrice Bélanger, Cédric Androuet,Viacheslav Koval, David Ek and Marc Charbonneau at the Structures Laboratory of École Polytechnique de Montréal for their invaluable assistance. The help of the undergraduate students working part-time at the laboratory is also acknowledged. I also thank Lucian Stefan and Antoine Rallu for helping me with numerical calculations.

The financial support provided by the Quebec Fund for Research on Nature and Technology (FQRNT) and the Natural Science and Engineering Research Council of Canada (NSERC) is acknowledged.

I wish to thank the external jury, Professor Omar Chaallal from École de Technologie Supérieure (ETS) and Professor Najib Bouaanani and Professor Sanda Koboevic from École Polytechnique de Montréal to have read and evaluated this Ph.D. dissertation.

Finally, I would like to express my deepest gratitude to my supportive wife who continuously encouraged me to finalize this research and my parent who always support me despite of thousand of miles between us.

RÉSUMÉ

Des analyses numériques réalisées par des chercheurs précédents ont montré que les tremblements de terre anticipés dans l'Est de l'Amérique du Nord, en raison de leur riche contenu en mouvements à hautes fréquences, pouvaient solliciter fortement les modes supérieurs de vibration des refends élancés en béton armé utilisés pour résister aux charges latérales dans les bâtiments. La contribution des modes supérieurs peut conduire à la formation de rotules plastiques dans la partie supérieure des murs, en plus de la rotule plastique qui est prévue à la base des murs lors de la conception des murs selon les normes et codes actuels. Les modes supérieurs peuvent également conduire à une amplification substantielle des efforts de cisaillement dynamiques à la base des refends, en excès du niveau de résistance exigé par les codes de conception. Pour étudier ces effets des modes supérieurs prédits par des simulations numériques pour les tremblements de terre de l'Est en Amérique du Nord, il était nécessaire de procéder à des essais en laboratoire sur des murs en béton armé soumis à de tels mouvements sismiques. Dans cette thèse, on présente et discute les deux programmes d'essais, ainsi que les études numériques complétées en parallèle, qui ont été réalisés sur les murs de refend en béton armé : essais statiques et essais dynamiques sur simulateur sismique.

La première série d'essais consistait en des essais monotones et cycliques sur des refends ductiles en béton armé conçus et détaillés conformément aux dispositions sismiques du CNBC 2005 et de la norme CSA-A23.3-04. Les tests ont été effectués à pleine échelle et à sur des modèles à échelle réduite 1:2.37 pour valider les règles de conception parasismique et les lois de similitude utilisées pour la réalisation d'essais à échelle réduite. Les essais sur spécimens à échelle réduite étaient essentiels car les essais dynamiques du second programme expérimental devaient être réalisés sur des modèles à échelle réduite. Dans ces essais, on a observé un comportement ductile en flexion sous les chargements monotoniques et cycliques, jusqu'à une ductilité en déplacement de 4.0, comme prévu par les codes. A ce niveau de déformation, les déformations inélastiques de cisaillement dans la rotule plastique correspondaient à environ 20% de la déformation totale. Dans les cycles suivants, la résistance des spécimens sous sollicitations cycliques s'est dégradée en raison du glissement en cisaillement qui s'est produit dans les fissures importantes de flexion

à la base du mur. On a obtenu une excellente concordance entre les résultats des essais à grandeur réelle et à échelle réduite, démontrant que l'utilisation d'un facteur d'échelle de l'ordre de 2.3 permettait de prédire adéquatement le comportement inélastique de refends en béton armé.

Pour ce programme d'essais, on a reproduit le comportement des spécimens en utilisant le logiciel d'éléments finis VecTor2. La comparaison entre les résultats expérimentaux et numériques a démontré qu'il était possible de prédire correctement avec ce type de modèle et de logiciel le comportement inélastique des refends en béton armé, incluant le mode de rupture observé sous chargement cyclique. Des modèles plus simples avec éléments de poutre et rotules plastiques concentrées ont également été utilisés pour la modélisation numérique. Les résultats ont montré que ce modèle pourrait bien reproduire la réponse en flexion des refends, mais les déformations de cisaillement ne pouvaient être reproduites, particulièrement dans le domaine non linéaire.

La deuxième série d'essais a consisté en des essais sur la table vibrante sur deux spécimens identiques, à l'échelle 1:2.33, d'un mur en béton armé de ductilité modérée de 8 étages conçus pour étudier les effets des modes supérieurs de vibration sur la réponse inélastique des murs sous des tremblements de terre produisant des mouvements de sol à haute fréquence attendus dans l'Est de l'Amérique du Nord. Les murs ont été conçus et détaillés conformément aux dispositions sismiques du CNBC 2005 et de la norme CSA-A23.3-04. Les objectifs étaient : 1) de valider et de comprendre la réponse inélastique de même que l'interaction entre les efforts de cisaillement, de flexion et axiaux dans les zones de rotule plastique des murs, en tenant compte des effets des modes supérieurs, et 2) d'examiner la formation d'une seconde rotule plastique dans la partie supérieure du mur en raison des réponses des modes supérieurs. Pour étudier l'évolution des dommages sous différents niveaux d'intensité, le premier spécimen a été testé sous des amplitudes de mouvement à la base incrémentées par tranches allant de 40% à 120% du niveau de conception. Pour le second spécimen, le premier essai a été réalisé à 100% du niveau de conception. Des essais additionnels ont ensuite été réalisés en augmentant l'amplitude par tranches successives jusqu'à 200% du niveau de conception.

Le second mode de vibration a significativement affecté la réponse des murs. Cela a donné lieu à des déformations inélastiques en flexion au niveau 6, avec une rotation plastique qui a atteint à peu près la même ductilité qu'à la base du mur. On a observé une amplification dynamique des forces de cisaillement à la base des deux murs. Dans le second mur, qui a été testé dans la condition initiale intacte, le pic de force cisaillement à la base a atteint environ 1.4 fois la résistance au cisaillement. Ce pic a est survenu avant que ne se forme la rotation inélastique à la base et la contribution à la résistance au cisaillement fournie par le béton, encore dans un état quasi non fissuré, a dépassé la valeur utilisée dans la conception et la rupture en cisaillement n'a pas été observée. Une fois que la rotation inélastique s'est produite, cette contribution du béton correspondait à la valeur obtenue en utilisant une valeur de 0.18 pour le coefficient de réduction pour tenir compte de la fissuration du béton.

La modélisation numérique de ces deux essais sur table vibrante a été réalisée afin d'évaluer les résultats du test et de valider les techniques actuelles de modélisation. Les analyses non linéaires dynamiques ont été effectuées à l'aide de modèles avec éléments de fibres en béton armé (programme OpenSees) et des éléments finis (programme VecTor2), en utilisant comme sollicitation les signaux enregistrés à la base des spécimens de murs sur la table vibrante. Une bonne concordance a été généralement obtenue entre les résultats numériques et expérimentaux. Les deux programmes ont permis de prédire la fréquence naturelle des murs dans les conditions intacte et avec dommages. Les deux techniques de modélisation ont permis de prédire que le moment maximal à la base des murs a atteint la capacité réelle des murs en flexion. Le programme OpenSees a prédit très bien le cisaillement maximal à la base, alors que le programme VecTor2 a surestimé les forces de cisaillement en comparaison avec les résultats expérimentaux. En termes de déplacement latéral au sommet, le programme OpenSees a donné un excellent résultat comparé aux mesures d'essais. Avec le programme Vector2, on a noté un décalage dans le temps entre la prédiction numérique et les résultats de l'expérience.

La réponse inélastique des murs, incluant le comportement de la seconde rotule plastique, ont pu être correctement reproduits à l'aide des programmes d'analyse avec éléments de fibres et par éléments finis. La méthode avec éléments de fibres est une bonne alternative en termes de temps de calcul. Elle produit des résultats raisonnables en comparaison avec la méthode des éléments

finis, bien qu'une attention particulière doive être accordée à la sélection des ratios d'amortissement. Les différentes analyses paramétriques dans cette thèse ont montré que, pour les deux modèles, l'ajout d'une petite quantité d'amortissement visqueux global en combinaison avec un modèle hystérétique raffiné pour le béton armé permettaient de bien prédire le comportement sismique des structures étudiées. Pour le programme VecTor2, un amortissement visqueux de 1% a conduit à des résultats raisonnables pour les murs en béton armé étudiés. Pour le programme OpenSees, 2% d'amortissement a donné lieu à une bonne concordance entre le test et les prédictions numériques pour l'essai à 100% du niveau de conception sur le mur initialement intact. Lorsque l'on augmente l'intensité du tremblement de terre, l'amortissement a dû être réduit entre 1.5% et 1% pour obtenir de bons résultats pour un mur endommagé avec des périodes de vibrations allongées.

Les résultats des essais et des analyses numériques sur les murs en béton armé soumis à mouvements de sols produits par des tremblements de terre anticipés dans l'Est de l'Amérique du Nord, ont démontré qu'il y a une forte possibilité d'avoir une seconde rotule plastique dans la partie supérieure des murs, en plus de celle à la base qui est considérée dans la conception. Cette seconde rotule plastique peut dissiper l'énergie induite par le tremblement de terre de façon plus efficace et diminuer les forces sur le mur. Une approche de conception considérant une seconde rotule plastique dans la partie supérieure du mur, en plus de celle à la base, pourrait donc être plus appropriée. Des recommandations préliminaires sont proposées dans cette thèse pour cette approche de conception pour les refends ductiles qui tient compte des effets des modes supérieurs sur la rotation plastique dans le haut du mur et sur les efforts de cisaillement à la base. Des études numériques ont montré que cette procédure de conception permettait de réduire les moments de flexion à mi-hauteur du mur, alors que les moments à la base du mur sont demeurés proches de la résistance nominale à la flexion. La seconde rotule plastique a également conduit à une réduction des efforts de cisaillement à la base, ce qui est bénéfique pour aussi réduire l'amplification dynamique de la réponse due aux modes supérieurs de vibration.

Après que le programme expérimental eut été terminé, les chercheurs de l'Université Concordia, le Professeur Khaled Galal et l'étudiant au doctorat Hosam El-Sokkary, en collaboration avec les chercheurs de l'École Polytechnique de Montréal, ont réparé les deux murs endommagés à l'aide

de polymère renforcé de fibres (PRF). Les murs ainsi réparés ont été testés de nouveau sur le simulateur sismique en utilisant la même séquence de mouvements sismiques. Ces tests visaient à comparer la réponse sismique des murs d'origine et réparés. Les fréquences naturelles mesurées pour les murs réhabilités étaient plus élevées que celles des murs d'origine dans la condition endommagée, à la fin du premier programme expérimental, Elles étaient cependant proches des valeurs mesurées pour les murs d'origine intacts. En appliquant les mouvements sismiques dont l’amplitude était graduellement augmentée par tranches, les dommages (fissuration, plasticité) se sont développés dans les étages non réhabilités.

ABSTRACT

Past numerical simulations performed by previous researchers have shown that higher mode response can be significant for high-rise reinforced concrete shear walls used in building structures to resist lateral loads, when subjected to ground motions rich in high frequency that are expected in earthquakes occurring in Eastern North America. Higher mode response can lead to the development of plastic hinges in the upper portion of walls, in addition to the base plastic hinge assumed in design according to current codes and design standards. Higher mode effects can also result in significant dynamic shear amplification at the base of walls, in excess of the shear resistance prescribed in current code documents. Experimental testing was needed on reinforced concrete walls under Eastern North America earthquake motions to validate these higher mode effects predicted by numerical simulations. This thesis presents two experimental programs together with companion numerical studies that were carried out on reinforced concrete shear walls: static tests and dynamic (shake table) tests.

The first series of experiments were monotonic and cyclic quasi-static testing on ductile reinforced concrete shear wall specimens designed and detailed according to the seismic provisions of NBCC 2005 and CSA-A23.3-04 standard. The tests were carried out on full-scale and 1:2.37 reduced scale wall specimens to evaluate the seismic design provisions and similitude law and determine the appropriate scaling factor that could be applied for further studies such as dynamic tests. Ductile flexural response was observed under cyclic loading up to a displacement ductility of 4.0. At this deformation level, inelastic shear deformations in the plastic hinge contributed to approximately 20% of the total lateral deformation. In the subsequent cycles, strength degradation took place due to shear sliding developing along the large flexural cracks at the wall base. Comparisons of the test results between prototype and reduced scale walls showed excellent agreement, which proved that using of scaling factor around 2.3 for the model wall could adequately predict the inelastic responses of prototype reinforced concrete shear walls.

The VecTor2 finite elements program was used to evaluate numerically the inelastic behaviour of model and prototype wall test specimens. Comparisons between experimental and numerical

results showed that the inelastic response and failure mode of the model and prototype walls as observed under cyclic loading could be adequately reproduced using the VecTor2 program. Simpler stick models with frame elements and lumped plastic hinges were also used as another numerical modeling technique. The results showed that these stick models could capture well the wall flexural response but shear deformations could not be reproduced.

The second series of experiments were shake table tests conducted on two identical 1:2.33 scaled, 8-storey moderately ductile reinforced concrete shear wall specimens to investigate the effects of higher modes on the inelastic response of slender walls under high frequency ground motions expected in Eastern North America. The walls were designed and detailed according to the seismic provisions of NBCC 2005 and CSA-A23.3-04 standard. The objectives were to validate and understand the inelastic response and interaction of shear, flexure and axial loads in plastic hinge zones of the walls considering the higher mode effects and to investigate the formation of second hinge in upper part of the wall due to higher mode responses. To investigate the progress of damage for the different levels of intensity, one specimen was tested under incremented ground motion amplitudes ranging from 40% to 120% of the design level. For the second specimen, the first test was performed at 100% of the design level and the amplitude was increased stepwise in subsequent tests up to 200% of the design level.

Second mode response significantly affected the response of the walls. This caused inelastic flexural response to develop at the 6^{th} level with approximately the same rotation ductility compared to that observed at the base. Dynamic amplification of the base shear forces was also observed in both walls. In the second wall, which was tested in the undamaged condition, peak base shear forces reached approximately 1.4 times of the wall shear capacity. That peak shear force demand occurred prior to significant inelastic rotation at the wall base and the contribution to shear resistance provided by the concrete, still nearly uncracked, exceeded the value used in design and shear failure was not observed. Once inelastic rotation had developed, that contribution corresponded to the value determined using a value of 0.18 for the reduction factor accounting for concrete cracking.

Numerical modeling of these two shake table tests was performed to evaluate the test results and validate current modeling approaches. Nonlinear time history analyses were carried out by the reinforced concrete fibre element (OpenSees program) and finite element (VecTor2 program) methods using the shake table feedback signals as input. Good agreement was generally obtained between numerical and experimental results. Both computer programs were able to predict the natural frequency of the walls in the undamaged and damaged conditions. Both modeling techniques could predict that the maximum bending moment at the base of the walls reached the actual wall moment capacity. The OpenSees program predicted very well the measured maximum base shear whereas the VecTor2 model estimated larger shear forces compared to the experimental values. In terms of top lateral displacement history, the OpenSees model led to excellent match with the experimental results but out-of-phase responses were observed between the VecTor2 predictions and the test measurements. .

The inelastic response and the dual plastic hinge behaviour of the walls could be adequately reproduced using the fibre element and finite element analysis programs. The fibre element method is a good alternative in terms of computing time. It produces reasonable results in comparison with the finite element method, although particular attention needs to be given to the selection of the damping ratios. The different parametric analyses performed in this thesis showed that, for both models, adding a small amount of global viscous damping in combination with a refined reinforced concrete hysteretic model could predict better the seismic behaviour of the tested structures. For the VecTor2 program, a viscous damping of 1% led to reasonable results for the studied RC walls. For the OpenSees program, 2% damping resulted in a good match between test and predictions for the 100% EQ test on the initially undamaged wall. When increasing the earthquake intensities, the damping had to be reduced between 1.5% and 1% to achieve good results for a damaged wall with elongated vibration periods.

According to the experimental results and numerical analyses on reinforced concrete shear walls subjected to ground motions from Eastern North America earthquakes, there is a high possibility of having a second plastic hinge forming in the upper part of walls in addition to the one assumed in design at the base. This second hinge could dissipate the earthquake energy more effectively and decrease the force demand on the wall. A dual plastic hinge design approach in which the

structures become plastic in the upper wall segment as well as the base could be therefore more appropriate. Preliminary design recommendations considering higher mode effects on dual hinge response and base shear forces for ductile slender shear walls are given in this thesis. Numerical investigation of this design procedure showed that bending moments could be reduced at the wall mid-height, whereas the moments at the base of the wall remained close to the wall nominal flexural strength. The dual-hinge design also led to a reduction of the base shear forces, which is beneficial in reducing dynamic amplification from higher mode response.

After completion of our shake table test program, researchers from Concordia University (Professor Khaled Galal and Ph.D. Candidate Hosam El-Sokkary), in collaboration with the researchers from École Polytechnique of Montréal, repaired the two damaged walls using Fibre Reinforced Polymer (FRP) wrapping. These repaired walls were then retested on the shake table using the same ground motion sequence. These tests aimed at comparing the seismic responses of the original and repaired walls. The natural frequencies of the rehabilitated walls were found to be higher than those of the original walls in the damaged state at the end of the initial test program, and were close to the values measured for the undamaged original walls. Upon applying seismic ground motion with stepwise incrementally increasing intensities, the damage (cracking, plasticity) was found to spread in the unrehabilitated storeys.

CONDENSÉ EN FRANÇAIS

A.1 Introduction

Avec le développement des sciences reliées aux tremblements de terre et de l'ingénierie des structures, les codes de construction des bâtiments et les provisions sismiques sont mis à jour à intervalles réguliers, mais il y a encore de nombreux aspects qui ne sont pas pleinement compris en raison de la nature aléatoire des mouvements sismiques et du caractère complexe de la réponse des structures en béton armé dans le domaine non linéaire. Parmi ces aspects, les effets des modes supérieurs de vibration sur les structures durant les séismes ont été des sujets d'études récentes.

Dans la norme CSA A23.3, l'effort de cisaillement pour la conception est l'effort qui correspond à l'atteinte de la capacité ultime en flexion probable du mur à sa base, après la formation d'une rotule plastique. Ce calcul est cependant effectué en ne considérant que le premier mode de vibration (Adebar et al. 2005).

Des analyses dynamiques récentes non linéaires de murs de refend soumis à des tremblements de terre ont montré que des forces de cisaillement au-delà des efforts calculés dans les codes usuels peuvent se développer en raison de la contribution des modes supérieurs de vibration de la réponse dynamique (Blakeley et al. 1975, Filiatrault et al. 1994, Amaris 2002, Panneton et al. 2006, 2006 Krawinkler, Velev 2007, Boivin et Paultre 2010). Ces forces de cisaillement élevées peuvent provoquer une rupture fragile en cisaillement des murs ou des défaillances par glissement à la base des murs.

Ces études numériques ont également révélé que l'amplification du moment au sommet du mur, aussi produit par les modes supérieurs, peut conduire à la formation de rotules plastiques dans la partie supérieure des murs, même lorsqu'ils sont conçus et détaillés pour qu'une rotule plastique ne se forme qu'à la base (Blakeley et al. 1975; Tremblay et al 2001; Panneton et al 2006).

En raison d'une amplitude plus faible des charges sismiques dans la zone de sismicité modérée de l'Est de l'Amérique du Nord, les refends en béton armé de la catégorie « à ductilité modérée » sont généralement préférés aux refends de la catégorie « ductile ». Les premiers sont plus simples à concevoir et, surtout, à construire, des avantages importants qui l'emportent sur des charges de conception plus élevées exigées pour ces murs. Les secousses produites par les tremblements de terre prévus dans l'Est de l'Amérique du Nord sont riches en mouvements à hautes fréquences par rapport aux secousses typiques de l'Ouest de l'Amérique du Nord, ce qui peut favoriser une réponse plus importante des murs aux modes supérieurs. Cette réponse peut se traduire par de l'amplification dynamique importante du cisaillement ainsi que l'amplification significative des moments de flexion sur la hauteur du mur. L'amplification dynamique peut conduire à la formation de rotules plastiques dans la partie supérieure du mur (Panneton et al. 2006).

Des recherches expérimentales sont essentielles afin de mieux comprendre la réponse dynamique sismique des murs en béton armé et développer une méthodologie de conception simplifiée mais réaliste pour utilisation dans la pratique. Une des méthodes les plus fiables pour obtenir des données sur le comportement sismique des murs est la réalisation d'essais sur table vibrante (Lestuzzi et al. 1999; Lu and Wu 2000; Kazaz et al. 2006; Panagiotou et al. 2007a, b). Un programme d'essais à grande échelle sur table vibrante a été réalisé récemment sur un mur rectangulaire de 7 étages soumis à un tremblement de terre en Californie (Panagiotou et al. 2007a, b). Ces essais ont confirmé que l'amplification dynamique due aux modes supérieurs pourrait augmenter le cisaillement à la base jusqu'à 1.5 fois la force de cisaillement correspondant à la sur-résistance de mur de refend.

A.2 Objectifs

Les objectifs de cette étude sont les suivants :
(a) examiner l'approche de conception pour la résistance au cisaillement proposée dans la norme CSA A23.3;
(b) vérifier les règles de similitude en comparant les résultats d'essais monotoniques et cycliques sur des murs prototypes et des modèles de murs à échelle réduite, ceci dans le but d'appliquer,

par la suite, des facteurs d'échelle similaires pour les essais sur la table vibrante sur des murs en béton armé;

(c) évaluer les capacités du logiciel VecTor2 pour reproduire la réponse inélastique et les modes de défaillance observés dans les essais pour les murs ductiles sous grandes déformations plastiques (essais monotoniques et cycliques);

(d) étudier, à l'aide d'essais sur table vibrante, les effets des modes supérieurs sur les murs en béton armé tels que l'endommagement, les efforts imposés et la réponse inélastique de murs sous un tremblement de terre de l'Est de l'Amérique du Nord (EAN);

(e) évaluer les résultats des essais et l'adéquation de la modélisation à l'aide d'éléments fibres (logiciel OpenSees) et d'éléments finis (logiciel Vector 2) pour les analyses dynamiques non linéaires sur murs en béton armé; et

(f) proposer une nouvelle approche de conception parasismique qui tienne compte des effets des modes supérieurs de vibration sur le comportement des murs de refend.

A.3 Méthodologie

Pour évaluer la procédure de conception sismique de la norme canadienne CSA A23.3 et étudier les effets des modes supérieurs sur les murs en béton armé sous les tremblements de terre à haute fréquence, des essais statiques et dynamiques ont été effectués sur des murs de refend en béton armé. Les essais ont été effectués au Laboratoire de génie des structures de l'École Polytechnique, Montréal, Canada. La modélisation numérique des murs a été réalisée par deux méthodes : éléments finis, avec le logiciel VecTor2, et éléments fibres, avec le logiciel OpenSees.

A.4 Contributions Originales

Les principales contributions scientifiques de ce projet de recherche sont les suivantes:

1. Reproduction avec des essais sur des spécimens à échelle réduite de la réponse sismique inélastique observée dans les essais monotoniques et cycliques sur des prototypes de refends en béton armé, y compris les déformations de flexion et de cisaillement et le mécanisme de défaillance (rupture en cisaillement après avoir atteint la ductilité cible).

2. Évaluation de la méthode « Disturbed Stress Field » implantée dans le code d'éléments finis VecTor2 (Vecchio 2000) en utilisant les résultats des essais monotoniques et cycliques sur des murs soumis à des déformations inélastiques significatives.
3. Utilisation d'un nouveau montage expérimental élaboré au Laboratoire de structure de l'École Polytechnique de Montréal pour les essais à grande échelle sur la table vibrante. Cette configuration d'essai vise à minimiser la charge axiale sur la table afin d'exploiter au maximum la résistance au moment de renversement de la table. Cela permet également de considérer un poids sismique réaliste et de considérer les effets P-delta sur la réponses des étages.
4. Réalisation des premiers essais à grande échelle sur table vibrante de murs de refend en béton armé à ductilité modérée de 9 m de haut représentant des prototypes de 21 m de haut sous une excitation sismique typique de l'Est de l'Amérique du Nord (ENA).
5. Démonstration claire des effets des modes supérieurs, y compris le comportement inélastique à la partie supérieure du mur conçu et détaillé conformément aux dispositions sismiques du CNBC 2005 et la norme CSA-A23.3-04 sous un tremblement de terre à hautes fréquences de l'ENA.
6. Démonstration que la méthode d'analyse avec éléments en fibres est capable de reproduire le comportement dynamique des murs en béton armé et de prédire la réponse non linéaire de la partie supérieure du mur sous l'effet des modes supérieurs.
7. Identification des paramètres d'amortissement visqueux réalistes permettant de corréler les résultats numériques et expérimentaux.
8. Démonstration que les paramètres d'amortissement doivent être modifiés lors de la réalisation d'analyses de structures soumises à des mouvements de sol successifs ayant des amplitudes différentes.
9. Proposition d'une approche de conception à double rotule plastique qui pourrait être appropriée pour des applications sismiques dans l'ENA. Des travaux de recherche plus approfondis sont cependant requis avant que la méthode ne puisse être codifiée.
10. Contribution à la conduite d'essais sur table vibrante de murs endommagés après l'application de techniques de réparation à l'aide d'un polymère renforcé de fibres afin d'améliorer le comportement sismique en condition réparée.

A.5 Résultats des essais monotoniques et cycliques

La première série d'essais consistait en des tests monotones et cycliques qui ont été effectués sur des murs en béton armé ductile conçus selon le CNBC 2005 et la norme CSA-A23.3-04 pour l'Ouest du Canada. Deux prototypes identiques ont été conçus, détaillés et fabriqués. Chacun des deux prototypes ont été testés sous chargement monotonique et cyclique, respectivement. Pour valider les lois de similitude et les facteurs d'échelle, deux modèles identiques à échelle réduite 1:2.37 des murs prototypes ont également été construits et soumis au même protocole de chargement (Fig. A.1).

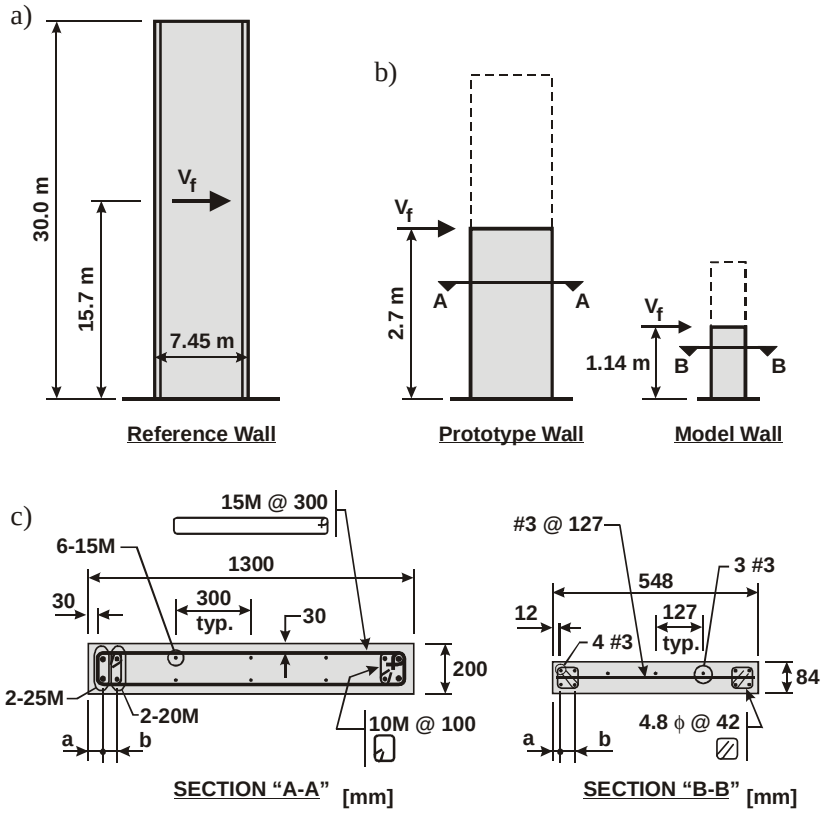

Fig. A.1: Description des refends en béton armé étudiés: a) mur du bâtiment de référence; b) Élévation des spécimens de mur; c) section des prototypes et des modèles à échelle réduite.

Les tests cycliques sur les prototypes et les modèle à échelle réduite ont montré que l'approche de conception par capacité spécifiée dans le code CSA A23.3 conduit à une réponse d'hystérésis stable dominée par la flexion jusqu'à une ductilité en déplacement de 4.0 (Fig. A.2).

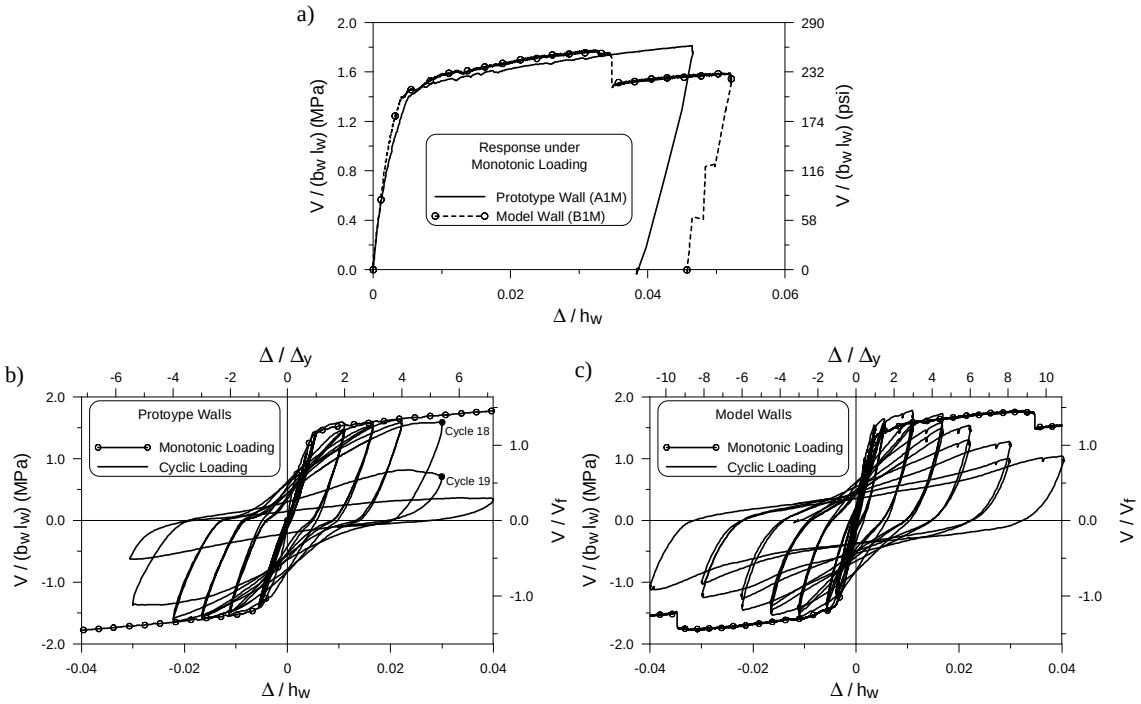

Fig. A.2 : Comportement en charge-déformation latérales des spécimens: a) comportement sous chargement monotonique; b) comparaison entre les comportements sous chargements monotonique et cyclique pour les prototypes; c) comparaison entre les comportements sous chargements monotonique et cyclique pour les modèles à échelle réduite.

Les murs peuvent atteindre et dépasser une ductilité égale à 3.5 telle que supposée dans les codes canadiens pour les murs ductiles. En raison de l'interaction entre les réponses inélastiques de cisaillement et de flexion, des déformations de cisaillement inélastiques se développent progressivement dans la région de la rotule plastique des spécimens. Ces déformations de cisaillement doivent être prises en compte dans la prédiction de la réponse inélastique sismique des murs. Dans les deux essais, le glissement en cisaillement s'est amorcé juste après avoir atteint la ductilité de conception de 3.5, ce qui a conduit à une dégradation significative de la résistance des murs. Dans les deux protocoles de chargement, on a obtenu un excellent accord entre les comportements du prototype et des modèles à échelle réduite (Fig. A.2). Ces résultats suggèrent que les modèles conçus avec un facteur d'échelle jusqu'à 2.4 et fabriqués avec du béton de résistance normale et des barres d'armature crénelées peuvent être utilisés pour étudier la réponse sismique des refends, y compris la flexion inélastique, les effets des déformations de cisaillement et le glissement en cisaillement.

Après les essais, on a réalisé des analyses numériques avec le programme d’analyse par éléments finis VecTor2 (VT2) pour évaluer la capacité de reproduire le comportement des spécimens d'essai sous les deux conditions de chargement. Les comparaisons entre les résultats expérimentaux et numériques ont montré que le logiciel VT2 peut prédire adéquatement les comportements inélastiques monotonique et cyclique des refends ductiles, y compris la rigidité initiale, les déformations de cisaillement, les efforts dans l'acier d’armature transversal, la dissipation d'énergie et les mécanismes de défaillance. Le logiciel VT2 a cependant surestimé la capacité ultime sous un chargement monotonique, probablement à cause d’une rigidité en tension (tension stiffening) excessive dans la région inélastique (Fig. A.3&4).

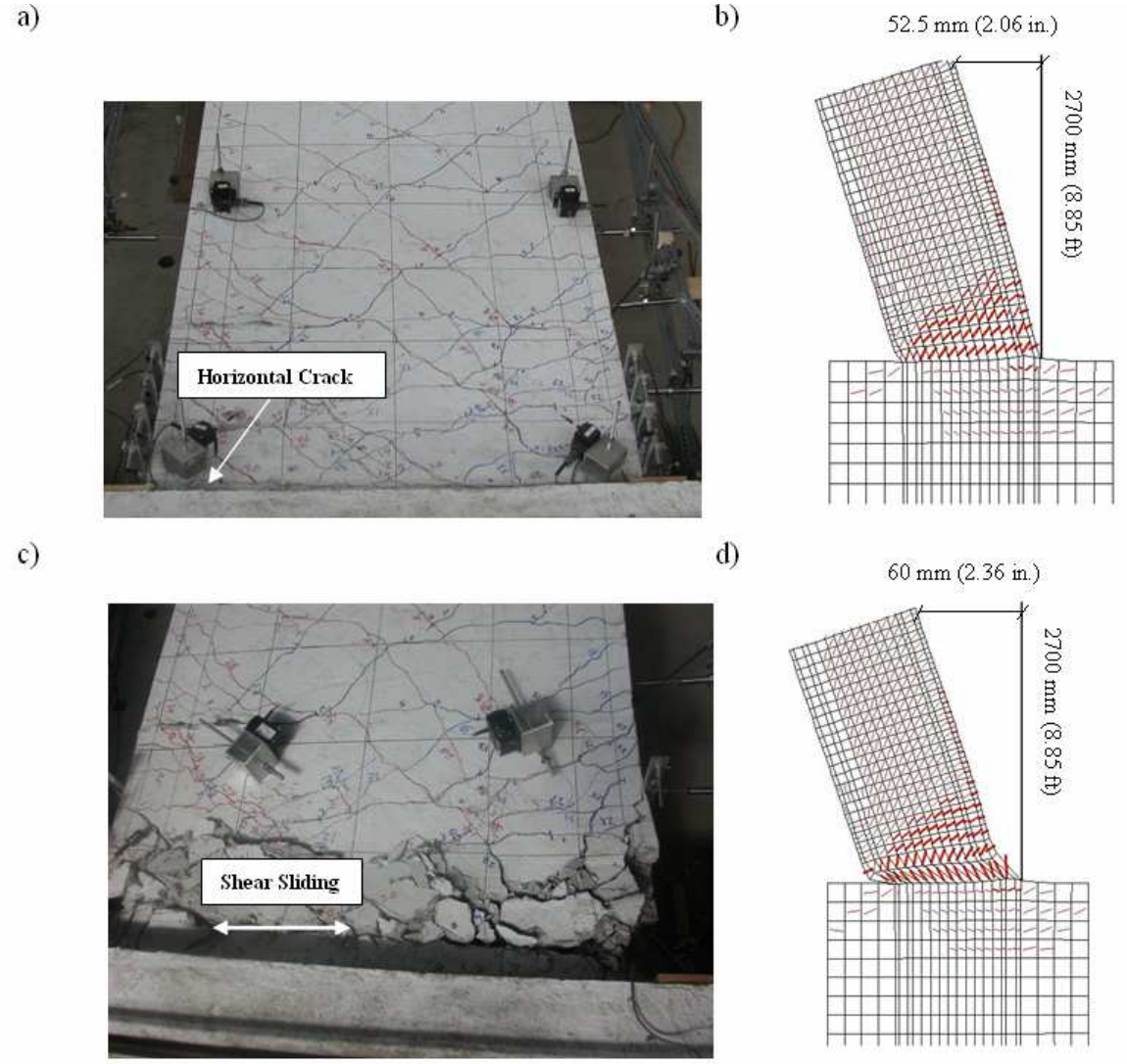

Fig. A.3 : Réseaux de fissures pour le prototype de mur sous chargement cyclique: a) Réseau de fissures observés à une ductilité de 3.5; b) Réseau de fissures obtenu de l'analyse VT2 à une ductilité de 3.5; c) Réseau de fissures observé à la rupture; d) Réseaux de fissures à la rupture obtenu de l'analyse VT2 .

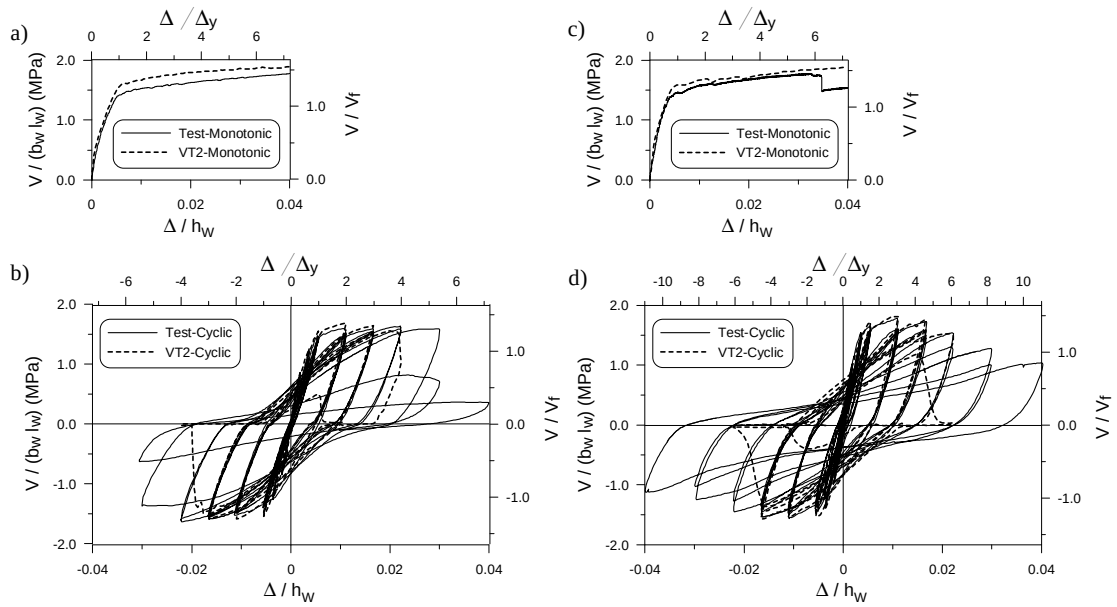

Fig. A.4 : Comportements en obtenus des essais et des analyses VT2 avec les propriétés des matériaux mesurées: a) comportements sous chargement monotonique pour les prototypes; b) comportement sous chargement cyclique pour les prototypes; c) comportements sous chargement monotonique pour les modèles à échelle réduite; d) comportements sous chargement cyclique pour les modèles à échelle réduite.

A.6 Résultats des essais sur table vibrante

La deuxième série de tests visait à étudier les effets des modes supérieurs par des essais sur table vibrante sur deux murs modèles identiques en béton armé représentant des refends d'un bâtiment de 8 étages situés sur un site de catégorie C à Montréal, QC, Canada. Les spécimens W1 et W2 ont été construits, le deuxième ayant la fonction d'assurer une redondance (deuxième chance) si certains problèmes inattendus se présentaient lors du premier essai. Les détails des spécimens sont donnés à la Fig. A.5.

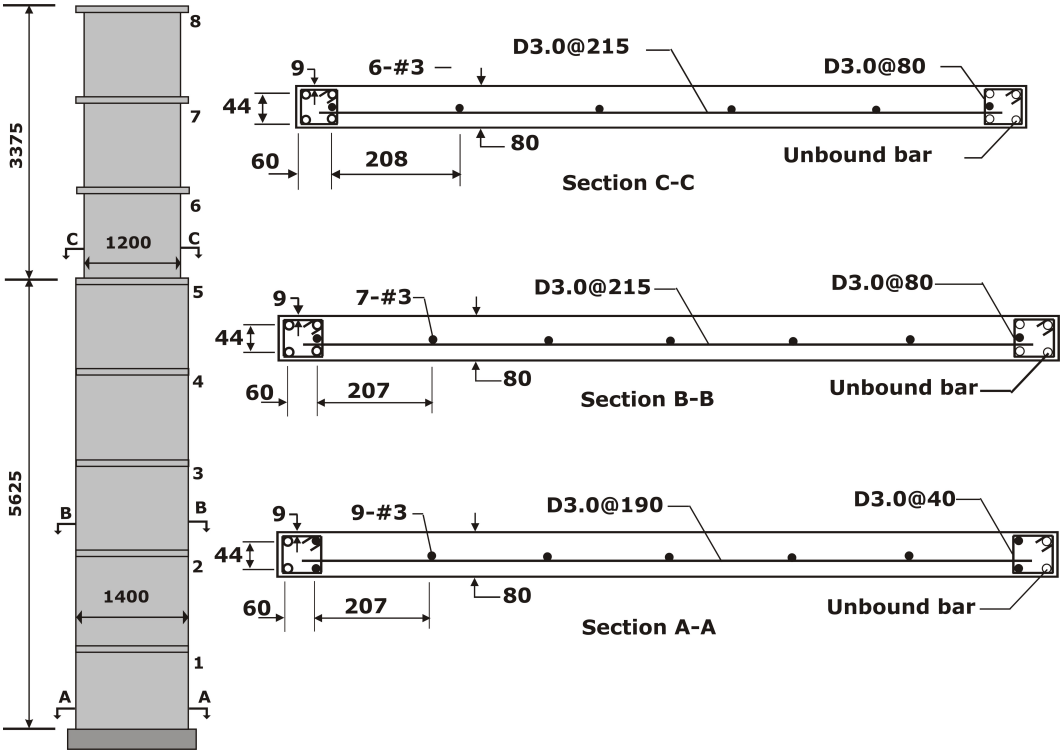

Fig. A.5: Dimensions des murs de modèle et de l'armature d'acier (les dimensions sont en mm)

Contrairement aux tests décrits au chapitre 3, un mur modérément ductile a été choisi pour éviter que la quantité d'acier d'armature minimum de flexion ne gouverne lors de la conception, ceci afin de pouvoir solliciter le spécimen jusqu'à sa capacité en flexion pendant les essais. Les spécimens de mur ont donc été conçus et fabriqués conformément aux codes de conception parasismiques du CNBC 2005 et la norme CSA A23.3 en supposant des murs de ductilité modérée.

Les deux spécimens ont été soumis à seul mouvement sismique correspondant à un tremblement de terre à haute fréquence, tel qu'anticipé dans l'Est de l'Amérique du Nord. Il s'agit d'un historique de mouvement de sols qui a été généré numérique (simulation) pour un séisme de magnitude 7.0 à 50 km. Le séisme a ensuite été modifié dans le domaine des fréquences de telle sorte que son spectre d'accélération s'harmonise au spectre de conception du CNBC 2005. Dans ce qui suit, ce signal correspond à 100% du séisme de conception (100% EQ). Le spécimen W1 a été soumis à une série d'essais successifs où l'amplitude des mouvements sismiques a été

incrémentée par paliers de 40% à 120% du niveau de conception parasismique du code. Pour le spécimen W2, la plage d'amplitudes était comprise entre 100% à 200% du niveau de conception.

Tel que prévu par les analyses préliminaires, lors de l'application des mouvements à la base correspondant à l'intensité de conception, les spécimens ont subi des déformations inélastiques en flexion limitées à la base du mur mais aussi au niveau 6. Le comportement inélastique au niveau 6 n'avait pas été considéré dans la conception. Il découle d'une réponse significative des modes supérieurs face aux hautes fréquences d'excitation. Durant les essais, ce comportement a été confirmé par la distribution verticale des forces d'inertie horizontales, par les efforts internes dans les spécimens ainsi que par des indicateurs de réponse en déformation (Fig. A.6).

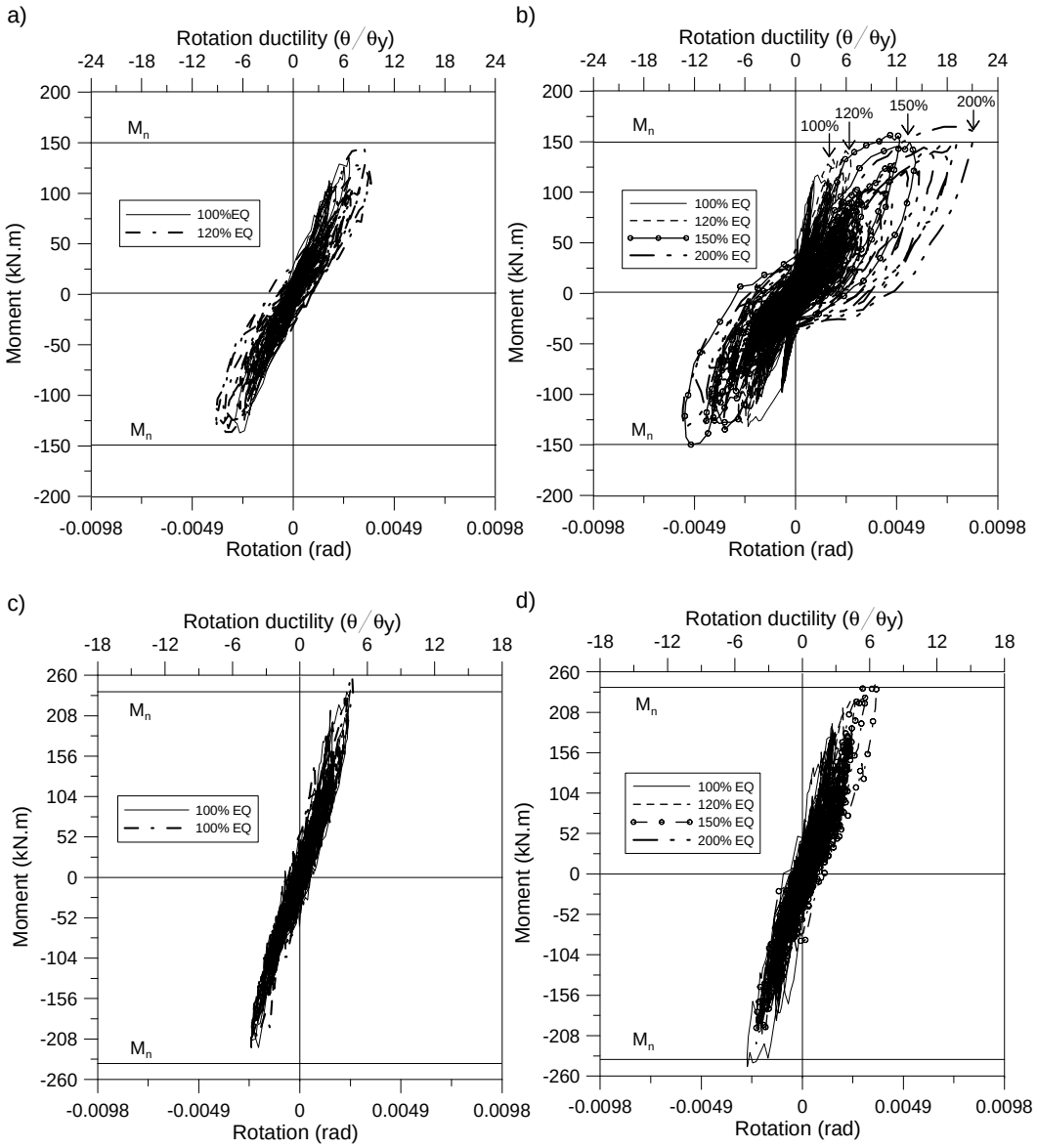

Fig. A.6 : Comportement moment-rotation : (a) au niveau 6 du spécimen W1; (b) au niveau 6 du spécimen W2; (c) à la base du spécimen W1, et (d) à la base du spécimen W2.

À la base des spécimens, on a observé de la fissuration en cisaillement et en flexion alors que seules des fissures de flexion se sont formées au niveau 6. En augmentant l'amplitude du mouvement sismique à la base au-delà de l'intensité de conception, la rotation inélastique additionnelle s'est seulement développée au niveau 6 (Fig. A.7).

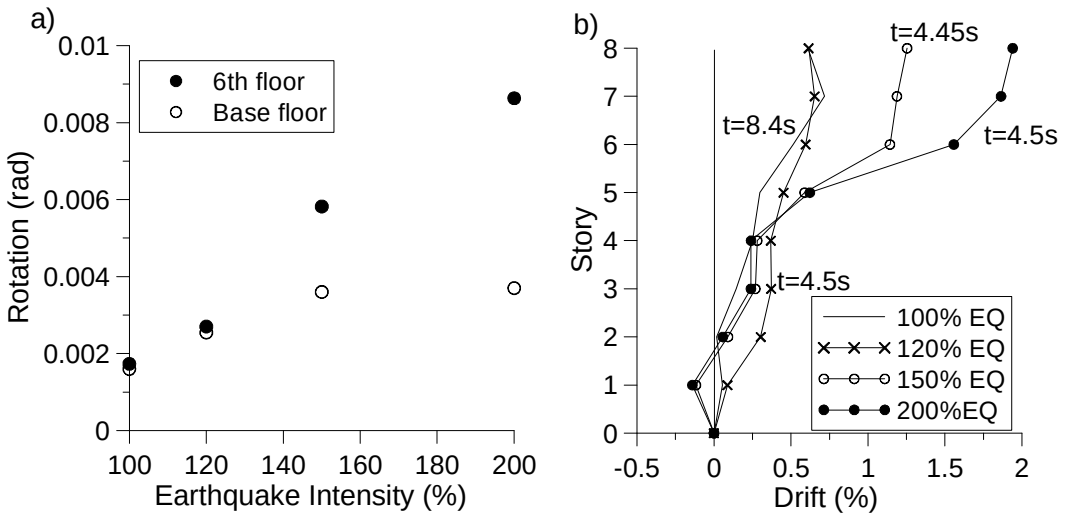

Fig. A.7: (a) Rotation maximale au niveau 6 et à la base du spécimen W2 en fonction de l'intensité du mouvement sismique; (b) Déplacements inter-étages de pointe sur la hauteur du spécimen W2 selon l'intensité du tremblement de terre.

Le moment de flexion maximum à la base des murs sous le mouvement sismique de conception a atteint la résistance réelle en flexion du mur, soit 1.3 fois la valeur de dimensionnement. Ce ratio correspond approximativement au facteur de sur-résistance R_o = 1.4 utilisé dans la conception.

La ductilité en déplacement maximale dans le haut des spécimen a été 35% plus élevée que le facteur de ductilité utilisé pour la conception. Cette différence a été causée principalement par la rotation inélastique qui s'est développée au niveau 6, plutôt qu'une rotation inélastique concentrée dans la rotule plastique à la base du mur comme on le suppose dans la conception. La rotation plastique maximale à la base des spécimens correspondait à la valeur prédite en supposant un comportement suivant le premier mode de vibration (Fig. A.8).

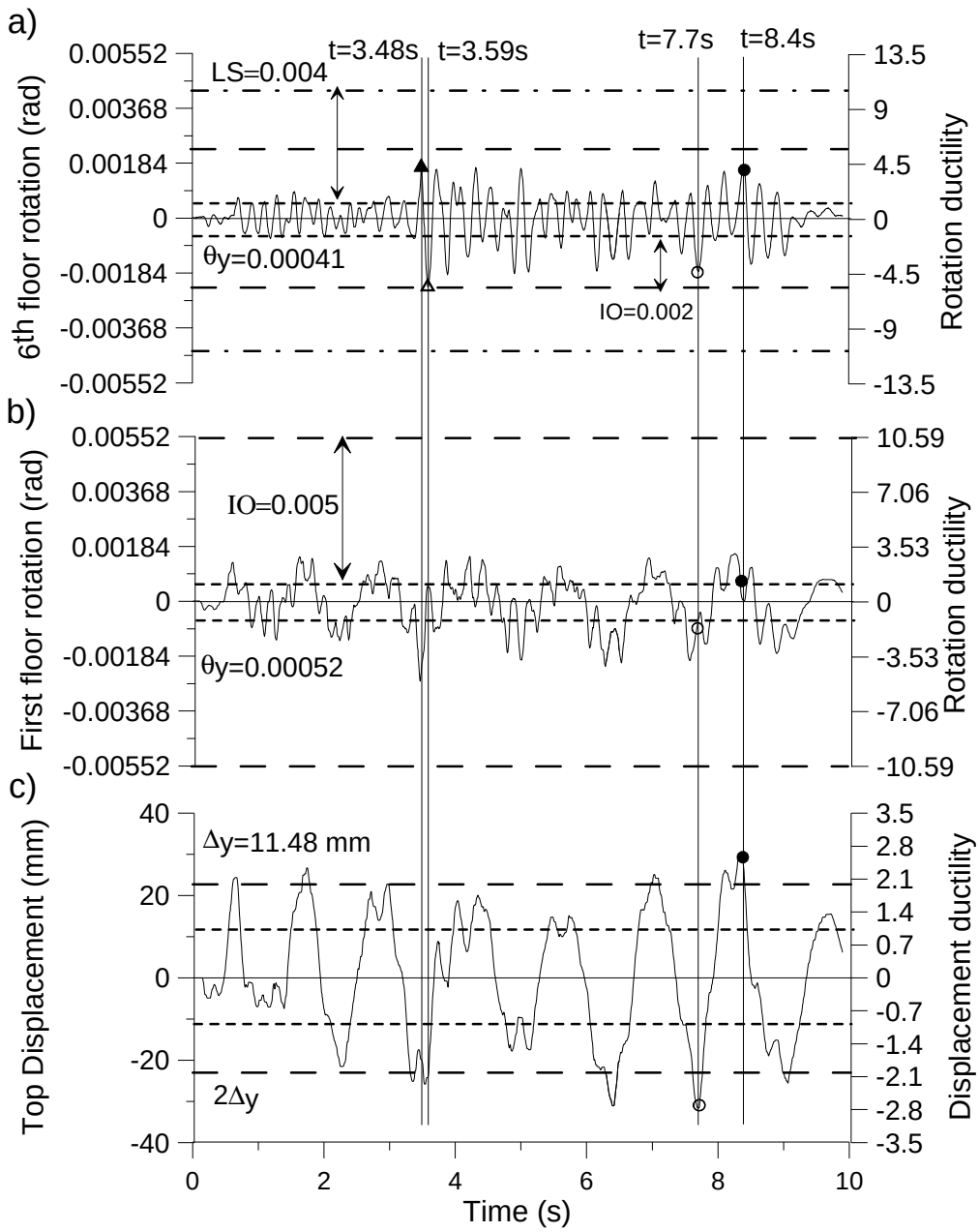

Fig. A.8 : Réponse du spécimen W2 en fonction du temps sous 100% EQ: (a) Rotation relative au 6^{e} étage, (b) Rotation à la base, et (c) Déplacement relatif en fonction de la hauteur du mur.

Les forces maximales de cisaillement à la base obtenues lors des essais ont atteint 1.82 fois l'effort qui avait été considéré pour la conception des spécimens. Ce facteur est réduit à 1.4. fois l'effort de cisaillement de conception déterminé en utilisant le signal enregistré sur le simulateur sismique qui a été effectivement appliqué aux murs. Ce rapport est proche du facteur d'amplification dynamique proposé dans le code NZS 3101 pour un mur de 8 étages (1.5). Malgré

ces forces excessives, aucune rupture en cisaillement n'a pas été observée, ce qui a été attribué à contribution plus grande que prévue du béton à la résistance au cisaillement. Cette capacité plus élevée du béton vient du fait que l'effort de cisaillement maximal s'est produit avant que ne se forme des fissures significatives en flexion due à la rotation inélastique à la base des murs (moment maximum se produit après le cisaillement maximum). Après la réponse inélastique en flexion, la résistance au cisaillement du béton correspondait à celle obtenue en utilisant une valeur de 0.18, au lieu de 0.10, pour le facteur de réduction β tenant compte de la résistance au cisaillement du béton fissuré dans la norme CSA A23.3. Ces résultats suggèrent qu'il serait approprié de spécifier dans la norme A23.3 un facteur d'amplification dynamique du cisaillement à la base, semblable à celui prescrit dans le code NZS 3101, afin de diminuer le risque de rupture par cisaillement.

En augmentant l'intensité des secousses sismiques à la base au-delà du niveau de conception, le cisaillement à la base a continué d'augmenter même si le moment à la base est resté pratiquement constant puisque limité par la résistance en flexion des spécimens.

Les résultats des essais sur table vibrante des deux murs W1 et W2 ont été examinés par des simulations numériques. Les murs ont été modélisés en utilisant la méthode des éléments finis (logiciel VT2) et la méthode des éléments fibres avec le logiciel OpenSees (OS). Les deux techniques de modélisation ont permis de prédire très bien les fréquences naturelles des murs, tant dans le domaine élastique que dans le domaine non linéaire considérant le cumul de l'endommagement. Les moments à la base obtenus par VT2 et OS étaient très proches des résultats des essais. Avec le logiciel OS, on a aussi pu reproduire la force de cisaillement à la base obtenue dans les essais. OS a aussi très bien prédit les déplacement latéraux mesurés au haut des spécimens (Fig. A.9).

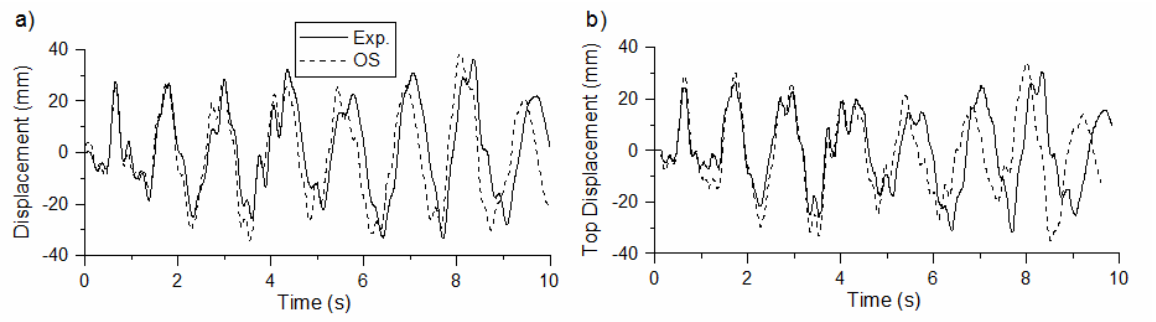

Fig. A.9 : Historique des déplacements du haut des spécimens W1 et W2 sous 100% EQ (a) OS vs essai pour le spécimen W1; (b) OS vs essai pour le spécimen W2

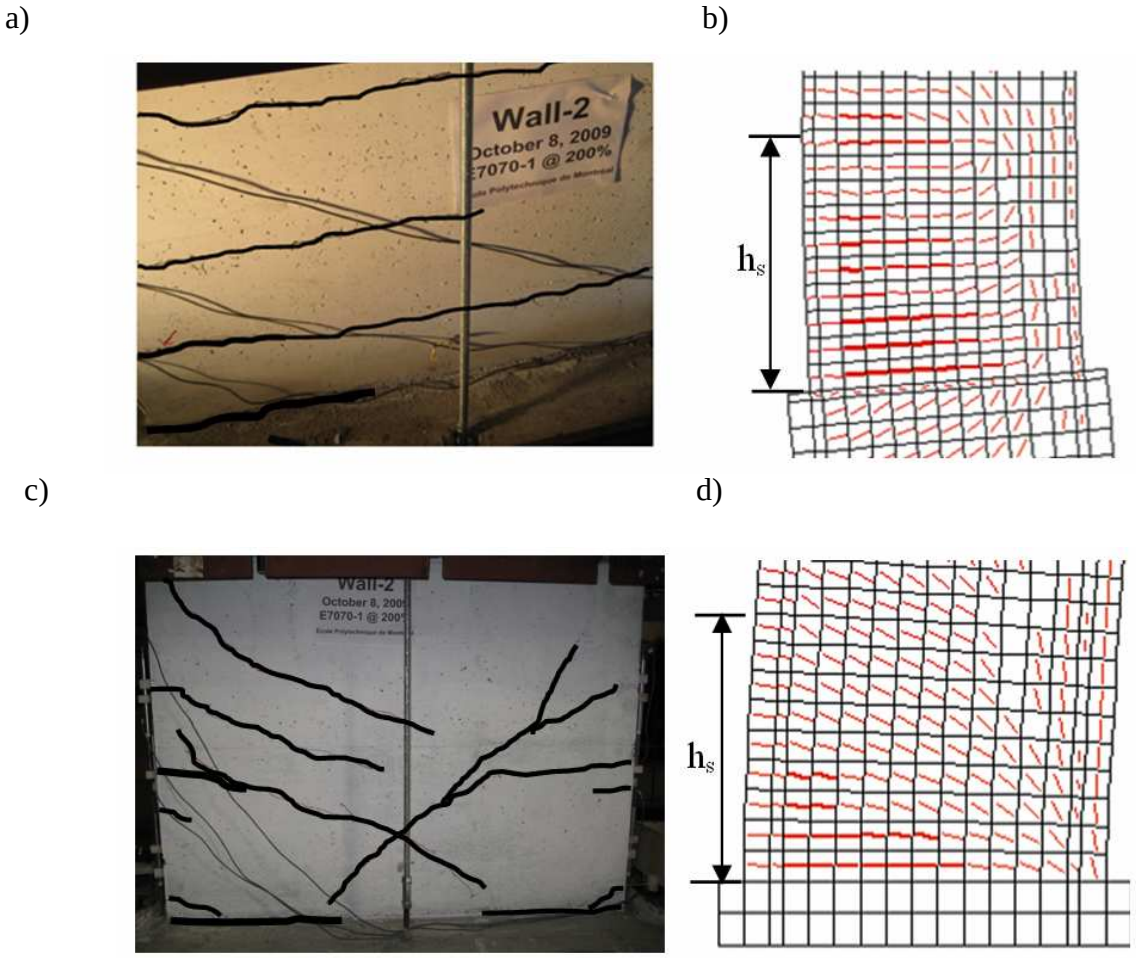

Fig. A.10: Réseaux de fissures accumulés dans le mur W2 pour 200% EQ: (a) observé au 6^{e} niveau lors l'essai; (b) obtenu de VT2 au 6^{e} niveau; (c) observé à la base lors de l'essai, et (d) obtenu de VT2 à la base.

Les réseaux de fissures à la base et au sixième niveau tels qu'obtenus avec le logiciel VT2 correspondaient très bien aux réseaux de fissures observés lors des tests (Fig. A.10). La formation d'une deuxième rotule plastique au 6^{e} étage a été observée dans la modélisation numérique et les résultats des analyses pour la relation moment-rotation sont en accord avec les résultats des essais (Fig. A.11).

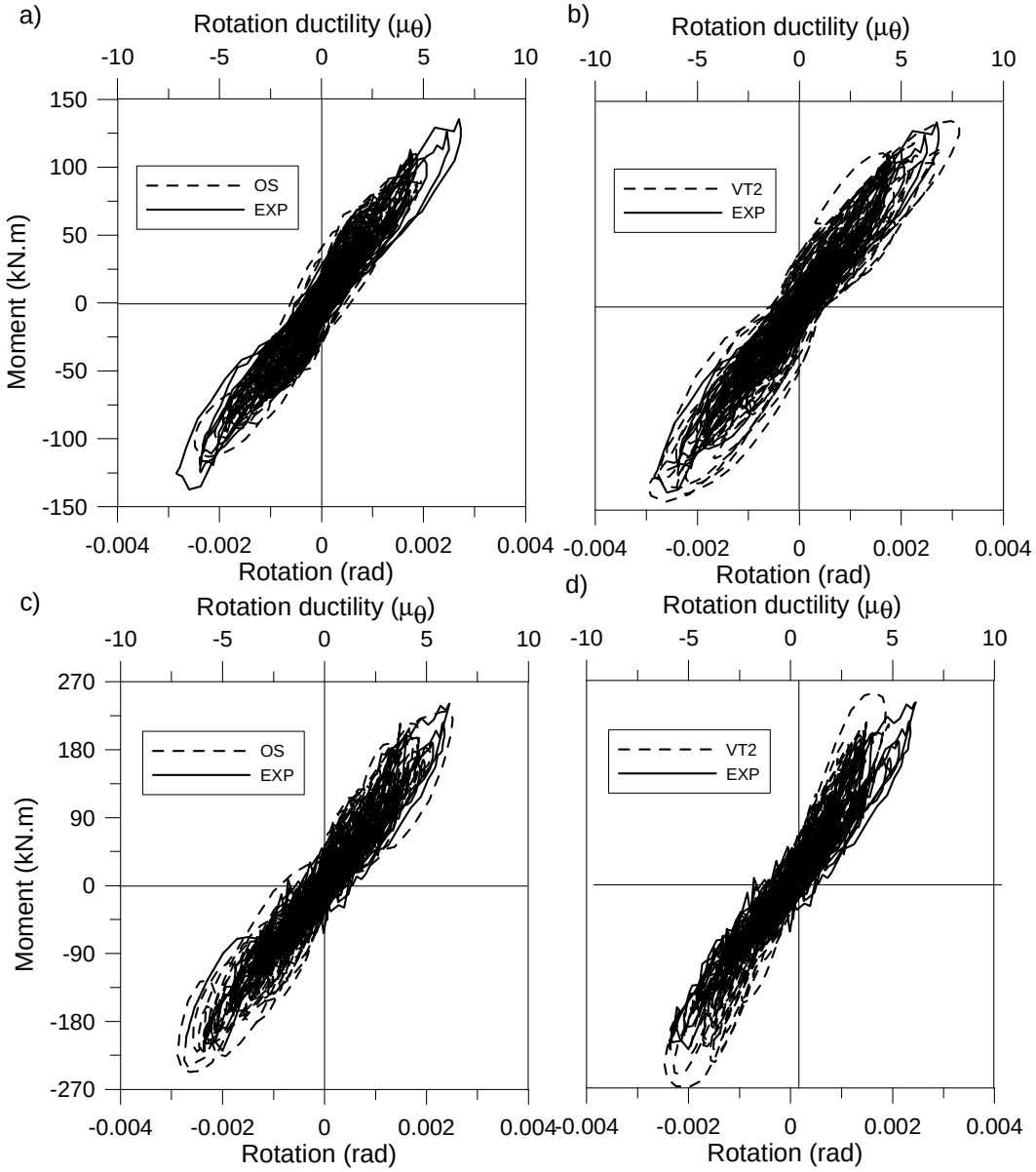

Fig. A.11: Comportement moment-rotation du spécimen W1 sous 100% EQ: (a) OS *vs* essai au niveau 6; (b) VT2 *vs* essai au niveau 6; (c) OS *vs* essai à la base, et (d) VT2 *vs* essai à la base.

Dans cette recherche, on a proposé et étudié une nouvelle approche de conception sismique dans laquelle on considère la formation d'une deuxième rotule plastique sur la hauteur du mur pour contrôler les effets des modes supérieurs sur la réponse des refends en béton armé. On définit cette approche comme la conception de murs avec double rotule plastique (dual hinge design approach). Des simulations numériques d'un mur conçu avec cette approche ont montré que le développement d'une seconde rotule plastique, en plus de celle prévue à la base, peut augmenter la dissipation d'énergie sismique et contribuer à réduire les forces sismiques imposées au mur.

A.7 Conclusions et Recommandations

Deux types d'essais statiques et dynamiques ont été effectués dans cette recherche pour étudier les effets des modes supérieurs de vibration sur le comportement sismique des refends en béton armé.

Les conclusions suivantes ont été obtenues à la suite des essais statiques:

1) Dans les essais cycliques, à la fois le prototype et le modèle ont présenté une réponse stable dominée par la flexion jusqu'à une ductilité en déplacement de 4.0, dépassant ainsi la limite en ductilité de 3.5 considérée par les codes de conception canadien pour les murs de refend ductiles. À une ductilité de 4.0, le glissement en cisaillement s'est amorcé dans les deux essais, ce qui a conduit à une dégradation significative de la résistance des spécimens. Les équations de la norme A23.3 concernant la résistance en cisaillement d'interface à la base des murs pourraient être revues pour assurer une protection suffisante contre ce mode de défaillance dans les structures avec refends ductiles.
2) Une excellente concordance a été obtenue entre le comportement du prototype et celui du modèle à échelle réduite sous les deux protocoles de chargement (monotonique et cyclique). Les modèles à échelle réduite conçus avec un facteur d'échelle allant jusqu'à 2.4 peuvent donc être utilisés pour étudier le comportement sismique des murs ductiles, y compris la flexion élastique, les déformations en cisaillement et le glissement en cisaillement.
3) Les comparaisons entre les résultats expérimentaux et numériques ont montré que le programme d'éléments finis VT2 peut prédire adéquatement le comportement inélastique

monotonique et cyclique des murs ductiles, y compris la rigidité initiale, les déformations en cisaillement, les efforts dans l'acier d'armature transversal, la dissipation d'énergie, et les mécanismes de défaillance.

Les conclusions suivantes ont été obtenues à la suite des essais dynamiques :

1) Sous le mouvement sismique de conception, les spécimens de murs à ductilité modérée ont démontré une réponse inélastique en flexion limitée à la base du mur et au niveau 6. Le comportement inélastique au niveau 6 est attribué aux effets des modes supérieurs de vibration et n'était pas prévu lors de la conception.
2) Les fissures à la base des spécimens ont été affectées par la flexion et par le cisaillement alors que seulement des fissures de flexion se sont formées au niveau 6. En augmentant l'amplitude de l'excitation sismique au-delà du niveau de conception, la rotation inélastique supplémentaire ne s'est développée qu'au niveau 6.
3) La ductilité en déplacement global basée sur les déplacements latéraux du toit a été 35% plus élevée que le facteur de ductilité spécifié dans le code, essentiellement parce que ces déplacements étaient causés par la rotation inélastique au niveau 6 et non par la rotation à la rotule plastique à la base, comme on le suppose lors de la conception. La rotation plastique a été maximale à la base et correspondait à la valeur obtenue en supposant que le premier mode de vibration domine la réponse du mur.
4) Le pic de force de cisaillement à la base du mur a atteint 1.82 fois l'effort utilisé dans la conception des spcéiemsn. Ce facteur est réduit à 1.4 si on considère l'effort de cisaillement de conception calculé en utilisant le signal enregistré sur le simulateur sismique et qui a été effectivement appliqué aux spécimens. Cette amplification dynamique est proche du niveau qui est prescrit pour cette structure dans le code de Nouvelle-Zélande NZS3101 et l'Eurocode EC8 (1.5). En augmentant l'intensité des secousses sismiques à la base au-delà du niveau de conception, le cisaillement à la base a continué d'augmenter même si le moment à la base est resté pratiquement constant.
5) Les spécimens ont pu résister à des forces de cisaillement à la base supérieures à la résistance au cisaillement du mur prescrite par le code, ce qui a été attribué au à une contribution du béton à la résistance au cisaillement plus élevée que prévue par le code

puisque le béton n'était pas fissuré en flexion au moment où le pic de force de cisaillement a été imposé (V_{max} s'est produit avant M_{max}).

6) Les deux méthodes d'analyse, soient celle par éléments finis (VT2) et celle avec éléments fibres (OS) ont permis de prédire adéquatement les périodes naturelles des spécimens pour les essais dans les conditions élastiques ou endommagées. Les logiciels OS et VT2 ont aussi permis de prédire les moments à la base des murs pour toutes les séries d'essais. Dans le domaine élastique ou partiellement endommagé, on a prédit avec le logiciel VT2 des forces de cisaillement plus élevées que les valeurs expérimentales. Les forces de cisaillement obtenues des analyses OS étaient cependant très proches des valeurs d'essais, en particulier pour le spécimen W2 qui était initialement dans un état non endommagé lorsque le mouvement sismique de conception a été appliqué.
7) Le taux d'amortissement calculé à la fin des analyses VT2 augmentait progressivement en raison de l'accumulation des dommages, et les valeurs sont proches des valeurs expérimentales.
8) Le logiciel VT2 a permis de prédire les fissures combinées de cisaillement et de flexion à la base des murs de même que les fissures de flexion au niveau 6. Une excellente concordance a été obtenue avec les réseaux de fissures observés durant les essais.
9) Les essais ont montrés qu'une deuxième rotule plastique se forme au niveau 6 des murs, en plus de celle qui s'est développée à la base, ceci en raison des effets des modes supérieurs de vibration. Ce comportement a également été prédit en utilisant les logiciels OS et VT2. Il y avait une bonne corrélation dans les courbes moment-rotation obtenues des essais et des modèles numériques.
10) Le développement d'une seconde rotule plastique dans la partie supérieure du mur, en plus de la rotule plastique à la base du mur, peut dissiper l'énergie sismique et contribuer à réduire les forces d'inertie imposées le long du mur. Une stratégie de conception a été proposée dans cette étude pour le développement d'une deuxième rotule plastique agissant comme un fusible dans la partie supérieure des murs.

La validité des modèles numériques dépend de plusieurs paramètres définis par l'utilisateur, en particulier pour les modèles d'amortissement. Cette étude a montré que l'ajout d'une petite

quantité d’amortissement visqueux global permet de bien prédire le comportement sismique des structures réelles, lorsque combiné avec un modèle hystérétique précis du béton armé.

Avec le logiciel VT2, un amortissement visqueux de 1% a conduit à des résultats raisonnables pour les murs étudiés. Pour le logiciel OS, 2% d'amortissement a donné lieu à des résultats qui se comparaient bien à ceux de l'essai sur le mur en bon état soumis au mouvement sismique de conception. Lorsque l'on augmente l'intensité du tremblement de terre, l'amortissement a dû être réduit à des valeurs comprises entre 1.5% et 1% pour obtenir de bons résultats pour le mur endommagé avec des périodes de vibration allongées. Il faut noter que ces valeurs d'amortissement ne s'appliquent que sur les murs considérés dans cette étude et peuvent ne pas être représentatives de l’amortissement présent dans les structures de bâtiments réels.

Le programme d'essais et les analyses ont confirmé que les murs à ductilité modérée soumis à une excitation sismique à haute fréquence peuvent présenter une réponse inélastique en flexion dans les étages supérieurs, de même qu’une amplification dynamique des forces de cisaillement horizontales à leur base.

Dans les bâtiments réels où les murs en béton armé sont utilisés en combinaison avec des cadres, plus d'amortissement est prévu par rapport aux spécimens examinées ici, et ces effets peuvent être moins prononcés que ceux mesurés lors de cette étude.

Pour développer d’avantage l’approche de conception basée sur la présence de deux rotules plastiques il est recommandé d'examiner de façon systématique à l’aide d’analyse paramétrique les réponses des modes supérieurs sur différents modèles numériques de murs à l’aide d’OpenSees (différentes hauteurs, différents coefficients d’amortissement différentes ductilité, différentes intensités de charges axiales …). Il s’agit tout d’abord de réduire autant que possible les amplifications dynamiques de cisaillement et, d'autre part, d'examiner les deux rotules plastiques et les détails d’acier d’armature pour la deuxième rotule.

Après les essais sur table vibrante, les deux murs d’origine ont été renforcés avec la collaboration de chercheurs de l'Université Concordia en utilisant deux méthodes différentes de réhabilitation

à l’aide de feuilles composites en fibres de carbone polymère renforcé (FCPR) à la région de rotule plastique (panneau de base et 6^{e} étages). Les murs réhabilités ont été testés en les soumettant aux mêmes niveaux d'excitations sismiques que celles appliquées aux murs d'origines. Les fréquences naturelles des murs réhabilités ont été jugées plus élevées que ceux des murs endommagés et proches des valeurs mesurées pour les murs d'origine en bon état. Les deux murs réhabilités montrent une meilleure résistance à la flexion au niveau du panneau du sixième étage. En augmentant l'intensité du mouvement à la base, les dommages (fissuration, plasticité) se sont propagés dans les autres étages non réhabilités.

TABLE OF CONTENTS

LIST OF TABLES

LIST OF FIGURES

LIST OF SYMBOLS

A_g	gross concrete section area
A_s	area of longitudinal steel bar
b_w	web thickness
c	depth of neutral axis
E_c	module of elasticity of concrete
E_s	module of elasticity of steel
E_h	accumulated hysteric energy
f_y	yield tensile stress of steel
f_u	ultimate tensile stress of steel
f'_c	compression stress of concrete
f_t	tensile stress of concrete
g	gravity acceleration
h_w	total height of wall
l_w	length of the wall
M_p	probable moment
M_f	factored moment
M_n	nominal moment resistance
M_r	factored moment
P	axial force
t_r	time scaling factor
R_d	force reduction factor
$R_o\&\varphi^o$	flexural overstrenght factor
S_a	spectrum acceleration
V_f	factored shear
V_r	factored shear resistance
V'_f	design shear capacity
V_n	nominal shear resistance
$V_{r,sf}$	factored shear resistance by friction

$V_{n,sf}$	nominal shear resistance by friction
V_y	yield lateral load
$V_{B,\ max}$	maximum shear at the base
$M_{B,\ max}$	maximum moment at the base
$M_{6,\ max}$	maximum moment at the 6^{th} floor
α	unloading stiffness factor
α_r	acceleration scaling factor
β	reloading stiffness factor, factor accounting for shear resistance of cracked concrete
γ_b	base shear strain
γ_6	6^{th} shear strain
γ_w	wall overstrength factor
Δ_f (Δ_{top})	wall top deflection
$\Delta_{top,\ res}$	residual wall top deflection
Δ_y	wall top yield deflection
Δ_{shear}	shear deformation
δ	storey drift
$\delta_{b\ res}$	base residual drift
$\delta_{6\ res}$	6^{th} residual drift
ε_{sh}	strain hardening of steel bar
ε_{su}	ultimate strain of steel bar
ε_{cu}	maximum compression strain of concrete
ε_0	peak compression strain of concrete
ε	longitudinal strain of steel bar
ξ	damping ration
θ_b	base rotation demand
θ_6	6^{th} rotation demand
$\theta_{b\ res}$	base residual rotation
$\theta_{6\ res}$	6^{th} residual rotation
θ_{id}	inelastic rotation demand

θ_p	plastic rotation
θ_{ic}	plastic rotation capacity
$\mu_{b\theta}$	base rotation ductility
$\mu_{6\theta}$	6^{th} rotation ductility
μ_{Δ}	displacement ductility
ϕ_c	resistance factor for concrete
ϕ_s	resistance factor for steel
ν_c	Poisson ratio of concrete
Ωo_M	moment overstrenght factor
Ωo_V	shear overstrenght factor
ω_v	shear amplification factor

LIST OF ACRONYMS AND ABBREVIATIONS

NBCC	National Building Code of Canada
CSA	Canadian Standard Association
NZS	New Zealand Standard
SPH	Single Plastic Hinge
DPH	Dual Plastic Hinge
RC	Reinforced Concrete
FRP	Fibre Reinforced Polymer
VT2	VecTor2
MCFT	Modified Compression Field Theory
DSFM	Disturbed Stress Field Model
FE	Finite Element
ACI	American Concrete Institute
ASTM	American Society for Testing Material
R2000	Response 2000
OS	OpenSees
ATC	American Technology Council
EC8	Eurocode 8
AIC	Adaptive Inverse Control
FEMA	Federal Emergency Management Agency
IO	Immediate Occupancy
LS	Life Safety
FQRNT	Quebec Fund for Research on Nature and Technology
NSERC	Natural Science and Engineering Research Council of Canada
PGA	Peak Ground Acceleration

LIST OF APPENDICES

INTRODUCTION

Motivation

With the development of earthquake and structure sciences, structure codes and seismic provisions are being updated, but there are still many aspects that are not fully understood due to the random nature of earthquake motions as well as the complex features of the response of reinforced concrete structures. Among these aspects, higher mode effects on structures during ground motions have been topical issues.

Current seismic provisions such as the Canadian CSA A23.3 standard, the New Zealand NZS3101 standard and the Eurocode EC8 (CEN 2004) have some design procedures to consider higher mode effects. For example in the Canadian and New Zealand standards, the design bending moments and shear forces above the base plastic hinge region must be amplified by the ratio of the actual flexural resistance in the hinge region to the design moment at that location. NZS3101 also prescribes modified design shear force envelopes along the building height, with shear amplification factors to account for higher mode effects. In Eurocode EC8, only the base shear forces are magnified to account for both flexural overstrength and dynamic amplification. In EC8, bending moments above the base hinge are amplified by applying a linear variation of bending forces from the expected flexural overstrength at top of hinge to near zero at the top of the wall. Shear amplification in NZS3101 is based on the number of stories whereas the period of the building and the shape of the design spectrum are considered in EC8. Rules in CSA A23.3 and EC8 vary depending on the level of ductility assumed in the calculation of the seismic loads.

On the contrary, no capacity design provisions or requirements for dynamic response effects are prescribed in the ACI (2008) provisions used in the U.S.

In CSA A23.3, the shear capacity should be obtained due to development of moment capacity of the wall at the base plastic rotation but the plastic rotation is evaluated assuming only first mode response (Adebar et al. 2005).

Nonlinear time history dynamic analyses of shear walls subjected to earthquake ground motions have shown that shear forces in excess of these capacity design values can develop due to the contribution of the higher modes of vibration to dynamic response (Blakeley et al. 1975, Filiatrault et al. 1994, Amaris 2002, Panneton et al. 2006, Krawinkler 2006, Velev 2007, Boivin and Paultre 2010). Such higher shear forces can cause brittle shear or sliding failure modes to occur.

Past numerical studies on cantilevered walls also revealed that the amplification of moment at top of the wall due to higher modes the plastic hinge can form in the upper part of walls, even when designed and detailed for plastic hinging at the base only (Blakeley et al. 1975; Tremblay et al. 2001; Panneton et al. 2006).

Due to low to moderate seismicity zone of Eastern North America, moderately ductile RC walls are generally preferred to ductile RC walls as the formers can be more easily designed and built while being cost effective in terms of required material. Ground motions expected in Eastern North America are richer in high frequency content compared to ground shaking typical of Western North America, which may promote relatively greater higher mode response of RC walls. This response can result in more severe dynamic shear amplification as wells as significant

amplification of bending moments at the wall mid height. The latter can lead to the formation of plastic hinges in the upper part of the wall (Panneton et al. 2006).

To understand better the dynamic seismic response of slender shear walls and develop consistent design methodologies for use in practice, further experimental research is clearly needed. One of the most reliable methods of generating the test data on the seismic behaviour of RC walls is large scale shaking table testing (Lestuzzi et al. 1999; Lu and Wu 2000; Kazaz et al. 2006; Panagiotou et al. 2007a, b). Full-scale shaking table test on 7-storey rectangular wall subjected to a California seismic ground motions confirmed that dynamic amplification due to higher mode response could increase the base shear up to 1.5 times the shear force corresponding to the wall flexural overstrength (Panagiotou et al. 2007a, b).

To evaluate the seismic design procedure of Canadian CSA A23.3 standard and investigate the higher mode effects on slender RC walls under high frequency ground motions, two series of large scale shaking table tests were carried out under Eastern North America ground motions in this research. The tests were performed at the Structural Engineering Laboratory of École Polytechnique, Montreal, Canada.

Objectives and Scopes

This research project is aimed at experimentally investigating higher mode effects on slender reinforced concrete shear walls subjected to Eastern North America (ENA) ground motions. These motions are expected to be rich in high frequencies, which represents a more critical condition for higher mode response. The tests permitted to examine the effect of higher mode responses on lateral deformation profiles, plastic hinging response, including yielding of the

reinforcement in the base and in upper levels, lateral load patterns and shear force demand, dynamic shear amplifications, and interaction between shear and bending moment demands.

The objectives of this study have been summarized as follow:

a) Examining the design approach for shear strength proposed in CSA A23.3.
b) Checking the rules of the scaling and similitude laws applied by comparing the results of tests on the walls of prototypes and models for application in tests of reinforced concrete walls on shake table.
c) Evaluating the capacity of VecTor2 program to replicate the inelastic response and failure modes observed in the tests for the wall under the high ductile plastic deformations.
d) Studying the effects of higher modes on the reinforced concrete walls such as damage, demand force, and the inelastic response of the wall under earthquake of Eastern North America (ENA).
e) Evaluating the shake table test results and the ability of Fiber Element (Open Sees) and Finite Element (VecTor2) models for nonlinear dynamic analysis of reinforced concrete walls.
f) Investigating the damping effects on numerical models by comparing to the experiments.
g) Proposing a new design approach that takes into account the effects of higher modes

Methodology

To investigate the higher mode effects on high-rise walls, the following experimental and analytical studies were conducted:

- In the summer of 2006, two pairs of prototype and scaled model of reinforced concrete walls (prototype: l_w=1.3m and h_w=2.7m, model: l_w=0.548 and h_w=1.14m) designed according to NBCC05 and CSA-A23.3-04 were tested under monotonic and cyclic loads at the Structural Engineering Laboratory of École Polytechnique, Montreal to verify the adequacy of the scaling rules between the prototype and model RC walls. Numerical simulations were performed using lumped plastic hinge based models and finite element models to reproduce the test results.
- In the winter of 2007, the wall prototype for the shake table test was selected from an 8-storey building located in Montréal, Canada. It was scaled down from 21 m to 9 m and redesigned according to NBCC05 and CSA-A23.3-04. The seismic response of the designed model wall was numerically investigated by finite element and fibre element methods to obtain an overview of the seismic behaviour of the wall before the tests.
- From summer 2007 to summer 2008, an innovative shake table test setup was designed and constructed by the group of researchers at École Polytechnique.
- From the Fall 2008 to the Spring 2009, the author constructed two identical wall specimens (Walls W1 and W2) of the designed model wall.
- From summer 2009 to winter 2010, the specimens were installed on the shake table and the tests were carried out. The author finalized the analysis and interpretation of the test results. The numerical modeling of the walls was carried out using finite element (VecTor2) and fibre element (OpenSees) methods.

After doing the tests on each of the two walls, the walls were rehabilitated using FRP wrapping by Prof. K. Galal and Ph.D. student Hosam Samy from Concordia University to investigate the seismic behaviour of the repaired walls. The tests were carried out at École Polytechnique of Montreal.

Original Contributions

The main scientific contributions of this research project follow as below:

1. Reproducing the inelastic seismic response of ductile shear walls including shear deformation effects, shear sliding behaviour and failure mode of prototype full scale with reduced scale specimens, as observed in monotonic and cyclic tests.
2. Evaluating the Disturbed Stress Field Method (Vecchio 2000) implemented in the finite element code VecTor2 using the monotonic and cyclic test results of walls subjected to significant inelastic deformations.
3. Applying the new test rig developed at the Structural Engineering Laboratory of Ecole Polytechnique of Montreal for the large scale shake table tests. This setup aims at minimizing axial load on the shake table to fully exploit its overturning moment capacity. It also allows to represents realistic seismic weight configurations and considers the P-delta effects on storey responses.
4. Performing the first large scale shake table tests on 9 m tall models of 21 m high moderately ductile prototype reinforced concrete shear walls under Eastern North America (ENA) seismic ground motions.

5. Clear demonstration of higher mode effects including plastic hinge in the upper part of the wall designed and detailed according to the seismic provisions of NBCC 2005 and CSA-A23.3-04 standard under the high frequency ENA earthquake.
6. Demonstrating that the fibre element method is capable of reproducing most of the dynamic behaviour of reinforced concrete shear walls and predicting the nonlinear response in the upper part of the wall under the higher mode effect.
7. Identification of suitable viscous damping parameters to correlate numerical and experimental results.
8. Showing that the damping parameters have to be modified when carrying out analyses of the structure subjected to successive ground motions with different amplitudes.
9. Proposing a dual hinge design approach that could be appropriate for ENA seismic applications; however, the method still needs further investigation before it can be codified.
10. Contributing to the conduct of shake table tests of the damaged walls after applying a Fiber Reinforced Polymer wrapping repair technique to improve their seismic behaviour.

CHAPTER 1

LITERATURE REVIEW

1.1 Introduction

To prevent the collapse of building structures under strong seismic ground motions, reinforced concrete (RC) shear walls must maintain a high proportion of their initial strength and stiffness and possess high energy-dissipation capacity (Paulay and Priestley 1992).

In current code seismic provisions such as CSA-A23.3-04 and New Zealand NZS3101 standard, ductile cantilever reinforced concrete walls must satisfy stringent design and detailing requirements such that they are capable of developing ductile flexural plastic hinging at their bases without significant shear distress or without failure modes causing rapid strength deterioration under cyclic inelastic loading (Adebar et al. 2005). Following capacity design principles, the wall should be able to carry the shear forces developed due to attainment of the probable flexural capacity at the wall base (Paulay and Priestley 1992, CAC 2006).

1.2 Analyses of RC Walls and Higher Mode Effects

The inelastic seismic response of tall and slender RC walls remains complex, however, as it involves the superposition of multiple modes of vibration in the nonlinear range, interacting flexural, shear and axial cyclic load demand, and the random nature of earthquake ground motions. Nonlinear time history analyses of shear walls under the ground motions have shown that the base shear forces in excess of the capacity design values prescribed in Codes can develop due to contributions of higher mode responses (Blakeley et al. 1975; Filiatrault et al. 1994; Tremblay et al. 2001; Priestley and Amaris 2002; Priestley 2003; Sullivan et al. 2006; Krawinkler 2006; Panneton et al. 2006; Boivin and Paultre 2010). This excess shear forces can cause brittle failure or sliding failure modes before the walls reach to their designed plastic rotations at the base. In the most of these analyses lumped plastic hinge method was used with hysteretic plastic hinges concentrated at their ends. Effects of shear sliding deformations along flexural cracks and shear stiffness degradation due to diagonal cracking were however omitted (Cheng et al. 1993, Thomsen and Wallace 2004).

D'Ambrisi and Fillipou (1999) proposed a computationally effective macroscopic member that includes elastic, spread plastic, interface bond-slip, and shear sub-elements connected in series. Nonlinear shear elements have also been used in combination with fibre discretization of wall cross sections to better capture the distribution of normal stresses while including shear deformation effects on the response (Petrangeli et al. 1999, Petrangeli 1999). Proper coupling between nonlinear flexural and shear responses however requires the use of realistic material constitutive laws in a finite element (FE) formulation. For instance, the compatibility, equilibrium, and constitutive relations of the Modified Compression Field theory (MCFT)

(Vecchio and Collins 1986) and Disturbed Stress Field Model (DSFM) (Vecchio 2000) have been implemented in the two-dimensional FE analysis program VecTor2 (VT2) (Wong and Vecchio 2002). Palermo and Vecchio (2003, 2004) extended the capability of this numerical tool to cyclic loading applications. Palermo and Vecchio (2007) showed that this methodology could lead to quick and reliable results for various wall designs and geometries using simple low-order rectangular elements with smeared material properties. The ability of FE procedures to adequately reproduce the nonlinear dynamic response of shear walls must be verified through shake table benchmark tests (Orbovic et al. 2004).

The effect of higher modes can be more significant under Eastern North America earthquake due to the higher frequency content of the ground motions they generate. To investigate the higher mode effects for this type of ground motions, nonlinear time history analyses were carried out by Panneton et al. (2006) on an eight-storey reinforced concrete shear wall building located in Montréal (24 m high). The building was braced by four simple shear walls and three cores. Fig. 1.1 shows the bending moments and the shear forces distributions for one of these walls along the height under different ground motions. The base shear forces obtained from nonlinear time history analysis is two time larger than the shear forces prescribed by the code (Fig. 1.1a). Fig. 1.2b also shows the amplification of bending moment at the mid-height of the wall. This amplification resulted in increased curvature demand in the upper levels and possible formation of a plastic hinge in that region (Fig. 1.2).

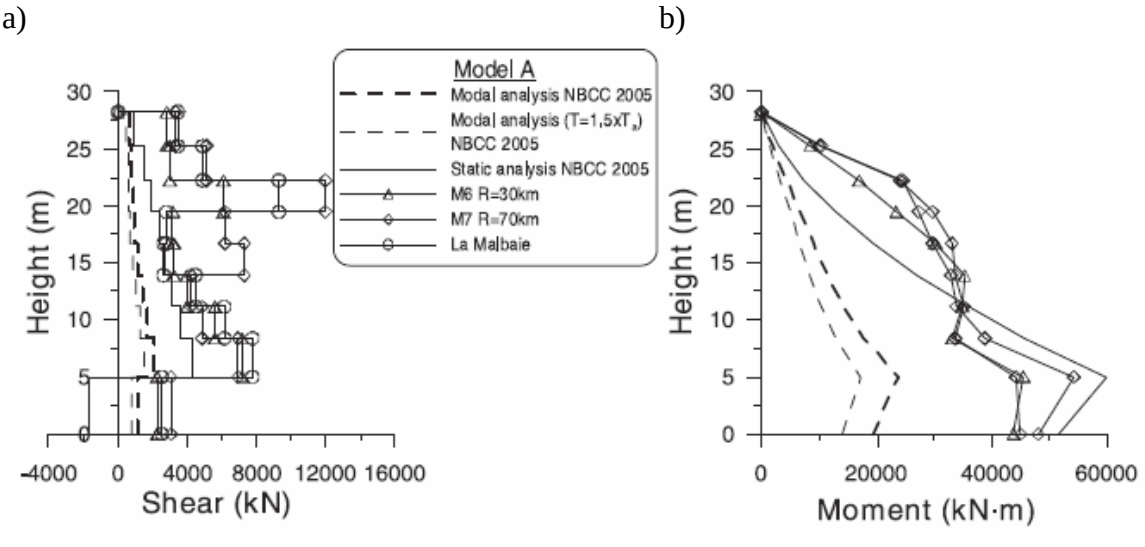

Fig. 1.1: Comparison of storey shear and bending moment for different analyses (Panneton et al. 2006); (a) shear distribution (b) moment distribution.

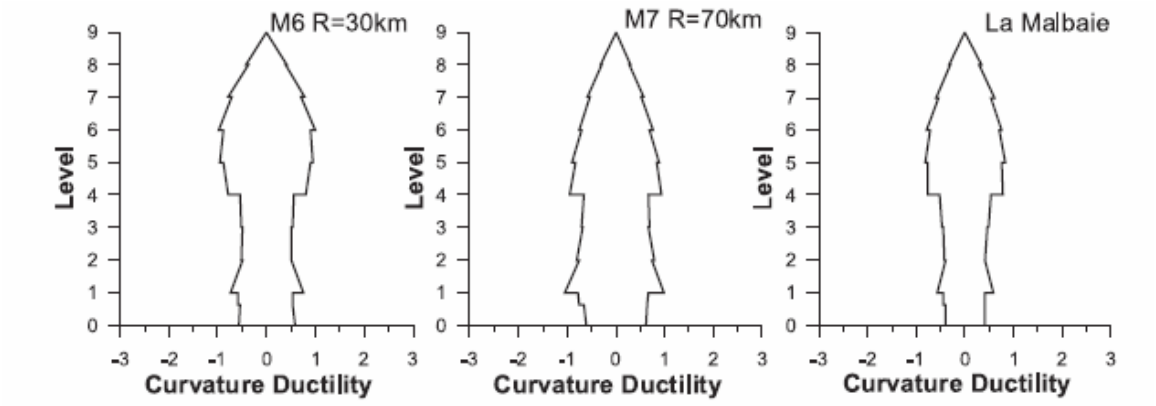

Fig. 1.2: Curvature ductility demand under seismic ground motions (Panneton et al. 2006)

1.3 Design Approach of Building Codes

Differences exist in seismic provision standards on how to achieve the desired ductile base flexural hinging response while accounting for the dynamic and higher mode effects in design.

In the Canadian CSA A23.3 standard (CSA 2004), the design bending moment above the base hinge, M_f, is obtained by multiplying the moment obtained from static or response spectrum analysis (M_{ST} or M_{RSA}) by the ratio M_r/M_{ST} or M_r/M_{RSA} calculated at the top of the hinge region where M_r is the factored moment resistance of the wall section. This force amplification is applied to take into account the higher mode effects (Fig. 1.3).

In CSA A23.3, the shear capacity depends on the base plastic rotation but the plastic rotation is evaluated assuming only first mode response. The design base shear in CSA A23.3 standard is increased to account for the wall flexural overstrength. This is done by multiplying the shear force from static or response spectrum analysis, V_{ST} or V_{RSA}, by the ratio of the wall probable capacity M_P for Ductile walls, or the nominal moment capacity M_n for Moderately ductile walls, at the wall base, to the moment M_{ST} or M_{RSA} at the wall base.

Among these two amplification factors described in two previous paragraphs the most critical one should be used as an amplification factor for the shear forces above the hinge to obtain the shear design forces.

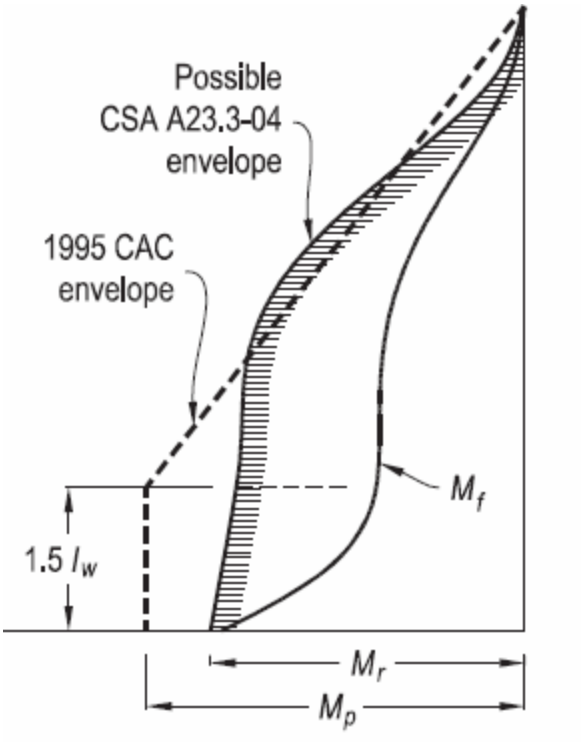

Fig. 1.3: Capacity design moment envelopes for ductile RC walls (Boivin and Paultre 2010).

In the New Zealand NZS3101 standard (NZS 2006), the design bending moments and shear forces above the base plastic hinge region must be amplified by the ratio of the actual flexural resistance in the hinge region to the design moment at that location. This standard also prescribes modified design shear force envelopes along the building height, with shear amplification factor (ω_V) to account for higher mode effects (Fig. 1.4). Shear amplification in NZS3101 is based on the number of stories:

$$\omega_V = 0.9 + n/10 \quad \text{For } n \le 6$$
$$\omega_V = 1.3 + n/30 \le 1.8 \quad \text{For } 6 < n \qquad \text{Eq. 1.1}$$

where n is the number of stories.

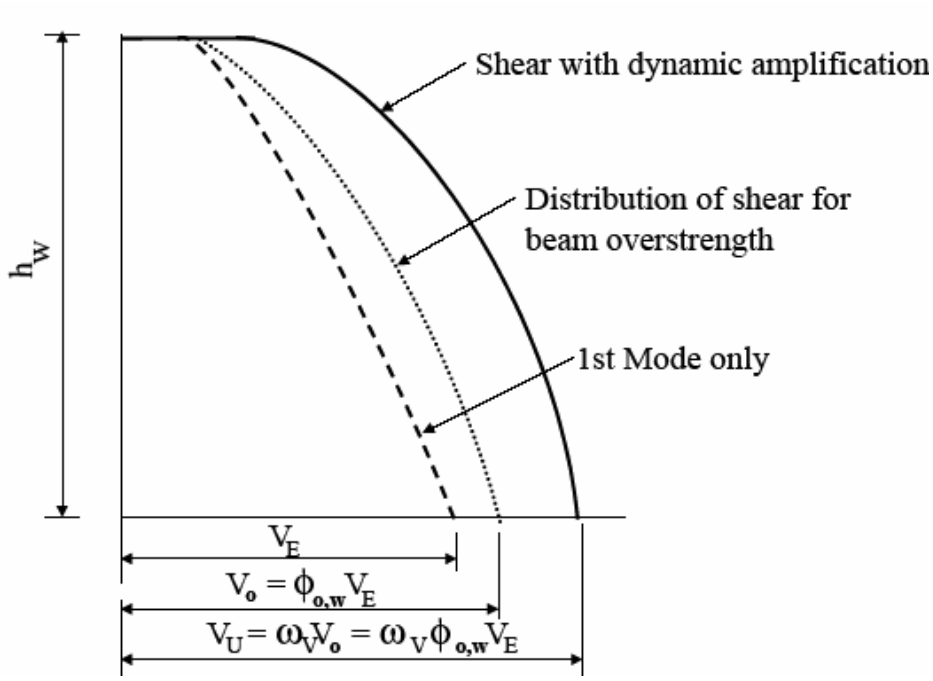

Fig.1.4: Distribution of shear force with over strength and dynamic amplification (NZS 2006)

In Eurocode EC8 (CEN 2004), a linear variation of bending moments should be considered from the expected flexural overstrength at the top of the base hinge to near zero at the top of the wall, as it is shown in Fig. 1.5. This increase in bending moment accounts for higher mode effects.

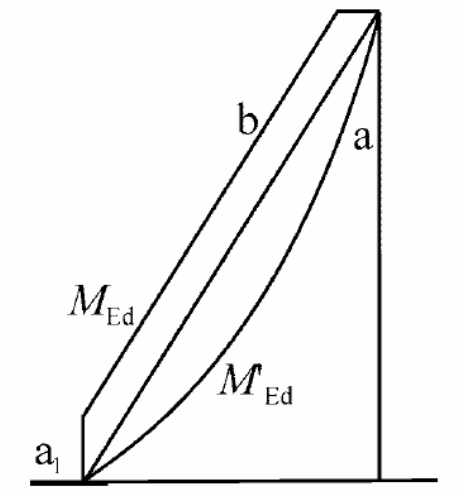

Key

a	moment diagram from analysis
b	design envelope
a_l	tension shift

Fig. 1.5: Design envelope for bending moments in slender walls (M'_{ED} and M_{ED} are analysis and design bending moment respectively) (CEN 2004)

In EC8, the shear forces obtained from analysis are increased by the dynamic magnification provided by Eq. 1.2. In this formulation, not only the flexural overstrength is considered but the period of the building and the shape of the design spectrum are taken into account to consider the dynamic amplification.

$$\varepsilon = q \cdot \sqrt{\left(\frac{\gamma_{Rd}}{q} \cdot \frac{M_{Rd}}{M_{Ed}}\right)^2 + 0{,}1\left(\frac{S_e(T_C)}{S_e(T_1)}\right)^2} \leq q \qquad \text{Eq. 1.2}$$

where

q	is the behaviour factor used in the design;
M_{Ed}	is the design bending moment at the base of the wall;
M_{Rd}	is the design flexural resistance at the base of the wall;
γ_{Rd}	is the factor to account for overstrength due to steel strain-hardening; in the absence of more precise data, γ_{Rd} may be taken equal to 1.2;
T_1	is the fundamental period of vibration of the building in the direction of shear forces V_{Ed};
T_C	is the upper limit period of the constant spectral acceleration region of the spectrum
$S_e(T)$	is the ordinate of the elastic response spectrum

On the contrary, no capacity design provisions or requirements for dynamic response effects are prescribed in ACI (2008).

Priestley et al. (2007) recently proposed a bilinear bending moment envelope to consider the higher mode moment amplification (Fig. 1.6). This envelope starts at the base with the expected flexural overstrength, ends at zero moment at the top and passes through a mid-height moment $M^{o}_{H/2}$ given by:

$$M^{\circ}_{H/2} = C_{1,T}\ \varphi^{\circ}\ M_{u,0} \quad \text{where } C_{1,T} = 0.4 + 0.075 T_1(\mu/\varphi^{\circ} - 1) \geqslant 0.4 \qquad \text{Eq. 1.3}$$

In which φ^{o} is the wall base expected flexural overstrength factor given by $M_p / M_{u,0}$, where M_p is the expected flexural overstrength that accounts for all sources of strength increase at the base of the wall, $M_{u,0}$ is the design base bending moment, T_1 is the fundamental period and μ is the displacement ductility factor.

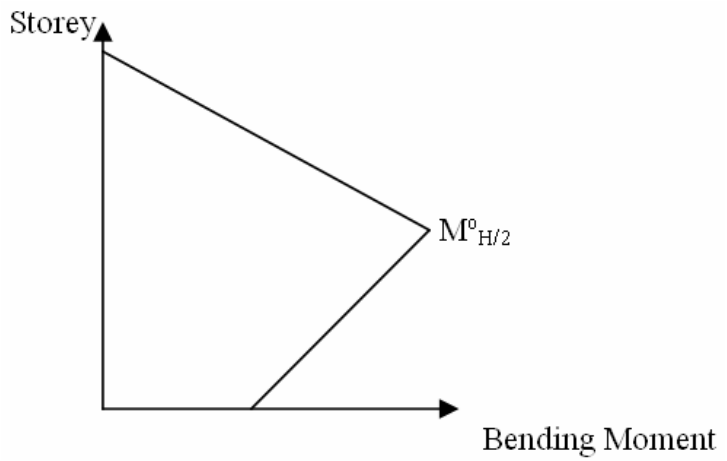

Fig. 1.6: Distribution of design moment along the height after formation of base plastic hinge proposed by Priestley et al. (2007).

1.5 Dual Hinge Design Concept

Having another plastic hinge at the mid-height of the wall in addition to the base could dissipate the earthquake energy more effectively and decrease the force demand on the wall (Panagiotou and Restrepo 2009). According to the dual plastic hinge design approach the structures can become plastic in the top part as well as at the base of the wall. The mid-height plastic hinge can be designed like the bottom plastic hinge to meet specific objectives such as minimum curvature ductility or strain demand. Reduction of the bending moment demand along the height of the wall due to formation of a second hinge will follow the reduction in longitudinal reinforcement. This behaviour can be observed from the numerical study carried out by Panagiotou and Restrepo (2009) on 10, 20 and 40 storey shear walls designed based on the single plastic hinge (SPH) and dual plastic hinge (DPH) concepts. Figure 1.7 compares the distribution of the bending moments in the three walls for the two design approaches. The single hinge approach leads to increased bending moments at the mid height of the walls whereas the dual hinge design reduced significantly these bending moments. This effect is more pronounced as the wall is taller because

the higher mode contributions in taller walls are more significant. In most cases, the base shear forces were also reduced when applying the dual hinge design approach (Fig. 1.8).

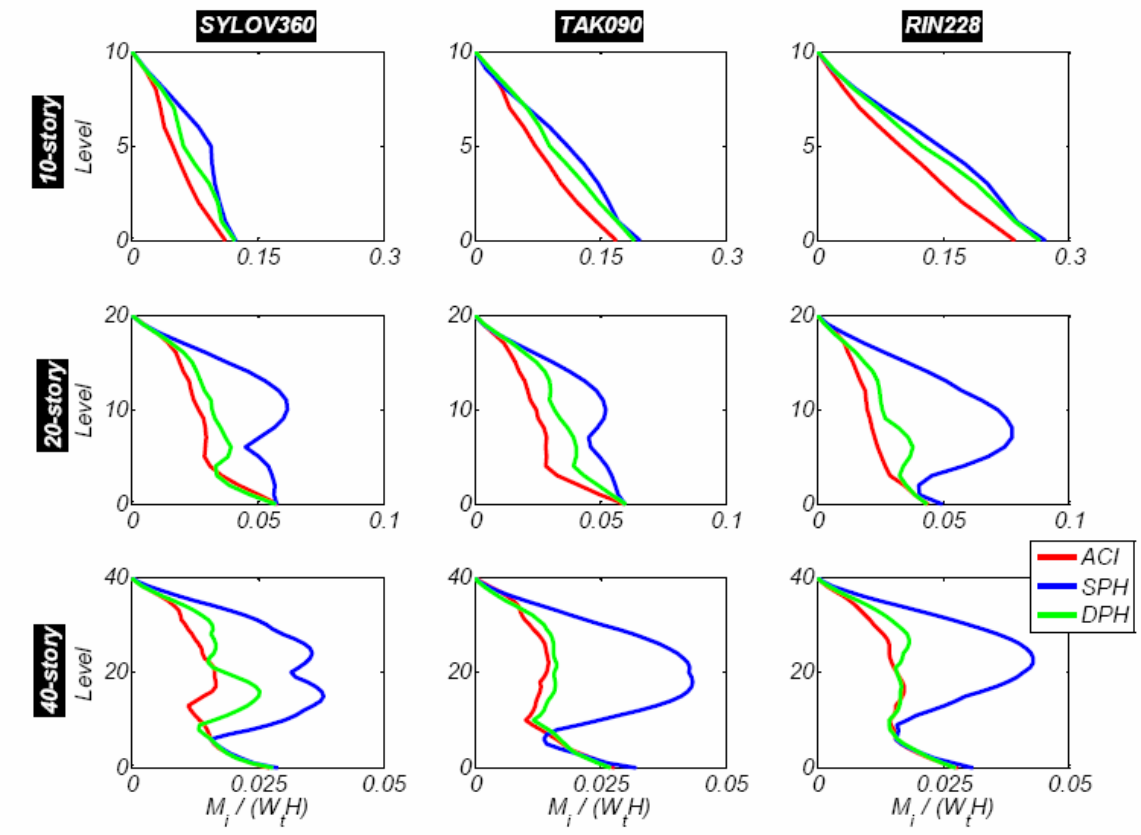

Fig. 1.7: Bending moment envelope obtained from analyses (ACI:ACI Code, SPH: Single Plastic Hinge, DPH: Dual Plastic Hinge) (Panagiotou and Restrepo 2009).

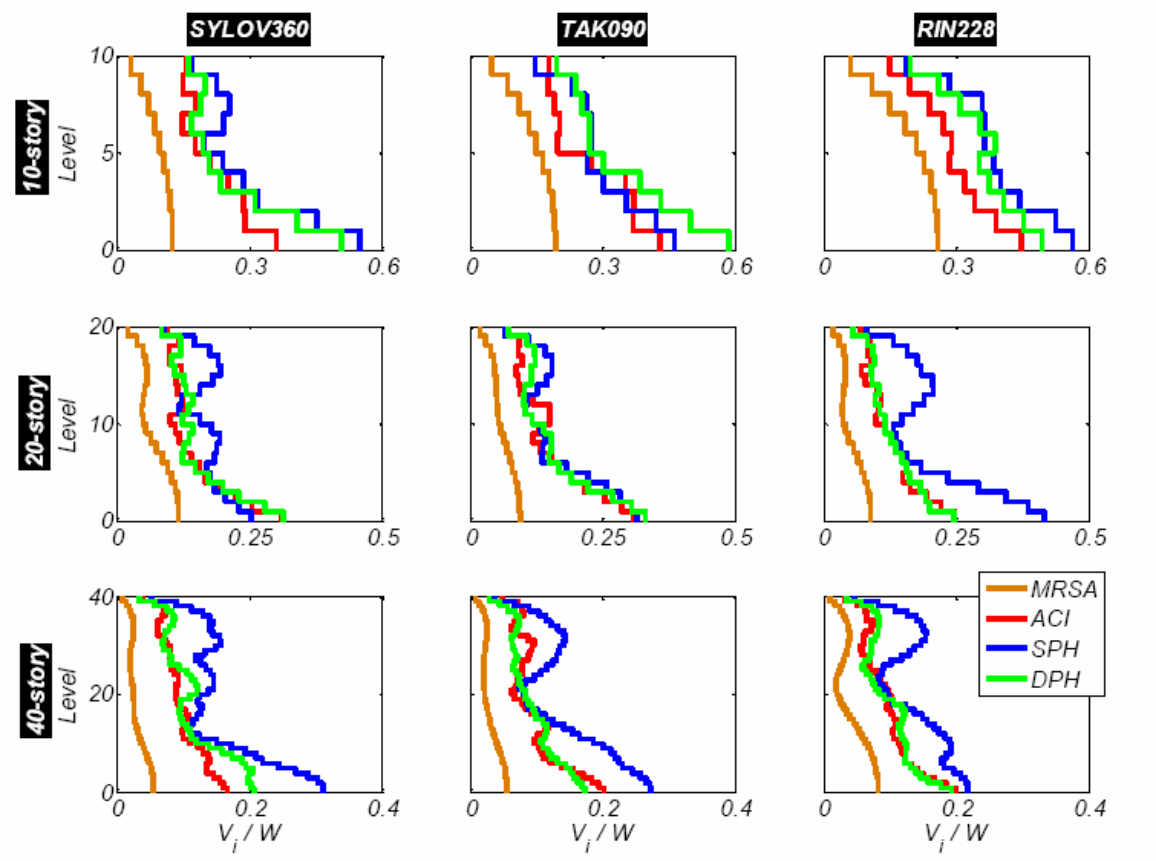

Fig. 1.8: Normalized shear force envelope obtained from analyses (MRSA: Modal Response Spectrum Analysis) (Panagiotou and Restrepo 2009).

1.6 Experimental Similitude of Ground Motions and Shake Table Tests

The previous discussions showed that some complexity still exists for higher mode effects in slender RC walls that have not been clearly understood. To investigate the seismic responses of the wall one of the best ways is to carry out experimental tests. Dynamic testing of structures complements and aids the validation of computational methods for studying the behaviour of structures under earthquake loads. Large scale shake table testing has been a reliable method of generating test data on the seismic behaviour of RC walls (Lestuzzi et al. 1999; Lu and Wu 2000; Kazaz et al. 2006; Panagiotou et al. 2007a, b). To fully understand and investigate the higher

mode effects and having a bench mark for test for numerical modeling, large scale shake table tests on high rise RC wall are needed. Recent full-scale shake table testing of 7-storey rectangular wall subjected to a California seismic ground motions (Panagiotou et al. 2007a, b) confirmed the dynamic amplification of shear forces due to higher modes. In these tests, the base shear overstrength reached up to 1.5 times the shear force associated to the wall flexural overstrength due to the influence of higher modes which lowered the position of the lateral loads compared to design assumptions.

In the current literature there is no large scale shake table test focusing on higher mode effects and damage and plasticity in wall upper levels caused by high frequency ground motions typical of Eastern North America (ENA) earthquakes.

CHAPTER 2

ORGANIZATION AND OUTLINE

The Introduction of this thesis presented background information on the research topic, the objectives of the research project, and the methodology that was adopted. Chapter 1 is the literature review reporting on past seismic analytical and experimental work on reinforced concrete shear walls. Seismic design provisions included in current code documents are also discussed in Chapter 2.

The subsequent three chapters respectively correspond to three technical papers that have either appeared or been submitted for publication in scientific journals:

Chapter 3 (Paper 1): Ghorbanirenani, I., Velev, N., Tremblay, R., Palermo, D., Massicotte, B., and Léger, P., "Modeling and Testing of Influence of Loading History and Scaling Effects on the Inelastic Response of Reinforced Concrete Shear Walls," *ACI Structural Journal*, V. 106, No. 3, May-June 2009, pp. 358-367.

Chapter 4 (Paper 2): Ghorbanirenani, I., Tremblay, R., Léger, P., and Leclerc, M. 2010. "Shake Table Testing of Slender RC Shear Walls Subjected to Eastern North America Seismic Ground Motions," *ASCE Journal of Structural Engineering*, (Submitted on July 6th, 2010 to the editor to begin the review process)

Chapter 5 (Paper 3): Ghorbanirenani, I., Léger, P., Tremblay, R., 2010. "Numerical Modeling of Shaking Table Test and Design Recommendations for Higher Modes in an 8-Story RC Shear Wall," *ASCE Journal of Structural Engineering*, (Submitted on July 6th, 2010 to the editor to begin the review process)

The content of these three chapters can be summarized as follows:

Chapter 3 presents the monotonic and reverse cyclic tests performed on prototypes and scaled down models of ductile RC walls designed according to NBCC 2005 and CSA-A23.3-04 for the Western of Canada. The objectives were to: (a) examine the design approach for shear capacity proposed in the CSA A23.3 standard, (b) verify the applied scaling rules by comparing the results of the tests on the prototype and model walls for application in the shake table tests of reinforced concrete walls, and (c) evaluate the capability of VecTor2 program to reproduce the inelastic response and failure mode observed in the tests for high ductile wall under the large ductility and large plastic deformations.

Chapter 4 presents a description and interpretation of the results from two series of shake table tests carried out in the Structural Engineering Laboratory of École Polytechnique, Montréal on 8-storey, 9 m high reinforced concrete shear wall models designed according to NBCC 2005 and CSA-A23.3-04. The objectives were to investigate the higher mode effects on reinforced concrete walls such as the damage, force demand and inelastic deformation response under Eastern North America (ENA) earthquake ground motions. Two identical wall models W1 and W2 were constructed. Wall W2 was to be used as backup in case of unexpected problems during the tests on Wall W1. No such problem occurred and Wall W1 was tested under the same ground motion but with stepwise incremented amplitudes starting at 40% of the design level earthquake. Wall W2 was tested directly under the 100% design level earthquake. In these tests, a Moderately ductile wall category was selected rather than the Ductile wall category considered in the tests described in Chapter 3, because minimum reinforcement requirements would have governed the design of the test specimens had the Ductile wall category been adopted.

The Moderately ductile wall category is also the one preferred by design engineers in eastern Canada.

Chapter 5 presents a study of the ability of different RC constitutive models to reproduce numerically the test results obtained from the shake table tests on the 8-storey RC walls described in Chapter 4. Numerical modeling is carried out using the finite element (VecTor2) and the fibre element (OpenSees) methods. The objectives were to evaluate the test results and the capability of different modeling techniques for nonlinear seismic time history analyses of reinforced concrete members. Based on experimental and numerical results, this chapter also proposes design guidelines and recommendations that consider higher mode effects on slender reinforced concrete walls.

The last Chapter of the thesis, **Chapter 6,** presents a general discussion of the results obtained from the tests and analyses with respect to the problems and observations discussed in the literature review.

In the course of the project, four additional technical publications on specific aspects of the work have been prepared and presented at national and international conferences. These papers are presented in the following Appendices of the thesis:

Appendix I: The objective was to investigate numerically the higher mode effects on RC walls under ENA earthquake ground motions using the different constitutive models. (Lumped Plastic Hinge, Fiber Element and Finite Element)

Ghorbanirenani, I., Tremblay, R., Léger, P., and Palermo, D. 2008. "Inelastic Seismic Evaluation of Slender Shear Walls Designed According to CSA-A23.3-04 and NBCC 2005" *Proc. Canadian Society of Civil Engineering (CSCE) 2008 Annual Conference*, Quebec, QC, Paper No. 520.

Appendix II: The objective was to numerically investigate the dynamic responses of RC walls with different geometries and designs to find the appropriate model to better observe the higher mode effects in shake table tests considering existing laboratory constraints.

Tremblay, R., Ghorbanirenani, I., Velev, N., Léger, P., Leclerc, M., Koboevic, S., Bouaanani, N., Galal, K., and Palermo, D. 2008. "Seismic Response of Multi-Storey Reinforced Concrete Walls Subjected to Eastern North America High Frequency Ground Motions" *Proc. 14th World Conference on Earthquake Engineering*, Beijing, China, Paper No. 05-01-0526.

Appendix III: The objective was to assess and compare the ductility demand in the upper part of a 10-storey RC shear wall building located in Montréal, Canada, and designed according to Canadian codes published in 1975, 1985, 1995 and 2005.

Ghorbanirenani, I., Léger, P., Tremblay, R., and Rallu, A. 2009. "Distribution of Inelastic Demand in Slender R/C Shear Walls Subjected to Eastern North America Ground Motions," *Proc. ATC&SEI Conf.*, Dec 2009, San Francisco, CA., USA.

Appendix IV: The objective of this paper was to present to the seismic engineering community preliminary results of the shake table tests carried out on RC walls under an ENA earthquake ground motion.

Ghorbanirenani, I., Tremblay, R., Léger, P., Leclerc, M., El-Sokkary, H., and Galal, K. 2010. "Shake Table Tests and Repair of Ductile Slender Reinforced Concrete Shear Walls subjected to ENA ground motions," *Proc. 9th US National and 10th Canadian Conference on Earthquake Engineering*, July 2010, Toronto, Canada, Paper No. 594.

CHAPTER 3

MODELING AND TESTING INFLUENCE OF SCALING EFFECTS ON THE INELASTIC RESPONSE OF SHEAR WALLS

3.1 Abstract

Monotonic and cyclic quasi-static testing was performed on ductile reinforced concrete shear wall specimens designed and detailed according to the seismic provisions of NBCC 2005 and CSA-A23.3-04 standard. The tests were carried out on full-scale and 1:2.37 reduced scale wall specimens. The behaviour under cyclic loading was characterized by ductile flexural response up to a displacement ductility of 4.0. At this deformation level, inelastic shear deformations in the plastic hinge contributed to approximately 20% of the total deformation. In the subsequent cycles, strength degradation took place due to shear sliding developing along the large flexural cracks at the wall base. Shear sliding was not observed under monotonic loading and the specimens exhibited significantly higher ductility capacity. Excellent agreement was found between prototype and reduced scale walls. The inelastic response and failure mode observed under cyclic loading could be adequately reproduced using the VecTor2 finite element analysis program. Simpler models with frame elements and lumped plastic hinges could capture well the wall flexural response but shear deformations could not be reproduced.

3.2 Introduction

In the 2005 National Building Code of Canada (NBCC) and the CSA-A23.3-04 standard, ductile cantilever reinforced concrete walls must satisfy stringent design and detailing requirements such that they are capable of developing ductile flexural plastic hinging at their bases without significant shear distress or without failure modes causing rapid strength deterioration under cyclic inelastic loading (Adebar et al. 2005). Following capacity design principles, the design shear forces are those corresponding to the attainment of the probable flexural capacity at the wall base (Paulay and Priestley 1992, CAC 2006). Nonlinear time history dynamic analyses of shear walls subjected to earthquake ground motions have shown that shear forces in excess of these capacity design values can develop due to the contribution of the higher modes of vibration to dynamic response (Filiatrault et al. 1994, Amaris 2002, Panneton et al. 2006). Such higher shear forces can cause brittle shear or sliding failure modes to occur. Walls in these nonlinear dynamic analyses were modeled using elastic frame elements with hysteretic plastic hinges concentrated at their ends. Effects of shear sliding deformations along flexural cracks and shear stiffness degradation due to diagonal cracking were however omitted (Cheng et al. 1993, Thomsen and Wallace 2004).

D'Ambrisi and Fillipou 1999 proposed a computationally effective macroscopic member that includes elastic, spread plastic, interface bond-slip, and shear sub-elements connected in series. Nonlinear shear elements have also been used in combination with fibre discretization of wall cross sections to better capture the distribution of normal stresses while including shear deformation effects on the response (Petrangeli et al. 1999, Petrangeli 1999). Proper coupling between nonlinear flexural and shear responses however requires the use of realistic material

constitutive laws in a finite element (FE) formulation. For instance, the compatibility, equilibrium, and constitutive relations of the Modified Compression Field theory (MCFT) (Vecchio and Collins 1986) and Disturbed Stress Field Model (DSFM) (Vecchio 2000) have been implemented in the two-dimensional FE analysis program VecTor2 (VT2) (Wong and Vecchio 2002) . Palermo and Vecchio 2003, 2004 extended the capability of this numerical tool to cyclic loading applications. Palermo and Vecchio 2007 showed that this methodology could lead to quick and reliable results for various wall designs and geometries using simple low-order rectangular elements with smeared material properties. The ability of FE procedures to adequately reproduce the nonlinear dynamic response of shear walls must be verified through shake table benchmark tests (Orbovic et al. 2004). Due to physical limitations of test facilities, these tests must be conducted on reduced scaled models and care must be exercised in selecting model materials and fabrication processes so that the applicable similitude requirements are satisfied and the experiment is representative of actual wall response. Wallace and Krawinkler (Wallace and Krawinkler 1985) reported that shear wall overall response could be predicted successfully using reduced scale models. They suggested that deformed bars should be used in models to adequately reproduce bond strength. Moncarz and Krawinkler (Moncarz and Krawinkler 1981) also stressed the importance of properly reproducing the strain hardening behaviour in model reinforcement to adequately capture the strength and the spread of cracking for members failing in a combined flexure and shear mode.

This chapter presents a test program performed on ductile reinforced concrete shear walls carrying low axial loads designed and detailed according to NBCC 2005 and CSA-A23.3-04 seismic provisions. Two identical full-scale specimens were built. One wall was tested under monotonic loading. The second one was subjected to quasi-static cyclic loading with stepwise

incremented deformation amplitudes. The tests were repeated on 1:2.37 reduced scale models and the results are compared to those obtained from the full-scale prototype specimens. Finite element analyses of the walls were performed using the VT2 program and the numerical predictions are compared with the test results. Additional analytical results are presented to examine the adequacy of simplified models based on frame elements with concentrated end plastic hinges.

3.3 Research Significance

The walls studied performed as intended under cyclic load up to the ductility of 3.5 assumed in design. Significant shear deformations and coupling between shear and flexural response was observed. Beyond a ductility of 4.0, failure occurred by sliding at the wall base along the flexural cracks that had progressively opened upon cyclic loading, indicating that limited margin exists to accommodate the uncertainty in the demand from ground motions. The test program also showed that the inelastic seismic response of shear walls including shear deformation effects and shear sliding behaviour can be reproduced in reduced scale models for future shake table test programs (Tremblay et al. 2005). The observed behaviour could be satisfactorily predicted using the DSFM (Vecchio 2000) implemented in a finite element code, which was not possible using the lumped plastic hinge beam-column formulation.

3.4 Test Program

3.4.1 Reference building wall

The test specimens were designed to reproduce the loading conditions and construction details of a typical shear wall used in a 10-story residential building located in Vancouver, BC. That reference wall is illustrated in Fig. 3.1a. The wall has length l_w = 7.45 m (24.1 ft) and height h_w = 30 m (98.4 ft). It complies with the special seismic requirements specified in NBCC 2005[1] and the CSA standard A23.3-04 for ductile shear walls, and the seismic loads were determined with ductility and overstrength related force modification factors R_d = 3.5 and R_o = 1.6, respectively. The building has a fundamental period of 1.32 s. The shear and bending moment demand were determined using the response spectrum analysis and the resulting base bending moment to base shear ratio, M_f/V_f, was equal to 15.7 m (51.5 ft) = 0.52 h_w. The shear span to wall length ratio, k = (M_f/V_f)/l_w = 2.11, is close to the 2:1 ratio that distinguishes between shear and moment dominated wall responses, The wall was located on the building perimeter, next to a stairway shaft. The applied gravity loads produced a compressive stress of 1% the nominal concrete compressive strength and were therefore ignored in the test program. The wall was constructed with normal strength concrete having a nominal compressive strength f'_c = 30 MPa (4.35 ksi) and a weldable grade 400 CSA-G30.16 reinforcing steel with nominal f_y = 400 MPa (58.0 ksi) and f_u = 550 MPa (79.8 ksi) was considered in the calculations, as required in CSA-A23.3-04 for systems designed with R_d greater than 2.5. The reinforcement was sized and detailed such that the factored flexural demand to resistance ratio M_f/M_r = 1.00. According to code capacity design procedures, sufficient shear reinforcement was provided to resist the shear force associated to the development of the probable moment resistance of the wall. The solution was a web thickness, b_w

= 200 mm (7.87 in.) with two layers of 15M @ 250 mm (9.84 in.) distributed reinforcement, which resulted in V_f/V_r ratio of 0.55. Capacity design aspects are discussed further in the design of the test specimens.

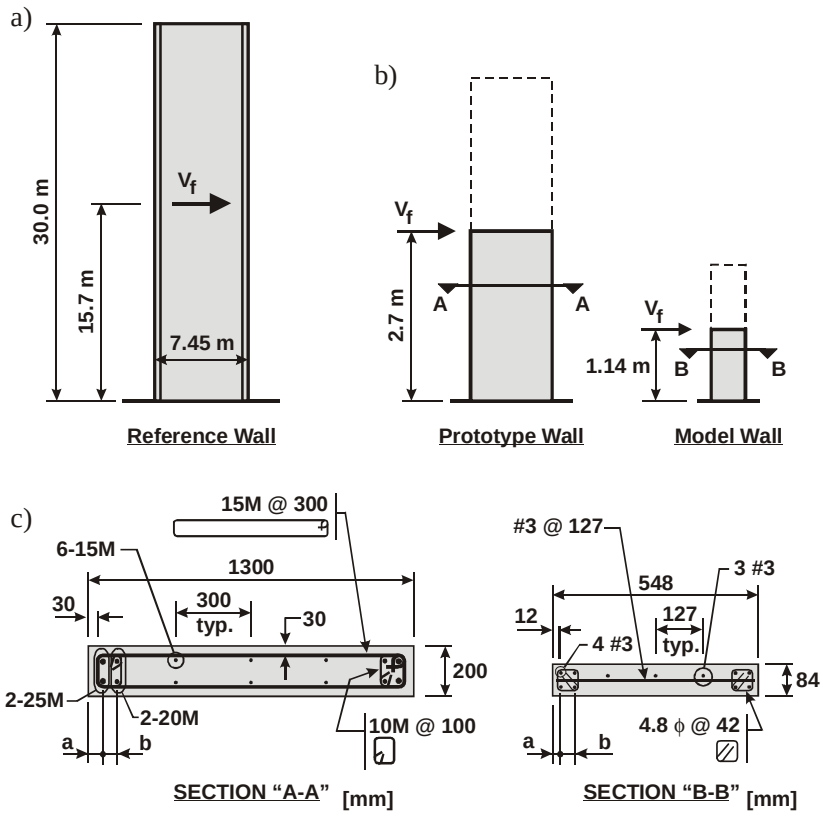

Fig. 3.1: Description of the shear walls studied: a) Reference building wall; b) Schematic elevation of the wall specimens; c) Cross-section of the wall specimens (End A at right, End B at left) (25.4 mm = 1 in. ; 0.305 m = 1 ft).

3.4.2 Design of the test specimens

The test program included a total of four specimens: two prototype specimens (Series A) and two reduced-scale model specimens (Series B). One specimen pair was subjected to monotonic loading (A1M and B1M) while cyclic loading was applied to the other two walls (A2C and B2C). In the tests, the specimens were subjected to a concentrated horizontal load representing the total earthquake load and only the portion of the wall located below the point of application of the resultant seismic load was considered, as shown in Fig. 3.1b. The prototype specimens were designed to reflect the main characteristics of the reference building wall. They were proportioned assuming the same material properties and following an iterative procedure to obtain the same shear span to wall length ratio k as well as the same strength-to-demand M_f/M_r and V_f/V_r ratios. A coarse aggregate size of 14 mm (0.55 in.) was considered for the concrete and a rectangular cross-section was selected for ease of fabrication. To mimic the shear resisting portion of the reference wall, the thickness of the prototype wall was set equal to that of the building wall web and a similar distributed reinforcement layout consisting of two layers of 15M @ 300 mm (11.8 in.) was specified. Several possible wall length and concentrated reinforcing steel arrangements were examined. A 1.3 m (4.26 ft) long x 2.7 m (8.85 ft) tall prototype wall was finally chosen (Fig. 3.1b) with V_f = 317 kN (71.3 kip) and M_f = 856 kN-m (631 kip-ft), which resulted in k = 2.08, M_f/M_r = 1.00, and V_f/V_r = 0.55. The cross-section of the prototype and model specimens is shown in Fig. 3.1c. The concentrated longitudinal steel was made of 20M and 25M bars enclosed by 10M closed stirrups. Dimensions a and b in Figs. 3.1c and 1d are given in Table 3.1.

Table 3.1: Date of testing and position of the concentrated longitudinal reinforcing steel.

Wall No.	Date of test (2006)	Nominal values		Measured values			
				End A(1)		End B(1)	
		a (mm)	*b* (mm)	*a* (mm)	*b* (mm)	*a* (mm)	*b* (mm)
A1M	May 7	56	95	90	75	55	64
A2C	Oct. 8	56	95	100	75	85	70
B1M	July 9	24	35	55	35	35	35
B2C	Sept. 15	24	35	30	35	53	35

(1) End A is under tension under positive storey shear (Fig. 3.1c).
Note: 25.4 mm = 1 in.

In CSA-A23.3, ductile shear walls must have a factored shear resistance, V_r, sufficient to resist the horizontal shear force, V'_f, that will develop when the wall reaches its probable moment resistance, M_p. The moment M_p is determined with resistance factors equal to 1.0 and assuming 1.25 f_y for the steel yield strength to account for strain hardening. For the prototype wall, M_p = 1258 kN-m (928 kip-ft) = 1.47 M_f, and the shear force, V'_f = 1.47 x 317 = 466 kN (105 kip). The resistance V_r is determined according to the general method proposed in CSA-A23.3, including the limitations to the shear resistance provided by the concrete in plastic hinging regions. These limits depend on the anticipated inelastic rotation demand on the wall, $\theta_{id} = \Delta_f (R_o R_d - \gamma_w)/(h_w - l_w/2)$, where Δ_f is the wall top deflection under the load V_f and γ_w is the wall overstrength factor, $\gamma_w = M_n/M_f$, with M_n being the wall nominal moment resistance obtained with resistance factor equal to 1.0. For the prototype wall, Δ_f = 3.15 mm (0.12 in.), M_n = 1036 kN-m (764 kip-ft), γ_w = 1.21, and θ_{id} = 0.0067, which led to V_r = 581 kN (131 kip), greater than V'_f = 466 kN (105 kip). These parameters are summarized in Table 3.2. The unfactored shear resistance, V_n, normalized with respect to the wall gross area ($b_w l_w$) is also given in Table 3.2 for reference. When comparing CSA-A23.3-04 and ACI-318-08 seismic design requirements, the main differences are the resistance factors and the spacing of the confinement reinforcement in the boundary zones.

For shear, CSA-A23.3 uses different ϕ factors for concrete (ϕ_c = 0.65) and steel (ϕ_s = 0.85) whereas ACI 318 uses only one ϕ factor (ϕ = 0.6) that applies to the nominal shear strength. For the prototype wall, the ACI 318 factored shear resistance is 3% less than the CSA value. Maximum spacing between confinement bars are 0.5 b_w and 0.33 b_w in CSA and ACI codes, respectively.

Table 3.2: Wall properties based on nominal and as-built specimen properties.

Parameter	Nominal properties		As-built test specimens			
	Prototype	Model	A1M	A2C	B1M	B2C
M_f (kN-m)	856	66.8	897	880	67.2	68.7
V_f (kN)	317	58.6	332.1	325.9	59.0	60.2
M_f/M_r	1.00	1.00	1.00	1.00	1.00	1.00
k	2.08	2.08	2.08	2.08	2.08	2.08
$\gamma_w = M_n/M_f$	1.21	1.21	1.21	1.21	1.21	1.21
$\gamma_p = M_p/M_f$	1.47	1.47	1.47	1.47	1.47	1.47
Δ_f (mm)	3.15	1.39	3.40	3.34	1.29	1.31
θ_{id} (rad)	0.0068	0.0071	0.0073	0.0072	0.0065	0.0067
θ_{ic} (rad)	0.0099	0.0093	0.0095	0.0084	0.0099	0.0083
V'_f	466	86.14	488.20	479	86.73	88.50
V_r (kN)	581	105	633	634	119	118
V_f/V_r	0.55	0.56	0.52	0.51	0.50	0.51
V_n (kN)	724	130	780	783	149	148
$V_n/b_w l_w$ (MPa)	2.78	2.82	3.00	3.01	3.24	3.21
$V_{r,sf}$ (kN)	554	98	606	606	108	108
$V_{n,sf}/b_w l_w$ (MPa)	3.28	3.29	3.59	3.59	3.61	3.61

Note: 1 kN = 225 lb; 25.4 mm = 1 in.; 1 MPa = 145 psi; 1 kN-m = 738 lb-ft

In design, the factored resistance by cohesion and friction against potential horizontal sliding of the wall base, $V_{r,sf}$, must also be checked against V'_f. That resistance was determined for the monolithically placed concrete condition, which corresponds to the fabrication process adopted in this experimental program. A cohesion stress of 1.0 MPa (145 psi) and a friction coefficient of 1.40 were used as specified in CSA-A23.3-04, which gives $V_{r,sf}$ = 554 kN (126 kip) when considering only the distributed vertical shear reinforcement and the area of the cross-section

resisting shear. This exceeds the maximum anticipated shear force V'_f. The unfactored resistance, $V_{n,sf}$, as normalized with respect to the wall cross section is given in Table 3.2. As a final step in design, the anticipated inelastic rotation, θ_{id}, was compared to the wall plastic rotation capacity prescribed in CSA-A23.3-04, θ_{ic}. The latter is given in Table 3.2 and the prototype wall specimens were deemed to possess adequate inelastic rotation capacity.

For the model specimens, the potential for distortions between full-scale and model material properties was minimized by selecting regular deformed bars for the main reinforcement and avoiding micro-concrete mixes. A geometric scaling factor of 2.37 was selected, as governed by the minimum available deformed bar size (No. 3) and concrete coarse aggregate size (5 mm = 0.20 in.). The model wall dimensions and reinforcement steel are illustrated in Figs. 3.1b and 1c. ASTM A706 grade 60 ksi (413 MPa) No. 3 bars (A_s = 71 mm^2 = 0.11 in^2, f_y = 413 MPa = 60 ksi, f_u = 552 MPa = 80 ksi) were selected for both the longitudinal and transverse reinforcement steels. Cold rolled plain bars 4.76 mm (0.18 in.) in diameter and made of SAE 1018-1020 steel (f_y = 220 MPa = 32 ksi, f_u = 400 MPa = 58 ksi) were used for the confinement reinforcement. These material properties met the similitude requirements between the prototype and model walls in terms of dimensions, steel reinforcement ratios, and aggregate sizes. However, due to physical constraints, the position of the concentrated longitudinal reinforcement (dimensions *a* and *b* in Table 3.1) could not be adjusted to exactly match the scaling factor. This and the differences in mechanical properties between ASTM A706 and CSA-G30.16 reinforcing steels induced small deviations between the model and prototype specimens. Design forces and resistances based on the model nominal properties are summarized in Table 3.2. As shown, the model values for the *k* factor and the M_f/M_r and V_f/V_r ratios are equal or very close to the prototype wall values. The

model specimens also had sufficient resistance in shear and shear friction to resist the anticipated shear force corresponding to the attainment of M_p at the wall base, and their plastic rotation capacity exceeded the anticipated rotation demand.

3.4.3 Predicted response with nominal properties

Prior to testing, analysis of the prototype and model specimens was carried out under monotonic and cyclic loading to verify the design assumptions. The Response 2000 (Bentz 2001) (R2000) non-linear plane sectional analysis program based on the MCFT (Vecchio and Collins 1986) was used for the monotonic member response. For the steel reinforcement, the following additional properties were used: modulus of elasticity, E = 200000 MPa (30000 ksi), deformation at initiation of strain hardening, ε_{sh} = 0.015, and ultimate deformation, ε_{su} = 0.13 and 0.12 for G30.16 and ASTM A706 steels, respectively. For the concrete, the Popovic-Thorenfeldt-Collins base curve with f'_c = 30 MPa (4.35 ksi) and tensile strength, f_t = 1.75 MPa (254 psi) was adopted. Compression softening according to Vecchio and Collins 1986 was also considered together with the tension stiffening model by Bentz 1999. A tension stiffening factor of 0.3 was used to reduce tension stiffening effects to predict the envelope under cyclic loading. The load - top lateral deformation responses of the prototype and model specimens are shown in Fig. 3.2a. The loads are normalized with respect to the wall cross-section areas and the deformations are normalized to the wall heights. The response is very similar for both specimen sizes, the small differences being attributed to the deviations from exact similitude requirements for the steel yield strength and location of the concentrated longitudinal bars. The program predicts failure by crushing of the concrete at the wall bases, with peak resistances attained at a top lateral deformation of 0.019

h_w and 0.018 h_w for the prototype and model specimens, respectively. These deformations approximately correspond to a displacement ductility of 4.5.

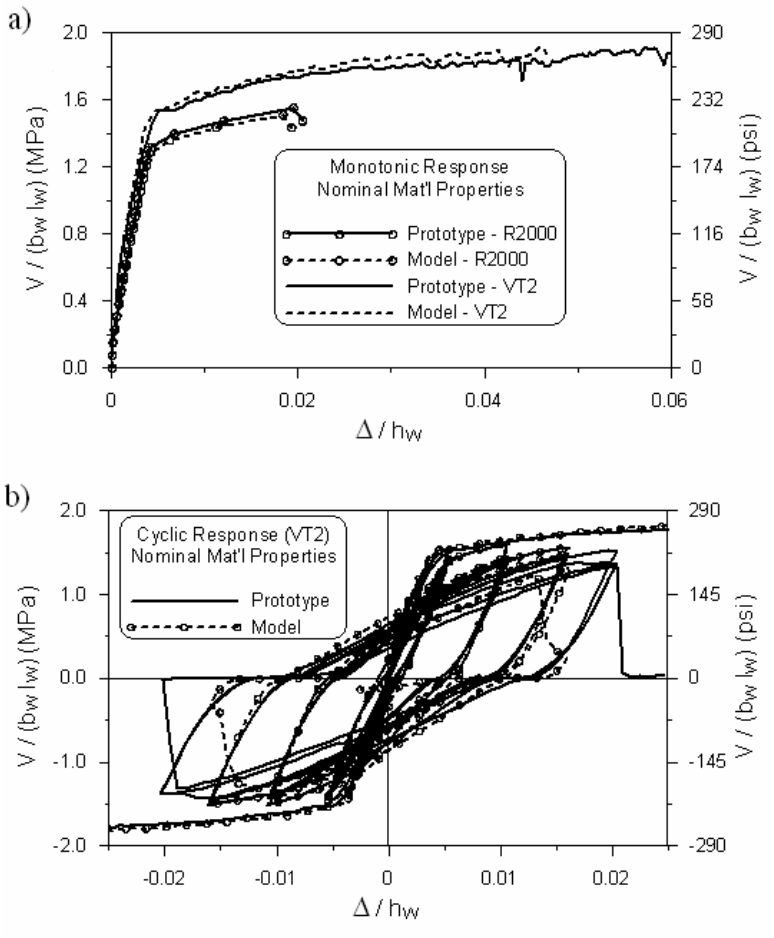

Fig. 3.2: Predicted specimen responses with nominal properties: a) Monotonic responses from R2000 and VT2 analyses; b) Monotonic and cyclic responses from VT2 analyses.

The VT2 program (Wong and Vecchio 2002) is based on the MCFT (Vecchio and Collins 1986) and the DSFM (Vecchio 2000) for the nonlinear finite element analysis of reinforced concrete membrane structures. The program was used to predict the behaviour of both specimens under monotonic and cyclic loadings. Plane stress rectangular elements with smeared reinforcement were used to discretize the wall, with a total of 16 elements in the shortest direction, as recommended by Palermo and Vecchio 2007. Convergence analysis confirmed the

appropriateness of the number of elements. Basic properties for the steel and concrete materials were the same as those specified in the R2000 analyses. The hysteretic model of the reinforcement was according to the Seckin model (Bauschinger). Reinforcement dowel action at the wall base was reproduced using the Tassios model based on a beam on an elastic concrete foundation theory (He and Kwan 2001). The dowel force varies as a function of shear slip and steel rebar properties. The pre-peak compression response of the concrete was based on the Popovics curve for normal strength concrete whereas the post-peak response followed the base curve. Tension stiffening effects according to Bentz 1999 were automatically accounted for in the analysis, depending on the average concrete principal tensile strain. Concrete strength enhancement due to confinement was considered within the regions of concentrated reinforcement. The Kupfer/Richart model appropriate for cyclic loading was used for that purpose (Wong and Vecchio 2002). In this model, the uniaxial compressive strength, f'_c, and the corresponding strain, ε_0, are both amplified by a concrete confinement factor that varies during the analysis depending on the principal stress state. The hysteretic response of the concrete was set according to Palermo and Vecchio 2002 (with decay), and the slip distortion was taken into account according to the Vecchio-Lai model (Vecchio and Lai 2004). As shown in Fig. 3.2a, the VT2 program predicts a larger capacity and significantly higher ductility for both specimens under monotonic loading when compared to the R2000 results. Both specimens reached a peak average shear stress of 1.9 MPa (275 psi), still well below the nominal unit shear resistance of the specimens, $v_n = V_n/b_w l_w$ = 2.8 MPa (406 psi) (see Table 3.2). The VT2 analyses predicted failure in flexure at drift ratios of 0.058 and 0.047 for the prototype and model specimens, respectively, corresponding to ductility levels of 11 and 8. The better performance predicted by the VT2 FE

analyses is mainly attributed to the fact that concrete confinement effects are implicitly considered, which is not the case for R2000.

Figure 3.2b shows the VT2 response of both walls under imposed cyclic top lateral displacement with stepwise incremented amplitudes. The VT2 monotonic response is reproduced in the first and third quadrants of the plot for comparison purposes. Up to a drift of 0.015 h_w, excellent match is found between the prototype and wall models, confirming the validity of the scaling assumptions adopted in the design of the specimens. The peak resistance developed by the cyclic specimens matched the monotonic response up to 0.01 h_w drifts on the positive side and 0.005 h_w in the other direction. Beyond these deformations, the resistance of both walls progressively decrease until a sudden and complete drop in strength occurs at $\Delta = 0.02\ h_w$ for the prototype wall and at $\Delta = 0.015\ h_w$ for the model wall, revealing much lower deformation capacities than that anticipated from monotonic response. Under cyclic loading, the longitudinal steel yields at both ends of the wall, resulting in large flexural cracking extending the full length of the wall. This reduces the ability of the concrete in the compression zone to resist the shear at the base of the wall leading to large shear sliding displacements. Under monotonic loading, this mechanism is delayed as cracking occurs from one direction only. Sliding occurs when the base flexural crack extends the full length of the wall.

3.4.4 Test setup and as-built specimen properties

Figure 3.3 shows the test setup used in the experimental program. All specimens included the test wall portion and a strong foundation block used to reproduce realistic base conditions. The specimens were mounted horizontally on the strong floor of the laboratory and the load was

applied by a high performance 1500 kN (337 kip) actuator with pinned end connections. The foundation blocks were firmly attached to steel framing members by means of pre-tensioned steel tie rods. The wall specimens were supported on rollers to prevent out-of-plane deformations. At a ductility of 4.0 for the prototype wall, the rotation of the actuator due to the lateral deformation reached 0.007 rad. This resulted in an axial load of 2.9 kN (0.65 kip) in the wall, which was considered as negligible. To avoid stress concentrations in the concrete components, flexible wooden pads were inserted between the steel plates attaching the test walls to the actuator and those attaching the foundations to the framing members. The foundation blocks were purposely designed significantly thicker than the test walls to limit cracking in the foundations.

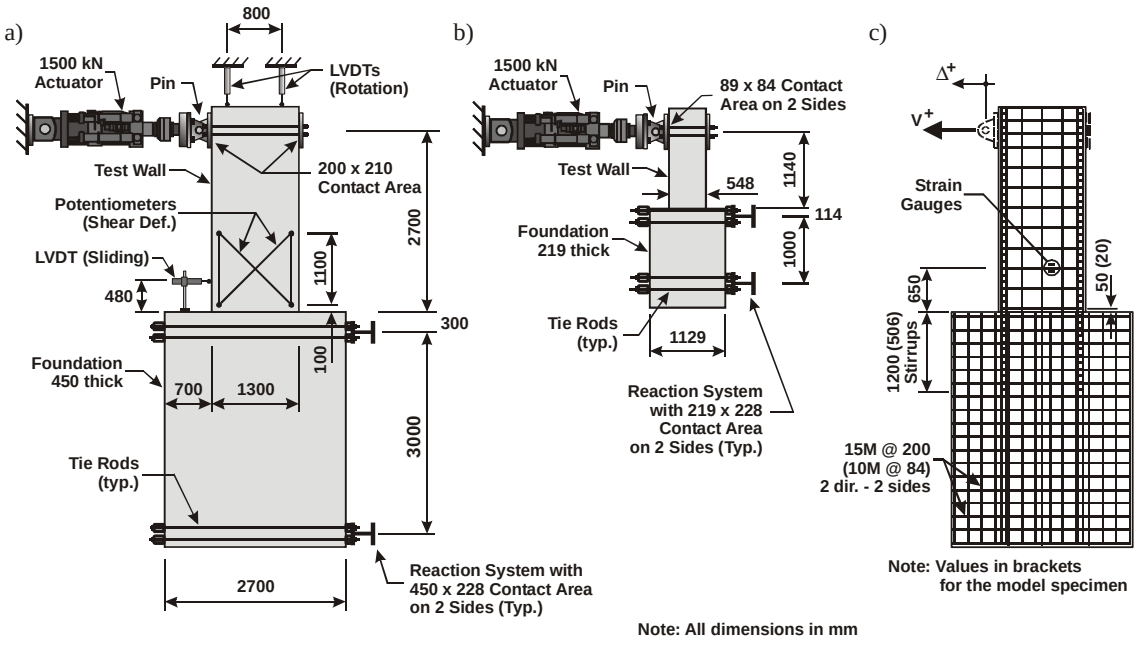

Fig. 3.3: Test set-up: a) Prototype wall; b) Model wall; c) Reinforcement lay-out for both specimen sizes. (Note: All dimensions in mm; 25.4 mm = 1 in.).

All specimens were poured in the horizontal position and super-plasticizer was used in both concrete mixes to ease concrete placement. The wall and foundation portions were cast

continuously without cold joints. The concrete of the prototype wall was supplied by a local supplier with a specified f'_c = 30 MPa (4.35 ksi), no added air, and 14 mm (0.55 in) traprock coarse aggregate. For the model, an in-house mix was prepared with Type GU cement (ASTM C 150, Type I), W/C = 0.55, 4-6 mm (0.16-0.24 in.) syenite type coarse-grained aggregate with 83% passing 5 mm (0.20 in.) sieve. The concrete used for the prototype walls was also used for the foundation of the two model specimens up to approximately 300 mm (11.8 in.) below the wall base. Pouring was performed on March 24, 2006 and the tests were performed between May 7th and October 8th of the same year. Testing dates are given in Table 3.1. Measured concrete strength values at 28 days are given in Table 3.3 and results of the tensile tests on the reinforcing steel are presented in Table 3.4. The range of measured values and the average value are given for each group of steel bars. During the specimen fabrication, it was difficult to properly place the concentrated reinforcement at the required position and maintain exactly that position during concreting. The measured as-built dimensions *a* and *b*, as defined in Fig. 3.1c, are given in Table 3.1 for each end of each specimen. The factored moment resistance, M_r, of each wall was determined using the measured material properties, and the equivalent design actions M_f and V_f could be determined assuming the M_f/M_r and k ratios obtained with the nominal specimen properties. The various design and resistance parameters for each wall were then computed and are given in Table 3.2.

Table 3.3: Measured concrete properties.

Wall	f'_c (MPa)	E_c (MPa)	ε_0	ν_c
Prototype	28.3	29140	0.00203	0.223
Model	47.0	32770	0.00260	0.236

Note: 1 MPa = 145 psi

Table 3.4: Measured reinforcing steel strength properties (average values in brackets).

Wall	Location	Size	f_y (MPa)	f_u (MPa)	ε_{sh}	ε_u
Prototype	Longitudinal	25M	429-443 (437)	621-636 (626)	0.010	0.146
	Longitudinal	20M	410-419 (412)	575-581 (579)	0.022	0.170
	Longitudinal	15M	440-456 (448)	662-685 (675)	-	-
	Horizontal	15M	449-458 (452)	667-680 (671)	-	-
Model	Longitudinal	#3	437-460 (450)	593-602 (597)	0.018	0.170
	Horizontal	#3	438-460 (450)	588-601 (594)	-	-

Note: 1 MPa = 145 psi

3.4.5 Test procedure

All tests were conducted by controlling the horizontal top displacement imposed by the actuator. Movements of the foundation blocks and actuator reaction system were monitored and removed to obtain the wall deformations relative to the foundation. The positive direction for loads and displacements is shown in Fig. 3.3c. In the monotonic tests, the lateral displacement was imposed at a constant rate of 1.0 mm/min (0.04 in/min). The tests were however interrupted to allow for observation of damage and photos to be taken. In the cyclic tests, a displacement controlled loading history based on the ATC-24 protocol (ATC 1992) was adopted: 3 cycles at 0.33 Δ_y, 0.66 Δ_y, 1.0 Δ_y, 2.0 Δ_y, and 3.0 Δ_y, followed by 2 cycles at 4.0 Δ_y, 2 cycles at $\Delta = 0.03\ h_w$, and 2 cycles at $\Delta = 0.04\ h_w$. The value of the top lateral displacement at yield, Δ_y, was set equal to 1.33 the deflection at first yield, the latter being taken equal to the lateral top displacement from the load-deformation curve from monotonic test at a moment equal to 75% of the yield lateral load, V_y, in accordance with the recommendation of ATC-24. The force V_y was set equal to the ordinates of the intersecting point between straight lines representing initial elastic response and average post-yield inelastic response up to the code limit drift angle of 0.025 rad. The Δ_y values for the prototype and model walls were respectively equal to 15.0 mm (0.59 in.) and 4.2 mm (0.16 in.).

The ratio between these two values (3.57) exceeded the geometric scaling factor and it was decided to use Δ_y = 15.0/2.37 = 6.33 mm (0.25 in.) to establish the cyclic displacement history for the model specimen.

3.5 Test Results

3.5.1 Response under monotonic and cyclic loading

Figure 3.4a shows the normalized lateral load-lateral deformation response under monotonic loading for specimens A1M and B1M, respectively. The response of both specimens is nearly identical up to Δ/h_w = 0.0348, where failure in tension of one the longitudinal bars occurred in the model wall, resulting in a reduced resistance at larger deformations. Inspection after testing revealed that this bar had been damaged during the installation of the instrumentation. For both specimens, the test was halted due to limitation of the loading apparatus, before failure of the specimens. The good match between the responses of the two specimens up to code allowed deformation (0.025 h_w) confirms that similitude rules apply well to reinforced concrete walls subjected to monotonic loading. The higher concrete strength in the model wall resulted in a greater wall stiffness prior to yielding but had a small influence on the inelastic wall response which is essentially governed by the reinforcing steel. Both specimens could exhibit ductility well in excess of plane section analysis predictions neglecting concrete confinement effects.

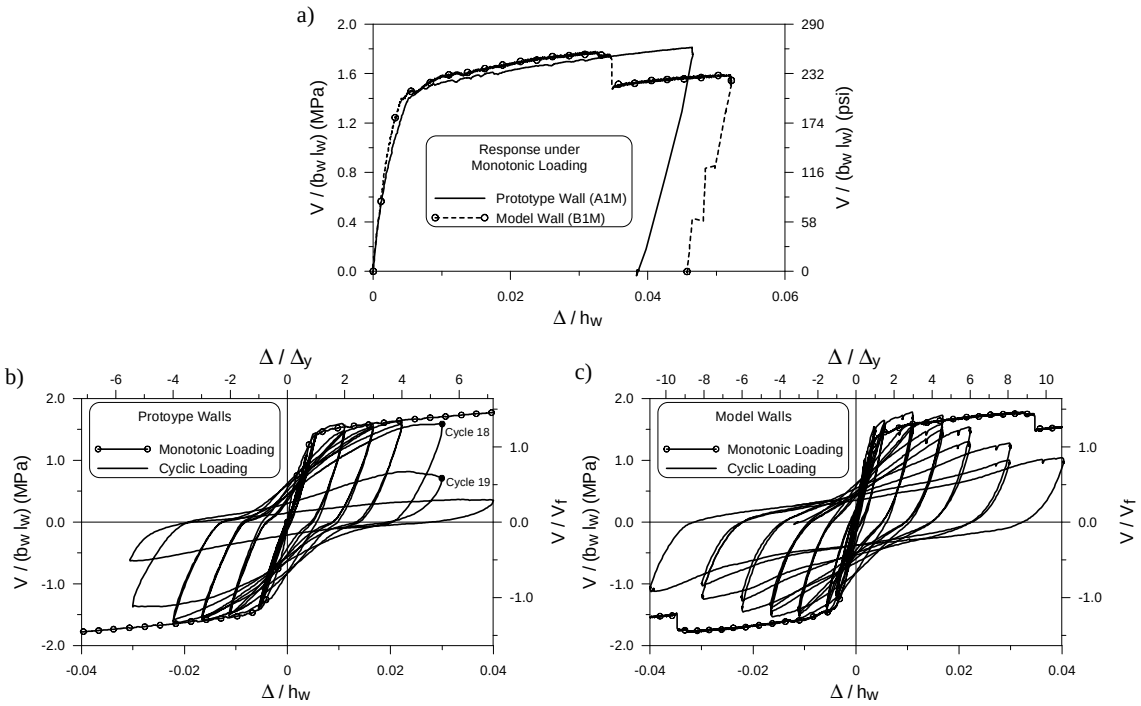

Fig. 3.4: Load-deformation responses from tests: a) Monotonic responses; b) Comparison between monotonic and cyclic responses of the prototype specimens; c) Comparison between monotonic and cyclic responses of the model specimens (1 MPa = 145 psi).

Figures 3.4b and 4c compare the response under cyclic and monotonic loadings for the prototype walls and the model walls, respectively. In these two figures, the monotonic responses have been mirrored in the third quadrant to ease comparisons. The load is divided by the wall cross-section on the left hand side axis and with respect to the design load V_f of the right-hand side axis. The deformations are normalized with respect to the wall height on the bottom axis and are expressed as displacement ductility along the top axis, with Δ_y = 15.0 mm (0.59 in.) and 4.2 mm (0.16 in.) for the prototype and model walls, respectively. Both specimens exhibited stable hysteretic responses matching the monotonic load-deformation curves up to a displacement ductility of approximately 4.0, thus satisfying the ductility capacity implied by the ductility-related factor R_d of 3.5 specified for this shear wall category. In Fig. 3.4c, the difference in strength between monotonic and cyclic responses of the model specimens in the positive direction is due to

differences between the positions of the main longitudinal reinforcement in the two specimens, the lever arm of the steel resisting flexure in the positive direction being longer for the cyclic specimen B2C (dimension *a* at end A, see Table 3.3). At a ductility of 3.5 under cyclic loading, flexural and diagonal shear cracking could be observed in the prototype and model walls, as illustrated for the prototype specimen in Fig. 3.5a. Strength degradation started at a ductility of 4.0 in both specimens. This degradation was associated with evidences of horizontal slippage along the main flexural cracks near the base of the wall, as shown in Fig. 3.5c for the prototype wall. This behaviour was not observed in the monotonic specimens. As shown in Figs. 3.4b and 4c, the strength decrease was steeper for the prototype wall.

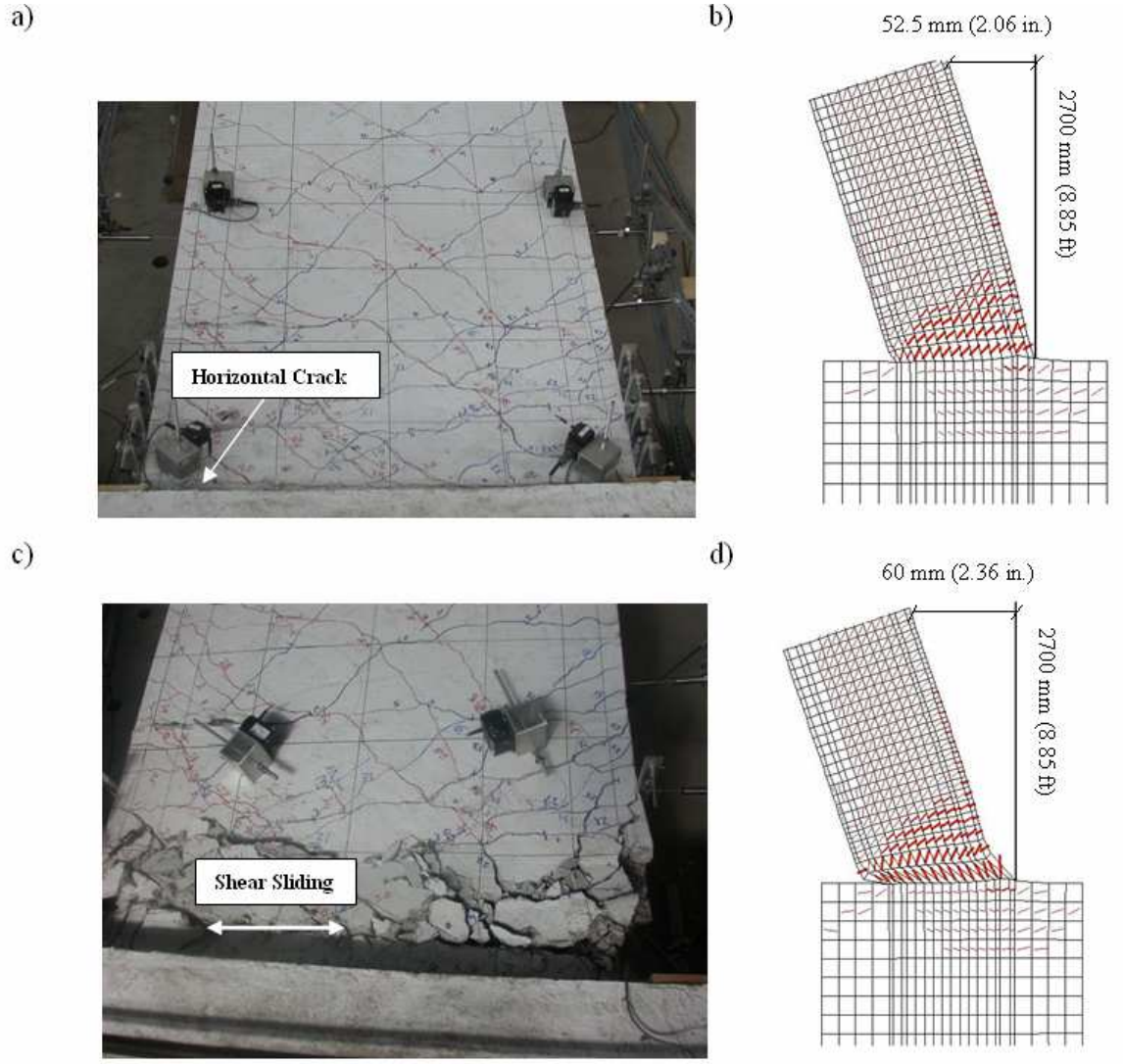

Fig. 3.5: Crack pattern for the cyclic prototype specimen: a) Observed crack pattern at a ductility of 3.5; b) Crack pattern at a ductility of 3.5 from VT2 analysis; c) Observed crack pattern at failure; d) Crack pattern at failure from VT2 analysis.

Figure 3.6a shows the hysteretic relation between the applied base shear and the measured shear deformations in the plastic hinge region, Δ_{shear}, for the prototype specimen under cyclic loading. The deformations were monitored with potentiometers longitudinally and diagonally mounted in the hinge zone of the specimen (Fig. 3.3a). The same shear deformations are plotted against the applied top displacements in Fig. 3.6b. Elastic linear response with limited shear deformations is observed in both figures up to initiation of flexural yielding of the specimen, i.e. for Δ less than

Δ_y in Fig. 3.6b. Beyond that point, a pinched hysteretic shear response progressively developed as diagonal shear cracking formed in the specimen (Fig. 3.6a). Figure 3.6b shows that shear deformations increased nearly linearly with the amplitude of the applied top displacement up to Δ/Δ_y = 4.0. At this ductility, shear deformations corresponded to approximately 20% of the total deformations (0.004 h_w / 0.02 h_w). Beyond that point, most of the applied deformation took place in the form of shear sliding. Similar response was observed for the model wall with shear deformations reaching 21% of the total deformation at ductility of 4.0.

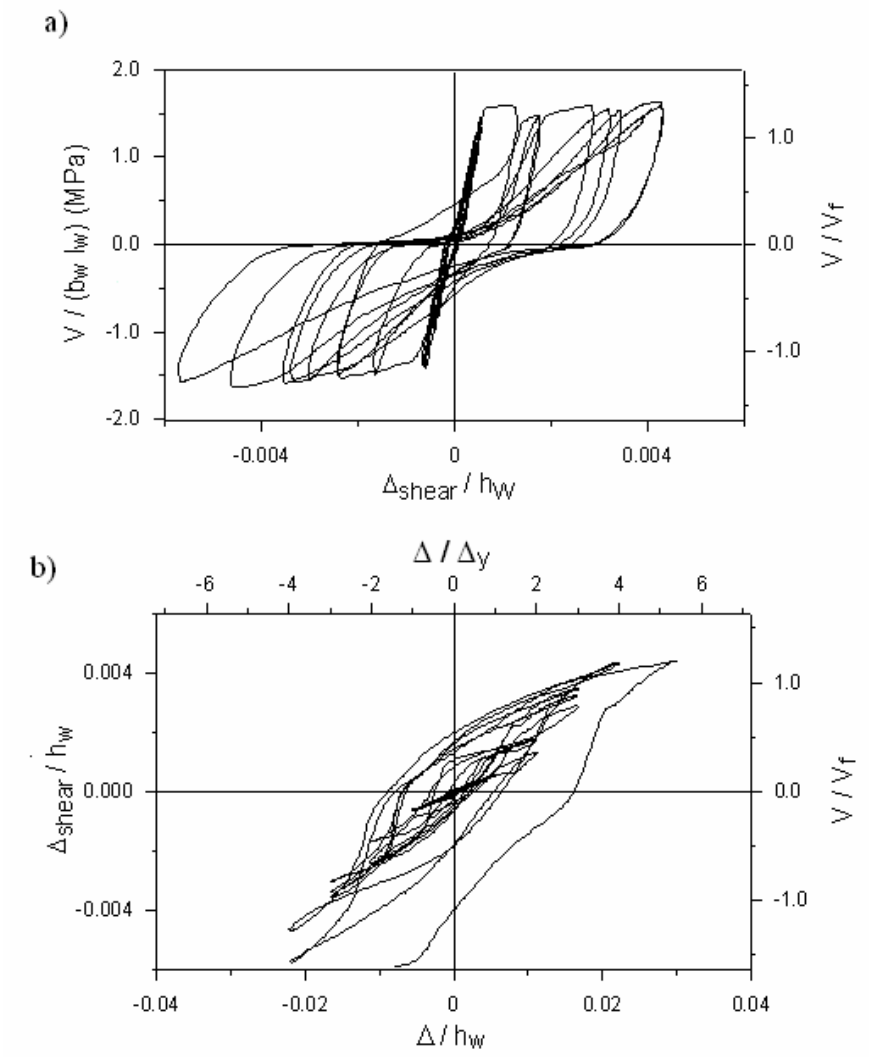

Fig. 3.6: Shear deformations in the prototype specimen under cyclic loading as a function of the: a) Applied lateral load; b) Applied top displacement (1 MPa = 145 psi).

At first attainment of a displacement ductility of 3.5 in the monotonic and cyclic tests, the applied shear forces in the two opposite directions reached between 1.25 and 1.28 V_f, which is less than the value of 1.47 V_f assumed in design, suggesting that strain hardening in the steel reinforcement was less than expected in design. The measured shear stress values at peak loads (approximately 1.6 MPa = 232 psi) were also significantly lower than the shear stresses associated to the unfactored shear resistance V_n (approximately 3.0 MPa = 435 psi, see Table 3.2) or the unfactored interface shear resistance $V_{n,sf}$ (approximately 3.6 MPa = 522 psi, see Table 3.2). In CSA-A23.3-04[2], the $V_{n,sf}$ assumes cohesive resistance from concrete over the full wall cross-section area. This resistance cannot be developed along the cracks at the wall base. In Eurocode 8[31], cohesion is omitted in the calculation of the shear sliding resistance for seismic applications. According to EC8, the unfactored shear sliding resistance is equal to 1.8 MPa (261 psi), which is close to the measured shear stress. In spite of this, significant shear deformations progressively took place in the plastic hinge region upon increasing inelastic rotation and failure occurred by shear sliding along flexural cracks just after reaching the ductility level implied in design. The absence of axial load in the test walls likely represented a critical condition for shear sliding but this condition was accounted for in code design equations for shear friction. The terms accounting for cohesion and friction in these equations may need to be revisited when assessing the capacity of members subjected to severe inelastic cyclic loading.

3.6 Analytical Predictions

Numerical simulations of the specimen's response were performed with the VT2 program using the as-built material and geometrical properties of the specimens. The program was used to predict the specimen response including crack patterns, load-deformation behaviour, shear

sliding, rotation at top, shear deformations, strain in the reinforcement, and hysteretic energy. Additional VT2 analyses were also performed to evaluate the effect of the axial loads on the wall response. The steel and concrete models used in all these analyses are the same as those adopted for the prediction of the wall responses with nominal properties, except that the Modified Park-Kent concrete model with a linearly descending branch was selected for the model walls because it is more appropriate than the base curve for higher strength concrete as measured in the laboratory (f'_c = 47 MPa (6.82 ksi)). In addition, the capability of reproducing the global specimen response with an elastic frame element with lumped plastic hinge model was assessed using the modified Takeda hysteretic hinge model (Otani 1981) in the Ruaumoko computer program (Carr 2004). For the hysteretic model, the envelope was based on the monotonic response from the R2000 program, as would be typically done when adopting a plastic hinge model. The as-built specimen properties were used in this prediction. The "Drain 2D" unloading model was adopted with an unloading stiffness parameter α = 0.15 and a reloading stiffness parameter β = 0.2 from the test data obtained herein. These values fall within the ranges suggested in the Ruaumoko program user's manual and were determined to best fit the test data obtained in this project.

3.6.1 Results

A comparison of the crack patterns observed in the test and predicted by the VT2 program is shown in Fig. 3.5 for the prototype specimen subjected to cyclic loading. At ductility of 3.5 (Figs. 3.5a and 5b), the diagonal and flexural crack patterns are clear in the plastic hinge zone in both the test and the VT2 prediction, with a major flexural crack extending the full width of the wall near the wall base. Figures 3.5c and 5d compare the responses of the specimen at failure.

Significant shear sliding of the specimen along the horizontal crack at the vicinity of the base of the wall can be observed in both figures. Note that the picture in Fig. 3.5c was taken at a top horizontal displacement of 81 mm (3.2 in.) whereas the analysis prediction of Fig. 3.5d is given at a displacement of 60 mm (2.36 in.), which was the deformation at failure in the analysis.

Figures 3.7a and 7b compare the monotonic and cyclic load-deformation responses from experiment and VT2 analysis for the prototype specimen. In the monotonic test, good agreement is found for the initial and post-yield stiffnesses but the VT2 program overestimates the wall strength by approximately 12%. That difference reduces to 4% if tension stiffening effects are deactivated in the analysis, indicating that the tension stiffening model employed possibly led to overstrength under large deformations. Omitting tension stiffening effects however reduced the initial stiffness by 60%, which is unrealistic. For the cyclic results, that are of major significance for future shake table tests, there is an excellent agreement between the test and VT2 prediction up to ductility 4.0. In VT2, shear sliding initiated at a ductility of 4.0 and led to a sudden and nearly complete loss in lateral capacity. The same failure mode was observed in the test but strength degradation started after a ductility of 4.5 and developed more gradually. Up to a ductility of 3.0, the accumulated hysteric energy, E_h, was the same in the test (112.5 kN-m = 83 kip-ft) and VT2 analysis (E_h=112.9 kN-m = 83 kip-ft). Figures 3.7c and 7d show the same comparisons between tests and numerical simulations for the model walls. Similar but smaller discrepancy in peak capacity was observed (8%) for the monotonic loading case. Failure of the tension reinforcement did not occur in the analysis as the observed defect in the rebar had not been replicated in the numerical model. Excellent agreement was obtained for the cyclic response up to a ductility of 6.0. Strength degradation under cyclic loading started after a ductility of 4.5 in both the test and the VT2 simulation. As was the case for the prototype, the VT2 program

predicted the observed failure mode but the strength degradation was more pronounced than in the test.

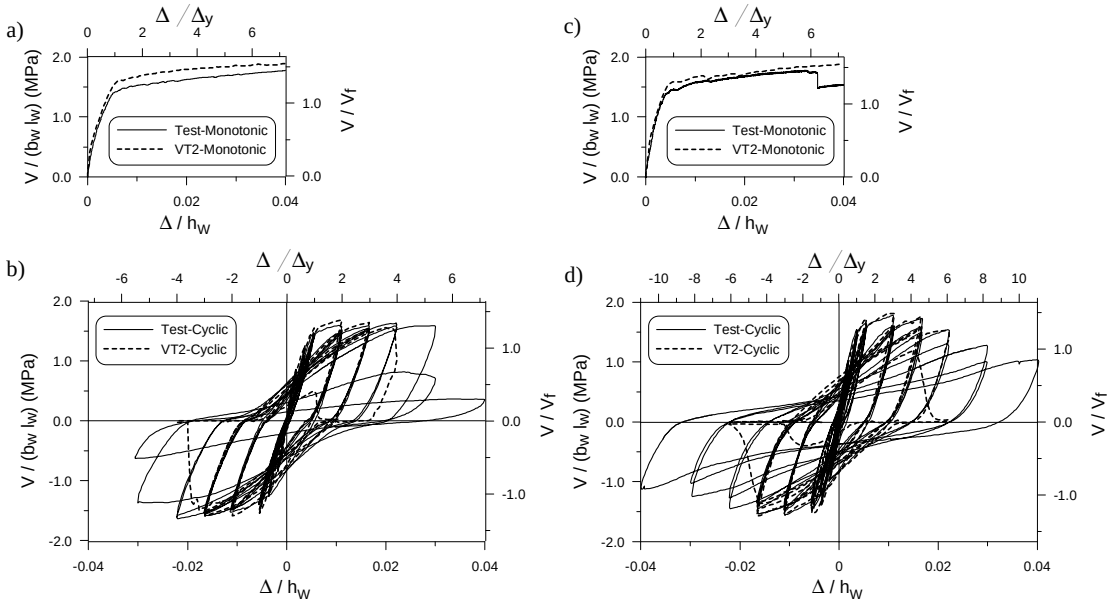

Fig. 3.7: Responses of the specimens from tests and VT2 analysis with the actual material properties: a) Monotonic responses of the prototype specimen; b) Cyclic responses of the prototype specimen; c) Monotonic responses of the model specimen; d) Cyclic responses of the model specimen (1 MPa = 145 psi).

The predicted and measured strains in the horizontal reinforcing steel of the prototype wall are plotted as a function of the normalized base shear in Fig. 3.8. Figure 3.3c shows the location of the strain gages used to collect this data. Excellent match is found between the test and VT2 values for the wall under monotonic loading. The monotonic responses also form the envelope of the cyclic responses. Good match between predicted and measured values was also obtained under cyclic loading. Both the numerical and experimental results show that the shear reinforcement did not yield (strains less than 0.002) up to the ultimate lateral displacements.

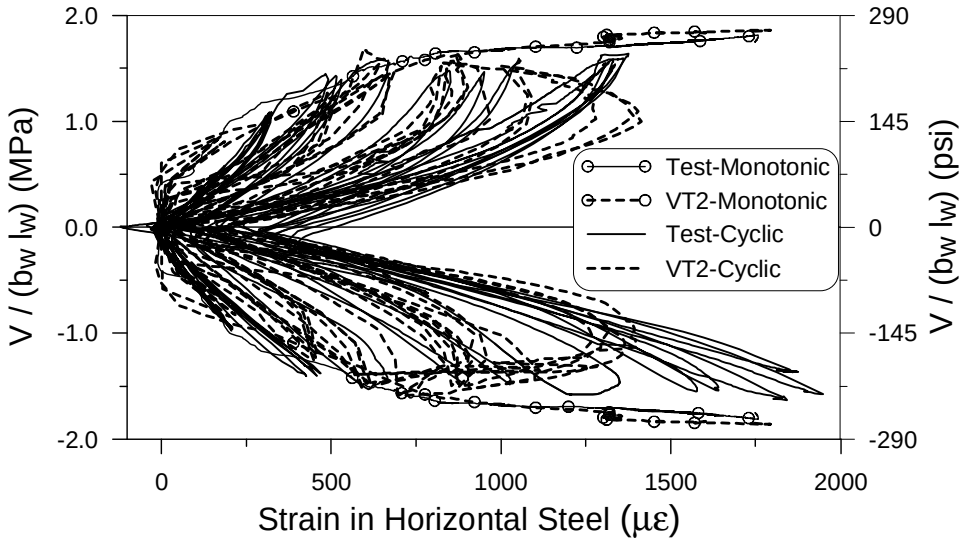

Fig. 3.8: Strain of horizontal steel-shear stress curve for monotonic and cyclic response of the prototype specimens.

Figure 3.9a shows that no sliding occurred for the monotonically loaded prototype specimens (test and VT2). Under cyclic loading, the VT2 program predicted sliding developing rapidly after a ductility of 4.0. In the test, sliding gradually developed at the same displacement ductility in cycles 18 and 19. Strength degradation in the test was also observed in the same cycles (Fig. 3.4b). Good agreement can be observed in Fig. 3.9b between test and VT2 shear strain values under monotonic and cyclic loading up to ductility 3.0. Note that anchorage of the potentiometers was damaged after cycle 18 and the test data shown for cycle 19 may include some error.

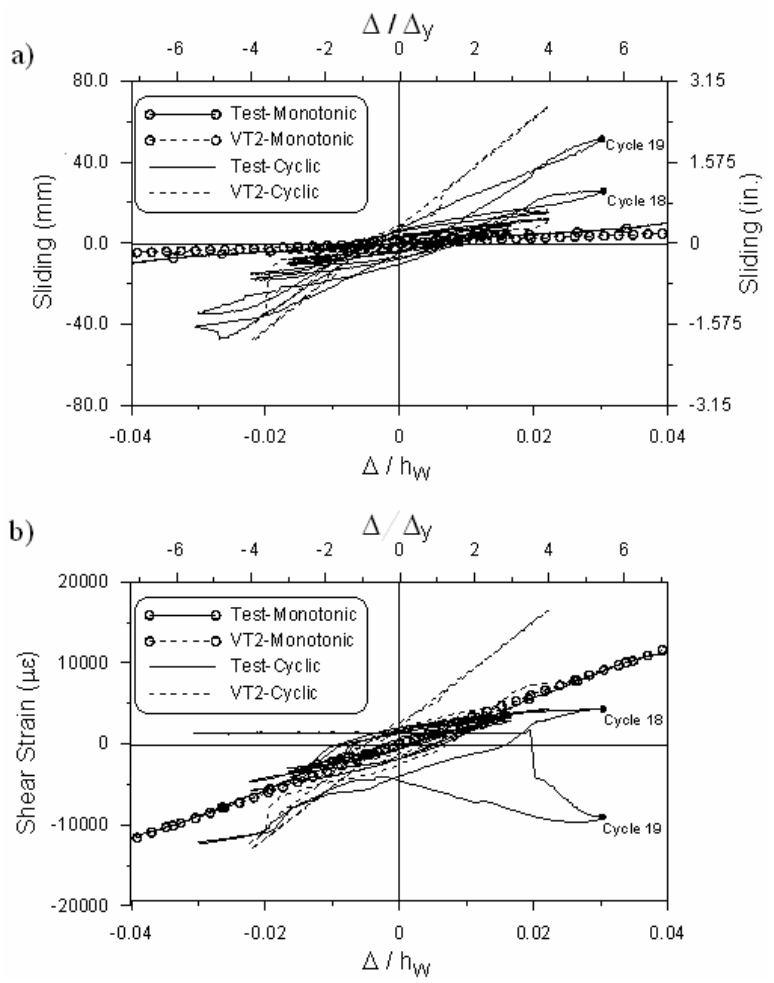

Fig. 3.9: Sliding and shear strain responses from tests and VT2: a) Sliding of monotonic and cyclic responses of the prototype specimens; b) Shear strain of monotonic and cyclic responses of the prototype specimens.

Figure 3.10a shows that the measured monotonic and cyclic load-deformation responses of the prototype wall was well predicted using the modified Takeda model with concentrated plastic hinge in terms of initial stiffness and strength. In the cyclic test, however, the pinching that gradually developed due to shear deformations and the strength degradation resulting from shear sliding could not be reproduced by the frame element with concentrated plastic hinge model. Figure 3.10b shows the cyclic base moment *vs* rotation at wall top response of the prototype wall from the test, the VT2 analysis, and the modified Takeda model. Good match is found between

the three curves up to large rotations (0.02 rad.), indicating that lumped plasticity models can be used to predict the quasi-static cyclic flexural response of shear walls.

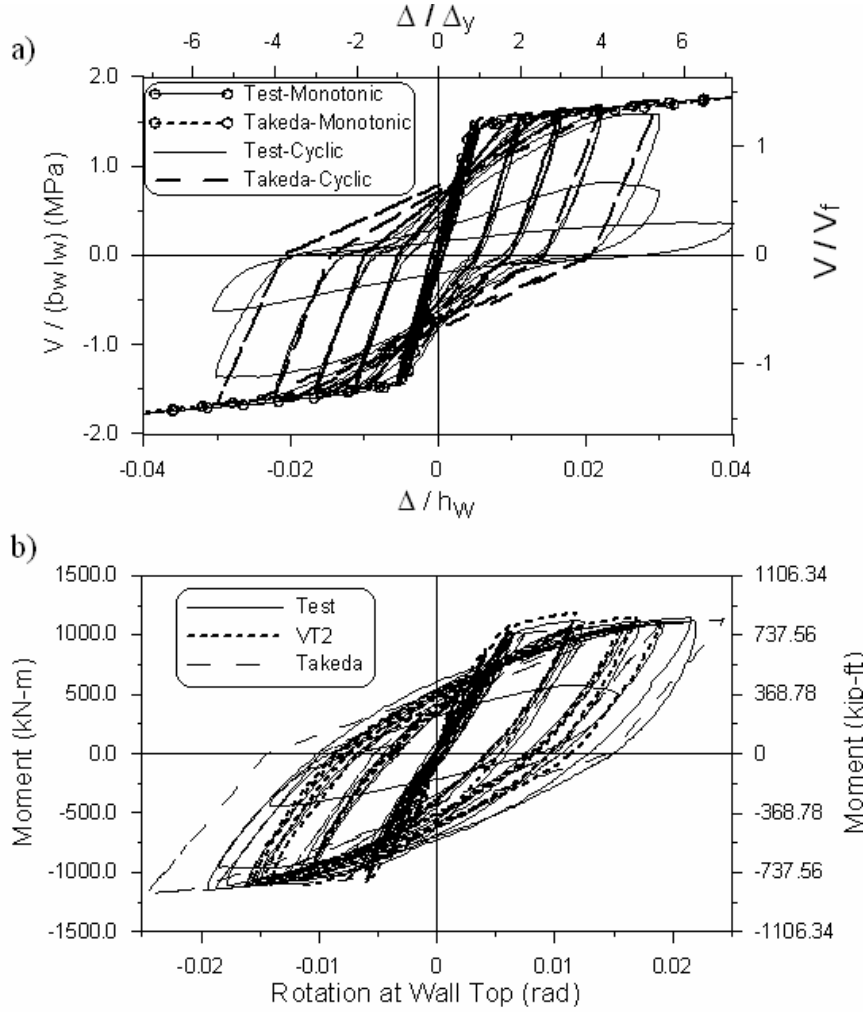

Fig. 3.10: Responses of prototype specimens from tests Takeda model and VT2: a) Load-deformation of monotonic and cyclic responses (1 MPa = 145 psi); b) Moment-rotation of the cyclic response.

The VT2 program was used to examine the influence on the cyclic response of the prototype wall of applying an axial load producing an average compressive stress of 0.10 f'_c. The addition of the axial load had no effect on the pre-cracking wall stiffness but the strength and the cracked stiffness of the specimen were increased by 32%. The lateral deformation at yield remained

unchanged but the accumulated hysteric energy up to ductility 3.0 increased by 13%. Failure by shear sliding occurred immediately after completion of the two cycles at a ductility of 4.0, which represents a marginal improvement compared to the specimen without axial load (sliding initiated in the first cycle at the same ductility).

3.7 Summary and Conclusions

Two identical prototype wall specimens were designed, detailed, and fabricated according to the provisions of NBCC 2005 and the CSA-A23.3-04 standard. The specimens were tested under monotonic and quasi-static cyclic loading, respectively. Two identical 1:2.37 reduced scale models of the prototype walls were also constructed and subjected to the same loading protocols. Numerical predictions of the specimen responses were carried out before testing to validate the design assumptions. Numerical analyses were also performed after testing to assess the ability to reproduce the test wall response under both loading conditions. The following conclusions and recommendations can be drawn from this study:

1. In the cyclic tests, both the prototype and model wall specimens exhibited a stable hysteric response dominated by flexure up to a displacement ductility of 4.0, thus exceeding the ductility capacity of 3.5 implied in Canadian code design provisions for ductile shear walls. Upon flexural inelastic response, inelastic shear deformations progressively developed in the plastic hinge region of the wall reaching approximately 20% of the total wall deformations at a ductility of 4.0. These shear deformations should be accounted for in the prediction of the inelastic seismic response of cantilevered wall structures. At a ductility of 4.0, shear sliding started to develop in both tests, which led to significant strength degradation of the wall specimens. Current code

equations for the interface shear resistance could be revisited to provide sufficient protection against this failure mode in ductile shear wall structures.

2. Both the prototype and reduced scale model walls exhibited large ductile flexural response with steadily increasing capacity upon yielding. Top displacements of up to 0.04 times the wall height were reached, as limited by the test setup, without the shear sliding response and associated strength degradation observed under cyclic loading. The measured response under monotonic loading matched very well the envelope of the ductile portion of the response under cyclic loading. Similarly, the monotonic demand on the transverse steel used in the plastic region of the wall corresponded to the envelope of the demand measured under cyclic loading.

3. Excellent agreement under both loading protocols was found between the responses of the prototype and the reduced scale model specimens. This suggests that reduced scale models designed with a scaling factor of up to 2.4 and constructed with normal concrete mixes and deformed bars for the main reinforcement can be used to examine the seismic response of ductile shear wall structures, including inelastic flexural and shear deformation effects and shear sliding mechanisms.

4. Comparison between the experimental and numerical results showed that the VecTor2 finite element program can adequately capture the inelastic monotonic and cyclic behaviour of ductile shear walls, including initial stiffness, shear deformations, force demand in the transverse steel, energy dissipation, and failure mechanisms. The VT2 program overestimated the ultimate capacity under monotonic loading, possibly due to excessive tension stiffening effects in the

inelastic range. Improvement to the program and related modeling procedures could also be made to better match the ultimate capacity and rate of strength degradation

In this test program, the interaction of bending moment and shear force at plastic hinge was investigated. Axial loading was not considered. Further testing would be needed to examine the interaction of bending, shear and axial load under dynamically applied seismic loading.

CHAPTER 4

SHAKE TABLE TESTING OF SLENDER RC SHEAR WALLS SUBJECTED TO EASTERN NORTH AMERICA SEISMIC GROUND MOTIONS

4.1 Abstract

This chapter presents shake table test results on two identical 1:2.33 scaled, 8-story moderately ductile reinforced concrete shear wall specimens under high frequency ground motion expected in Eastern North America. The walls were designed and detailed according to the seismic provisions of NBCC 2005 and CSA-A23.3-04 standard. The objectives were to validate and understand the inelastic responses and interaction of shear, flexure and axial loads in plastic hinge zones of the walls considering the higher mode effects. One specimen was tested under incremented ground motion amplitudes ranging from 40% to 120% of the design level. The range was increased from 100% to 200% for the second specimen. The response of the walls was significantly affected by the second mode, causing inelastic flexural response to develop at the base as well as the 6^{th} level. Dynamic amplification of the base shear forces was also observed in both walls. In the second wall, which was tested in the undamaged condition, peak base shear forces occurred prior to significant inelastic rotation and the contribution to concrete to shear resistance exceeded the value used in design. Once inelastic rotation had developed, that

contribution corresponded to the value obtained using a value of 0.18 for the reduction factor accounting for concrete cracking. Inelastic rotation in the upper wall region was found to limit the force demand imposed by higher mode response.

4.2 Introduction

To ensure the survival of building structures under strong seismic ground motions, reinforced concrete (RC) shear walls must maintain a high proportion of their initial strength and stiffness, and possess high energy-dissipation capacity (Paulay and Priestley 1992). For individual cantilevered shear walls, the primary energy dissipation mechanism is flexural yielding at the wall bases and seismic design provisions have been developed to confine inelastic response in that plastic hinge region and prevent brittle shear failure.

The inelastic seismic response of tall and slender RC walls remains complex, however, as it involves the superposition of multiple modes of vibration in the nonlinear range, the post-elastic behaviour of reinforced concrete under dynamically applied and interacting flexural, shear and axial cyclic load demand, and the random nature of earthquake ground motions. In particular, past numerical studies showed that greater than expected horizontal shear forces can develop in multi-story cantilevered walls as a result of higher mode response in the inelastic range (Blakeley et al. 1975; Filiatrault et al. 1994; Tremblay et al. 2001; Priestly and Amaris 2002; Priestley 2003; Sullivan et al. 2006; Krawinkler 2006; Panneton et al. 2006; Boivin and Paultre 2010). Dynamic amplification of shear forces was also confirmed in recent full-scale shake table testing of 7-story rectangular wall subjected to a California seismic ground motions (Panagiotou et al. 2007a, b). In these tests, the base shear overstrength reached up to 1.5 times the flexural

overstrength due to the influence of higher modes which lowered the lower position of the lateral loads compared to design assumptions. The high shear force demand observed in this test program could be reproduced numerically by Martinelli and Filippou (2009). Past numerical studies on cantilevered walls also revealed that plastic hinges can form in the upper part of walls, even when designed and detailed for plastic hinging at the base only (Blakeley et al. 1975; Tremblay et al. 2001; Panneton et al. 2006).

Differences exist on how to achieve the desired ductile base flexural hinging response while accounting for these dynamic effects in design. In the New Zealand NZS3101 standard (NZS 2006) and the Canadian CSA A23.3 standard (CSA 2004) for the design of concrete structures, the design bending moments and shear forces above the base plastic hinge region must be amplified by the ratio of the actual flexural resistance in the hinge region to the design moment at that location. In Eurocode EC8 (CEN 2004), only the design shear forces are increased to account for flexural overstrength. NZS3101 and EC8 both prescribe modified design bending moment envelopes along the building height, together with shear amplification factors to account for higher mode effects. Shear amplification in NZS3101 is based on the number of stories whereas the period of the building and the shape of the design spectrum are considered in EC8. Rules in CSA A23.3 and EC8 vary depending on the level of ductility assumed in the calculation of the seismic loads. On the contrary, no capacity design provisions or requirements for dynamic response effects are prescribed in ACI (2008). In CSA A23.3, the shear capacity depends on the base plastic rotation but the plastic rotation is evaluated assuming only first mode response (Adebar et al. 2005). Panagiotou and Restrepo (2009) recently proposed a design method that accounts for the possibility of a plastic hinge forming in the top part of walls.

Further experimental research is clearly needed to understand better the dynamic seismic response of slender shear walls and develop consistent design methodologies for use in practice. Large scale shake table testing has been a reliable method of generating test data on the seismic behaviour of RC walls (Lestuzzi et al. 1999; Lu and Wu 2000; Kazaz et al. 2006; Panagiotou et al. 2007a, b). This chapter presents a shake table test program realized on two identical 1:2.33 scaled models of an 8-story cantilever RC shear wall with rectangular cross-section. The prototype structure is wall with moderate ductility designed in accordance with Canadian seismic provisions for a class C site in Montréal, Quebec, Canada. This wall system and seismic conditions are typical of several other major urban centers in Eastern North America such as Ottawa, Toronto, Boston, and New York. The study therefore complements well previous studies focusing on ductile wall systems designed for and subjected to earthquakes typical of the Pacific west coast of North America. Ground motions in Eastern North America are also expected to be rich in high frequencies, a more critical condition for higher mode response. The tests permitted to examine lateral deformation profiles, plastic hinging response in the upper levels, lateral load patterns and shear force demand, the interaction between shear and bending moment demand. The two wall specimens were subjected to stepwise incremented ground motions: starting at 40% of the design level for Wall 1 and at 100% of the design level for Wall 2, thus allowing the study of the influence of damage experienced in previous smaller amplitude earthquakes on the response under strong ground motions. Next chapter presents a comparison of the test results with predictions from numerical models together with design recommendations for higher mode response.

4.3 Experimental Program

4.3.1 Prototype Building and Scaling Factors

The test program was carried out with the unidirectional shake table facility of the Structural Engineering Laboratory at École Polytechnique of Montréal. The program involved two identical scaled specimens of individual RC shear walls of the moderately ductile wall category complying with the seismic design provisions of the National Building Code of Canada (NBCC) (NRCC 2005) and the CSA A23.3 standard for the design of concrete structures in Canada. The properties of the test specimens were selected to represent the 8-story residential RC shear wall building located in Montréal, QC, Canada studied by Panneton et al. (2006). The reference prototype structure had a total height of 20.97 m (8 x 2.621 m) and a scaling factor l_r = 0.429 was adopted to meet the 9.0 m test height limitation with a story height in the models of 1.125 m. A preliminary quasi-cyclic test program was performed to verify the adequacy of the chosen scaling factor for the purpose of this study (Ghorbanirenani et al. 2009a). An artificial mass simulation was selected to meet similitude requirements (Moncarz and Krawinkler 1981). The method was modified to introduce a scaling factor on acceleration, a_r = 2.65, to keep the seismic weight per floor close to 60 kN. This resulted in a scaling factor on time, t_r = 0.403. A rectangular wall cross-section was adopted and the dimensions were adjusted such that the fundamental period of the model falls in the 0.5-0.8 s range, which corresponds to the 1.2-2.1 s period range estimated for the prototype structure, depending on cracked flexural stiffness assumptions considered. The geometry and reinforcing steel for the test specimens are detailed in Fig. 4.1. As discussed later, the cross-section was intentionally reduced at the 6th level to closely match the bending moment demand at that location. In the tests, a constant axial load of 2.7% of $A_g f'_c$ was applied to the

specimens, where A_g is the wall gross cross-section area at the wall base and f'_c is the concrete nominal compressive strength. This low axial load is representative of lightly axially loaded walls located along the perimeter of buildings or against stairways or elevator shafts.

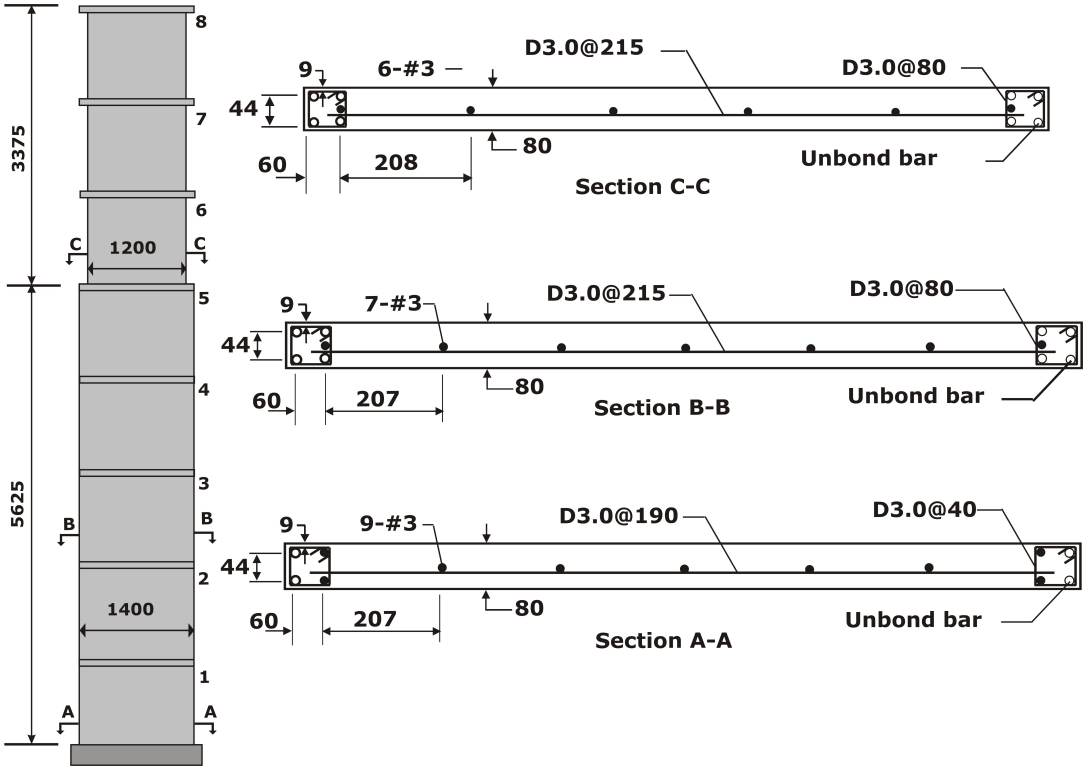

Fig. 4.1: Model wall dimensions and steel reinforcement (dimensions are in mm).

4.3.2 Seismic Design of the Test Specimens

The design is presented herein for the reduced scale model to ease comparisons with test results. The seismic shear forces and bending moments were obtained from response spectrum analysis using specific uniform hazard spectra (UHS) specified in NBCC 2005 for a class C site in Montréal, QC. Cracked flexural stiffness properties as specified in CSA A23.3 were used in the analyses, which led to periods in the first and second modes T_1 = 0.73 s and T_2 = 0.13 s,

respectively. For Type MD walls, the elastic force demand is divided by a ductility-related factor, R_d, of 2.0 and an overtrength-related factor, R_o = 1.4, and the resulting shear and bending moment distributions, M_{RSA} and V_{RSA} are illustrated in Fig. 4.2. The longitudinal reinforcement was made of ASTM A706 No. 3 bars (A_s = 71 mm^2, f_y = 414 MPa, f_u = 552 MPa) and f'_c = 30 MPa was adopted for design. At the wall base, the amount of longitudinal reinforcement was such that the wall factored moment resistance, M_r, exactly matched the moment M_{RSA}. The height of the plastic hinge region was taken equal to the length of the wall (1.4 m). This exceeded the first-story height and the hinge longitudinal rebars were extended up to the second floor. In absence of clear indication for shear and moment amplification above the plastic hinge, we applied the requirements according to CSA A23.3 for Ductile Walls. The design bending moment above the base hinge, M_f, are obtained by multiplying the moment M_{RSA} by the ratio M_r/M_{RSA} calculated at the top of the hinge region, 1.4 m from the base. For the wall specimens, that ratio was equal to 1.45 and the resulting M_f profile is shown in Fig. 4.2. The longitudinal reinforcement in the third and upper floors was gradually reduced such that M_r corresponded as closely as possible to M_f. Above the 5th floor, the wall length was reduced to better match the bending moment demand in the upper levels. Bonding for one of the longitudinal rebar of the concentrated reinforcement was also eliminated using greased sleeves to meet the required flexural strength while providing for the minimum confinement steel. The M_r/M_f ratio at the base of 6th level was equal to 1.0, as was the case at the wall base. In the upper levels, flexural overstrength resulted from minimum reinforcement requirements.

The design base shear was obtained by multiplying the shear force V_{RSA} by the ratio of the wall nominal flexural strength, M_n, to the moment M_{RSA} at the base. This ratio was equal to 1.145. Above the hinge region, as it was mentioned, the design horizontal shear forces V_f were obtained

by multiplying V_{RSA} by the 1.45 amplification factor used for bending moments. In CSA A23.3, the contribution of concrete to the factored shear resistance of members is based on the parameter $\beta\sqrt{f_c'}$, where β accounts for shear resistance of cracked concrete. In plastic hinge regions of walls, special β values apply in view of the anticipated inelastic rotation demand. For moderately ductile shear walls, $\beta = 0.10$ is recommended in CSA A23.3. Alternatively, β can be determined based on the expected hinge inelastic rotation: $\beta = 0.18$ if the inelastic rotation is less than 0.005 rad and $\beta = 0.0$ if the inelastic rotation exceeds 0.015 rad. Linear decrement is permitted between these two limits. The inelastic rotation is obtained from the plastic portion of the anticipated roof displacement including inelastic deformation effects assuming a rigid plastic wall model with plastic hinging only at the base. For the test specimen, the computed roof displacement including inelastic effects was 33.6 mm and the resulting inelastic rotation in the base hinge was equal to 0.00216 rad. For such a small rotation, $\beta = 0.18$ could have been used, but the first option ($\beta = 0.10$) was adopted in the design of the specimens. Deformed D3.0 wire made of ASTM A496 steel (A_s = 19.26 mm^2, f_y = 515 MPa, f_u = 585 MPa) was used for the transverse and confinement reinforcement. The amount of shear reinforcement was adjusted along the height to meet the shear force demand V_f as well as the minimum steel requirements for ductility. The resulting factored shear resistance, V_r, as supplied, is shown in Fig. 4.2. Minimum reinforcement requirements led to significant shear overstrength in the upper levels, as is typically the case in actual structures. It is noted that no dynamic amplification is prescribed in NBCC 2005 and CSA A23.3 for shear walls. For the test specimens studied herein, a dynamic amplification factor of 1.5 would be prescribed in both the NZS3101 and EC8 provisions, but this amplification was not considered in the design.

Check the ductility of the wall:

$\gamma_w = (M_n/M_f)_{base} = 1.145 > 1.3$ NO $\longrightarrow \gamma_w = 1.3$

$\theta_{id} = (\Delta_f R_d R_o - \gamma_w \Delta_f)/(h_w - l_w/2) = (12x2x1.4-1.3x12)/(9000-1400/2) = 0.00216 > 0.003$ NO

$\theta_{ic} = (\varepsilon_{cu} l_w/2c-0.002) = (0.0035x1400/2x142-0.002)=0.015 > \theta_{id} = 0.003$ O.K

The two wall specimens were constructed simultaneously, in the vertical position, with single-story lifts poured in sequence to replicate actual construction practice. At every level, floor slab segments were fabricated on both sides of the walls to transfer inertia forces from the seismic weights to the wall and to include floor slab effects during the tests. The measured properties of the reinforcing steel are given in Table 4.1a. An in-house concrete mix was prepared for the models with Type GU cement, W/C = 0.69, 4-6 mm syenite type coarse-grained aggregate with 83% passing 5 mm sieve. The measured properties of the concrete at 28 days and the day of testing are given in Table 4.1b. The nominal shear and bending wall resistances using actual material properties are plotted in Fig. 4.2. Each wall was built with a stiff base footing that was anchored on the shaking table with pre-tensioned high strength bolts to prevent base uplift due to rocking.

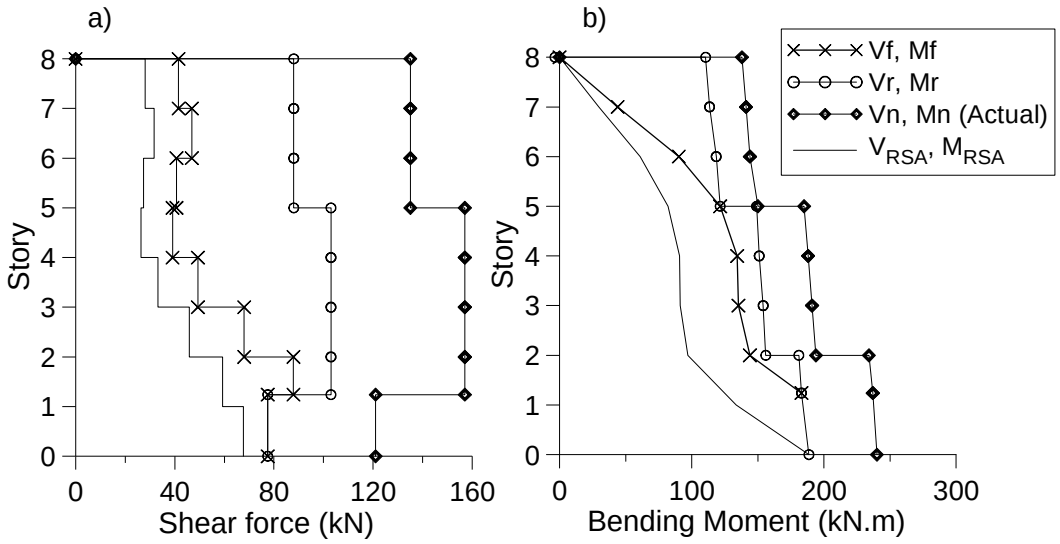

Fig. 4.2: Computed and design forces in test specimens: (a) Shear forces; (b) Bending moments.

The slab of the floors is also fabricated to consider the floor effects during the test. Fig. 4.3a and 3b show the formworks and purring the concrete of the walls respectively.

a) b)

Fig. 4.3: Photos of constructing of the walls; (a) formworks; (b) purring of concrete.

Table 4.1: Material property. a) Steel; b) Concrete.

a) Steel material properties

Bar type	Size	f_y (MPa)	f_u (MPa)	ε_{sh}	ε_u
Longitudinal	#3	441-492(455)	629-749 (706)	0.011	0.13
Horizontal	D3.0	493-503(496)	585-633 (601)	-	-

b) Concrete material properties

Time		f'_c (MPa)	f_t (MPa)	E_c (MPa)	ε_0	ν_c
28 Day		30.0	2.9	-	-	
Day of test	W1	30.0	2.9	26632	0.0026	0.22
	W2	33.3	2.9	26670	0.0020	0.22

4.3.3 Test Setup and Instrumentation

A test specimen and the shaking table test setup are illustrated in Figs. 4.4a&b. The total weight of the wall was 52 kN, including the weight of the base footing (11 kN). At each level, the seismic weight tributary to the wall studied was simulated by horizontal steel plates that were supported on independent steel columns resting on the laboratory strong floor beside the shake table (Fig. 4.4b and 5a). The masses were connected to the test wall by rigid arms to transfer the seismic loads to the specimen. This seismic weight arrangement also reproduced the gravity load carrying system laterally braced by shear walls in buildings, so that P-delta effects could be directly included in the tests. At the base of the gravity load system, the steel columns were mounted on frictionless roller bearings and pin-connected to horizontal steel members extending up to the earthquake simulator to which they were connected. Hence, the base of the gravity system was subjected to the same horizontal displacements as the shake table. This configuration allowed seismic weight much larger than the 15 ton (145 kN) payload capacity of the table: the steel plates weight was approximately 62 kN per floor, resulting in a total gravity/seismic weight of 500 kN for the 8 floors. The axial load P_0 was applied to the specimen by means of two post-tension tendons anchored to the base footing, one on each side of the wall. At the wall top, coil springs were inserted in the tendon anchorage system to mimimize variations in the axial load applied during the tests (Fig. 4.4c and 4.6). The model walls and seismic weight system were surrounded by an independent braced steel frame to provide for safety and lateral stability. At each level, a horizontal guiding system with PTFE sliding interface was used to brace the specimen in the transverse direction (Fig. 4.4b).

The instrumentation used to measure the deformations, accelerations and forces is shown in Fig. 4.5a. Load cells were mounted in the stiff connecting arms to measure the horizontal inertia forces induced by the steel plates simulating the seismic weights (Fig. 4.4b). Accelerometers were also used at every floor to the evaluate inertia forces from the wall self-weight. Additional load cells were used to monitor the vertical load applied by the tendons. Displacement transducers were installed to measure the lateral displacements of the structure as wells as the localized wall rotation and shear deformations at the expected plastic hinge locations, i.e. at the wall base and at the 6^{th} level. During the tests, the forces from the shake table actuator as well as the shake table displacement and acceleration feedback signals were also recorded. The horizontal equilibrium of the whole system could then be verified by comparing the summation of all story inertia forces to the force applied by the actuator, Figure 4.5b shows an example of such a verification. Excellent match could be obtained, demonstrating the adequacy of the test setup. Variations of the applied wall axial loads were found to be small, generally less than 5%, as also illustrated in Fig. 4.5b.

a)

b)

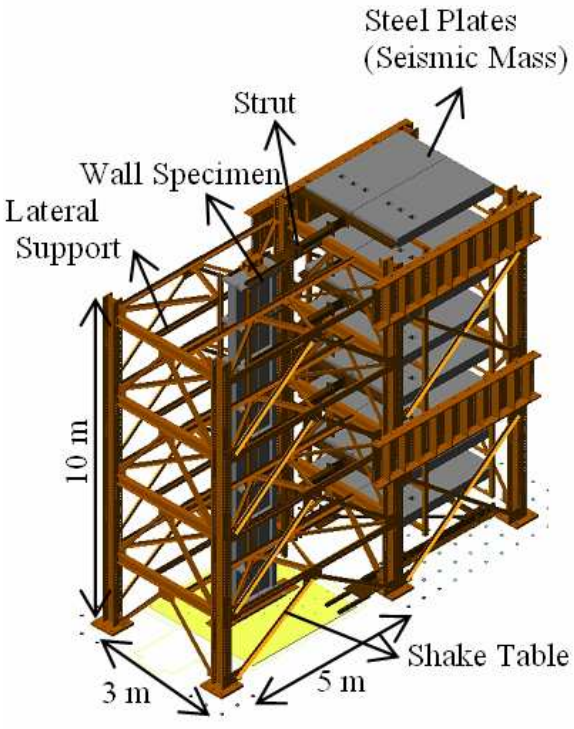

c)

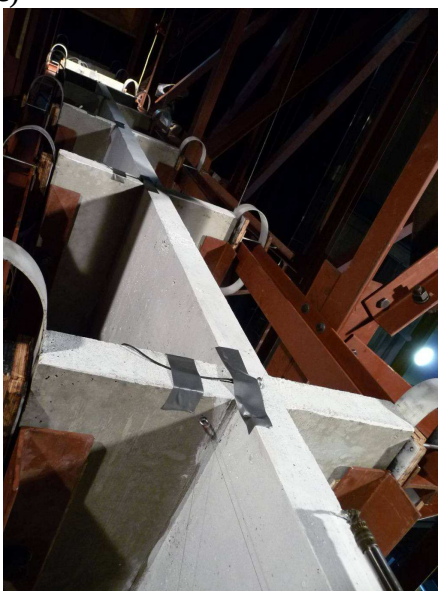

Fig. 4.4: Test setup: (a) Test specimen prior to installation in the test setup; (b) Test specimen on shake table and seismic weight system; (c) Wall lateral supports and load cells for horizontal inertia force measurements at floor levels.

a)

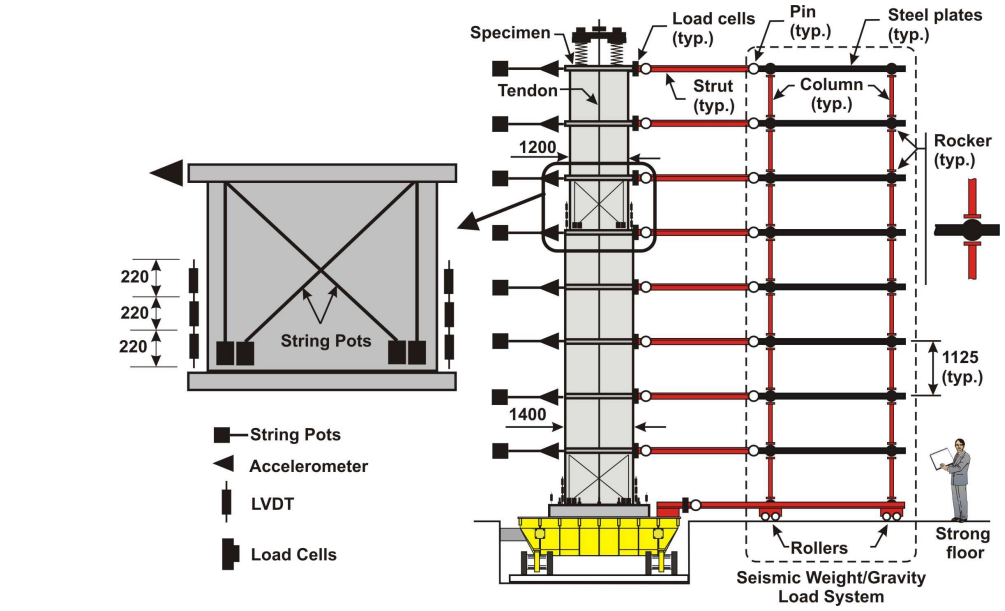

b)

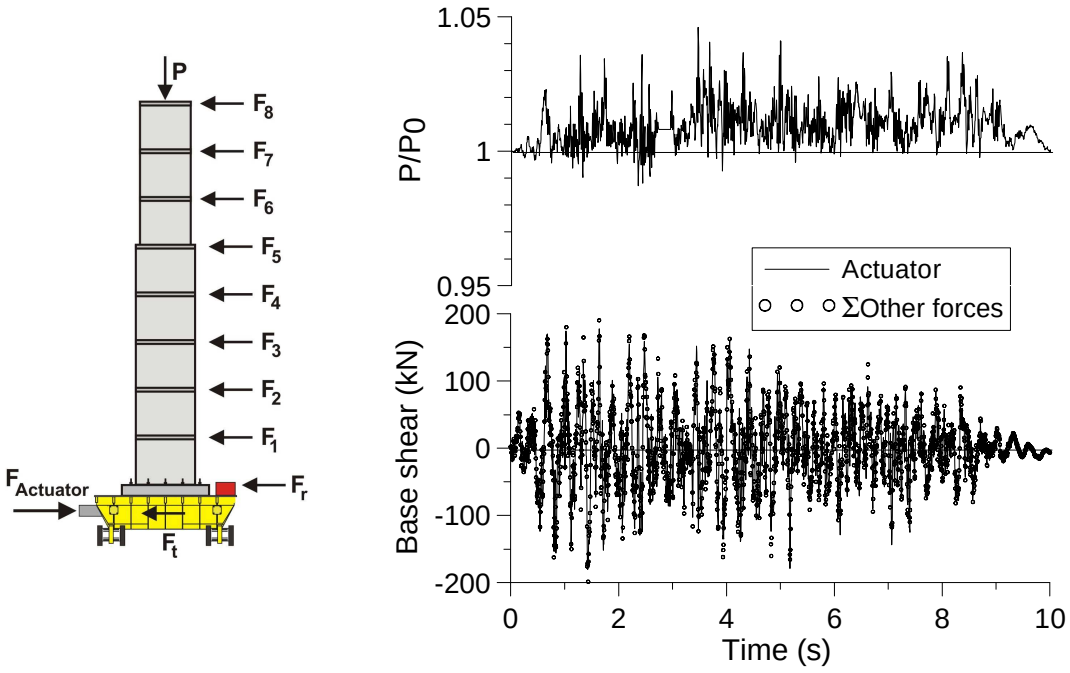

Fig. 4.5: (a) Elevation of test setup with instrumentation; b) Horizontal force equilibrium and variation of axial load during a test.

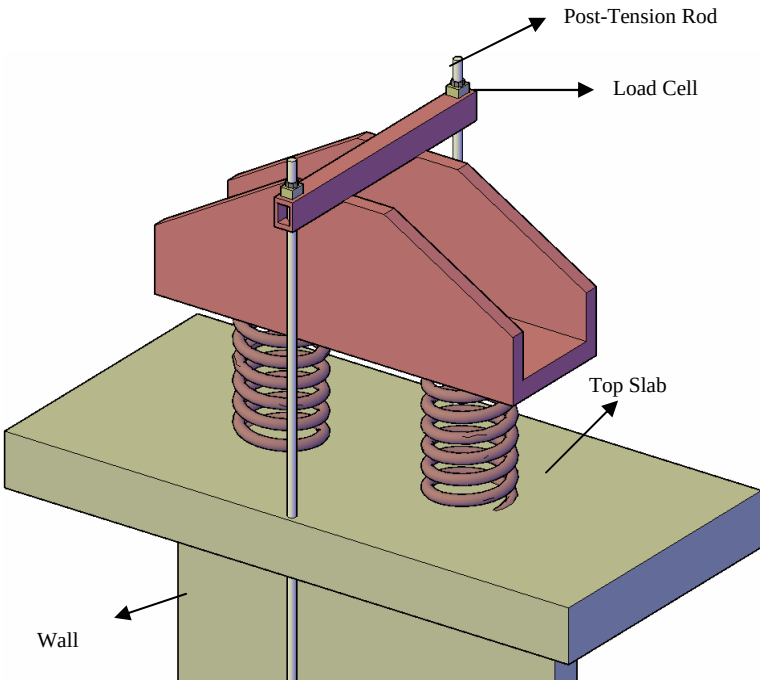

Fig. 4.6: Spring setup to apply the axial load.

4.3.4 Test Ground Accelerations

A simulated time history corresponding to an M7.0 event at 70 km was selected for testing as this magnitude-distance scenario dominates the hazard in Montréal (Tremblay and Atkinson, 2001). The original record was modified using a close spectral matching technique to fit the site specific NBCC 2005 UHS used in design. This modified ground motion is referred to herein as 100% EQ. The NBCC UHS and the 5% damped ground motion spectra are compared in Fig. 4.7a and the 100% EQ ground motion is plotted in Fig. 4.7b (acceleration and time are presented at the model scale). Wall 1 was subjected to 10%, 40%, 100%, 80%, and 120% EQ intensities. For Wall 2, 100% EQ was applied first on the undamaged specimen. Subsequent tests on this wall were performed at 120%, 150%, and 200% EQ levels. The 5% damped response spectra of the acceleration feedback signal recorded during the tests are shown in Figs. 4.7c&d. The periods of

the walls in their first three vibration modes, as measured before the test at 100% EQ, are also indicated in the figures.

Tuning of the shake table controller was performed on the bare shake table and subsequently finalized under low amplitude motions with Specimen W1 installed on the table, prior to applying the 10% EQ test. An Adaptive Inverse Control (AIC) technique was activated to mitigate amplification in the high frequency range due to resonance with the oil column of the earthquake simulator. This tuning setting was used for the 10%, 40%, and 100% EQ level tests on Wall W1. As shown in Fig. 4.7c, amplification occurred for periods shorter than the specimen second mode period. Repeating the 100% EQ test without AIC revealed better match with the target spectra and AIC was no longer used for the remaining of the tests on Wall W1. No attempt was made to improve the table settings when installing Wall W2, as the intent was to apply the same input to both specimens. Hence, all tests on W2 were performed without AIC. The amplified input in the high frequency mainly affected the response in mode 3 and higher, but relatively higher demand was also imposed in second mode, as will be discussed later. It is noted that such exceedence in very short periods is typical for actual earthquakes at near-source distances in Eastern North America as the NBCC2005 spectrum is capped at periods shorter than approximately 0.1 s (at the model scale) whereas ground motion spectra continue to rise until the period reaches 0.02 s (Atkinson 2009). Spectra of two such ground motions from an historical earthquake are plotted in Fig. 4.7a. The applied test signals were then still representative of actual seismic motions rich in high frequencies.

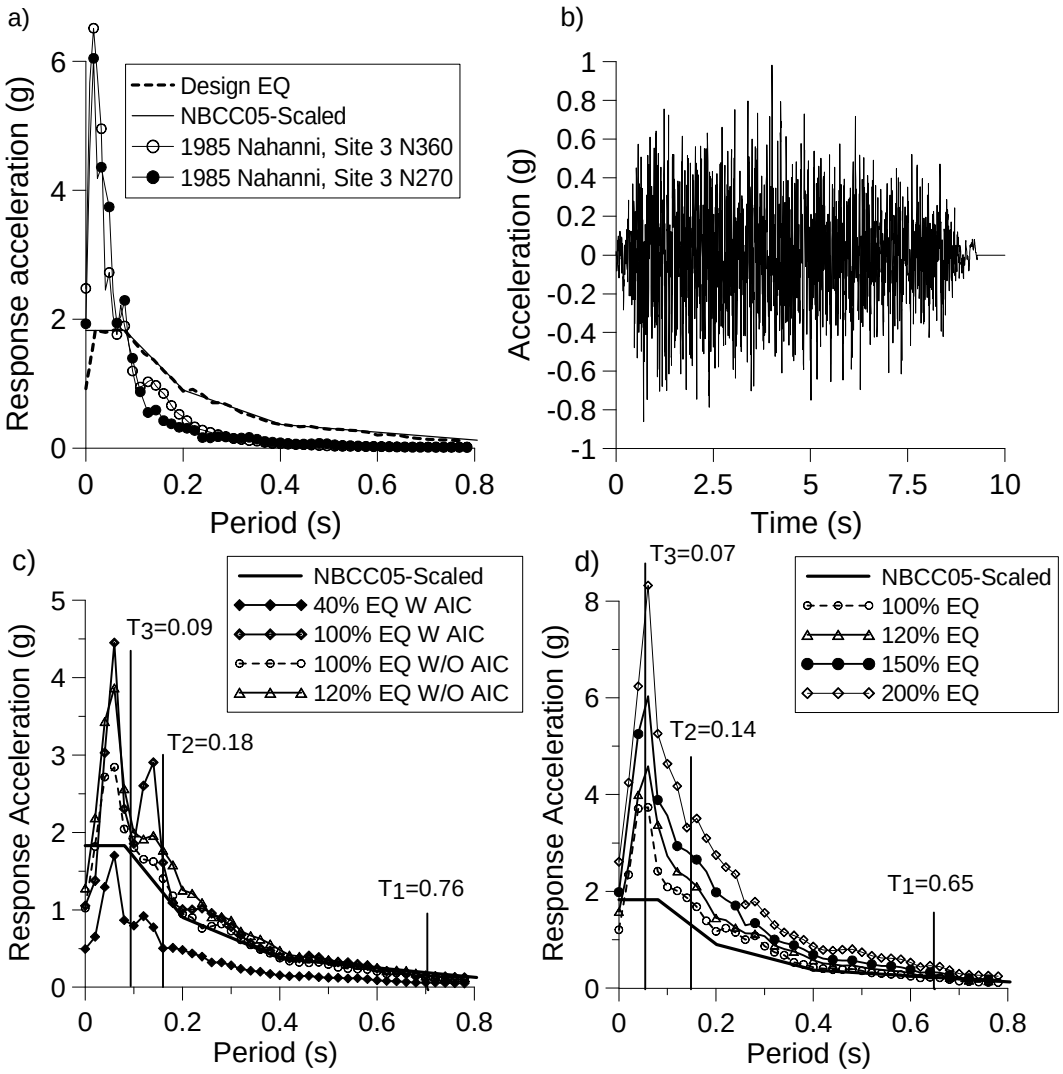

Fig. 4.7: Ground motions: (a) Scaled 2005 NBCC UHS, response spectra of 100% EQ, and response spectra from 1985 Nahanni records; (b) Time history of 100% EQ; (c) Response spectra of feedback acceleration records in W1 tests; and (d) Response spectra of feedback acceleration records in W2 tests. Notes: acceleration and time are scaled values; periods shown are those measured before the 100% EQ tests.

4.4 Dynamic Characteristics of The Wall Specimens

Tables 4.2 and 4.3 give the measured dynamic characteristics and peak response parameters for Walls W1 and W2, respectively. In the tables, the dynamic properties are those measured through low amplitude impact tests immediately after the seismic test. The modal properties of Wall W1 after all tests before the 100% EQ (Test No. 3) are close to each other, indicating that the specimen remained essentially elastic in these tests. This is also confirmed by comparing the top displacement (10.3 mm), the base rotation (0.00051 rad) and the rotation in the 6^{th} level (0.00044 rad) measured in Test No. 2 (40% EQ) with the corresponding deformations at yield: roof displacement of 11.48 mm, base rotation of 0.00052 rad and rotation at the 6^{th} level of 0.00041 rad. For both Walls W1 and W2 after 100% EQ, significant period elongation due to nonlinearity can be observed for the first three modes. Damping ratios in the first two modes (ξ_1 and ξ_2) are given in the tables. The high measured values likely reflect the conditions under the impact tests, with friction between test components significantly affecting the very small amplitude wall response. Lower damping ratios, in the order of 1-2%, are deemed to better represent the situation under strong ground motions, as demonstrated in the next chapter when comparing experimental and numerical results.

Table 4.2: Measured dynamic characteristics and peak response parameters for Wall W1

Test No.	Initial	1 – 10% AIC	2 – 40% AIC	3 – 100% AIC	4- 100% no AIC	5 – 80% no AIC	6 – 120% no AIC
PGA (g)		0.111	0.493	1.051	1.278	1.099	1.537
$S_a(T_1)$ (g)		0.015	0.059	0.130	0.094	0.080	0.095
T_1 (s)	0.67	0.680	0.72	0.76	0.90	0.850	0.960
T_2 (s)	0.14	0.14	0.15	0.18	0.20	0.22	0.240
T_3 (s)	0.097	0.097	0.11	0.093	0.091	0.098	0.10
ξ_1 (%)	6.7	4.2	3.3	6.3	3.8	3.4	4.0
ξ_2 (%)	-	4.2	5.1	6.3	6.0	6.4	9.5
$V_{B, max}$ (kN)		20	57	124	118	105	139
$M_{B, max}$ (kN-m)		40	111	214	241	191	261
$M_{6, max}$ (kN-m)		27.5	78.4	126	137	102	144
Δ_{top}(mm)		-2.18	10.3	30.0	36.0	29.5	41.3
$\Delta_{top, res}$ (mm)		0	0.38	-0.25	0.99	0.96	1.28
δ_6 (%)		0.040	0.161	0.490	0.69	0.52	0.770
$\delta_{6, res}$ (%)		0	0.013	-0.0075	0.0063	0.00533	0.0029
θ_B (rad)		0.00014	0.0005	-0.00222	0.0024	0.00198	0.0026
$\theta_{B, res}$(rad)		0	1.5e-5	-1.5e-6	8.17e-5	6.7e-5	7.94e-5
θ_6 (rad)		-3e-6	0.00044	-0.0024	-0.0028	0.0021	0.00376
$\theta_{6, res}$(rad)		0	-1.5e-5	-6.5e-5	-4.8e-6	-3.0e-6	5.3e-5
$\mu_{\theta B}$		0.27	0.98	4.2	4.6	3.8	5.0
$\mu_{\theta 6}$		0.007	1.07	5.8	6.8	5.1	9.1
ε_B ($\mu\varepsilon$)		325	1100	2240	2350	1830	2360
ε_6 ($\mu\varepsilon$)		43	1440	12300	10920	7000	9800
γ_B		0	1.21e-4	4.8e-4	8.9e-4	5.6e-4	7.46e-4
γ_6		0	1.32e-4	2.25e-4	3.15e-4	2.8e-4	5.55e-4

Table 4.3: Measured dynamic characteristics and peak response parameters for Wall W2

Test No.	Initial	1 –100%	2 –120%	4- 150%	5 –200%
PGA (g)		1.2	1.58	2.0	2.6
$S_a(T_1)$ (g)		0.21	0.11	0.11	0.16
T_1 (s)	0.65	0.96	1.0	1.03	1.31
T_2 (s)	0.14	0.24	0.27	0.33	0.36
T_3 (s)	0.073	0.096	0.10	0.12	0.16
ξ_1 (%)	5.4	14.	21.	29	26
ξ_2 (%)	-	11	17	14	11
$V_{B, max}$ (kN)		140	140	172	183
$M_{B, max}$ (kN-m)		250	225	243	253
$M_{6, max}$ (kN-m)		132	141	157	165
Δ_{top}(mm)		-31.3	38.4	52.4	71.5
$\Delta_{top, res}$ (mm)		-1.13	0.94	7.50	10.1
δ_6 (%)		-0.60	0.69	1.22	1.5
$\delta_{6, res}$ (%)		-0.034	0.018	0.13	0.19
θ_B (rad)		-0.0027	0.0025	0.0036	0.0037
$\theta_{B, res}$(rad)		-0.00011	0.00015	0.00035	0.00041
θ_6 (rad)		-0.0023	-0.0027	0.0058	0.0086
$\theta_{6, res}$(rad)		-4.18e-5	-9.0e-5	0.00031	0.00082
$\mu_{\theta B}$		5.2	4.8	6.9	7.1
$\mu_{\theta 6}$		5.6	6.6	14.1	20.9
ε_B ($\mu\varepsilon$)		2174	5535	11430	11368
ε_6 ($\mu\varepsilon$)		7118	15100	17880	-
γ_B		7.8e-4	8.2e-4	9.6e-4	1.5e-3
γ_6		-	-	-	-

4.5 Seismic Response of the Wall Specimens

4.5.1 Observed Damage and Crack Patterns

Cracks and damage to the wall specimens were traced after each test. Because the specimens were under compression axial loads, most of the cracks were closed and were not visible. Under 100% EQ, cracking was mainly observed at the base and 6th levels for both specimens. Figure 4.8 shows the crack patterns at these two locations for Wall W2 after the 100% EQ and 200% EQ tests. Combined shear and flexural cracks, approximately 0.1 mm in width, were observed at the base of the wall after the 100% EQ (Fig. 4.8c). At the wall edges, cracks are nearly horizontal and dominated by flexure. They changed to more inclined, shear cracks towards the middle of the wall section. The crack pattern is the same, although more pronounced, after the 200% EQ. No horizontal flexural cracking developed at the joint with the footing. At Level 6, there was only one horizontal crack at the joint with the 5th floor slab after the 100% EQ (Fig. 4.8a). No other cracks could be observed at the 6th level storey height. After the 200% EQ, additional flexural horizontal cracks developed in the wall over the 6th level story height (Fig. 4.8b). The absence of shear cracks at the 6th level is due to the larger shear capacity to demand ratio at the 6th level compared to the wall base (see Fig. 4.2a). Figure 4.9 shows the strain in the longitudinal bars at the base and 6th levels during the 100% EQ. The strain readings indicate that higher flexural demand developed at the 6th level. Compared to Wall W2, Wall W1 experienced more damage due to the previous test at 100% EQ (Test No. 3), but similar cracking patterns were observed after the 100% EQ and 120% EQ tests.

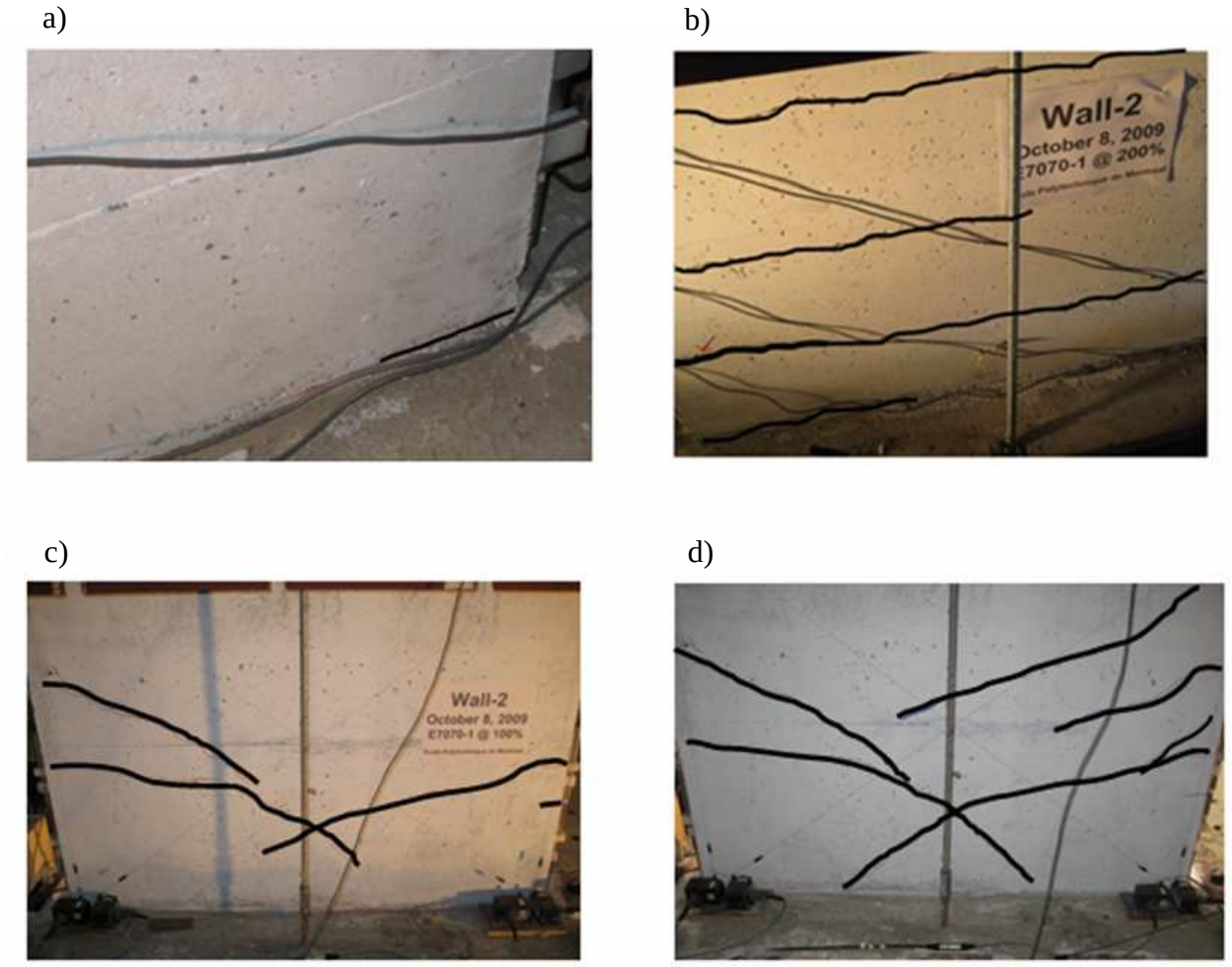

Fig. 4.8: Crack pattern in Wall W2 at: (a) 6th level after 100% EQ; (b) 6th level after 200% EQ; (c) Base level after 100% EQ; and (d) Base level after 200% EQ.

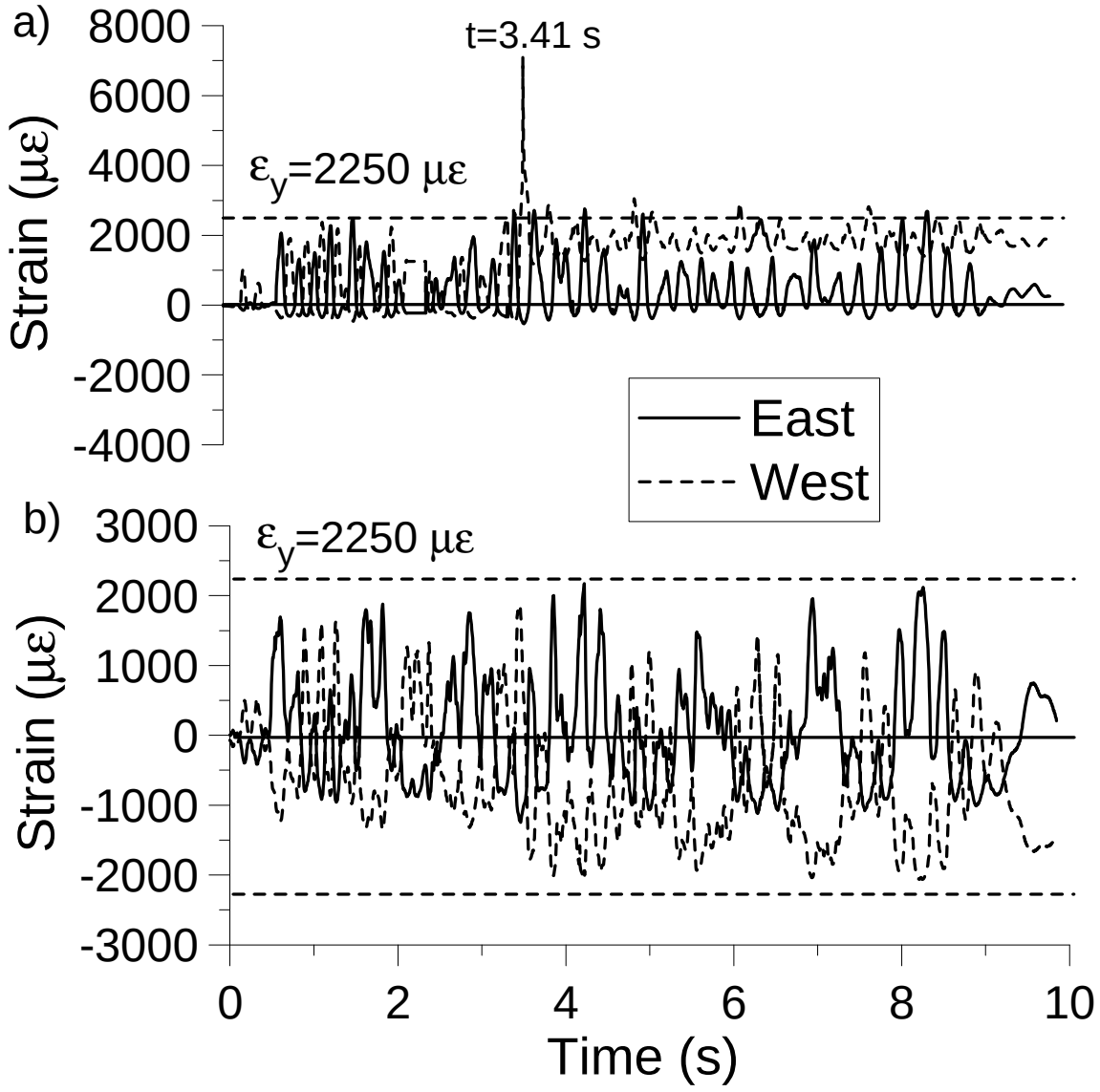

Fig. 4.9: Strain history in longitudinal bar in Wall W2 under 100% EQ at : 6th floor; (b) Base.

4.5.2 Deformation Response

Peak values of the top horizontal displacement (Δ) and rotation (θ) measurements at the base and 6th levels are given in Tables 4.2 and 4.3 for all tests. Figure 4.10 shows the time history of these parameters for Wall W2 under 100% EQ. In the figure, base rotation and top displacements are governed by both the first and 2nd modes, whereas the rotation at the 6th level is essentially due to

2^{nd} mode response. The peak rotation ductility levels measured at the base and 6^{th} level are 5.2 and 5.6, respectively. The 6^{th} floor rotation reached and slightly exceeded the Immediate Occupancy (IO) level as defined in FEMA356 (0.002 rad), whereas the one at the base remained well below the IO level. Peak positive and negative rotations at the 6^{th} floor occurred at t = 3.48 s and 3.59 s, respectively. These peaks correspond to the first significant inelastic rotation excursions at that level ($\theta > \theta_y$). They also coincide with the large strain demand measured in the longitudinal bar at that level (t = 3.41 s in Fig. 4.9). The influence of the 6^{th} floor rotation on the top displacement time history is evident in Fig. 4.10c. Peak base rotation occurred at t = 3.46 s, just before and in the direction opposed to the peak rotation at the 6^{th} level, confirming 2^{nd} mode response. The plastic portion of the base rotation at this time, θ_p, is equal to 0.0021 rad. This is nearly equal to the value predicted when following code design procedure ($\theta_{p,\,code}$ = 0.00216 rad), but this rotation was not associated to a single base hinge plastic (first mode) response, as assumed in design. Peak top displacement occurred later in the test and reached a value of -31.4 mm at t = 7.7 s. This displacement is close to the predicted value of 33.6 mm, but does not result from base hinge rotation. In fact, peak displacements in both directions occurred at the same times (7.7 s and 8.4 s) as local maxima of rotations at the 6^{th} level, and not to maxima of base rotations. The measured peak roof displacement corresponds to a global displacement ductility of the 2.7, as determined with a yield roof displacement obtained from nonlinear pushover analysis based on actual material properties. This is 35% higher than the ductility force modification factor specified in NBCC 2005 (R_d = 2.0).

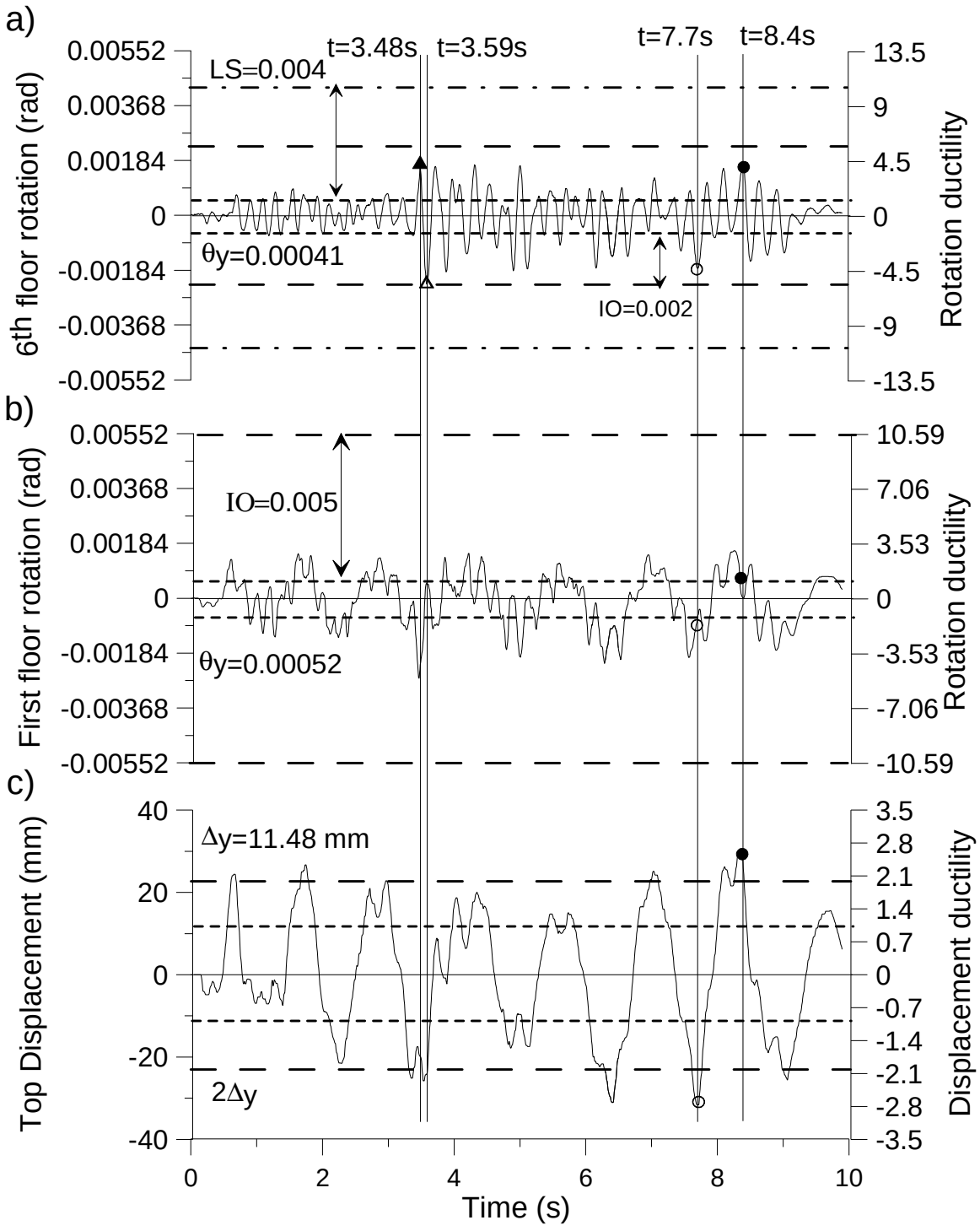

Fig. 4.10: Time history response of Wall W2 under 100% EQ: (a) Relative 6th floor rotation; (b) Base rotation; and (c) Relative top displacement.

The influence of second mode response and rotation at the 6th level can be observed further by examining the vertical profiles of the wall lateral deformations and accelerations for Wall W2 under 100% EQ. Snapshots of the lateral deformations at positive and negative peak top displacements and peak rotations at the 6th level are presented in Fig. 4.11a. Peak roof displacements at 7.7 s and 8.4 s occur when base rotations are small and they mainly result from deformations in the upper part of the wall. In particular, a marked change in slope at the 5th floor slab, which coincides with wall rotation in the 6th level, is observed at t = 8.4 s. The figure also shows that large rotations occurred in opposite directions at the base and 6th levels at t = 3.48 s. Figure 4.11b shows the lateral acceleration profiles at the same points in time. Those correspond to inertia force, or seismic load profiles. At peak roof displacements, the force patterns are far from the triangular first mode shape traditionally assumed in design. At maximum 6th level rotations, the inertia force patterns nearly adopt a second mode deformation profile.

When compared to the design spectrum, the test ground motion signals contained excessive energy in the period range corresponding to second and higher modes of the specimens (Fig. 4.7d). This discrepancy likely contributed to the observed response. As mentioned, however, similitude exists between the signals imposed in the tests and actual high frequency dominated ground motions from earthquakes in Eastern North America, indicating that the observed behaviour could in fact occur in future earthquakes. Furthermore, numerical simulations described in the next chapter show that similar response with plastic rotation at the wall base and at the 6th level would have been obtained under the spectrally matched ground motion time history of Fig. 4.7b.

Peak inter-story drifts (δ) at the 6th level are given in Tables 4.2 and 4.3. The values under 100% EQ are much smaller than typical limits prescribed in building codes (2.0-2.5%). The comparisons of the results for Test No. 4 in Table 4.2 to the values from Test No. 3 in Table 4.3 suggest that the peak response parameters under design ground motion level are not significantly influenced by previous damage experienced by a wall. Residual deformations are also given in Tables 4.2 and 4.3. For both walls, the values after the 100% EQ are very small, partly due to the re-centering behaviour induced by gravity loads. For both test specimens, peak and residual deformations steadily increased when applying larger ground motion amplitudes.

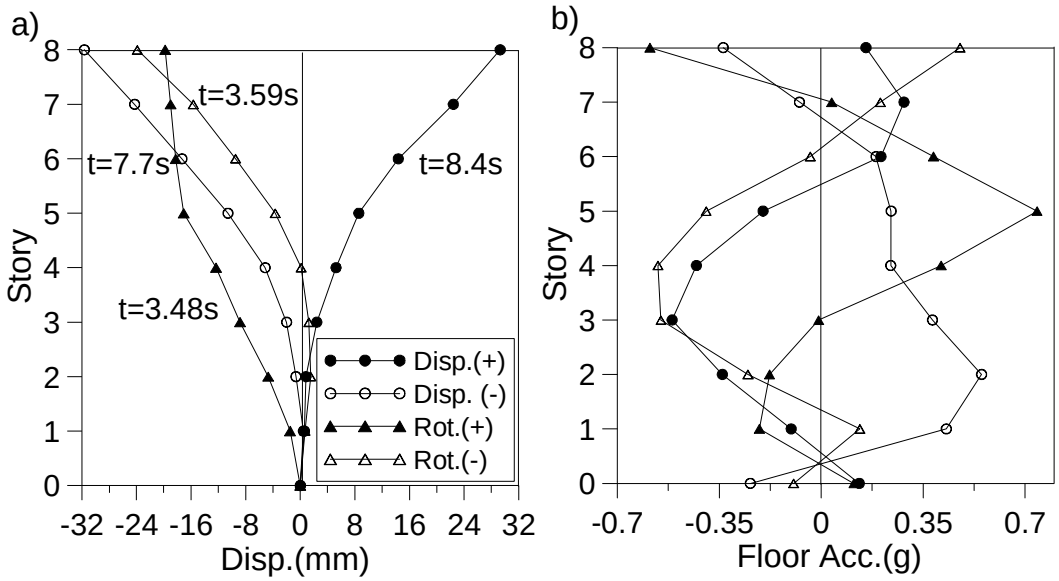

Fig. 4.11: Response of Wall W2 under 100% EQ at time of maximum top displacement and 6th level rotation: (a) Lateral displacement profiles; (b) Floor horizontal acceleration profiles.

4.5.3 Flexural Demand

Figures 4.12a&b show the distribution of acceleration along the height of both walls W1 and W2 under the 100% EQ at the time of maximum base shear and bending moments, respectively. As was the case at times of peak roof displacements and 6th level rotations in Fig. 4.11, the distribution of story forces along the height of both walls are mainly contributed by second mode response. In both walls, maximum base shear force took place before maximum base moment, and the height of the resultant forces producing maximum base moment is located about two times higher than the resultant forces producing maximum base shear. This confirms that peak bending moments and shears are not produced by the same loading patterns. Furthermore, the resultant forces producing maximum bending moments and maximum shears are both located two times higher in Wall W2 compared to Wall W1. This difference is attributed to the damage experienced by Wall W1 in the previous test at 100% EQ (Test No. 3 with AIC): cracking at the base reduced the lateral forces from first mode response and flexural cracking at the 6th level caused the upper part of the wall to be more flexible and, thereby, lag being the lower portion of the wall and attract less inertia forces at times of maximum base shear and base moment.

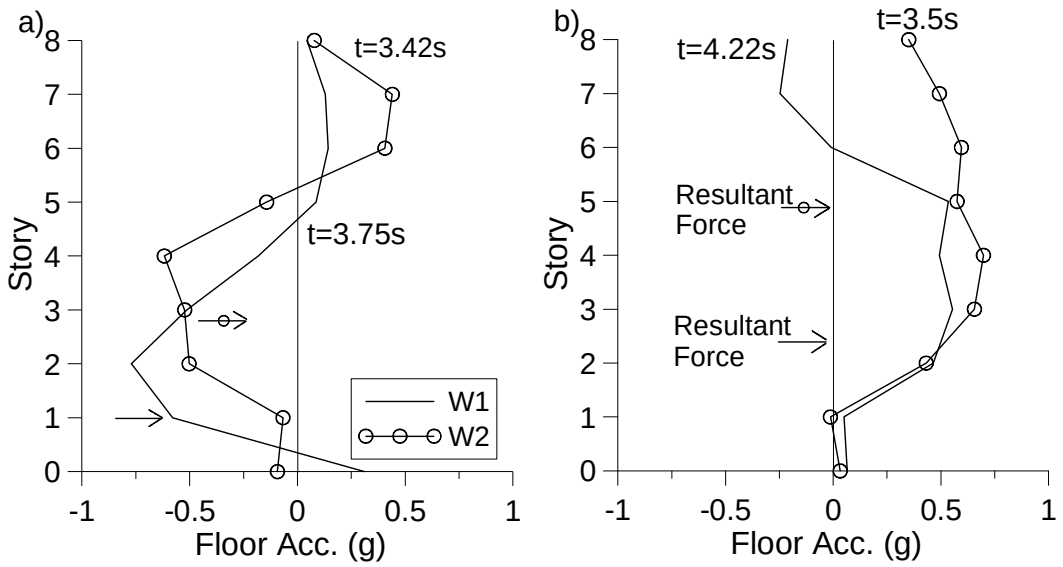

Fig. 4.12: Floor horizontal acceleration profiles in Wall W2 under 100% EQ at time of: (a) Maximum base shear; (b) Maximum base moment.

Envelopes of bending moments measured in Walls W1 and W2 under 100% EQ are illustrated in Figs. 4.13a & b, respectively. The flexural wall nominal capacity based on actual material properties, M_n, is also shown in the figures. For both walls, the bending moments reached and slightly exceeded M_n at the base and nearly reached M_n just above the 5th floor. The base moments reached 1.3 times the design moment in Fig. 4.2, which compares well with the overstrength-related modification factor R_o = 1.3 specified in NBCC 2005 for this wall category. Both measured envelopes exhibit shapes that are strongly influenced by higher mode response, similar to the demand predicted from response spectrum analysis at the design stage (see Fig. 4.2b). The two envelopes also have similar amplitude, in spite of the fact that one wall (W1) had been damaged, mainly because moments are bounded by the capacity of the walls.

Due to the differences between target and actual input test signals, the measured flexural demand must be compared to the bending moment computed from elastic response spectrum analysis using the feedback signal imposed by the shake table. In Figs. 4.13a&b, the elastic values so

computed, $M_{RSA,e}$, were scaled down by the $M_n/M_{RSA,e}$ ratio at the bases of the walls so that the resulting diagrams, referred to as $M_{RSA,n}$ in the figures, are anchored to M_n at the bases to account for inelasticity. These $M_{RSA,n}$ diagrams very closely match the measured bending moments, except in the bottom portions of the two walls where they underestimate the observed flexural demand.

The bending moments $M_{RSA,e}$ based on the table feedback signal can also be used to determine the bending moment diagram M_f that is recommended in CSA A23.3 for the design of walls for moments above the base hinge region: the $M_{RSA,e}$ values above the hinges are scaled by the $M_r/M_{RSA,e}$ ratio calculated at the top of the hinge region. The resulting M_f values are larger than the values used in the design of the specimens (Fig. 4.2) due to the amplification of the shake table motion in the short period range (Fig. 4.7). They approximately correspond to the demand just above the plastic hinge but then become much larger than the measured values in the upper levels. This overestimation is mainly attributed to the fact that the vertical distribution of bending moments from response spectrum analysis is based on wall elastic response whereas cracking and inelastic rotation was observed at the base and 6th levels. Scaling the results from response spectrum analysis by the ratio $M_r/M_{RSA,e}$ at the top of the assumed hinge region is not sufficient to fully account for these inelasticity effects, partly because there is no physical reasons why the moment will reach M_r at that location when yielding occurs or M_n is attained at the wall base. More importantly, perhaps, is the inelastic response at the 6th level that likely contributed to reducing the demand below the code design M_f values in the upper portion of the wall. The variation in bending moments in Wall 2 upon increasing ground motion amplitudes illustrates this effect. Peak moments at the base and 6th levels, respectively M_B and M_6, are given in Table 4.3 and the moment envelope measured under the 200% EQ test is plotted in Fig. 4.13b. While the

moment varies only slightly at the wall base, as was expected, the moment at Level 6 gradually increases until reaching and slightly exceeding M_n at that location.

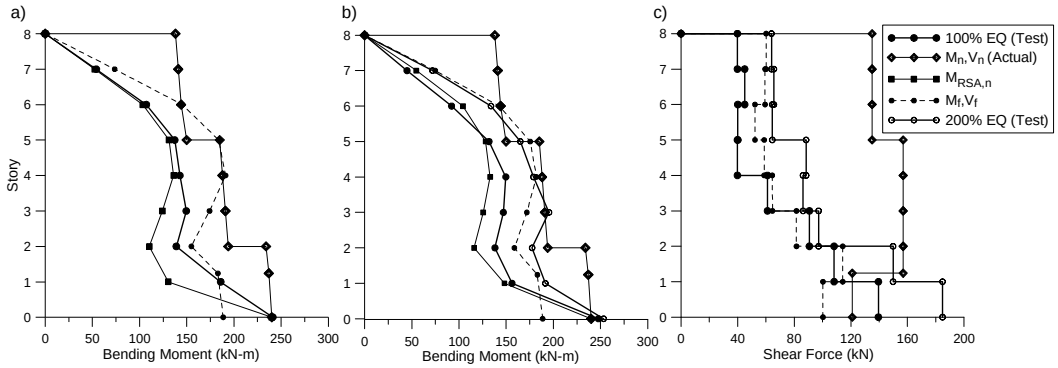

Fig. 4.13: Envelope of: (a) Bending moments in Wall W1; (b) Bending moments in Wall W2; and (c) Horizontal shear forces in Wall W2.

Hence, flexural hinging at the wall base only cannot, by itself, limit the moments induced by higher mode response in the upper portion of the wall. Inelastic flexural response must also occur in that wall segment. The results under increasing amplitude ground motions also showed that plastic hinging at the wall base does not protect either against large inelastic rotation to develop in the top floors of slender shear walls. This can be seen in Fig. 4.14 in which the moment-rotation response at the base and 6th levels of the two walls in the 100% and larger EQ tests is shown. For Wall 2, the corresponding peak plastic rotations measured at the two same locations are plotted in Fig. 4.15a and peak inter-story drifts recorded along the wall specimens are shown in Fig. 4.15b. All these response parameters reveal that inelastic demand gradually concentrated at the 6th level upon increasing the base motion amplitude. The possibility of controlling the bending moment demand in the upper part of the wall and the need to accommodate inelastic response in that part of the wall can be achieved simultaneously by intentionally allowing and detailing for a plastic hinge to form in the upper part of shear walls. This design approach has

been recently investigated by Panagiotou and Restrepo (2009) and is examined further in the next chapter.

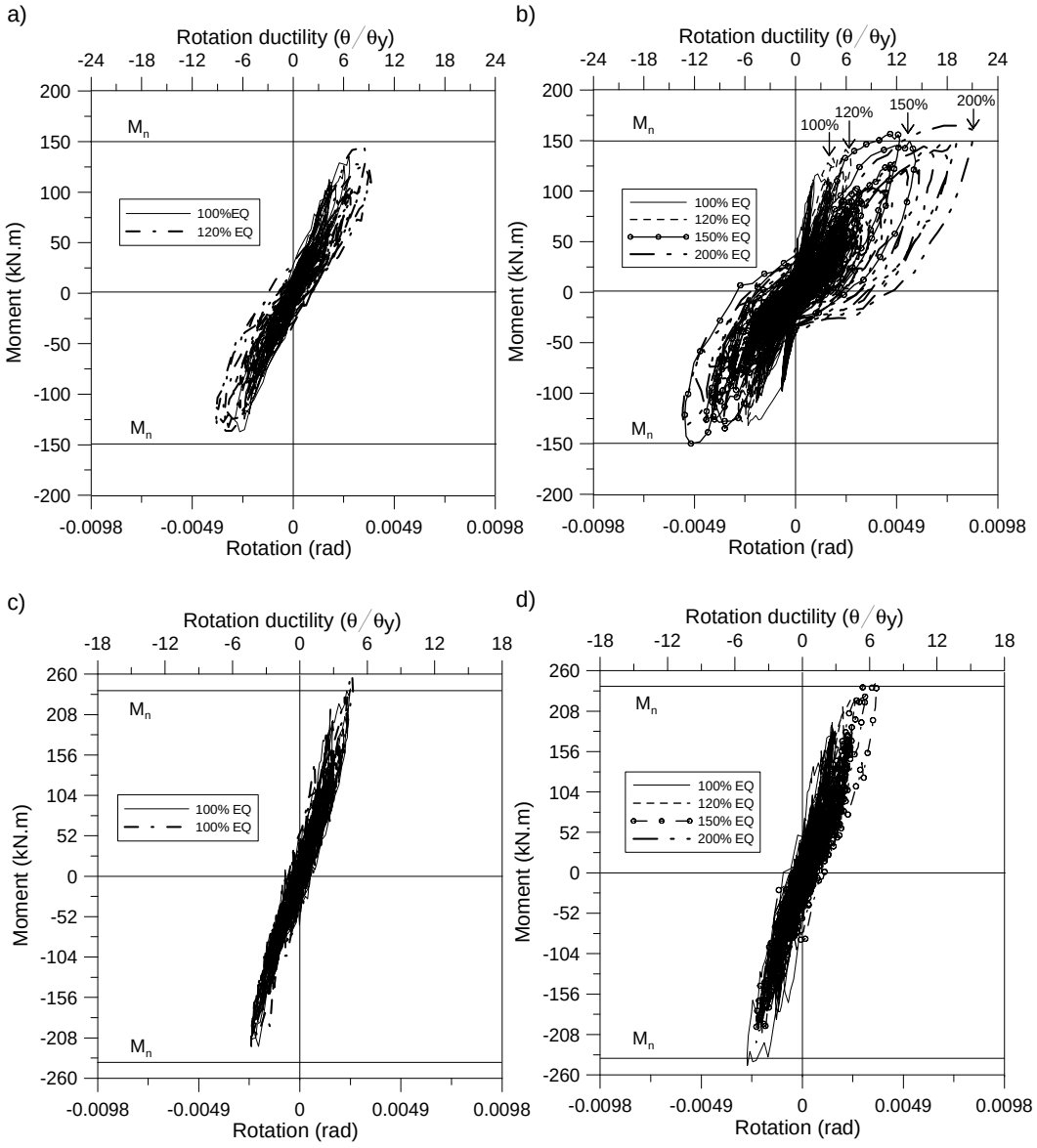

Fig. 4.14 Moment-rotation responses at: (a) 6th level of Wall W1; (b) 6th level of Wall W2; (c) Base of Wall W1; and (d) Base of Wall W2.

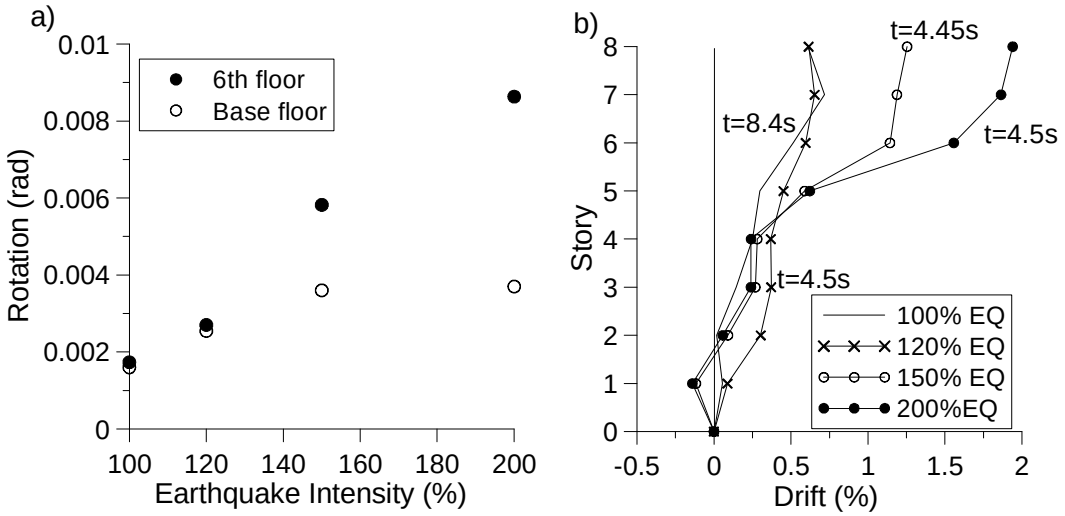

Fig. 4.15: (a) Maximum rotation at 6th and base levels of Wall W2 under increasing earthquake intensities; (b) Interstory drift angle in Wall W2 at time of maximum top displacement under increasing earthquake intensities.

4.5.4 Horizontal Shear Demand

Peak shear forces and shear angular deformations, γ, measured the base and 6th levels are given in Tables 4.2 and 4.3 for the two walls. The horizontal shear force in Wall W2 is shown in Fig. 4.13c. In the figure, V_f corresponds to the design shear force determined according to the code procedure described above but using the shears from an elastic response spectrum analysis performed with the table feedback signal. The shear envelope measured under the 100% EQ exceeds V_f in the lower floors and is less than V_f in the upper half of the wall. At the base, the maximum shear reached 1.4 V_f. Such dynamic amplification approaches the level specified in NZS3101 and EC8 codes for this structure (1.5). Shear dynamic amplification is also demonstrated by comparing the ratios of the maximum measured values at the wall base to the original design values (Fig. 4.2) for bending moments and shears at the base of the wall: 1.32 for

the moment and 1.82 for shear. Further amplification was also observed when increasing ground motion amplitude with the ratios of peak moment and shear values recorded in the 200% and 100% EQ tests being equal to 1.02 and 1.31, respectively.

The shear force-shear deformation hysteretic responses measured at the base level of Walls 1 and 2 are shown in Figs. 4.16a&b, respectively. Nonlinear response was observed in both walls under 100% EQ, which is consistent with the observed diagonal shear cracks (Fig. 4.8). No significant shear deformations were measured at the 6th level, which is also in line with the observed crack patterns. Nonlinearities at the base increased in Wall W2 when applying 200% EQ. The time history of the longitudinal strain in the horizontal shear reinforcement at the base of Wall W2 is given in Fig. 4.16c. As shown, the steel remained elastic under both ground motion levels, indicating that the shear strength as supplied was not fully mobilized. In Fig. 4.13c, however, the base shear demand under 100% EQ is found to exceed by approximately 15% the wall actual nominal shear capacity as reduced in anticipation of concrete cracking ($\beta = 0.10$).

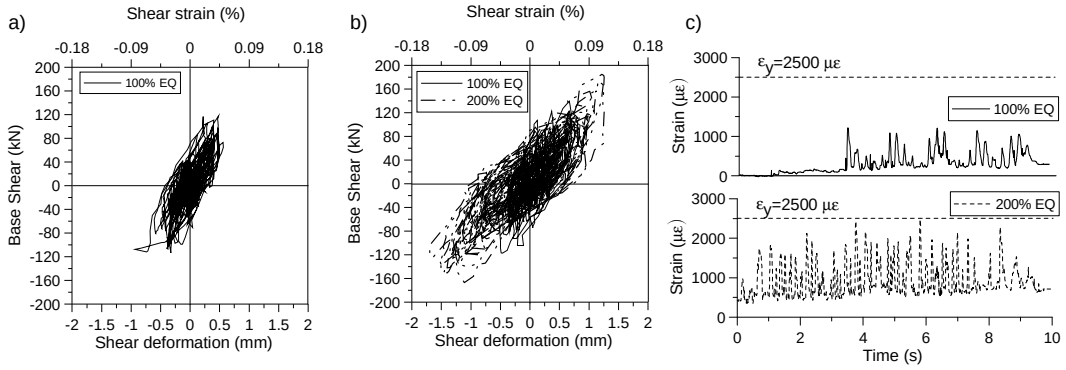

Fig. 4.16: (a) Hysteretic shear response at the base of Wall W1; (b) Hysteretic shear responses at the base of Wall W2; (c) Strain time history in horizontal reinforcement at the base of Wall W2.

This apparent discrepancy is due to the limited base plastic rotation experienced by the wall. This is illustrated in Fig. 4.17 where the shear resistances contributed by the concrete and the

horizontal reinforcement are plotted against the total applied base shear for Wall W2 in the 100% and 200% EQ tests. The shear resisted by the steel could be obtained from the measured steel strain and the concrete shear was obtained by subtracting the steel contribution from the total shear. In Fig. 4.17a, the β factor corresponding to the concrete shear is also given. In that figure, the upper right quadrant of the plots, the concrete shear force varies nearly linearly with the base shear (Fig. 4.17a) whereas the steel contribution remains small and constant (Fig. 4.17b), indicating that most of the base shear is resisted by concrete. The β factor reaches a value of 0.27, much greater than the value adopted in design, the reason being that the plastic rotation reached remained very small (θ_p = 0.0006 rad). In the third quadrant of the plots in Figs. 4.17a&b, the concrete contribution is capped to β approximately equal to 0.18 after a plastic rotation of 0.0022 rad was first attained under 100% EQ, even if θ_p in subsequent cycles remained small. As shown, the additional shear was then resisted by steel. In the design of the wall specimens, β = 0.10 was conservatively adopted although a value of 0.18 was also permitted in CSA A23.3 for moderately ductile shear walls. These tests tend to confirm that β = 0.18 would be appropriate for this application.

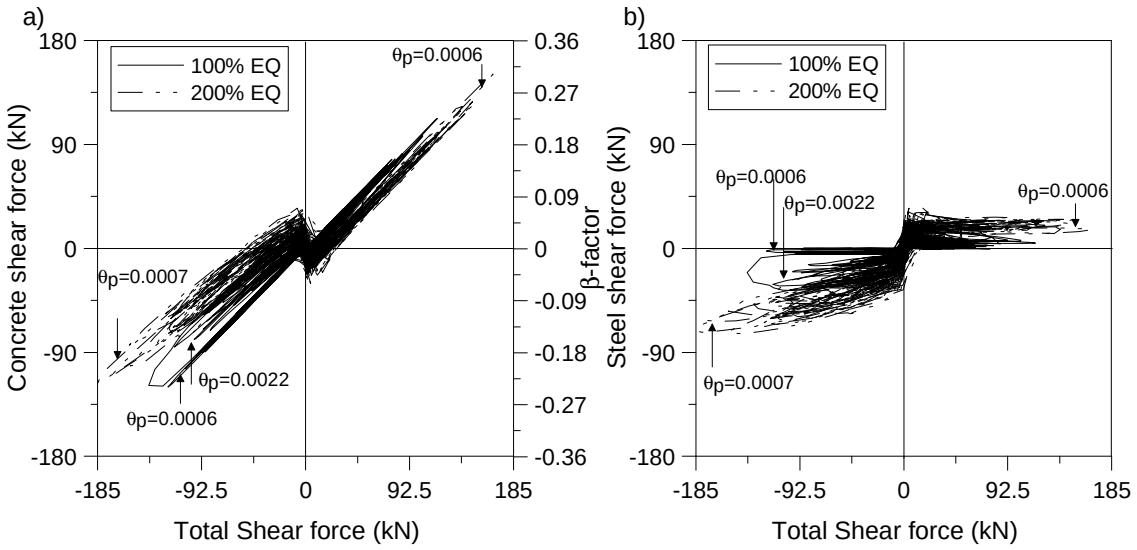

Fig. 4.17: Contribution to total base shear in Wall W2 of: (a) concrete; (b) steel (θ_p is the wall plastic rotation)

4.6 Summary and Conclusions

Shaking table tests were carried out on two identical models of an individual reinforced concrete shear wall in an 8-story residential building located in Montréal, QC, Canada. The specimen walls were designed and fabricated according to the seismic provisions of NBCC 2005 and CSA A23.3 standard for moderately ductile walls. The specimens were subjected to a ground motion record rich in high frequency energy, as anticipated in Eastern North America, and tests were performed at different ground motion amplitudes. The following conclusions and recommendations can be drawn from this study:

1. Under the design level base motion, the specimens experienced limited inelastic flexural response at the wall base, as anticipated, as well as at the 6th level, which was not expected in design. This behaviour resulted from significant higher mode response under the high frequency motions, as was confirmed by the vertical distribution of horizontal

loads, internal forces and other deformation response indicators. Cracking at the base was affected by both flexure and shear whereas flexural cracks only formed at the 6th level, which is consistent with the respective shear force demand to supply ratios at the two locations. When increasing the ground motion amplitude beyond design level, additional inelastic rotation only developed at the 6th level.

2. Under the design level base motion, the bending moment at the wall base reached the actual flexural resistance of the walls, and the ratio between the measured maximum moment and design moment values was equal to 1.3, approximately corresponding to the overstrength-related factor R_o = 1.4 assumed in design. The global displacement ductility based on roof displacements was 35% higher than the ductility-related factor specified in NBCC, essentially because it was associated to drift caused by inelastic rotation at the 6th level and not base hinge rotation, as assumed in design. The maximum plastic rotation at the base however corresponded to the value obtained assuming first mode response.
3. Under the design level base motion, the peak base shear force reached 1.82 times the value assumed in design. The amplification reduces to 1.4 when considering the design values are recomputed using the actual ground motion signal that was actually applied to the specimens. This dynamic amplification is close to that prescribed for this wall structure NZS3101 and EC8 code documents (1.5). Upon increasing the ground motion beyond the design level, the base shear continued to increase although the base moment remained nearly constant.
4. The walls could sustain base shear forces exceeding the wall actual shear strength, essentially due to a greater than expected contribution from concrete to shear resistance. This higher concrete capacity resulted from peak shear force demand occurring before development of significant cracking and inelastic rotation at the wall base. After inelastic

response, the concrete shear strength corresponded to that obtained using a value of 0.18, instead of 0.10, for the reduction factor β accounting for shear resistance of cracked concrete.

5. Damage from previous earthquakes resulted in slightly more pronounced higher mode, as the wall was already weakened at the base and 6^{th} level in flexure, resulting in larger rotation at the 6^{th} level and top displacements. The peak shear force and bending moment demand remained comparable.

The test program confirmed that slender moderately ductile shear walls subjected to high frequency ground motions can experience inelastic flexural response in the upper floor region and dynamic amplification of horizontal shear forces at their bases. Higher damping is expected in actual building structures compared to the test specimens examined herein, and these effects may be less pronounced than measured in the tests. Further study is needed to quantify these differences and propose design and detailing rules to address these phenomena. The tests showed that flexural hinging in the wall upper segment can be used to control the force demand imposed by higher mode response. This design alternative is examined in the next chapter.

CHAPTER 5

NUMERICAL MODELING OF SHAKING TABLE TEST AND DESIGN RECOMMENDATIONS FOR HIGHER MODES IN AN 8-STORY RC SHEAR WALL

5.1 Abstract

This chapter presents the numerical modeling of two large scale shake table tests of two slender 8-story reinforced concrete shear wall models performed to investigate higher mode effects on the response of high rise walls to ground motion records representing high frequency Eastern North America seismic excitation. These effects have been described in previous chapter and include plastic hinges forming in the upper part of the walls, as well as the base, and base shear demand exceeding the capacity design shear forces prescribed in codes. Nonlinear time history analyses were carried out by the reinforced concrete fibre element (OpenSees) and finite element (VecTor2) methods using shake table feedback signals. Good agreement was obtained between numerical and experimental results. The inelastic responses and the dual plastic hinge behaviour of the wall could be adequately reproduced using finite element and fibre element analysis programs. The fibre element method is a good alternative in terms of computing time and it produces reasonable results in comparison to the finite element method, although particular attention needs to be given to the selection of the damping ratios. Based on the experimental and

numerical results, this chapter also gives preliminary design recommendations considering higher mode effects on dual hinge response and base shear forces for ductile slender shear walls.

5.2 Introduction

In previous chapter, shake table tests were performed on two slender, moderately ductile reinforced concrete (RC) shear walls when subjected to high frequency ground motions expected in Eastern North America. The tests showed that higher mode effects can play an important role in the seismic responses of such walls, as was predicted in past numerical studies (Filiatrault et al. 1994; Priestly and Amaris 2002; Panneton et al. 2006; Sullivan et al. 2008; Panagiotou and Restrepo 2009) and in recent test program (Panagiotou et al. 2007a, 2007b). In particular, the tests confirmed the possibility that inelastic flexural response develops in the upper part of tall walls and that base shear forces exceed the values corresponding to the attainment of the wall flexural strength at the base. Such effects are not considered in seismic design provisions such as ACI-318 (ACI 2008) in the United Stated or CSA A23.3 (CSA 2004) in Canada. Amplification of base shear is required in New Zealand (NZS 2006) and in Eurocode (CEN 2005).

Large scale shaking table tests are among the best methods to understand the real behaviour of structures under dynamically applied seismic ground motions, but performing such tests is very costly and time consuming. Therefore, experimental studies must be complemented by extensive parametric studies to develop a deeper understanding of the seismic behaviour of structures. RC shear walls in most past nonlinear dynamic analyses were modeled using elastic frame elements with hysteretic lumped plastic hinges concentrated at their ends. Although inelastic flexural seismic responses can be predicted reasonably well with these models (Takeda et al. 1970;

Clough and Johnston 1966), these analyses did not account for shear sliding deformations along large flexural cracks and degradation of shear stiffness due to diagonal cracking that can develop in walls subjected to large cyclic inelastic deformations (Cheng et al. 1993; Thomsen IV and Wallace 2004). Failure of the compressive zone due to the combination of shear, flexure, and axial loads in critical regions was also ignored. Prediction of the inelastic response of reinforced concrete structural walls requires accurate, effective, and robust modeling and analysis tools that incorporate important material characteristics and behavioural response features such as tension stiffening, opening and closing of cracks, confinement, and takes into account the interaction of axial, shear- and flexural forces.

Finite element analysis has been successfully used to capture most of these effects and that technique has been successfully used to reproduce shake table test response of shear wall structures (e.g., Lu and Wu 2000; Kazaz et al. 2006). Multi-fibre beam element models based on Euler-Bernoulli theory represents an attractive alternative to finite element modeling as it can reproduce in details the dominant inelastic flexural response anticipated in shear walls (Orackal and Wallace 2006; Grange et al. 2009), while being significantly computationally less demanding that finite element analysis, especially if 3D building models are considered. Shear deformations in fibre models are generally considered independently assuming linear elastic shear response, without interaction with flexural response. Fibre element models are now available in commercial software that are used in day-to-day practice for seismic analysis of RC structures (e.g., CSI 2006a, 2006b). Engineers would therefore benefit from validations performed against dynamic seismic test data that could improve the reliability of this simpler analysis technique.

In this chapter, the finite element and the fibre discretization techniques are verified against the shake table tests described in the previous chapter. The VecTor2 (VT2) computer program, which is based on 2D plane stress finite element theory (Wong and Vecchio 2003), is a software that includes most of the features present in RC members. The program was used to reproduce the seismic response of shear walls from quasi-cyclic tests (Palermo and Vecchio 2007; Ghorbanirenani et al. 2009a). Dynamic seismic analyses were performed with VT2 (Tremblay et al. 2008; Ghorbanirenani et al. 2009b) but no validation has been performed yet against shake table test data. The OpenSees (OS) computer program (Mazzoni et al. 2006) is selected for fibre element modeling. The program has already been used to predict shake table results for RC walls subjected to large inelastic demand from ground motions expected in Western U.S. (Martinelli and Filippou 2009). The walls studied herein are of the moderately ductile category and are subjected to high frequency ground motions typical of earthquakes anticipated in Eastern North America (ENA). The response of the walls is dominated by higher mode effects, and the inelastic response is limited. This makes the response more sensitive to cracking and damping modeling assumptions. Appropriate constitutive models developed in the study could then be extended with confidence to study the seismic response of similar wall structures in large ENA urban areas located in regions of moderate seismicity of such as Boston, Montréal or Ottawa. In the second part of the this chapter, OS modeling is applied to investigate a dual plastic hinge design approach intended to reduce the bending moment and shear force demand due to higher mode effects in slender RC walls.

5.3 Summary of Test Program

The experimental program is described in the previous chapter and consisted of shake table testing of two identical wall models W1 and W2 designed with a scaling factor of 0.43. The specimens are representative of an individual slender reinforced concrete wall of an 8-story residential building located in Montréal, QC, Canada, and designed according to the 2005 NBCC (NRCC 2005) with combined inelastic force reduction factor $R_dR_o = 2.8$. The models have a total height of 9 m, with a uniform story height of 1.125 m. The wall length is 1.4 m up to the 6^{th} level and 1.2 m above. The wall thickness is 80 mm. The seismic weight at each floor is about 62 kN. A simulated ground motion time history developed for Eastern North America seismic conditions and spectrally matched to the design spectrum was used in the test program. This motion is referred to herein as 100% EQ. The first wall (W1) was initially tested under 40% EQ. The intensity of the record was subsequently increased up to 80%, 100% and 120% EQ levels. The second wall (W2) was tested directly under 100% EQ level, simulating an initially undamaged wall exhibiting uncraked stiffness when the design seismic event occurs. The earthquake record intensity for Wall W2 was then successively increased to 120%, 150% and 200% of the design earthquake. Unless otherwise noted, all analyses presented in this chapter were performed using the shake table acceleration feedback signals measured during the tests as input. For each specimen, the signals from all tests performed have been applied with 5 seconds of zero motion between each test, so that cumulative damage effects experienced during the entire test series could be accounted for in the analysis.

5.4 Model Parameters

5.4.1 Fibre Element Model

Nonlinear beam elements with fibre discretization of the cross-section were used in the OpenSees program. Shear deformation was modeled by including linear elastic shear cross-sectional stiffness coefficients. The measured material properties of the wall were used in the numerical model. The fibres and constitutive models used for material properties are shown in Fig. 5.1. In the model 50 and 10 concrete fibres were used along the length and the width of the wall respectively. Confinement effects on concrete response in the regions of concentrated reinforcement were accounted for in the model. In the numerical simulations, the applied seismic excitations corresponded to the measured shake table accelerations. Therefore, the shake table was not included in the numerical models. The natural periods obtained from the models were in good agreement with the experiment (Table 5.1). The mass and initial (elastic) stiffness proportional Rayleigh damping model was used to reproduce damping effects. The coefficients were determined using the frequencies in modes 1 and 2 as measured in the tests. These modeling coefficients were found to depend on the shaking intensity levels and damage progress. Parametric identification using back analyses with various values of viscous damping was performed for Walls W1 and W2 to obtain the best match in top displacements between the experiment and the OpenSees (OS) results. For each analysis, only one value of damping was used for all tests of the test series because damping could not be modified from tests to tests during the analysis. Values given in Table 5.2 are the amount of damping that led to the best match for particular tests during the entire analysis and, therefore, only represent approximations as different values of damping should have been used for each of the tests in a series.

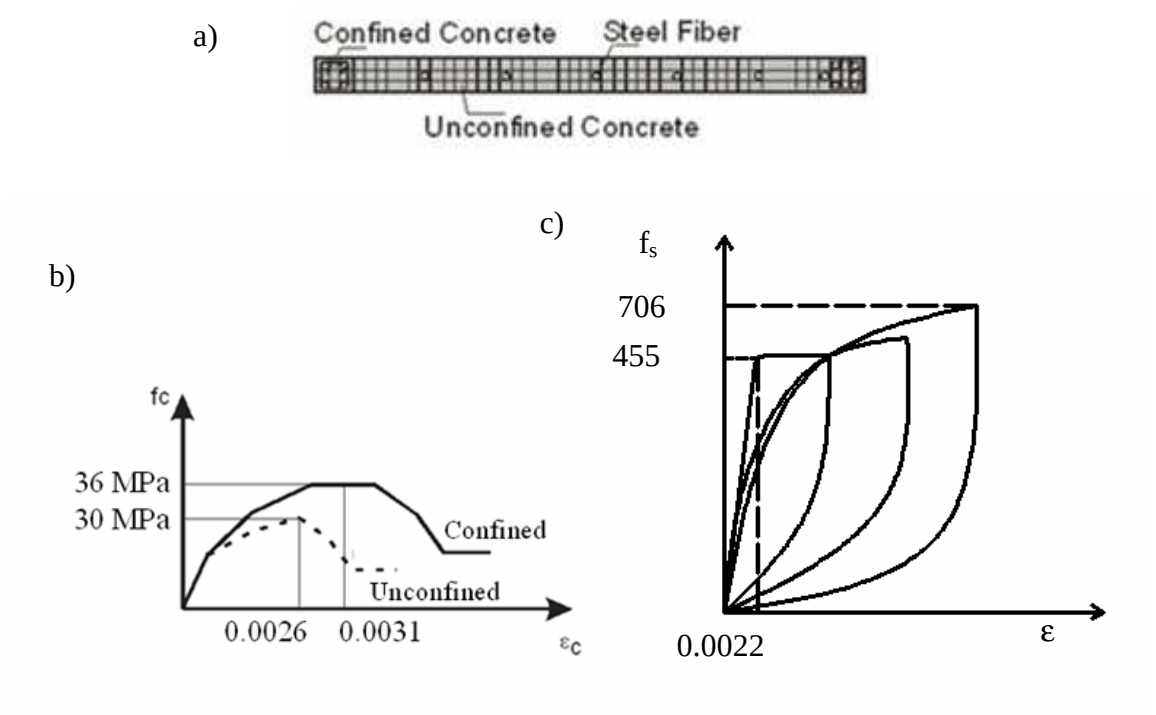

Fig. 5.1: OpenSees model: (a) Cross-section fibre discretization; (b) Concrete properties; (c) Steel properties.

Table 5.1 Experimental and numerical dynamic characteristics and peak responses for Walls W1 and W2.

		W1			W2			
Parameter	**Method**	**40%**	**100%**	**120%**	**100%**	**120%**	**150%**	**200%**
T1	**EXP**	0.72	0.90	0.96	0.96	1.0	1.03	1.31
	OS	0.67	1.1	1.00	0.93	1.02	1.1	1.23
	VT2	0.61	0.94	1.06	0.97	1.03	1.29	1.6
ξ^1(%)	**EXP**	5.1	6.0	9.5	11.0	17.2	14.4	10.7
	OS	6.7	4.0	1.5	4.8	3.0	2.2	2.8
	VT2	6.2	6.9	7.3	7.0	7.0	8.4	12.3
$V_{b\ max}$ (kN)	**EXP**	57	118	139	139	140	172	183
	OS	58	135	148	142	140	188	206
	VT2	114	165	191	186	195	179	191
$V_{6\ max}$ (kN)	**EXP**	21	40	46	40	45	46	66
	OS	22	48	58	47	55	60	76
	VT2	42	58	61	56	65	64	57
M_{max} (kN.m)	**EXP**	111	241	261	250	225	243	253
	OS	123	247	253	256	252	258	257
	VT2	200	269	269	269	267	281	271
$\Delta_{max\ (top)}$ (mm)	**EXP**	10	36	41	31	38	52	71
	OS	11	37	39	33	40	47	63
	VT2	10	29	36	28	36	45	57
$\mu_{\theta 6}$	**EXP**	1.07	6.8	9.1	5.6	6.6	14.1	20.9
	OS	1.3	6.0	11.2	5.6	7.6	10.5	17
	VT2	1.9	7.3	9.7	6.3	9.7	10.7	19.5
$\mu_{\theta b}$	**EXP**	0.9	4.6	5.0	5.2	4.8	6.9	7.1
	OS	0.9	5.9	6.7	5.3	6.9	7.1	8.0
	VT2	1.6	4.6	5.7	3.6	4.8	8.6	7.7

Table 5.2 Viscous damping ratios assumed in OpenSees for Walls W1 and W2

Wall	**Wall W1**			**Wall W2**			
Test	**40%**	**100%**	**120%**	**100%**	**120%**	**150%**	**200%**
ξ(%)	4.5	1.5	1.0	2.0	1.5	1.0	1.0

5.4.2 Finite Element Model

The VT2 program is based on the Modified Compression Field Theory and the Disturbed Stress Field Model for nonlinear finite element analysis of reinforced concrete membrane structures (Vecchio 2000; Vecchio and Collins 1986). For these analyses, 2D plane stress rectangular elements with smeared reinforcement were used. Saatci (2007) have shown that this program is

capable of modeling most of the damage, cracks and hysteretic energy dissipation mechanisms. Therefore only a small amount of viscous damping is needed, mainly to achieve numerical convergence. Comparative analyses by Tremblay et al. (2009) showed that 1% viscous damping is applicable in VecTor2 for reinforced concrete walls responding in the nonlinear range to seismic ground motions. In this study 1% Rayleigh viscous damping was used. As for the fibre models, the material properties used in FE models corresponded to as-built material properties measured in the laboratory at the time of the tests, as described in the previous chapter.

The pre-peak compression response of the concrete was based on the Popovics curve for normal strength concrete whereas the post-peak response followed the base curve (Fig. 5. 2a). The hysteretic response of the concrete was set according to Palermo and Vecchio (2002) (with decay) and tension stiffening effects according to Bentz et al. (2006) were automatically accounted for in the analysis, depending on the average net concrete axial strain. Figures 5.2a and 5.2b show the hysteric response of concrete in both compression and tension. The slip distortion was taken into account according to the model by Vecchio and Lai (2004). Concrete strength enhancement due to confinement was considered using the Kupfer/Richart model for the concrete located within the region of concentrated reinforcement.The hysteretic model of the reinforcement was according to the Seckin model (Bauschinger) shown in Fig. 5.3. Figures 5.4a and 5.4b show the test walls in the laboratory and finite element meshes with seismic lumped masses used for the analyses of the walls in VT2. The axial force (90.7 kN) induced by post-tensioned vertical bars was considered as a static force and modeled as a point load at top of the wall. The self weight of the wall was considered for both the static axial load and seismic loads. The seismic mass of each floor was distributed at the nodes of that floor.

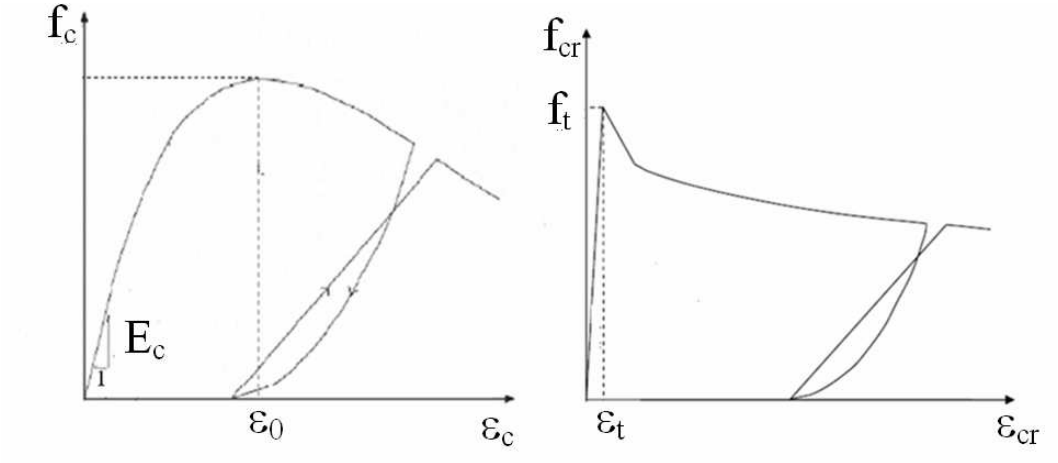

Fig. 5.2: Hysteretic response of concrete in VecTor2 program: (a) Compression; (b) Tension.

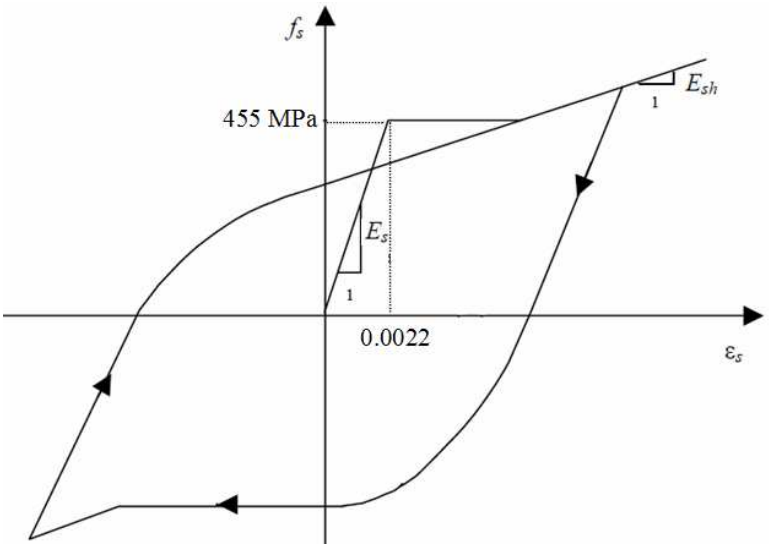

Fig. 5.3: Hysteretic response of steel reinforcement in VecTor2 Program.

a) b)

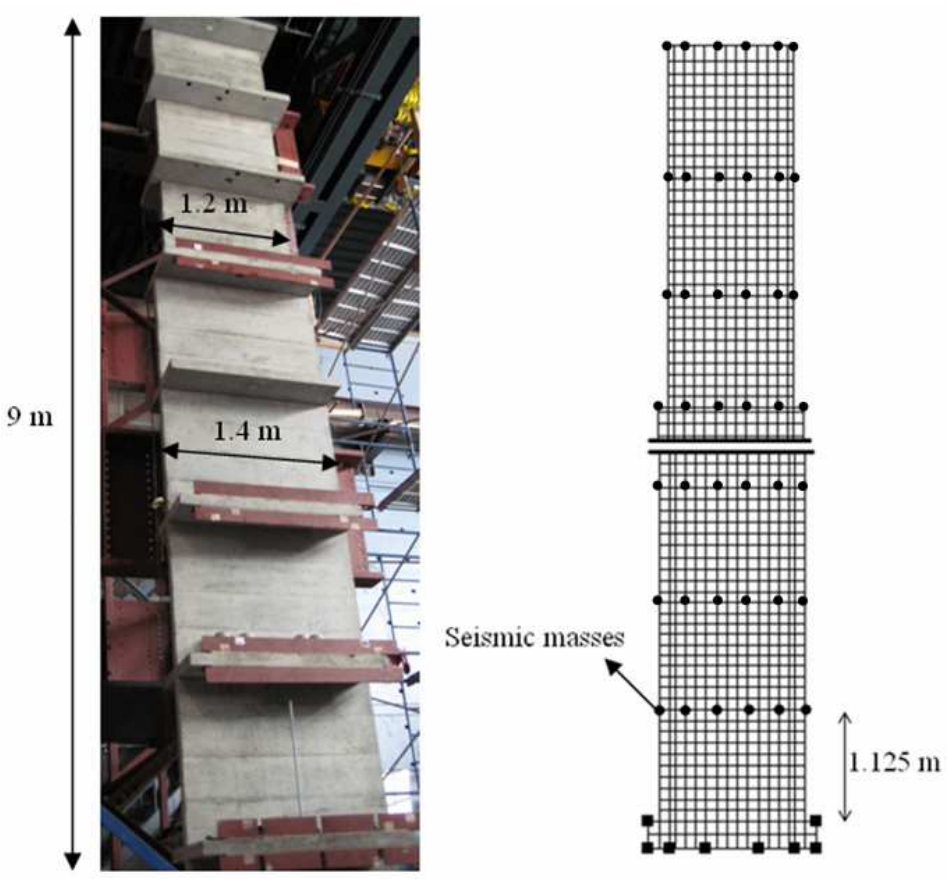

Fig. 5.4: (a) Model walls tested in the laboratory; (b) FE model created in VecTor2.

5.5 Comparison of Seismic Responses between Experiments and Numerical Models

5.5.1 Dynamic Characteristics

Table 5.1 compares the dynamic characteristics and peak responses of the walls obtained from the experiment and numerical models. The first natural periods obtained from analyses are shown in Table 5.1. They are generally close to the values obtained from free vibration response of the wall specimens in impact tests. As nonlinearity is increased in the walls, the numerical natural

periods of the walls elongate approximately in the same proportion as the experimental values, which shows that stiffness degradation and plasticity are well captured by the RC constitutive models.

Although 1.0% constant viscous damping was used for VT2 analyses, the damping calculated with VT2 from free vibration response at the end of each test is significantly larger and closer to the experimental values, except for the first three tests on Wall W2. This could be due to friction between the wall lateral supports and the wall itself. The additional damping in VT2 could also come from the hysteretic behaviour of the steel and concrete materials and from the energy dissipation by opening and closing of the cracks as well as from tangential crack motions modeled in VT2.

5.5.2 Damage and Crack Patterns

Under the 100% design earthquake, the crack pattern observed in the tests and computed from VT2 analysis are in fair agreement. The ability of the program to predict cracking and damage is illustrated in Fig. 5.5 where the crack patterns observed in Wall W2 under the 200% EQ (maximum intensity) is compared to the prediction by VT2. The lengths of the plastic hinge at the base and at the 6^{th} level are equal to the story height in both, the test observations and the FE model. The cracks at the base are a combination of inclined shear cracks and horizontal bending cracks (Fig. 5.5c), which is well predicted by the FE model (Fig. 5.5d). In the tests, shear cracks were not observed at the 6^{th} level (Fig. 5.5b) and the crack pattern obtained from FE analysis (VT2) agrees very well with the test results (Fig. 5.5c).

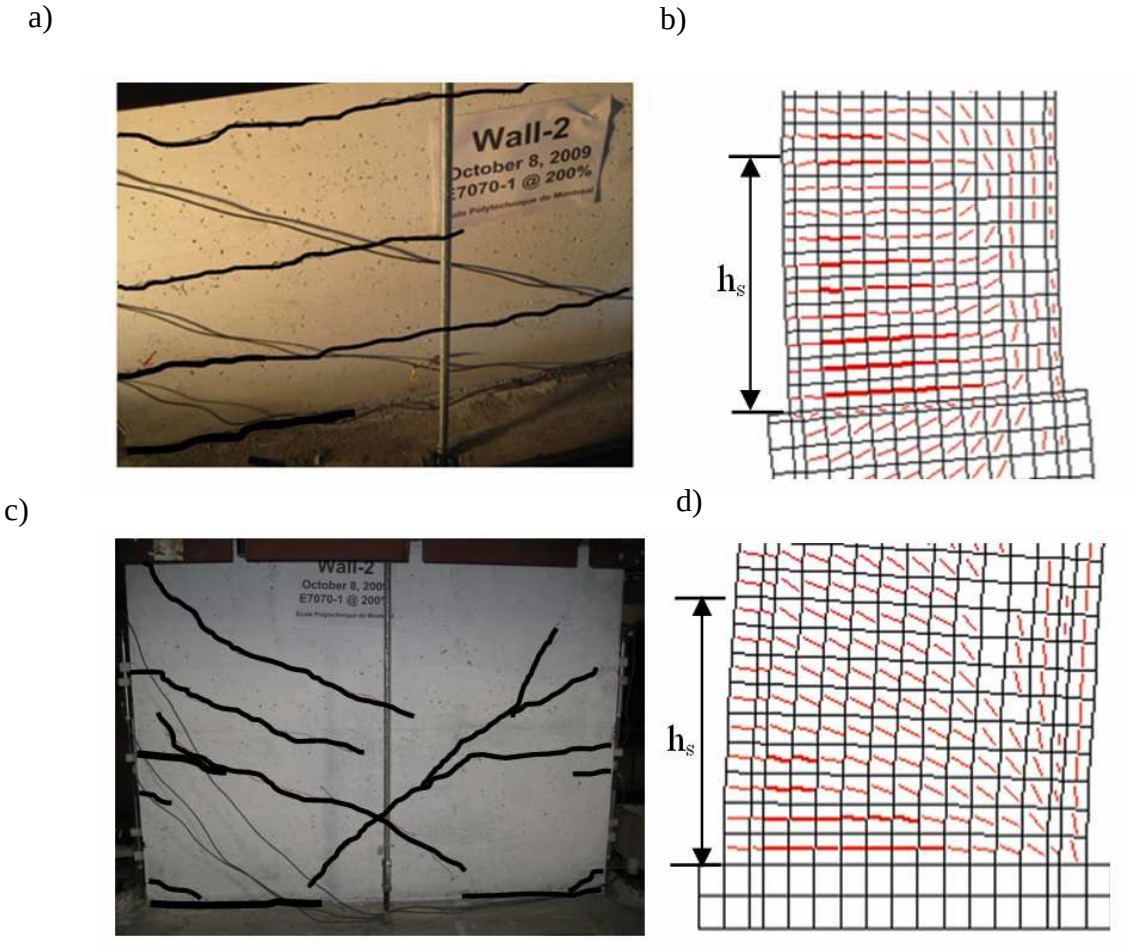

Fig. 5.5: Cumulative crack patterns in Wall W2 under 200% EQ: (a) 6th level from test; (b) 6th level from VecTor2; (c) at the base from test; and (d) at base from VecTor2.

5.5.3 Displacement Response

In Table 5.1, the maximum top displacements ($\Delta_{max\ (top)}$) of Wall W2 under the 100% EQ that are obtained from OS and VT2 are very close to the experimental values. This is especially the case for Wall W2 under 100% design earthquake which was initially undamaged. Figure 5.6 compares the top displacement histories of Walls W1 and W2 under the 100% EQ to the top displacements obtained from OS and VT2. Results from OS in Figs. 5.6a and 5.6b agree well with the

experimental values. Although VT2 in Figs. 5.6c and 5.6d leads to out-of-phase responses in comparison with the experiments, the prediction follows the same displacement patterns as in the test. Figures 5.7a&b compare the distribution of the drifts along the height of Walls W1 and W2 under the 100% EQ. VT2 produced values closer to the experiment, whereas OS generally follows the same deformation pattern but with slightly larger deformations.

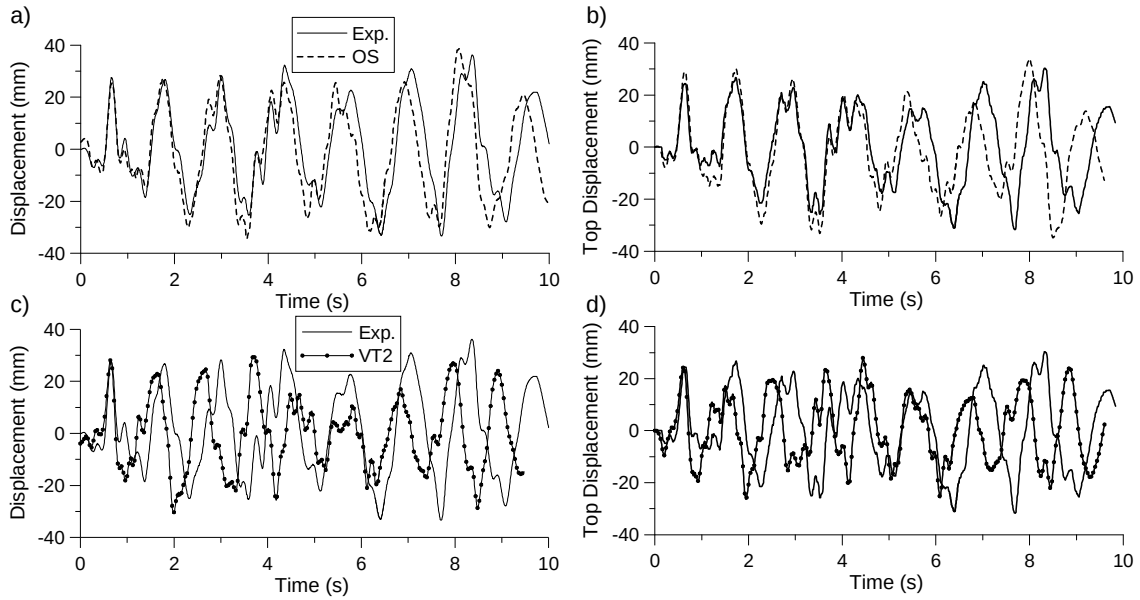

Fig. 5.6: Top displacement history for Walls W1 and W2 under 100% EQ: (a) OS *vs* Test for Wall W1; (b) OS *vs* Test for Wall W2; (c) VT2 *vs* Test for Wall W1; and (d) VT2 *vs* Test for Wall W2.

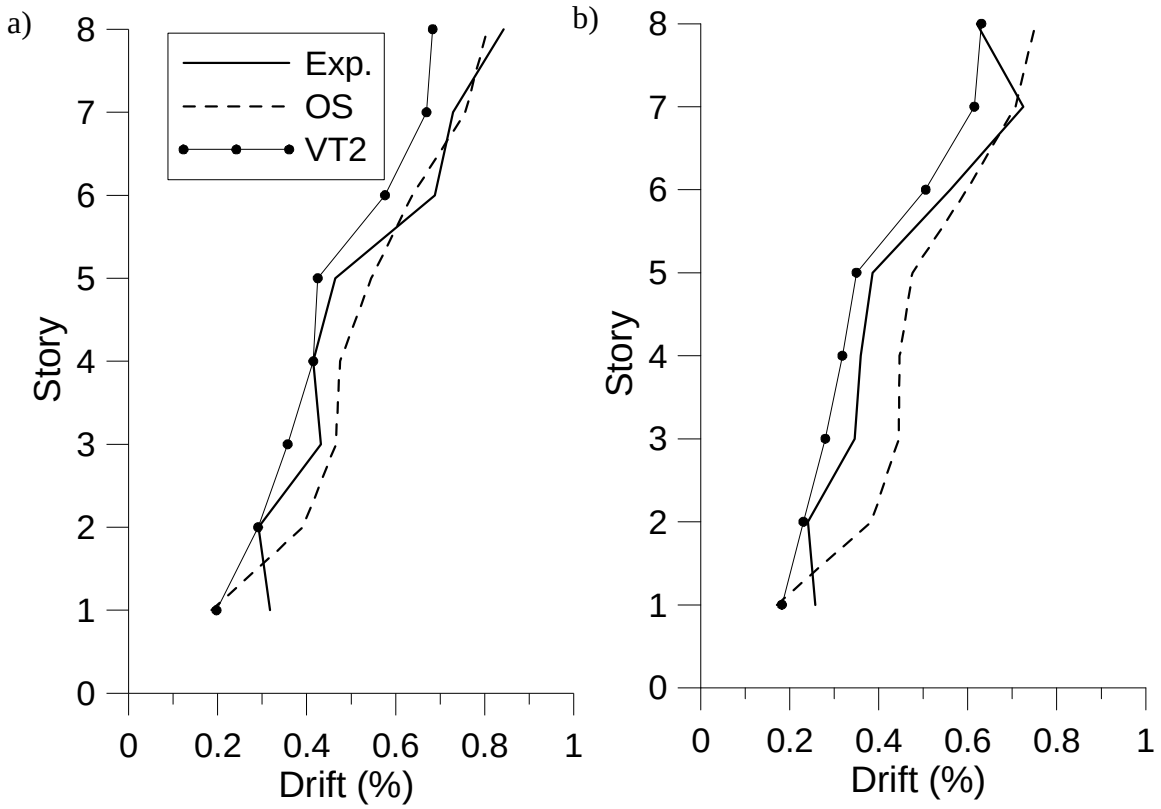

Fig. 5.7: Vertical distribution of drifts under 100% EQ for Wall: (a) W1; (b) W2.

5.5.4 Flexural and Shear Responses

In Table 5.1, the maximum base shear, the shear at the 6th level, and the bending moment at the base that are obtained from numerical modeling are compared to the experimental results. The shear forces from OS are in good agreement with the experiment. The moments at the base of Walls W1 and W2 from OS and VT2 are very similar to the experiment results. Figure 5.8 compares the shear and moment distributions along the height of Walls W1 and W2 as obtained from tests and the numerical models under the 100% EQ. The moment distributions obtained from OS in Figs. 5.8b&d are nearly the same as the test values. In Fig. 5.8a, base shear obtained from OS for wall W1 is around 16% more than the test, that could be due to previously damaged condition of wall W1 but as the wall W2 was undamaged initially, OS could predict very well the

distribution of the shear forces (Fig. 5.8c). VT2 predictions of the base moments in Figs. 5.8b&d for W1 and W2 fairly close to the experimental values. Due to higher mode response, the base shears in the walls were amplified in both the tests and the numerical modeling.

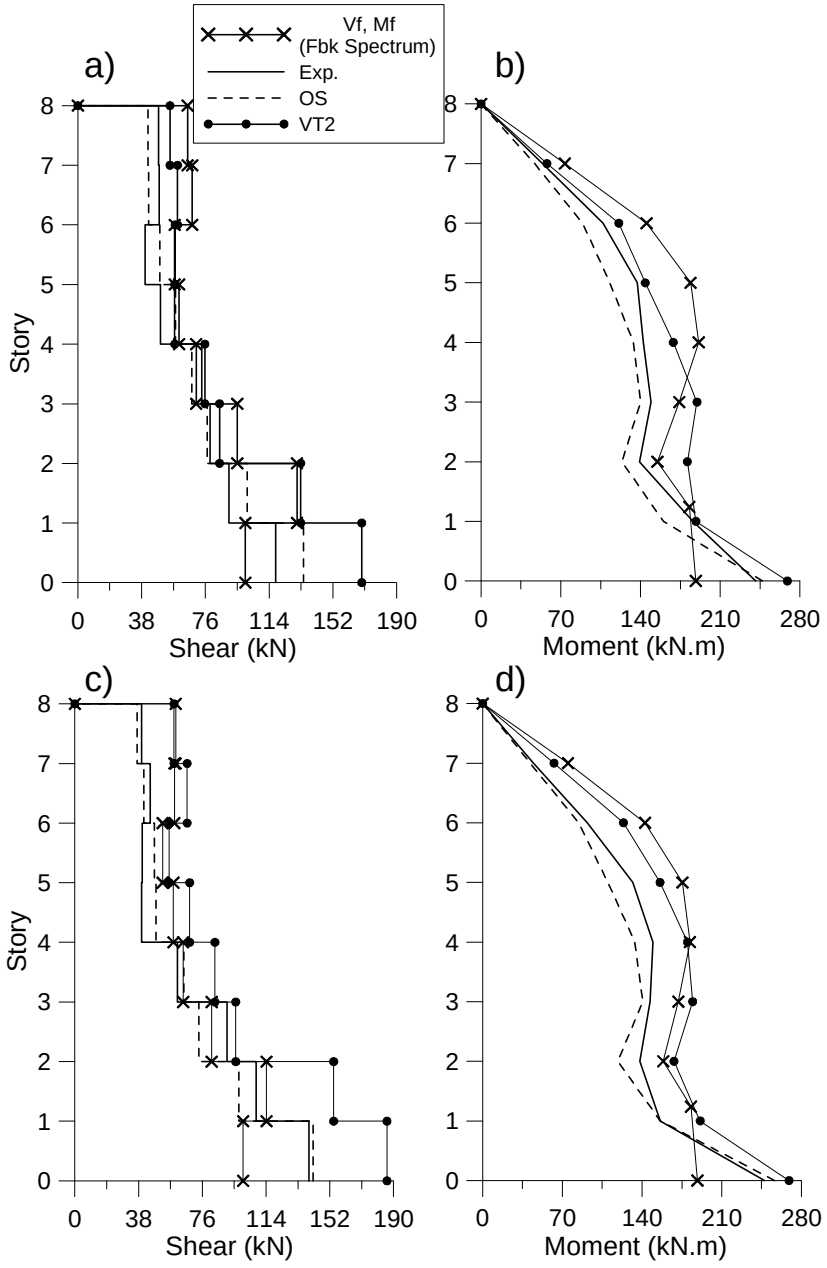

Fig. 5.8: Vertical force distribution under 100% EQ: (a) Shear distribution for Wall W1; (b) Moment distribution for Wall W1; (c) Shear distribution for Wall W2; and (d) Moment distribution for Wall W2.

Figures 5.9a&b present the vertical distribution of the horizontal accelerations along the height of Walls W1 and W2 at the time of maximum base shear under 100% EQ. Lateral inertia forces, or seismic loads, acting on the walls directly correspond to the accelerations shown. The lateral force patterns obtained from tests show significant contributions from the second and third modes of vibration. Both OS and VT2 predict the same patterns, especially for Wall W1.

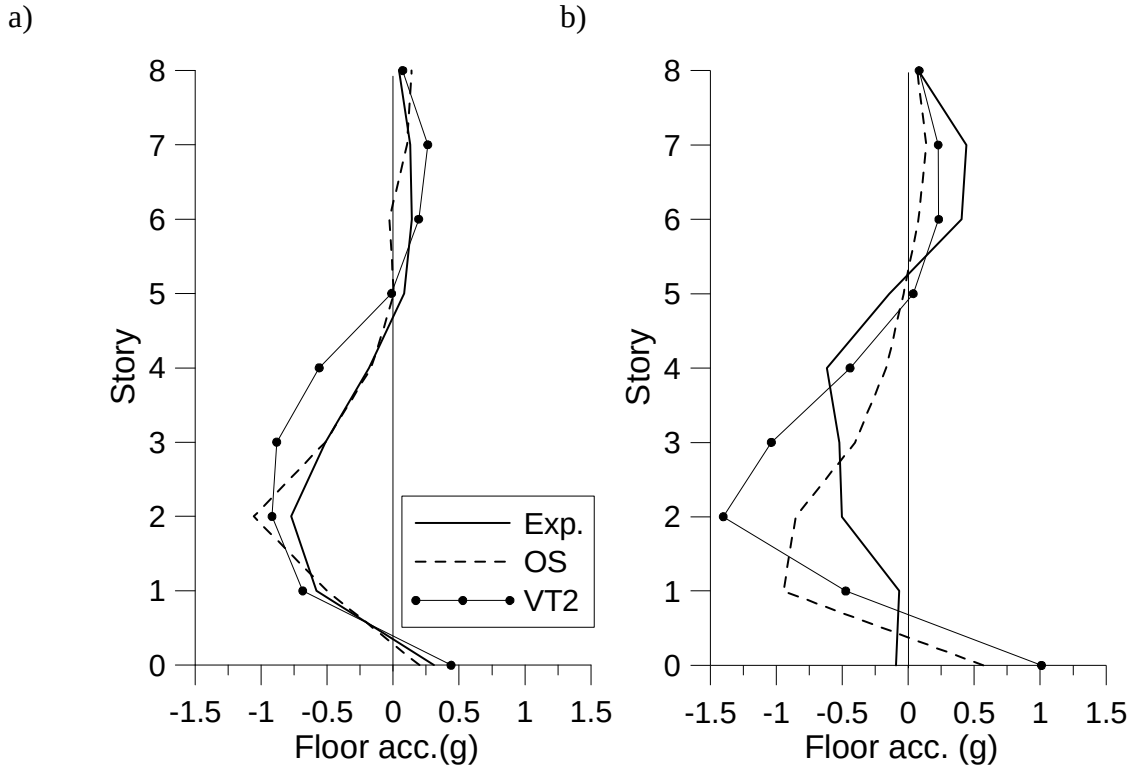

Fig. 5.9: Vertical distribution of horizontal accelerations under 100% EQ for Wall: (a) W1; (b) W2.

5.5.5 Hysteretic responses

Figures 5.10 and 5.11 show the comparison of the moment-rotation responses from numerical and experimental results for Walls W1 and W2 under 100% EQ. In both walls, inelastic rotations could be observed at the base and at the 6^{th} level of the walls. Both the VT2 and OS programs

give flexural stiffnesses that are close to the measured values. In Figs. 5.10a&c and Figs. 5.11a&c, OS predictions match fairly well the test hysteric responses at the 6th level as the computed force demand and rotational ductility are very close to the test results. VT2 also showed good match with the experimental hysteretic moment-rotation curves, especially for Wall W1 (Fig. 5.10). In Fig. 5.11b, the moments and rotations obtained from the VT2 analysis at 6th level of Wall W2 are larger than the corresponding experimental values.

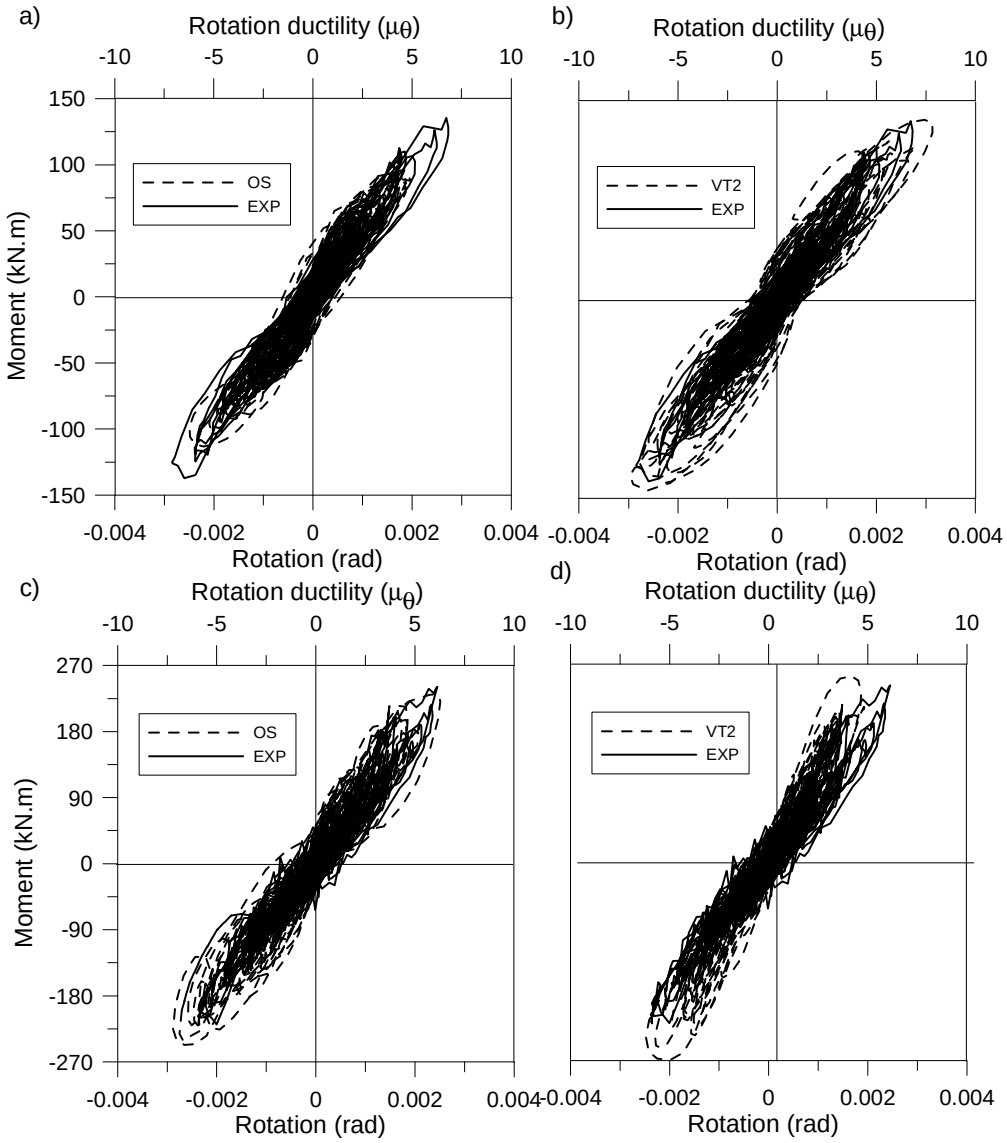

Fig. 5.10: Moment-Rotation response of Wall W1 under 100% EQ: (a) OS *vs* Test at the 6th level; (b) VT2 *vs* Test at the 6th level; (c) OS *vs* Test at the base; and (d) VT2 *vs* Tests at the base.

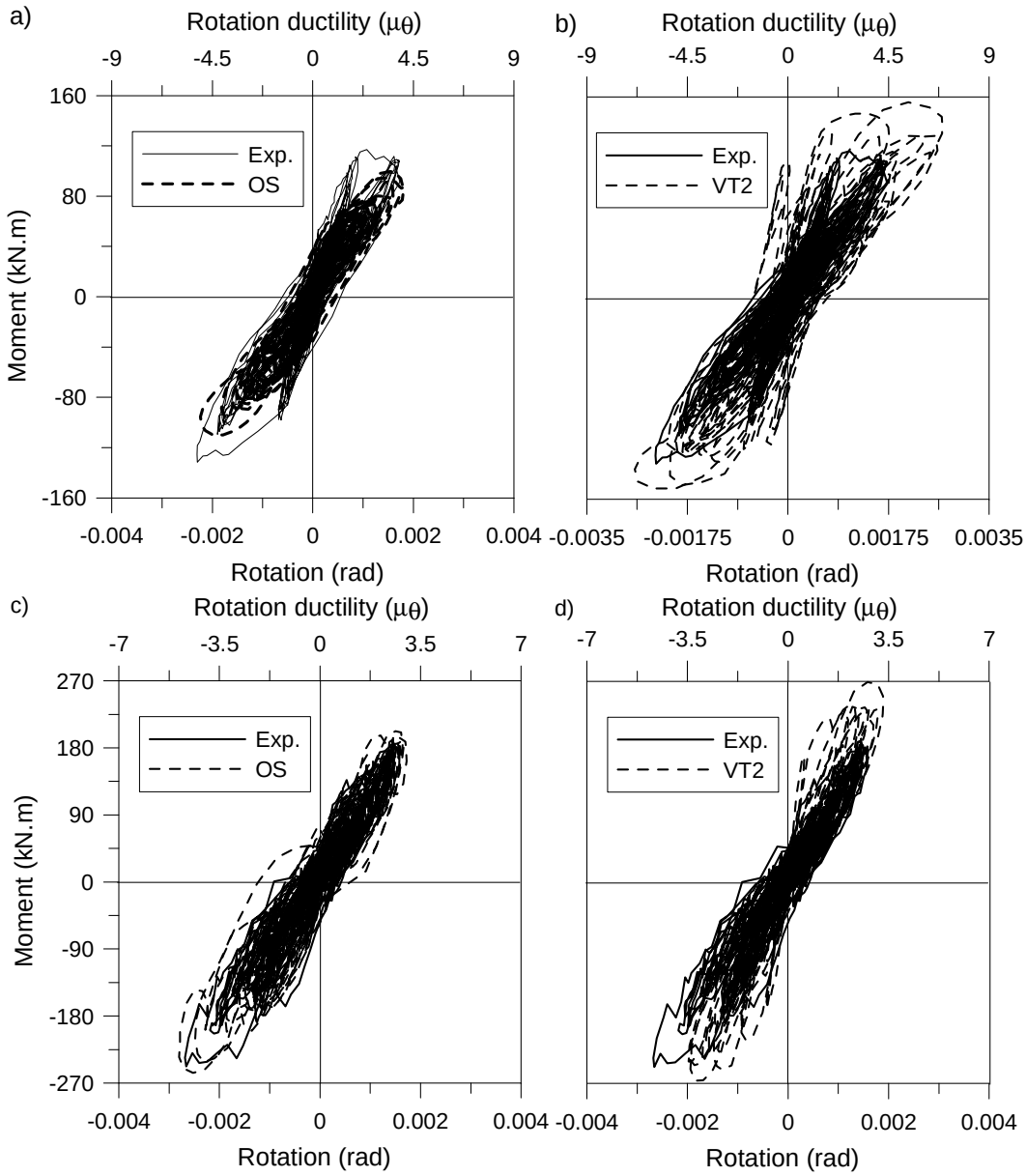

Fig. 5.11: Moment-Rotation response of Wall W2 under 100% EQ: (a) OS *vs* Test at the 6th level; (b) VT2 *vs* Test at the 6th level; (c) OS *vs* Test at the base; and (d) VT2 *vs* Tests at the base.

The VT2 program has the ability to predict cracking due to shear and bending, the interaction of these cracks in concrete members, and the shear deformation responses including the reduction in shear stiffness due to bending and shear cracks. Fig. 5.12 shows for Wall W2 the shear deformations in the base level versus the base shears under the 200% EQ, as obtained from the test and VT2. According to this figure, the average shear stiffness reduced by 88% in the test.

The figure shows that it was possible to reproduce well that stiffness degradation with the VT2 program. Good agreement for the maximum shear deformations is achieved between the test results and the VT2 prediction.

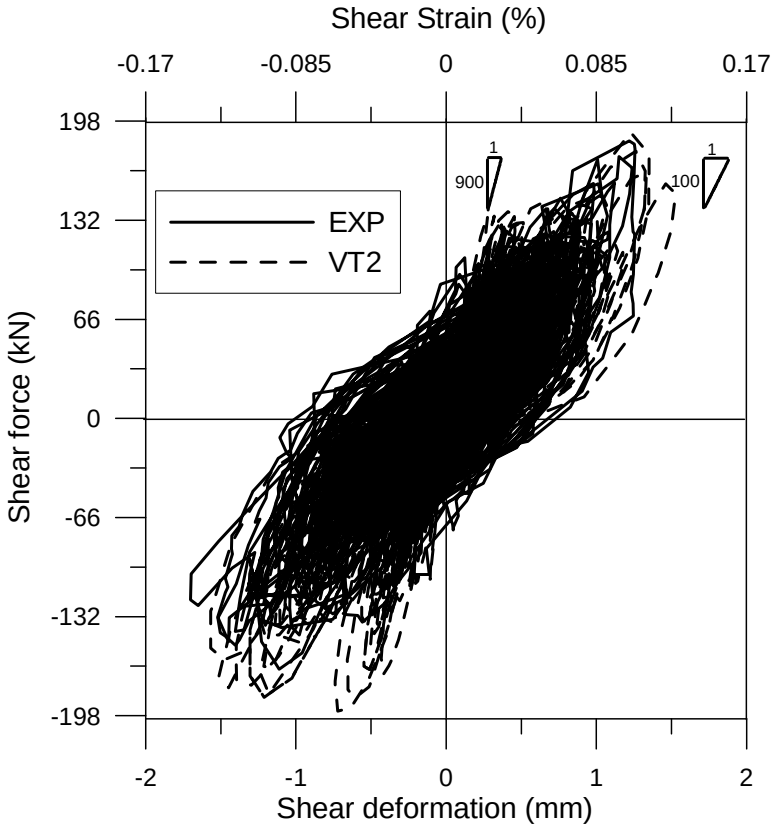

Fig. 5.12: Base shear vs. shear deformation response of Wall W2.

5.5.6 Time history of Shear *vs* Plastic Rotation Demand

The maximum base shears reached in wall W2 under 100% EQ reached approximately 1.15 times the wall nominal shear strength computed using the actual material properties. No shear failure was observed in that test. The wall could even resist the 30% greater shear demand that was imposed when applying the 200% EQ. In CSA-A23.3, the contribution to the cracked concrete to shear resistance varies with the expected hinge inelastic rotation: it is maximum up to an inelastic

rotation of 0.005 rad and decreases linearly to zero as the inelastic rotation reaches and exceeds 0.015 rad. The shear resistance of concrete is neglected for plastic rotation greater than 0.015 rad. The shear and rotation measured at the base of Wall W2 are plotted in Fig. 5.13 for the 100% and 200% EQ tests. The predictions from OS are also given in the graphs. For both the 100% and 200% intensities, it is noted that maximum base shear occurred before the maximum plastic rotation. That time lag before maximum rotation and maximum base shear is due to the fact that the former is dominated by the first mode shape whereas the second is governed by second and higher mode response. This behaviour can be of significance when assessing the performance of shear wall structures as the contribution of the concrete to shear resistance may depend on the sequence of these peak rotation and shear demand values. The figure shows that the OS analysis was capable of predicting accurately this behaviour.

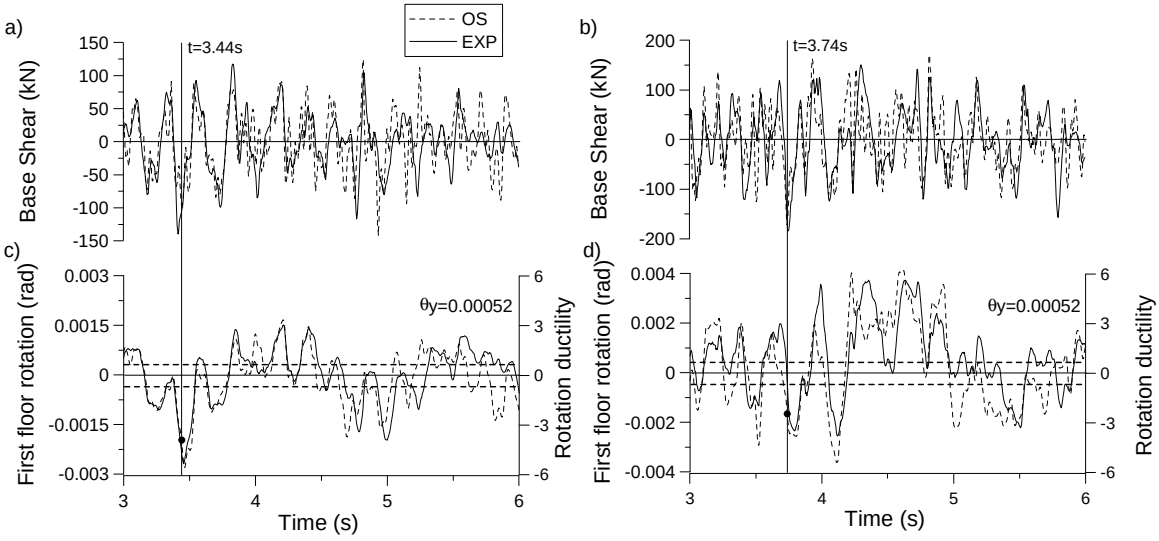

Fig. 5.13: (a) Base shear history for Wall W2 under 100% EQ: (b) Base shear history for Wall W2 under 200% EQ; (c) Base rotation in Wall W2 under 100% EQ; and (d) Base rotation in Wall W2 under 200% EQ.

5.5.7 Summary

The above comparisons show that OS can be used for the reinforced concrete shear walls dominated by flexural modes where the flexural stiffness reduction is more significant than the shear stiffness reduction, otherwise using of VT2 could be more beneficial if we are looking at the shear stiffness reduction coupled with the bending moment..

5.6 Dual Hinge Seismic Design for Higher Mode Effects

The CSA-A23-04 seismic design provisions are based on the assumption that a single plastic hinge will form at the wall base. The wall is first designed for flexure at the base and bending moments above the plastic hinge region and all shear forces from analysis are then amplified based on the bending moment resistance that is supplied at the wall base. This approach is proposed as an attempt to ensure that the wall will not fail in shear and will not develop inelastic flexural response above the plastic hinge. The analyses presented in this chapter and test results presented in the previous chapter show that higher mode effects under high frequency ground motions can lead to inelastic rotation at or above the wall mid height. Adding more longitudinal reinforcement steel at these locations to keep an elastic response in that region is likely to increase further the higher mode demand on the wall, especially the base shear forces (Ghorbanirenani et al. 2009b; Panagiotou and Restrepo 2009).

An alternative approach consists in allowing and designing for a second plastic hinge to form in the upper part of the wall, in addition to the base hinge, so that seismic energy can be dissipated more effectively and the force demand on the wall be controlled by yielding at predefined

location that have been properly detailed. In such a dual plastic hinge design approach, the question is to determine the best location and the flexural strength that must be assigned to that second (top) hinge so that inelastic flexural response is well balanced between the two hinges. For high ductility walls, Panagiotou and Restrepo (2009) proposed to locate the second hinge at mid-height of the wall and to design the wall for flexure at this location for 33% of the wall expected flexural strength at the base, including material overstrength and strain hardening effect. For walls with moderate ductility, we propose a different approach in which the two plastic hinges are designed for the bending moments that are obtained from response spectrum analysis without, any amplification. The two hinge regions are detailed according to current seismic provisions to sustain the anticipated inelastic demand. Bending moments and shear forces from analysis are then amplified for the design of the wall segments outside of the two hinge regions, i.e., in segments AB and CD in Fig. 5.14a. The amplification is based on the ratio of the factored moment resistance, M_r, and the factored bending moment from analysis, M_f, calculated above the base and upper hinges for segments AB and CD, respectively. The hinge regions should be designed for the shear forces that correspond to the development of their nominal moment.

Wall W2 is used herein to illustrate this dual hinge design procedure. Bending moments are first obtained from elastic response spectrum analysis using the NBCC 2005 design spectrum for the site studied, and are then reduced by the product of the overstrength- and ductility-related force modification factors, R_oR_d = 2.8, as described in the previous chapter. In the original design of the wall specimen, the flexural steel at the base was determined from that demand. The design moments above the base hinge region and the shear demand over the wall height was amplified based on the flexural strength supplied at the hinge, as also described in the previous chapter. The wall was analyzed under simulated ground motion that has been spectrally matched to the design

spectrum (see Chapter 4) using the OS modeling technique. Inelastic rotations θ_p = 0.0018 rad and 0.0016 rad developed at the base and 6th levels, respectively. In the dual-hinge concept, the wall is redesigned for plastic hinge at the 6th level, where it occurred in the original design. The design moment in that hinge region was taken equal to the value obtained from analysis and reduced by R_oR_d, but without amplification. In that case, inelastic rotations θ_p = 0.0013 rad and 0.0018 rad developed at the base and the 6th level. Although the rotation responses at 6th level look similar, an important difference is that inelastic rotation in the dual-hinge wall is forced to develop in areas where proper detailing has been provided, which is not the case in the conventional single-hinge design. Finally, the single-hinge design was modified by adding reinforcing steel in the upper floors such that inelastic response at the 6th level is prevented. The envelope of shear forces and bending moments obtained from analysis of the dual-hinge design and the modified single-hinge design are plotted in Figs. 5.14b and c, respectively. Design shears and moments used for the dual-hinge wall are also shown in the figure. In Fig. 5.14b, the moment demand along the wall height resulting from the dual-hinge concept is lower than the demand on the wall designed for hinging at the base only. The reduction in bending moments is maximum at the wall mid-height, whereas the moments at the base of the wall remained close to the wall nominal flexural strength. The dual-hinge design also led to a reduction of the base shear forces, an indication that this design approach can be beneficial in reducing dynamic amplification from higher mode response. As pointed out by Panagiotou and Restrepo (2009), more pronounced reductions in internal forces resulting from dual-hinge design can be expected for taller walls, including reductions in base shear forces.

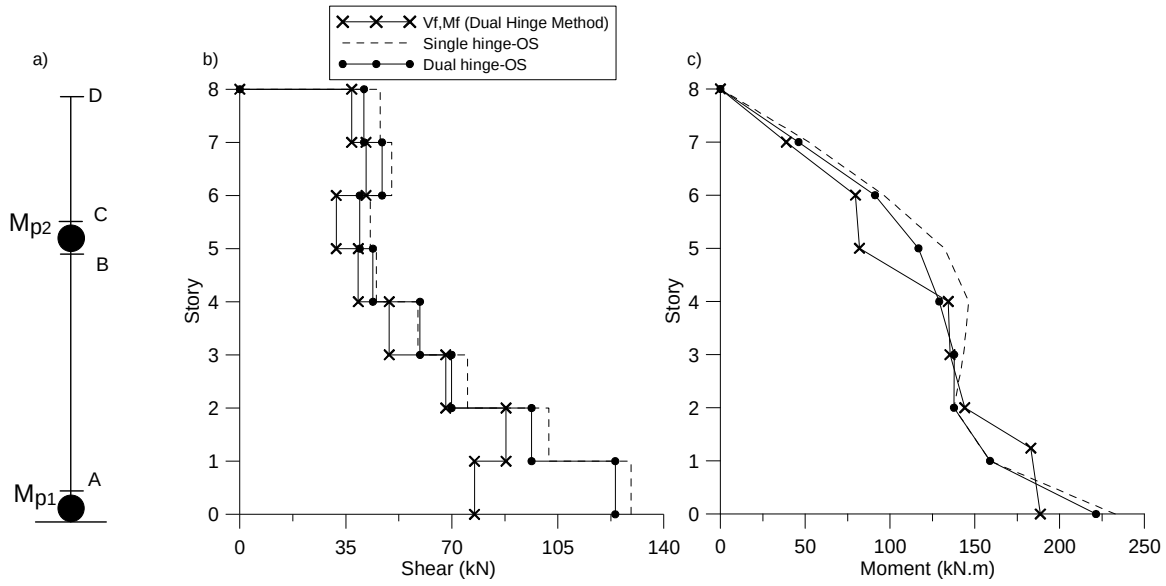

Fig. 5.14: Analysis of Wall W2 based on the dual-hinge and modified single-hinge design approaches: (a) Location of hinges; (b) Shear force distribution along the wall height; and (c) Moment distribution along the wall height.

5.7 Conclusions

In this chapter, the results of two series of shake table tests on high rise reinforced concrete walls were analyzed through numerical simulations. The walls were modeled using the finite element method using the VecTor2 (VT2) program and with the fibre element method using the OpenSees (OS) platform. An innovative seismic design approach involving the formation of two plastic hinges along the wall height has been proposed to address and control the higher mode actions on the response of slender reinforced concrete shear walls. The following conclusions and recommendations can be drawn from this study:

1- Both the finite element (VT2) and fibre element (OS) methods could predict the wall natural periods for the tests in the elastic or damaged conditions. The OS and VT2 models could predict well the wall base moments for all test series. In the elastic range or partially damaged situations, VT2 predicted shear forces larger than the experimental values whereas the shear forces from OS

analyses were very close to the test values, especially for Wall W2 which was initially in the undamaged condition when the design seismic excitation was applied.

2- The damping ratios computed at the end of the VT2 analyses gradually increased due to the accumulation of damage, and the values were close to the experimental results.

3- The VT2 program was able to predict the combined shear-flexural cracks at the base and the bending cracks at the 6^{th} level. Excellent match was obtained with the observed crack patterns from the tests.

4- The tests showed that a second plastic hinge formed at the 6^{th} level of the walls, in addition to the base hinge, due to higher mode effects. This behaviour was also computed using the OS and VT2 modeling techniques and there was a good agreement in moment-rotation responses between the test results and numerical models.

5- Comparison between the shear force-shear deformation responses from VT2 and tests showed that the VT2 program is able to predict shear deformations and shear stiffness degradations of walls due to shear cracking. The shear deformations obtained from the tests were very close to the values predicted by VT2.

6- The results of the tests and numerical models showed that the single plastic hinge design concept prescribed in CSA A23.3 standard is inadequate and that the formation of a second plastic hinge in upper level of slender individual walls is unavoidable. Development of the second plastic hinge in addition to the base hinge can dissipate more seismic energy and contribute to reducing the force demand on the wall. A design strategy was proposed in this study for the development of a second hinge acting as a fuse in the upper portion of walls. Due to higher mode response, the base shear forces obtained in the tests and from OS analyses were up to 40% larger than the shear capacity of the wall prescribed by the code. However, shear failure was not observed because the base plastic rotation associated to the higher mode producing the

larger shear forces shear remained small compare to first mode shape, contributing to maintaining high shear resistance from concrete.

The adequacy of the numerical models depends on several user defined parameters, especially for the damping models. This study showed that the addition of a small amount of global viscous damping in combination with a refined reinforced concrete hysteretic model could predict well the seismic behaviour of real structures. With the VT2 program, a viscous damping of 1% led to reasonable results for the studied RC walls. For the OS program, 2% damping resulted in a good match between test and predictions for the 100% EQ test on the initially undamaged wall. When increasing the earthquake intensities, the damping had to be reduced between 1.5% and 1% to achieve good results for a damaged wall with elongated vibration periods. It must be noted that those damping values only apply to the test specimens considered in this study and may not be representative of the damping present in actual building structures.

Additional analyses must be carried out on prototype structures to refine and validate further the multi-hinge design concept for the control of higher mode response. It was shown in this study that fibre element models would be adequate for this purpose and could be used for different height of shear wall structures.

CHAPTER 6

GENERAL DISCUSSIONS

The problem of higher mode effects in slender reinforced concrete walls have been investigated analytically by previous researchers (Blakeley et al. 1975; Filiatrault et al. 1994; Tremblay et al. 2001; Priestly and Amaris 2002; Priestley 2003; Sullivan et al. 2006; Krawinkler 2006; Panneton et al. 2006; Boivin and Paultre 2010). Although the current seismic codes (CSA 2004, CEN 2004, NZS 2006) are applying various approaches to consider the higher mode responses in RC walls, the results of analyses have shown different dynamic responses in compare to Codes. To clarify higher mode effects experimentally, large scale shear wall shake table testing are needed. Due to physical limitations of test facilities, shake table tests must be conducted on reduced scaled models and care must be exercised in selecting scaling factors, model materials and fabrication processes so that the applicable similitude requirements are satisfied and the experiment is representative of actual wall response.

Static and quasi static cyclic loadings tests carried out on RC walls at Structural Laboratory of École Polytechnique, showed that using of scaling factor of 2.3 could be adequate for reinforced concrete walls. The tests confirmed that plastic rotation behaviours, ductility and failure modes could be reproduced well in comparison to those of the actual wall. The capacity design procedure presented in CSA-A23.3-04 standard provides the desired ductility capacity confirmed by the tests. Upon flexural inelastic response, inelastic shear deformations progressively developed in the plastic hinge region of the wall and followed by shear sliding, which led to

significant strength degradation of the wall specimen right after the design ductility. Current code equations for the interface shear resistance should be revisited to provide sufficient protection against this failure mode in ductile shear wall structures. Coupling of nonlinear flexural and shear responses requires the use of realistic material constitutive laws in a finite element (FE) formulation. VecTor2 program used for validation of the tests is able to consider this coupling. This program can adequately capture the most of the nonlinearity responses. Possibly due to excessive tension stiffening effects in the inelastic range, VecTor2 program overestimated the ultimate capacity under monotonic loading. Improvement to the program and related modeling procedures could also be made to better match the ultimate capacity and rate of strength degradation.

Before selecting the prototype wall for shake table test, some preliminary nonlinear time history analysis were carried out on high rise reinforced concrete walls designed according NBCC 2005 and CSA A23.3-04. In these studies three different computer programs were used: Ruaumoko (lumped plasticity), VecTor2 (planar finite elements), and Perform 3D (1D and 2D fibre elements) (Appendices I, II). The aims of the analyses were to evaluate the seismic behaviour of wall and check the wall capacity for shake table tests.

Higher mode effects in slender reinforced concrete shear walls are an important problem that should be considered in design as flexural plastic hinges occur in the upper part of tall walls. This type of seismic inelastic behaviour is not anticipated by the code. Experimental shake table tests were thus planned to validate the predictions made by reinforced concrete wall constitutive models currently used by practicing engineers and researchers. According to the result of the tests, it could be interpreted that the moderate ductile wall (R_oR_d=2.8) designed according to CSA

A23.3-04 have the potential for formation of second hinge at top of the wall. In ductile walls the requirement for minimum steel at top of the wall is more restrict than for wall with moderate ductility. The larger plastic rotation at the base results in more energy dissipation, and top of the wall is less intended to form the second hinge. This could be one possible reason for elastic responses in the upper part of a wall observed from the numerical analyses carried out by Boivin and Paultre 2010. This behaviour also needs more study and analyses for different cases to be clarified.

Although the codes (CSA 2004, CEN 2004, NZS 2006) are trying to prevent the formation of upper hinge, development of another plastic hinge in addition to the base hinge could dissipate more earthquake energy and reduce the demand forces on the wall. The design procedure proposed in this thesis in section 5.6 develops another hinge at top to act as a fuse. This design approach is more effective in high rise walls (10-storey and higher) when higher modes are dominant.

Base shear forces obtained from tests are larger than the nominal shear capacity of the wall. However the shear failure was not observed due to larger concrete shear strength in comparison to the value prescribed by the code (CSA 2004). The time occurrence of maximum rotation and maximum base shear is a key point, because due to maximum plastic hinge rotation the concrete shear strength could be reduced (CSA A23.4 Clause 21.6.9.6, Appendix IV). Usually it was observed and computed that the maximum base rotation occurs in the first mode that dominates the response. While the maximum shear force occurs when higher mode shapes were significantly contributing to the response. Therefore the probability of shear failure due to higher modes becomes less when the transient nature of the response is recognized.

Complementary studies (Appendix III) indicated that in all the reinforced concrete walls designed between 1975-2005 in Montréal Canada, the base shear forces obtained from nonlinear time history analyses exceeded significantly the design shear forces prescribed by codes. Significant attention is also needed for walls designed before 1975 when the capacity design approach was not yet introduced. The analysis results of this type of wall showed very large plasticity at the mid height and large base shear forces in comparison to the design shear force (NBCC 1975).

The shake table test results were also applied to validate the numerical modeling by OpenSees and VecTor2. Fibre element method is a faster solution to get the results of large slender wall and for the structures dominated by bending effects. The results are in good agreement with the experiment. For the structures that have large nonlinear shear deformation and shear failure is expected, VecTor2 program which is based on finite element method could be a useful instrument. This program is able to reproduce fairly well the nonlinear shear deformation coupled with the moment and the shear sliding of the structures, as it was shown in the cyclic test of this thesis.

As VecTor2 is able to model the most of nonlinearity behaviour of reinforced concrete, very small viscous damping should be used just for convergence. Using of 1% damping in this study showed the top deformation of the wall is 9% less than the experiment and just for verification, an additional analysis showed that 0.5% damping gave the top deformation of 9% more than the test results, so using values of 0.5%-1.0% damping in VecTor2 could be adequate for reinforced concrete walls (Appendix I). In OpenSees program that some source of nonlinearity such as shear cracks and slips could not be modeled. Higher value of damping should thus be applied. As much as damage is developed inside the structure, the system dissipate more energy and less

damping should be used for different level of ground motion amplitudes, which was between 2%-0.5% in this study.

More complete details related to this general discussion can be found in Appendixes:

- I (Inelastic Seismic Evaluation of Slender Shear Walls Designed According to CSA-A23.3-04 and NBCC 2005),
- II (Seismic Response of Multi-Storey Reinforced Concrete Walls Subjected To Eastern North America High Frequency Ground Motions),
- III (Distribution of Inelastic Demand in Slender R/C Shear Walls Subjected to Eastern North America Ground Motions), and
- IV (Shake table tests and repair of ductile slender reinforced concrete shear walls).

CONCLUSIONS AND RECOMMENDATIONS

In this research project two types of static and dynamic testing were carried out on reinforced concrete shear wall models.

The first series of tests were to evaluate the capacity design approaches applied in Canadian standards. Two identical prototype wall specimens were designed, detailed, and fabricated according to the provisions of NBCC 2005 and the CSA-A23.3-04 standard. The specimens were tested under monotonic and quasi-static cyclic loading, respectively.

To validate the similitude laws and scaling factor, two identical 1:2.37 reduced scale models of the prototype walls were also constructed and subjected to the same loading protocols. In the cyclic tests, both the prototype and model wall specimens showed that the capacity design approach specified in codes led to a stable hysteric response dominated by flexure up to a displacement ductility of 4.0. The walls could achieve and exceed the ductility capacity of 3.5 implied in Canadian code design provisions for ductile shear walls. Due to coupling of shear and flexural inelastic responses, inelastic shear deformations progressively developed in the plastic hinge region of the wall specimens. These shear deformations should be accounted for in the prediction of the inelastic seismic response of cantilevered wall structures. Just after reaching the design ductility of 3.5, shear sliding started to develop in both tests, which led to significant strength degradation of the wall specimens. Current code equations for the interface shear resistance could be revisited to provide sufficient protection against this failure mode in ductile shear wall structures. Excellent agreement under both loading protocols was found between the responses of the prototype and the reduced scale model specimens. This suggests that reduced scale models designed with a scaling factor of up to 2.4 and constructed with normal concrete

mixes and deformed bars for the main reinforcement can be used to examine the seismic response of ductile shear wall structures, including inelastic flexural and shear deformation effects and shear sliding mechanisms.

Numerical analyses were also performed with the VecTor2 finite element program after testing to assess the ability to reproduce the test wall response under both loading conditions. Comparison between the experimental and numerical results showed that VecTor2 can adequately capture the inelastic monotonic and cyclic behaviour of ductile shear walls, including initial stiffness, shear deformations, force demand in the transverse steel, energy dissipation, and failure mechanisms. The VT2 program overestimated the ultimate capacity under monotonic loading, possibly due to excessive tension stiffening effects in the inelastic range.

The second series of tests were to investigate higher mode effects through shake table testing on two identical models of an individual reinforced concrete shear wall representative of an 8-storey residential building located in Montréal, QC, Canada. The specimen walls were designed and fabricated according to the seismic provisions of NBCC 2005 and CSA A23.3 standard for moderately ductile walls. The specimens were subjected to a ground motion record rich in high frequency energy, as anticipated in Eastern North America, and tests were performed at different ground motion amplitudes.

Under the design level base motion, the specimens experienced limited inelastic flexural response at the wall base, as anticipated, as well as at the 6^{th} level, which was not expected in design. This behaviour resulted from significant higher mode response under the high frequency motions, as was confirmed by the vertical distribution of horizontal loads, internal forces and other deformation response indicators. Both bending and shear cracks were observed at the wall bases

whereas flexural cracks only formed at the 6th level, which is consistent with the respective shear force demand to supply ratios at the two locations. When increasing the ground motion amplitude beyond design level, additional inelastic rotation only developed at the 6th level.

The maximum bending moment at the base of the walls under the design level base motion reached to the actual flexural resistance of the wall which is 1.3 times of design value. This ratio approximately corresponds to the overstrength factor R_o = 1.4 assumed in design. The maximum top displacement ductility of the walls was 35% higher than the ductility-related factor specified in NBCC associated to drift. This difference was caused by the inelastic rotation that developed at the 6th level, rather than being concentrated in the base plastic hinge, as assumed in design. The maximum plastic rotation at the base however corresponded to the value obtained assuming first mode response.

The maximum base shear forces obtained from tests exceeded the wall design shear strength by the factor of 1.4. This value is close to dynamic amplification proposed in NZS 3101 for an 8-storey wall. However shear failure was not observed due to a greater than expected contribution from concrete to shear resistance. This higher concrete capacity resulted from peak shear force demand occurring before the development of significant cracking and inelastic rotation at the wall base. After inelastic response, the concrete shear strength corresponded to that obtained using a value of 0.18, instead of 0.10, for the reduction factor β accounting for shear resistance of cracked concrete. These results suggest that it could be beneficial to apply a base shear dynamic amplification factor, similar to the one specified in the NZS 3101 standard, in CSA A23.3 to decrease the risk of shear failure.

By increasing the ground motion amplitudes, higher mode response of the walls was slightly more pronounced and it resulted in higher rotation at the 6th level.

After the shake table testing, the two original walls were rehabilitated with the collaboration of Concordia University using two different rehabilitation schemes utilizing carbon fibre-reinforced polymer (CFRP) composite sheets at the plastic hinge locations (base panel and 6th storey). The rehabilitated walls were retested by subjecting them to the same ground motion excitation levels applied to the original walls. The natural frequencies of the rehabilitated walls were found to be higher than those of the damaged original walls and close to the values measured for the undamaged original walls. Both rehabilitated walls performed efficiently showing improved flexural strength at the 6th storey panel. Upon increasing the seismic ground motion intensity, the damage (cracking, plasticity) was found to spread in the other unrehabilitated storeys.

The results of shake table tests on two original slender reinforced concrete walls were analyzed through numerical simulations. The walls were modeled using the finite element method with the VecTor2 (VT2) program and the fibre element method using the OpenSees (OS) platform. The natural frequencies of the walls were predicted very well by both modeling techniques, both in the elastic and nonlinear ranges. The base moment obtained from VecTor2 and OpenSees were very close to the test results and OpenSees could estimate well the base shear force obtained from the tests. The crack pattern computed with VecTor2 at both the wall base and 6th levels matched very well with the crack patterns observed in the tests. The formation of a second plastic hinge at the 6th floor was observed in the numerical modeling and the numerical moment-rotation responses were in good agreement with the test results.

In this research, an innovative seismic design approach involving the formation of two plastic hinges along the wall height was proposed to address and control the higher mode actions on the

response of slender reinforced concrete shear walls. Numerical simulations of a so-designed wall showed that the development of a second plastic hinge in addition to the base plastic hinge can increase the seismic energy dissipation and contribute to reducing the force demand on the wall.

The adequacy of the numerical models depends on several user defined parameters, especially for the damping models. This study showed that the addition of a small amount of global viscous damping in combination with a refined reinforced concrete hysteretic model could predict well the seismic behaviour of real structures. With the VecTor2 program, a viscous damping of 1% led to reasonable results for the studied RC walls. For the OpenSees program, 2% damping resulted in a good match between test results and numerical predictions for the test on the initially undamaged subjected to the design level earthquake ground motion. When increasing the earthquake intensities, the amount of damping had to be reduced between 1.5% and 1% to obtain good results for a damaged wall with elongated vibration periods. It must be noted that those damping values only apply to the test specimens considered in this study and may not be representative of the damping present in actual building structures.

The test program and analyses confirmed that slender moderately ductile shear walls subjected to high frequency ground motions can experience inelastic flexural response in the upper floor region and dynamic amplification of horizontal shear forces at their bases. In actual buildings where the RC walls are used in combination with frames, higher damping is expected compared to the test specimens examined herein, and these effects may less be pronounced than measured in the tests.

To develop the proposed design guideline considering the higher mode responses, different numerical modeling (e.g. OpenSees) could be done on prototype scale. This design guideline

should follow two directions, first to reduce as much as possible the dynamic shear amplifications and, second, to consider the dual plastic hinge concept and seismic detailing for the second hinge.

Although the shaking table test is one of the best methods to investigate the dynamic behaviour of structures, care is needed to calibrate the frequency response of the shake table to be as much as possible close to the target spectra. This could be done by playing with the acceleration, velocity and displacement parameters of the table while the specimen is installed. Adaptive Inverse Control (AIC) is another option that could be used but it requires more attention.

In this test program, the base excitation was applied in one direction only and the effect of in-plane torsion was neglected. In actual buildings, especially in irregular buildings, the torsion can significantly affect the dynamic responses of the walls. Torsional response could be considered in tests performed on a shake table that can apply the base excitation in two or three directions. In numerical simulations, structural walls should be modeled in 3D to consider the torsion effects and interaction with the other walls.

Usually shaking table tests are very costly and need extensive experimental work. Hybrid testing is another experimental technique that could be considered as a replacement. In this method, only the part of the wall of interest (e.g., 6^{th} floor) can be constructed in the laboratory, with proper boundary conditions, and the rest of the structure is numerically modeled. This technique not only reduces the massive experimental work but also gives the opportunity to do the tests on larger scale, sometime full scale, specimens to validate the design procedures.

REFERENCES

Adebar, P., Mutrie, J., and DeVall, R. (2005). Ductility of Concrete Walls: the Canadian Seismic Design Provisions 1984 to 2004. Canadian Journal of Civil Engineering, 32, (6), 2005, 1124–1137.

ACI (2008). Building Code Requirements for Structural Concrete (ACI 318-08) and Commentary (ACI 318R-08). American Concrete Institute, Farmington Hills, MI, USA.

Amaris, A. (2002). Dynamic Amplification of Seismic Moments and Shear Forces in Cantilever Walls. M.Sc. Thesis, Rose School of Engineering, Pavia, IT, 75 pp.

ATC (1992). ATC-24, Guidelines for Cyclic Seismic Testing of Components of Steel Structures. Applied Technology Council, Redwood City, CA, U.S.A.

Atkinson, G.M. (2009). Earthquake Time Histories Compatible with the 2005 NBCC Uniform Hazard Spectrum. Canadian Journal of Civil Engineering, 36 (6), 991–1000.

Bentz, E.C. (1999). Sectional Analysis of Reinforced Concrete Members. Ph.D. Thesis, Department of Civil Engineering, University of Toronto, Toronto, ON, Canada.

Bentz, E.C. (2001). Response-2000 Reinforced Concrete Section Analysis, Version 1.05. User Manual. Department of Civil Engineering, University of Toronto, ON, Canada.

Bentz, E.C., Vecchio, F.J., and Collins, M.P. (2006). The simplified MCFT for calculating the shear strength of reinforced concrete elements. ACI Structural Journal, 103(4), 614-624.

Blakeley, R. W., Cooney, R. C., and Megget, L. M. (1975). Seismic shear loading at flexural capacity in cantilever wall structures. Bull. New Zealand Nat. Soc. Earthquake Eng., 8(4), 278-290.

Boivin, Y., and Paultre, P. (2010). Seismic performance of a 12-Storey ductile concrete shear wall system designed according to the 2005 National building code of Canada and the 2004 Canadian Standard Association standard. Canadian Journal of Civil Engineering, 37(1), 1-16

CAC (2006). Concrete Design Handbook, 3rd Ed. Cement Association of Canada, Ottawa, ON, Canada.

Carr, A.J. (2004). Ruaumoko-2D (User's Manual), two- dimensional version. Department of civil engineering, University of Canterbury, Christchurch, New Zealand.

CEN. (2004). En 1998-1, Eurocode 8, Design of structures for earthquake resistance, Part 1: General rules, seismic actions and rules for buildings. European Committee for Standardization, Brussels, Belgium.

Cheng, F.Y., Mertz, G. E., Sheu, M. S., and Ger, J. F. (1993). Computed versus Observed Inelastic Seismic Low-Rise RC Shear Walls. Journal of Structural Engineering, ASCE, 119 (11), 3352-3275.

Clough, R.W., Johnston, S.B. (1966). Effect of stiffness degradation on earthquake ductility requirements. Proceedings of the Japan Earthquake Eng. Symp., Tokyo, Japan, 195-198.

CSA. (2004). CSA-A23.3-04, Design of Concrete Structures. Canadian Standards Association, Mississauga, ON, Canada.

CSI. (2006a). SAP 2000: Structural Analysis Program, Computer and Structures, Inc., Berkeley, CA.

CSI. (2006b). Perform 3D: Nonlinear Analysis and Performance Assessment for 3D Structures, Computer and Structures, Inc., Berkeley, CA.

D'Ambrisi, A., and Filippou, F.C. (1999). Modeling of Cyclic Shear Behaviour in RC Members. Journal of Structural Engineering, ASCE, 125 (10), 1143-1150.

EUROPEAN STANDARD (2003). Eurocode 8: Design of structures for earthquake resistance. European Committee for Standardisation, Brussels, Belgium.

Filiatrault, A., D'Aronco, D. and Tinawi, R. (1994). Seismic shear demand of ductile cantilever walls: a Canadian code perspective. Canadian Journal of Civil Engineering, 21 (3), 363-376.

Ghorbanirenani, I., Tremblay, R., Léger, P., and Palermo, D., (2008). Inelastic Seismic Evaluation of Slender Shear Walls Designed According to CSA-A23.3-04 and NBCC 2005. Canadian Society of Civil Engineering (CSCE), Quebec, CA.

Ghorbanirenani, I., Velev, N., Tremblay, R., Palermo, D., and Massicotte, B., and Léger, P. (2009a). Modeling and testing of influence of loading history and scaling effects on the inelastic response of reinforced concrete shear walls. ACI Structural Journal, 106(3), 358-367.

Ghorbanirenani, I., Rallu, A., Tremblay R., and Léger, P. (2009b). Distribution of inelastic demand in slender R/C shear walls subjected to Eastern North America ground motions. ATC&SEI Conference on Improving the Seismic Performance of Existing Buildings and Other Structures, San Francisco, CA, U.S.A.

Ghorbanirenani, I., Tremblay, R., Léger, P., Leclerc, M., El-Sokkary, H., Galal, K., (2010). Shake Table Tests and Repair of Ductile Slender Reinforced Concrete Shear Walls subjected to ENA ground motions. 9th US national and 10th Canadian Conference on Earthquake Engineering, Toronto, Canada.

Grange, S., Kotronis, P., and Mazars, J. (2009). Numerical modelling of the seismic behaviour of a 7-story building: NEES benchmark. Material and Structures, 42(10), 1433-1442.

He, X.G., and Kwan, A.K.H. (2001). Modeling Dowel Action of Reinforcement Bars for Finite Element Analysis of Concrete Structures. Computers and Structures, 79 (6), 595-604.

Kazaz, I., Yakut, A., and Gülkan, P. (2006). Numerical simulation of dynamic shear wall tests: a benchmark study. Computers and Structures, 84(8-9), 549-562.

Krawinkler, H. (2006). Importance of good nonlinear analysis. Struct. Design Tall Spec. Build. 15(5), 515–531.

Lestuzzi, P., Wenk, T., and Bachmann, H. (1999). Dynamic tests of RC structural walls on the ETH earthquake simulator. Report No. 240, IBK, ETH Zurich, Switzerland.

Lu, X., and Wu, X. (2000). Study on a new shear wall system with shaking table test and finite element analysis. Earthquake Engineering and Structural Dynamics, 29(10), 1425-1440.

Martinelli, P., and Filippou, F.C. (2009). Simulation of the shaking table test of a seven-story shear wall building. Earthquake Engineering and Structural Dynamics, 38(5), 587–607.

Moncarz, P.D., and Krawinkler, H. (1981). Theory and Application of Experimental Model Analysis in Earthquake Engineering. Report No. 50, John A. Blume Earthquake Engineering

Center, Department of Civil and Environmental Engineering, Stanford University, Stanford, CA, U.S.A.

NRCC. (2005). National Building Code of Canada, 12th ed. National Research Council of Canada, Ottawa, ON, Canada.

NZS. (2006). NZS 3101.1&2:2006, Concrete Structures Standard: Part 1 – The Design of Concrete Structures. New Zealand Standard, Wellington, New Zealand.

Orackal, K. and Wallace, W. (2006). Flexural modeling of reinforced concrete walls experimental verification. ACI Structural Journal, 103(2), 196-206.

Orbovic, N., Berge-Thierry, C., Bouchon, M., Stojadinovic, B., Arichi, Y., Hong, S., and Mosalam, K. (2004). Safety Significance of Near Field Earthquakes –IRSN Report (Institute for Radioprotection and Nuclear Safety- in French). Paris, France.

Otani, S. (1981). Hysteresis Models of Reinforced Concrete for Earthquake Response Analysis. Joumal of Faculty of Engineering, University of Tokyo, Tokyo, Japan, Series B, 36 (2), 1981, 407-441.

Panneton, M., Léger, P., and Tremblay, R. (2006). Inelastic Analysis of a Reinforced Concrete Shear Wall Building According to the NBCC 2005. Canadian Journal of Civil Engineering, 33 (7), 854-871.

Petrangeli, M., Emilio Pinto, P.E., and Ciampi, V. (1999). Fibre Element for Cyclic Bending and Shear of RC Structures. I:Theory. Journal of Engineering Mechanics, ASCE, 125 (9), 994-1001.

Petrangeli, M. (1999). Fibre Element for Cyclic Bending and Shear of RC Structures. II:Verification. Journal of Engineering Mechanics, ASCE, 125 (9), 1002-1009.

Palermo, D., and Vecchio, F. J. (2002). Behaviour of three-dimensional reinforced concrete shear walls. ACI Structural Journal, 99(1), 81-89.

Palermo, D., and Vecchio, F. J. (2003). Compression Field Modeling of Reinforced Concrete Subjected to Reversed Loading: Formulation," ACI Structural Journal, 100 (5), 616-625.

Palermo, D., and Vecchio, F. J. (2004). Compression Field Modeling of Reinforced Concrete Subjected to Reversed Loading: Verification," ACI Structural Journal, 101 (2), 155-164.

Palermo, D., and Vecchio, F. J. (2007). Simulation of Cyclically Loaded Concrete Structures Based on the Finite-Element Method. Journal of Structural Engineering, ASCE, 133(5), 728-738.

Panagiotou M., Restrepo J.I., Conte J.P. (2007a). Shake table test of a 7-story full scale reinforced concrete structural wall building slice phase I: rectangular wall section. SSRP 07-07 Report, Dept. of Struct. Eng., Univ. of California at San Diego, CA.

Panagiotou M., Restrepo J.I., Conte J.P. (2007b) Shake table test of a 7-story full scale reinforced concrete structural wall building slice phase II: T-wall. SSRP 07-08 Report, Dept. of Struct. Eng., Univ. of California at San Diego, CA.

Panagiotou, M., and Restrepo, J.I. (2009). Dual-plastic hinge design concept for reducing higher-mode effects on high-rise cantilever wall buildings. Earthquake Engineering and Structural Dynamics, 38(12), 1359-1380.

Paulay, T. and Priestley M.J.N. (1992). Seismic design of reinforced concrete and masonry buildings, John Wiley & Sons, Inc., New York, NY, USA.

Priestley, M.J.N., and Amaris, A.D. (2002). Dynamic amplification of seismic moments and shear forces in cantilever walls. Research Report ROSE No. 01, Rose School, University of Pavia, Pavia, Italy.

Priestley, M.J.N. (2003). Does capacity design do the job? An examination of higher mode effects in cantilever walls. Bull. New Zealand Soc. for Earthquake Eng., 36(4), 276–292.

Priestley MJN, Calvi GM, Kowalsky MJ., (2007). Displacement Based Seismic Design of Structures. IUSS Press: Pavia, Italy.

Saatci, S., (2007). Behaviour And Modeling Of Reinforced Concrete Structures Subjected To Impact Loads. PhD Thesis, University of Toronto, Canada.

Sullivan, T.J., Priestley, M.J.N., and Calvi, G.M., (2006). Shear forces in RC walls of frame-wall structures. Proc. of the 8th U.S. National Conference on Earthquake Engineering, San Francisco, CA, USA.

Sullivan, T.J., Priestley, M.J.N and Calvi, G.M. (2008). Estimating the higher-mode response of ductile structures. Journal of Earthquake Engineering, 12(3), 456–472.

Takeda, T., Sozen, M.A. and Nielsen, N.N. (1970). Reinforced concrete response to simulated earthquakes. Journal of Structural Engineering, ASCE, 96(12), 2557-2573.

Thomsen IV, J.H., and Wallace, J.W. (2004). Displacement-based design of slender reinforced concrete structural walls - experimental verification. Journal of Structural Engineering, ASCE, 130(4), 618-630.

Tremblay, R., Léger, P., and Tu, J. (2001). Inelastic seismic response of concrete shear walls considering P–delta effects. Canadian Journal of Civil Engineering, 28(4), 640-655.

Tremblay, R., Velev, N., Merzouq, S., Blais, C., Leclerc, M., Léger, P., Massicotte, B., and Rogers, C. (2005). Multi-Purpose Earthquake Simulation Testing Set-Up for Seismic Force Resisting Systems of Multi-Story Buildings. Proceedings First Int. Conf. on Advances in Experimental Structural Engineering, Nagoya, Japan, Paper No. 533.

Tremblay, R., Ghorbanirenani, I., Velev, N., Léger, P., Leclerc, Koboevic, S., Bouaanani, N., Galal, K., and Palermo, D. (2008). Seismic response of multi-storey reinforced concrete walls subjected to Eastern North America high frequency ground motions. Proc. 14WCEE, Beijing, China, Paper no. 05-01-0526.

Vecchio, F.J. and Collins, M.P. (1986). The modified compression-field theory for reinforced concrete elements subjected to shear. ACI Structural Journal, 83(2), 219-231.

Vecchio, F.J. (2000). Disturbed Stress Field Model for Reinforced Concrete: Formulation. Journal of Structural Engineering, ASCE, 126 (9), 1070-1077.

Vecchio, F.J. and Lai, D. (2004). Crack Shear-Slip in Reinforced Concrete Elements. Journal of Advanced Concrete Technology, 2 (3), 289-300.

Wallace, B.J. and Krawinkler, H. (1985). Small-Scale Model for Experimentation on R/C Assemblies, U.S. Japan Research Program. Report No. 74, John A. Blume Earthquake Engineering Center, Department of Civil and Environmental Engineering, Stanford University, Stanford, CA, U.S.A.

Wong, P.S., and Vecchio, F.J. (2002). VecTor2 & Formworks User's Manuals. Department of Civil Engineering, University of Toronto, Toronto, ON, Canada.

APPENDICES

Appendix I

Inelastic Seismic Evaluation of Slender Shear Walls Designed According to CSA-A23.3-04 and NBCC 2005

I. Ghorbanirenani, R. Tremblay, P. Léger, and D. Palermo

2008 CSCE Annual Conference, Quebec City - June 10-13, 2008

Abstract

The initial approaches used in most building codes to design reinforced concrete shear walls for earthquake resistance follow the equivalent lateral force procedure, which is based on the first vibration mode; corrections for higher mode effects derived from linear analyses are suggested. The maximum base shear can be obtained from capacity design considering the formation of a plastic hinge at the base of the wall. However, analyses of slender walls under strong ground motions show that base shears computed from nonlinear time history analyses can exceed the shear capacity prescribed by the code. In nonlinear range, the higher modes in tall walls can amplify the base shear. The moment at storey levels higher than the base can also be amplified due to higher mode effects, which could lead to the formation of a plastic hinge in the upper part of the wall. The large magnitude of the forces, in particular at the base and in upper levels, suggests that current code approaches do not provide adequate provisions for higher mode actions. In this paper, a reinforced concrete shear wall of an eight-story building located in Montréal was studied. This wall was designed according to CSA-A23.3-04 and NBCC 2005 and was subsequently scaled down as a model wall for the purposes of future shake table tests. Extensive non-linear dynamic analyses were carried out on the model wall using different constitutive models to investigate the higher mode effects on the internal shear forces and moment magnitude and distribution. The paper also presents the experimental shake table test program that is planned to validate the numerical simulations.

1- INTRODUCTION

With the development of seismology and structural engineering, structure codes and seismic provisions are being updated, but there are still many aspects that are not fully understood due to the random nature of earthquake motions as well as complex features of reinforced concrete structure responses. The behaviour of structural wall systems can be relatively complex. Among these aspects, higher mode effects on structures during ground motions have been an important issue.

To ensure adequate seismic performance, a reinforced concrete wall must have sufficient strength, particularly, shear strength greater than shear demand associated with flexural hinging, and sufficient displacement capacity (Paulay and Priestley 1992, Adebar et al. 2005).

The behaviour of tall RC walls during an earthquake is a vibration problem. The seismic motions of the ground cause the structure to vibrate, and the amplitude and distribution of dynamic deformations and their duration are of concern to the engineer. In general, tall walls respond to seismic motions somewhat differently than low-rise shear wall buildings. In many cases these low rise buildings can be treated as a single degree of freedom system corresponding to the fundamental mode. However, where the first mode is well out of resonance with the earthquake motions but the second and third mode periods are close to resonance, shear at higher storey levels are likely to be dominated by higher modes. Hence, there is usually a need to carry out multi-mode analyses, rather than just fundamental-mode analyses for tall RC walls (Booth 1994). The behaviour of tall walls under earthquakes is therefore different from the equivalent static analysis code procedure which is based on a first mode inverted triangular inertia force distribution along the wall.

Nonlinear dynamic analyses based on lumped plastic hinge in reinforced concrete shear walls showed that in the higher storey level of the wall there are local nonlinearities leading to the formation of another plastic hinge in addition to the plastic hinge at the base which is due to amplification of the shear and moment near the top (Panneton et al. 2005). The base shear

obtained from nonlinear time history analyses is often larger than the value prescribed by the code (Sullivan et al. 2006, Tremblay et al. 2005, Amaris 2002, Filiatrault et al. 1994).

The higher shear demand at the base of the wall, which is the location of the plastic flexural hinge, induces a reduction of the shear stiffness as well as a reduction in bending stiffness and strength by coupled interaction in the plastic hinge. This interaction of shear and bending should be considered in the design of the walls.

In order to develop a better understanding of the seismic behaviour of RC walls under higher mode effects, experimental large scale testing and advanced numerical analysis based on experimental results are necessary. This paper describes an analytical investigation of the higher mode effects on an 8-storey building reinforced concrete wall. Different constitutive models are used to predict the dynamic inelastic response of the wall. This analytical study was carried out in preparation of a shake table test program.

2- PROTOTYPE BUILDING AND TEST MODEL

Panneton (2004) examined the seismic behaviour of an eight-storey residential building located in Montréal, Quebec. The building was 23 m high and was laterally braced by four flat rectangular shear walls and three core walls. One of the flat shear walls of that building was selected as the prototype wall for a shake table test program to be conducted in the Structural Laboratory of École Polytechnique in Montréal. This paper presents an analytical study of the seismic response of the 1:2.33 reduced-scale model that was designed for the shake table tests.

The prototype wall was re-designed according to the seismic provisions of NBCC 2005 (NRCC 2005) and CSA-A23.3-04 (CSA 2004). The wall was assumed to be of the moderate ductility category with a ductility-related force modification factor, Rd = 2.0. Site Class C was assumed in design. The scaled model of the wall examined in this study has a height of 9.0 m. Due to laboratory limitations; the geometry of the wall was changed from a rectangular to a dumbbell-shaped cross-section while maintaining the original fundamental frequency of vibration of the

prototype building (0.71 Hz). The fundamental frequency of the scaled model was however increased to 1.8 Hz when applying the similitude requirements. The 2rd and 3rd mode frequencies of the model wall are equal to 10.1 Hz and 24.4 Hz, respectively. Figure 1 shows the factored shear forces and bending moment in the model wall as obtained from response spectrum analysis. This figure also shows the factored shear and flexural resistances of along the wall height. Following the code-prescribed capacity design approach, the factored shear force at the base corresponds to the shear force at the development of the nominal moment capacity of the wall.

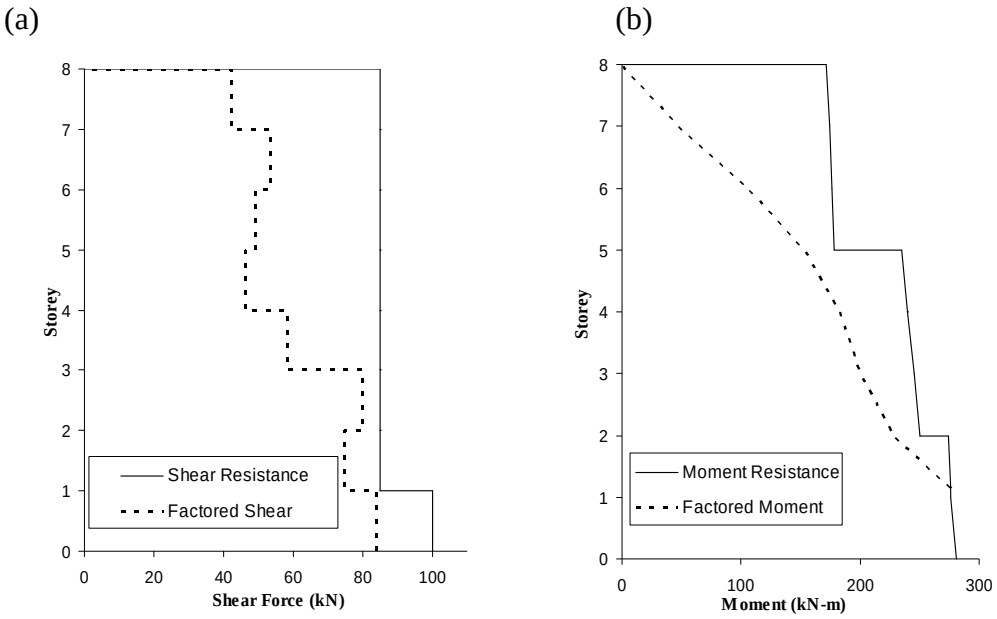

Figure 1- Distribution of forces along the height; (a) distribution of the factored shear forces and resistances; (b) distribution of the factored bending moments and factored bending moment resistances.

Figure 2 shows the elevation and section views of the wall including the rebar pattern along the height. ASTM A706 grade 60 ksi (413 MPa) No. 3 bars (As = 71 mm2, fy = 413 MPa, fu = 552 MPa) were selected for the longitudinal reinforcement steel. Wired deformed bars D 3.0, without a yield plateau, (As= 19.25 mm2, fy = 515 MPa, fu = 585 MPa) were used for transverse direction and confinement. For the last three stories, two No.3 bars at the boundary zone provide the moment resistance but two additional non bonded bars were used to satisfy the confinement requirements specified in the seismic provisions of CSA-A23.3 04. The seismic weight of the each floor is 60 kN which is the maximum weight that can be used in laboratory. The axial load,

125.5 kN, is assumed constant along the height. External post-tensioned cables will be used in the model to represent the axial load in the shake table tests.

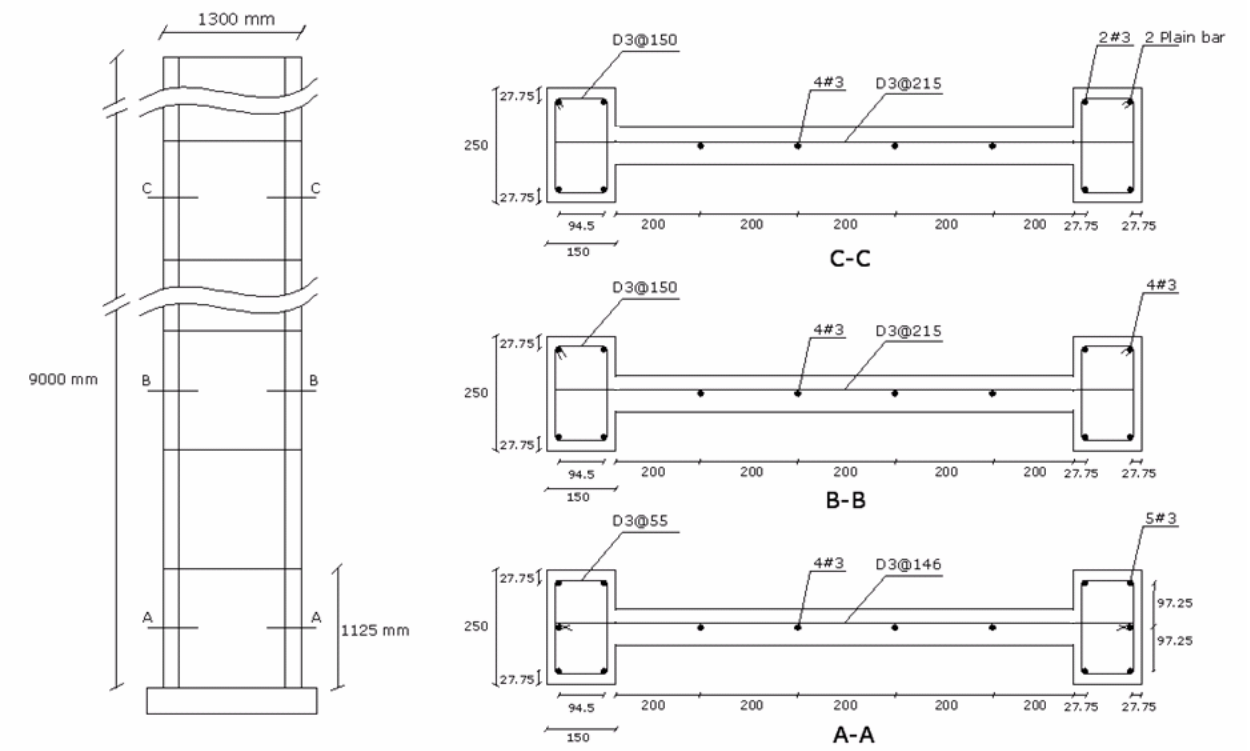

Figure 2- Elevation and section views of the model wall (mm) (section views are not scaled)

3- NUMERICAL MODELING

Different time history nonlinear analyses were carried out on the model wall using three different computer programs featuring different reinforced concrete constitutive models: Ruaumoko (Carr 2004), VecTor2 (Wong and Vecchio 2004, Vecchio and Collins 1986) and Perform 3D (CSI 2006). In all models, results from tensile tests were used for the reinforcing steel: fy = 450 MPa, fu = 590 MPa for the longitudinal steel and fy = 515 MPa fu = 585 MPa for the transverse reinforcement. The actual concrete strength was not known at the time of this study and f'c = 30 MPa was assumed in the calculations.

The model in Ruaumoko (Figure 3a) is based on beam elements with plastic hinges lumped at the member ends. The modified Takeda model (Otani 1981) shown in figure 3b was used to model the hysteretic moment curvature behaviour in the plastic hinges. In the modified Takeda model, the unloading and reloading stiffness factors were assumed equal to α=0.15 and β=0.2,

respectively. The back-bone of the hysteretic curve was obtained from plane section analysis program. The yielding stiffness rko varied between 0.2% to 0.12% of the initial stiffness along the wall height. Elastic response was anticipated in shear as a result of the capacity design approach that was adopted in design. Therefore, a linear shear deformation behaviour was assumed for the beam elements.

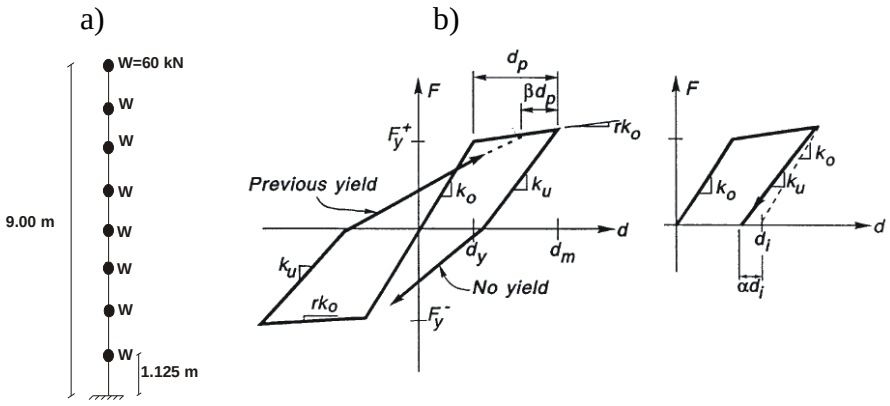

Figure 3- a) modeling of the wall in Ruaumoko; (b) modified Takeda model applied in Ruaumoko model.

VecTor2 is a finite element software for reinforced concrete structures based on the Modified Compression Field Theory. Figure 4a shows the finite element mesh of the wall. Figures 4b and 4c .show the stress-strain behaviour adopted for the concrete (Palermo and Vecchio 2003) and steel (Seckin 1981) materials. The effects of concrete confinement in VecTor2 were considered according to the amount of confinement steel (Kupfer et al. 1969).

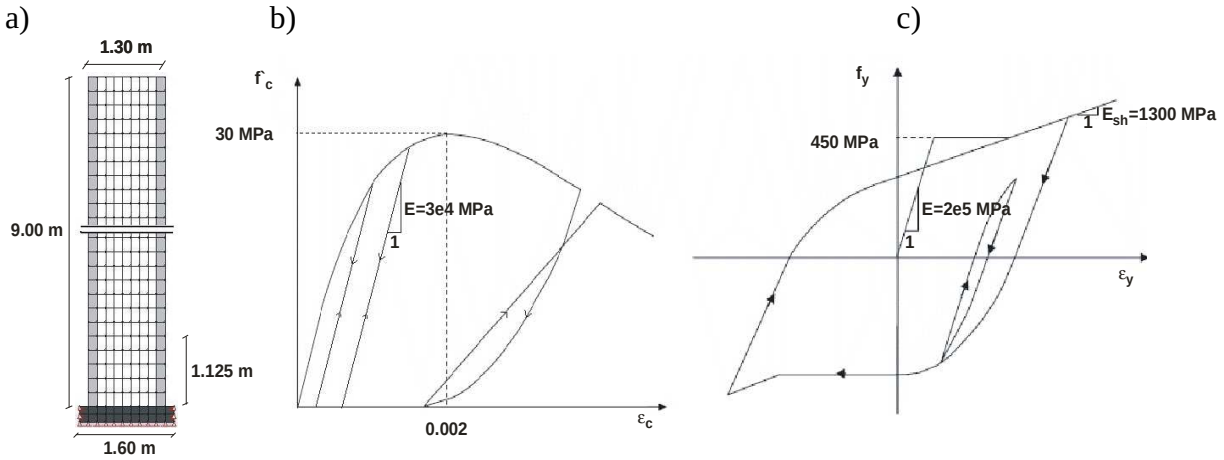

Figure 4- (a) Finite element mesh of the model wall in VecTor2; (b) Palermo hysteretic model of the concrete response in compression (Wong and Vecchio 2004); (c) Seckin model of the hysteretic response of the vertical reinforcement (Wong and Vecchio 2004)

Perform 3D models are based on fibre discretization of the cross-section, either for a wall model (2D elements) or a wall considered as a column member (1D element). The section of the wall was divided into concrete and steel fibres, as shown in figure 5a. Figures 5b and 5c show the stress-strain behaviour of the concrete and steel materials, respectively. In the boundary zones of the wall, the concrete material was defined as confined concrete and in the other regions it was defined as unconfined concrete.

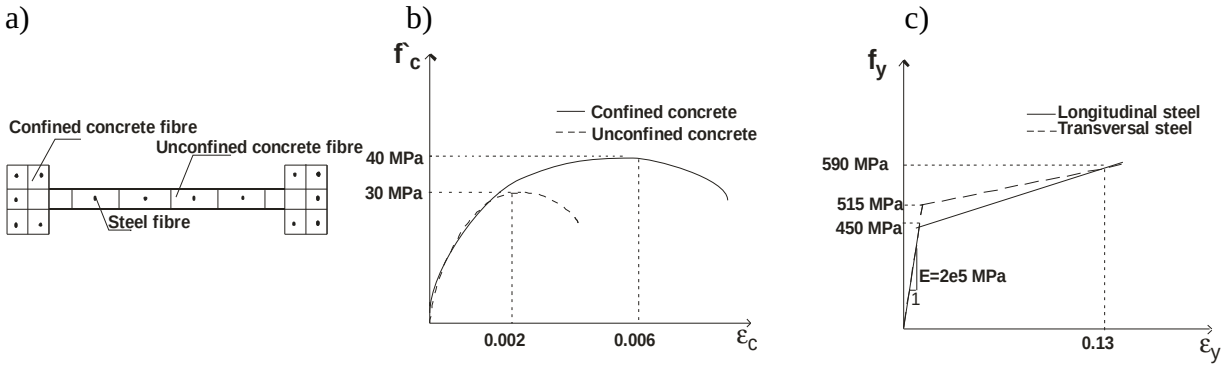

Figure 5- (a) fibre section of the wall in perform 3D; (b) stress-strain curve of unconfined and confined concrete; (c) stress strain curve of longitudinal and transversal steel.

As in the Ruaumoko model, it was assumed that the shear strength demand/capacity ratio would be less than 1.0 in the wall and a linear shear deformation response was assumed in the Perform 3D models. However, according to CSA.A23.3-04, the shear strength of the section in the plastic hinge region decreases due to the hinge plastic rotation (Figure 6). In the Perform 3D models, the interaction between the shear strength and the rotation of plastic hinge was considered in assuming a linear shear strength degradation for the hinge region. As described later, the shear force demand from the analyses was found to exceed the wall shear capacity. A second 2D Perform 3D model was therefore constructed to capture the nonlinear shear force-shear deformation behaviour of the wall. An elastic-plastic response was assumed with the shear strength being set equal to the ultimate shear strength (without resistance factors) of the wall section based on the actual concrete and steel material properties (152.6 kN).

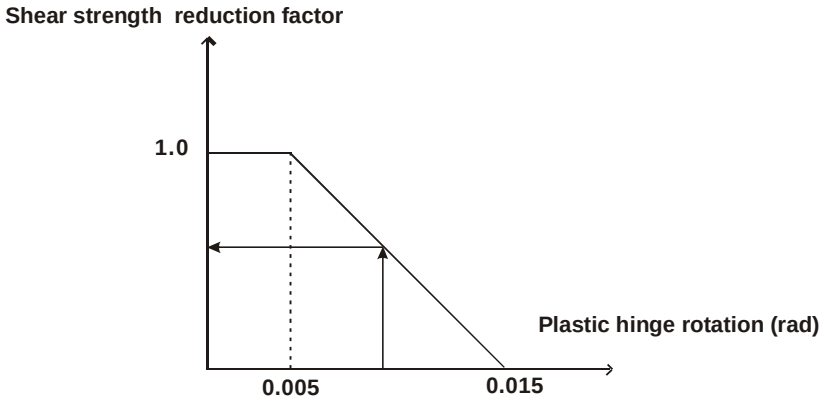

Figure 6- Effect of rotation on shear strength

Rayleigh damping proportional to the mass and the elastic stiffness of 3% of critical damping was specified in the first and second modes. Figure 7a shows the time history record of the ground motion that was selected for the test program. It is a spectrum compatible time history representative of a MW7.0 at 70 km earthquake scenario. The motion was scaled in time and amplitude according to applicable shake table similitude requirements. This scaled motion is referred to herein as the design ground motion level. The 5% damped acceleration earthquake spectrum is compared to the NBCC 2005 design spectrum in Figure 7b. As discussed later, the effects of scaling further the amplitude of the ground motion and modifying its frequency content were examined in the analytical study.

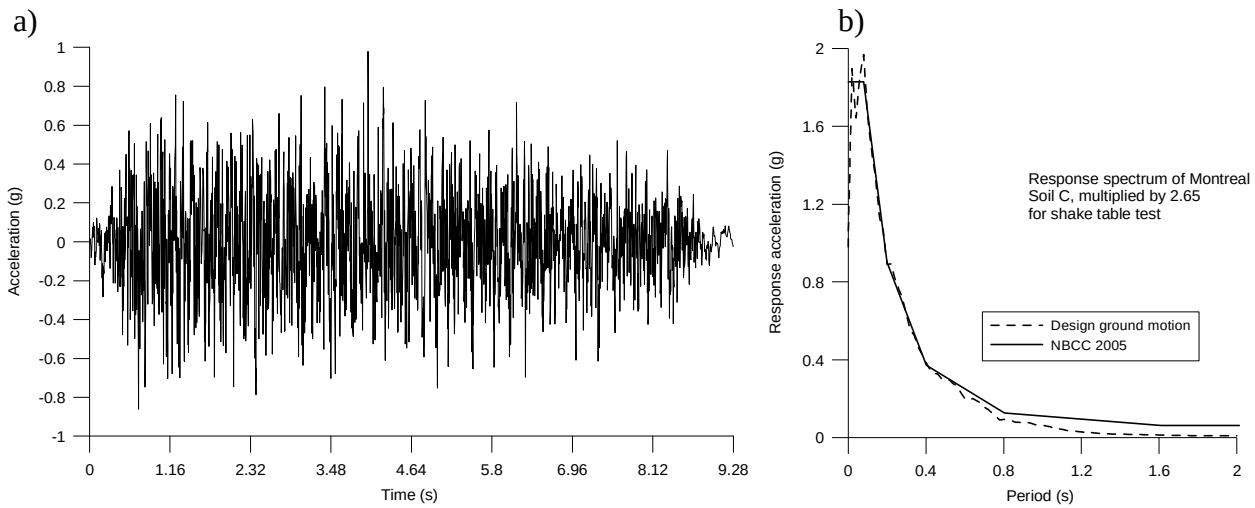

Figure 7- (a) time history record of scaled design ground motion;
(b) corresponding spectra and NBCC 05 spectrum compatibility.

4- ANALYSIS RESULTS

The peak values of key response parameters used as indicators of the seismic behaviour for these analyses are presented in Table 1. The selected parameters are the roof displacement, Δ, the bending moment at the base, M, the shear force at the base, V, the curvature ductility levels at the wall base, $\mu_{\phi 1}$, and at the 6th level, $\mu_{\phi 6}$.

The model wall under the design earthquake level shows that the Ruaumoko (lumped plasticity) model and Perform 3D model with wall fibre elements both predicted a curvature ductility of approximately 2.0 at the wall base, which is consistent with the ductility-related force modification factor used in design. Both models also predicted ductility levels higher than 1.0 at the sixth floor, indicating local nonlinearities near the top part of the wall. For the column element model in the Perform 3D program, the curvature of the section at sixth floor was very close to the yield curvature indicating a potential for nonlinear response (accounting for uncertainties). The VecTor2 FE software gave much lower curvature demand for the design earthquake. This could be related to the effect of high tension stiffening (Ghorbani-Renani et al. 2008). Table 1 indicates that all base shears under the design earthquake are larger than the shear forces obtained from capacity design (100 kN, see Figure 1a). This higher shear force demand

can induce nonlinearities in the wall shear response. The interaction of nonlinear shear and flexural responses can affect the results, and should ideally be considered in the analyses.

4-1- Effect of ground motion intensity

In order to investigate the effect of the higher ground motion intensities for the shake table tests, Additional analyses were performed using 1.5 and 2.0 times the intensity of the design earthquake. The latter ground motion intensity approximately corresponds to the capacity of the earthquake simulator apparatus. Table 1 gives the peak values of the performance parameters for the analyses under 1.5 and 2.0 times the design earthquake.

The increase in ground motion amplitude produced an increase in the amount of damage and curvature ductility demand at the base and in the upper part of the wall, as indicated by Ruaumoko and Perform 3D models. However, the predictions from the VecTor2 finite element model indicated that the wall specimen will remain elastic in the upper part, even at the maximum intensity.

The plastic hinge rotation demand computed at the wall base with Perform 3D under the maximum ground motion intensity was equal to $\theta p = 0.0015$ rad. This is much smaller than the 0.005 rad limit specified in the A23.3 code (Figure 6). The shear strength reduction of the section due to flexural hinge rotation was therefore negligible.

4-2- Effect of nonlinear shear deformations

The computed shear forces at the wall base were significantly greater than the shear resistance of the wall cross-section. The ultimate shear strength of the section based on the actual concrete and steel material properties is 152.6 kN. The average value of the of shear demand/capacity ratios from all analyses is approximately equal to 1.2. For this reason, another series of analyses were carried out using the third Perform 3D model that included nonlinearities in shear deformations and stiffness. The results are presented in the last column of Table 1. Comparisons with previous analyses indicate that under the design earthquake, the base shear and bending moment both

decreased when considering nonlinear shear behaviour. When increasing the earthquake intensity, a significant reduction of the shear forces was observed, probably due to the reduction of stiffness in shear and the occurrence of large plastic shear strains (γ_p = 1.3 x 10-3 m/m at maximum intensity). The shear stiffness reduction likely also contributed to the decrease in ductility demand at the wall base and in the upper section of the wall.

4-3- Effect of the ground motion frequency content

In the proposed test program, it is important to emphasize the effect of higher modes of the wall on its seismic response. The design ground motion record was then filtered to reduce the energy content of the signal in the 1.8-5.0 Hz frequency range, thus close to the first mode frequency of the wall. The wall was then analysed using 1.5 times the intensity of the filtered motion. The results are shown in the last row in Table 1. The top lateral deformation of the wall is much less than the values obtained from the previous analyses. The curvature ductility demand of the wall at the base ranges between 0.95 and 1.6. This indicates that the wall base remains mostly elastic. However, much higher curvature ductility demand (between 0.75 to 5.0) is observed at the sixth floor. This shows the direct effects of the higher modes on the seismic response of the upper part of the wall if the base remains elastic. The wall base shear demand did not change significantly, suggesting that the base shear forces are essentially due to the wall higher mode response.

Table 1- Peak values of the response parameters obtained with the different models and earthquake motions considered.

Ground Motion	Parameters	Ruaumoko	VecTor2	Perform 3D (Wall)	Perform 3D (Column)	Perform 3D (Wall) (NL. Shear def.)
EQ design	Δ (mm)	21.65	23	29	30	29
	M (kN-m)	355	334	380	326	355
	V (kN)	182	167	198	198	165
	$\mu_{\phi 1}$	2.2	0.8	1.9	1.2	1.4
	$\mu_{\phi 6}$	2.0	0.1	1.1	0.8	1.1
1.5 X EQ design	Δ (mm)	31	28	44	45	44
	M (kN-m)	356	361	400	400	355
	V (kN)	194	171	250	255	185
	$\mu_{\phi 1}$	3.24	1.0	3.25	3.35	3.00
	$\mu_{\phi 6}$	4.8	0.55	1.78	1.0	1.25
2.0 X EQ design	Δ (mm)	45	42	60	59	60
	M (kN-m)	356	372	450	500	390
	V (kN)	210	240	245	270	177
	$\mu_{\phi 1}$	4.9	1.35	5.0	5.5	4.0
	$\mu_{\phi 6}$	5.8	0.75	3.15	1.73	2.4
1.5 X EQ Filtered	Δ (mm)	9.5	6.56	16	12.0	16
	M (kN-m)	337	270	350	270	320
	V (kN)	240	180	215	150	166
	$\mu_{\phi 1}$	0.95	0.5	1.60	0.95	1.3
	$\mu_{\phi 6}$	5.00	0.75	2.00	1.2	1.70

5- CONCLUSION

Nonlinear time history analyses were carried out to investigate the seismic behaviour of a slender reinforced concrete shear wall structure. Three different computer programs were used: Ruaumoko (lumped plasticity), VecTor2 (planar finite elements), and Perform 3D (1D and 2D fibre elements). The shear wall studied was a 9 m tall, reduced-scale model considered for future shake table tests. The reference prototype wall is a 23 m tall wall part of an eight storey building located in Montréal, QC. The wall was designed as a moderately ductile shear wall according to CSA-A23.3-04 and NBCC 2005.

The results of the analyses under the design ground motions showed that there is a possibility of the formation of a plastic hinge in the upper part of the wall in addition to the base flexural hinge. This is attributed to the action of higher modes on tall shear walls. Current seismic design provisions do not account for this phenomenon and further studies (experimental and numerical) are needed to revisit the seismic design provisions, if necessary.

The analyses indicated that the base shear demand under the design earthquake was approximately 20% larger than the ultimate shear strength of the section as required by the code. This higher shear demand can cause nonlinearity in the shear response, which can result in shear stiffness degradation, detrimental sliding displacements at the wall base and reduction of base shear at plastic hinge and ductility demand.

The analyses for different ground motion intensities showed that increasing the motion amplitude can induce higher wall damage and ductility demand. To validate the predictions of different wall constitutive models, as implemented in the three computer programs considered, experimental data are needed. Shake table tests for different ground motion intensities will be done. The experimental program will permit to better evaluate the bending and shear stiffness, as well as cyclic strength degradation of the wall.

Filtering the low frequencies of the design ground motion showed that the ductility demand and the damage in the upper part of the wall have a direct relation to the higher frequency content of the records. The base shear demand remained nearly unchanged, suggesting that the main portion of the base shear forces is due to higher mode action.

This paper showed that the higher mode effects on slender reinforced concrete shear walls are an important problem that should be considered in design as flexural plastic hinges are likely to occur in the upper part of tall walls. This type of seismic inelastic behaviour is not anticipated by the code. Experimental shake table tests are thus planned to validate the predictions made by reinforced concrete wall constitutive models currently used by practicing engineers and researchers.

ACKNOWLEDGEMENTS

This project was supported by the Fonds québécois de la recherche sur la nature et les technologies (FQRNT) of the Government of Quebec, Canada.

References

Amaris, A., 2002, *Dynamic Amplification of Seismic Moments and Shear Forces in Cantilever Walls*, M.Sc. Thesis, Rose School of Engineering, Pavia, Italy.

Adebar, P., Mutrie, J., and DeVall, R., 2005, Ductility of Concrete Walls: the Canadian Seismic Design Provisions 1984 to 2004, *Canadian Journal of Civil Engineering*, 32(6): 1124-1137.

Booth, E., 1994, *Concrete Structures in Earthquake Regions: Design and Analysis*, Longman Scientific &Technical, 1st ed., UK, 368 pp.

Carr, A.J., Ruaumoko-2D, 2004, *User's Manual of Two- Dimensional Version of Ruaumoko*, Department of Civil Engineering, University of Canterbury, Christchurch, New Zealand.

CSA, 2004, CSA-A23.3-04, *Design of Concrete Structures, Canadian Standards Association*, Mississauga, ON, Canada.

CSI 2006, Perform 3D: *Nonlinear Analysis and Performance Assessment for 3D Structures, Computer and Structures*, Inc., 1995 University Avenue Berkeley, California 94704 USA.

Filiatrault, A., D'Aronco, D. and Tinawi, R., 1994, Seismic Shear Demand of Ductile Cantilever Walls: a Canadian Code Perspective, *Canadian Journal of Civil Engineering*, 21(3): 363-376.

Ghorbani-Renani, I., Velev, N., Tremblay, R., Palermo, D., Massicotte, B., Léger, P., 2008, Modeling and Testing The Influence of Scaling Effects on The Inelastic of Scaling Effects on The Inelastic Response of Shear Walls, *ACI Structural Journal*, Submitted on November 2007.

Kupfer, H., Hilsdorf, H.K.and Rusch, H., 1969, Behaviour of Concrete under Biaxial Stress, *ACI Structural Journal*, 87(2): 656-666.

NRCC, 2005, *National Building Code of Canada, 12th ed., National Research Council of Canada*, Ottawa, ON, Canada.

Otani, S., 1981, Hysteresis Models of Reinforced Concrete for Earthquake Response Analysis, *Joumal of Faculty of Engineering*, University of Tokyo, Tokyo, Japan, Series B, 36(2): 407- 441.

Palermo, D., and Vecchio, F. J., 2003, Compression Field Modeling of Reinforced Concrete Subjected to Reversed Loading: Formulation, *ACI Structural Journal*, 100(5): 616-625.

Panneton, M., Léger, P., and Tremblay, R., 2006, Inelastic Analysis of a Reinforced Concrete Shear Wall Building According to the NBCC 2005, *Canadian Journal of Civil Engineering*, 33(7): 854-871.

Panneton, M., 2004 , *3D Seismic Analysis of a Building Braced by Reinforced Concrete Walls Designed According to The National Building Code of Canada 2005*, M.Sc. Thesis, École Polytechnique, Montreal, Canada.

Paulay, T. and Priestley M.J.N., 1992, *Seismic Design of Reinforced Concrete and Masonry Buildings*, John Wiley & Sons, Inc., New York, NY, USA, 744 pp.
Seckin, M., 1981, *Hysteretic Behaviour of Cast-in-Place Exterior Beam-Column-Slab Subassemblies*, Ph.D. Thesis, Department of Civil Engineering, University of Toronto, 266 pp.

Sullivan, T.J., Priestley, M.J.N. and Calvi, G.M., 2006, Shear Forces in RC Walls of Frame-Wall Structures, *Proceedings of the 8th U.S. National Conference on Earthquake Engineering*, April 18-22, San Francisco, California, USA, Paper No. 1188, 10 pp.

Tremblay, R., Velev, N., Merzouq, S., Blais, C., Leclerc, M., Léger, P., Massicotte, B., and Rogers, C., 2005, Multi-Purpose Earthquake Simulation Testing Set-Up for Seismic Force Resisting Systems of Multi-Story Buildings, *Proceedings First Int. Conference on Advances in Experimental Structural Engineering*, Nagoya, Japan, Paper No. 533, 8 pp.

Vecchio, F.J. and Collins, M.P., 1986, The Modified Compression-Field Theory for Reinforced Concrete Elements Subjected to Shear, *ACI Structural Journal*, Proceedings, 83(2): 219-231.

Wong, P.S., and Vecchio, F.J., 2002, *VecTor2 & Formworks User's Manuals*, Department of Civil Engineering, University of Toronto, Toronto, ON, Canada.

Appendix II

Seismic Response of Multi-Storey Reinforced Concrete Walls Subjected To Eastern North America High Frequency Ground Motions

R. Tremblay, I. Ghorbanirenani, N. Velev, P. Léger, M. Leclerc, S. Koboevic,
N. Bouaanani, K. Galal, and D. Palermo

14th World Conference on Earthquake Engineering, Beijing, China, Paper No. 05-01-0526.

ABSTRACT

A research program has been undertaken to better characterizing the contribution of higher modes of vibration on the bending moment and shear force demand on cantilevered reinforced concrete shear walls. Emphasis is put on constructions located in eastern North America. Ground motions in this region have higher dominant frequency, which leads to relatively more significant higher mode response. An example of higher mode contribution is given for two sites in Canada exhibiting different seismic settings. A shake table test program is currently being prepared to examine the influence of damping and shear and flexural stiffness degradation on higher more response. The design of the test specimens and the results from prediction analyses are discussed. A preliminary test program conducted to validate assumptions in the use of reduced-scale wall test models is also presented.

1. INTRODUCTION

Cantilevered concrete shear walls are extensively used in Canada to provide lateral resistance to reinforced concrete as well as steel frames structures. For seismic design, reduced horizontal loads can be used provided that the wall is designed and detailed to exhibit a ductile inelastic flexural response under strong earthquake ground motions. For instance, a plastic hinge region must be created at the wall base where inelastic rotation will take place during severe earthquakes. The design shear forces from analysis are amplified to match the base shear associated with the attainment of the probable yield moment of the wall at its base. This approach

has been introduced in the 2005 National Building Code of Canada (NBCC) (NRCC 2005) and the CSA A23.3 (CSA 2004) standard for the design of reinforced concrete structures.

Several past studies have shown that applying these capacity design principles may not be sufficient to guard against shear demand in excess of the design values or plastic rotation above the plastic hinge region, in areas not detailed to sustain inelastic flexural demand (Filiatrault et al. 1994, Tremblay et al. 2001, Priestley and Amaris 2002, Panneton et al. 2006, Sullivan et al. 2006, Boivin et al. 2008). Such undesirable behaviour has been mainly attributed to the contribution of the higher mode of vibration of the wall, even upon yielding of the wall at its base. Dynamic shear magnification factors have been introduced in the New Zealand building code to prevent brittle shear failure (Priestley 2002). No explicit guidance is given in CSA A23.3 to account for this behaviour.

This paper outlines some aspects of a research project that has been undertaken to enhance our understanding of this phenomenon and develop guidelines that would be applicable to Canada and other regions of the world with similar seismicity. Particular interest is devoted to eastern Canada where anticipated seismic ground motions are likely to be richer in high frequency energy, which would lead to a greater influence of the higher modes on wall response. A 15-storey shear wall application is first introduced to illustrate this situation. A preliminary test program that was carried out to validate the use of reduced scale physical models to reproduce the inelastic cyclic flexural and shear responses of R/C wall is then presented and discussed. The design and preliminary analysis of a wall specimen to be used in a shake table test program are also described. The analytical work is also used to highlight other parameters influencing the bending moment and shear demand on shear wall structures, namely the flexural and shear stiffness degradation and damping.

2. HIGHER MODE RESPONSE OF R/C SHEAR WALLS

The influence of the seismicity at the site on higher mode effects is illustrated for a 15-storey reinforced concrete shear wall building located at two different sites in Canada: Vancouver, BC, and Montreal, QC. The hazard at Vancouver, which is also moderate, is representative of that for other cities in the Pacific Northwest region, including Seattle, Portland, and Victoria. The hazard at Montreal is representative of that of many eastern cities located in moderately-active seismic zones, including cities such as Boston, New York. Site Class C corresponding to very dense soil or soft rock was assumed at both sites.

The storey height for the walls is 3 m and the total wall height is 45 m. The walls are designed according to the seismic provisions of NBCC 2005 (NRCC 2005) and CSA A23.3 (CSA 2004). In Vancouver, the wall is designed as a ductile shear wall with an Rd factor of 3.5. The wall in Montreal is a moderately-ductile shear wall with a ductility-related force modification factor, Rd = 2.0. In Montreal, minimum reinforcement requirement often governs and there is no motivation to select a more ductile system. The wall cross-sections and periods of vibration in the first three modes are given in Fig. 1. The periods are those obtained using the cracked cross-sectional properties recommended in CSA A23.3. A dynamic (response spectrum) analysis method is used to determine the bending moment and shear forces along the height of the walls. According to CSA A23.3 provisions, the design moment is maintained equal to the base moment over the height of the plastic hinge zone. Above, the plastic hinge, the moments from analysis are increased to match the design moment at the top of the plastic hinge. For Vancouver, the base shear force is increased to Vp, the shear force associated to the probable moment resistance at the wall base, including strain hardening effects. For Montreal, Vp is associated to the nominal moment resistance. Resistance to Vp is maintained over the plastic hinge length and the shear force demand from analysis above the plastic hinge is amplified accordingly. Although the wall in Montreal is designed with a lower Rd factor, the resulting design seismic loads are lower due to the lower hazard and the wall has a smaller cross-section and longer fundamental period than in Vancouver (Fig. 1).

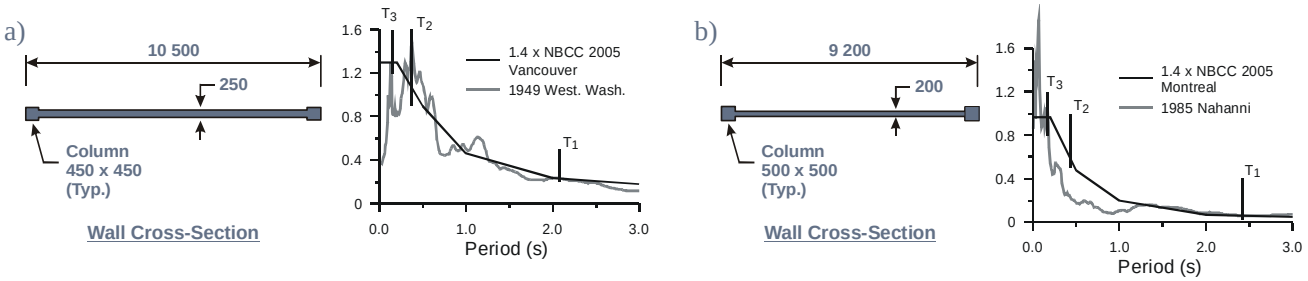

Figure 1. Wall cross-section and acceleration spectra for: a) Vancouver; b) Montreal.

The wall in Vancouver is subjected to a record from the 1949 Western Washington earthquake while an acceleration record from the 1985 Nahanni earthquake is used for the Montreal site. In design, the seismic effects were increased by 40% to account for torsional effects. Only 2D analysis is performed herein and the same amplification factor was applied to both records to achieve a proper supply-demand ratio. The structures were modeled with a cross-section fibre discretization using the wall element in the Ruaumoko computer program (Carr 2004). The Kent-Park model was used for the concrete material and the Al Bermani hysteresis rule was applied for the reinforcing steel. Figure 2 presents the computed time history response at both sites. Only the first 30 seconds of the Western Washington ground motion is presented but the same time scale was preserved for both records in the figure to more easily compare frequency effects.

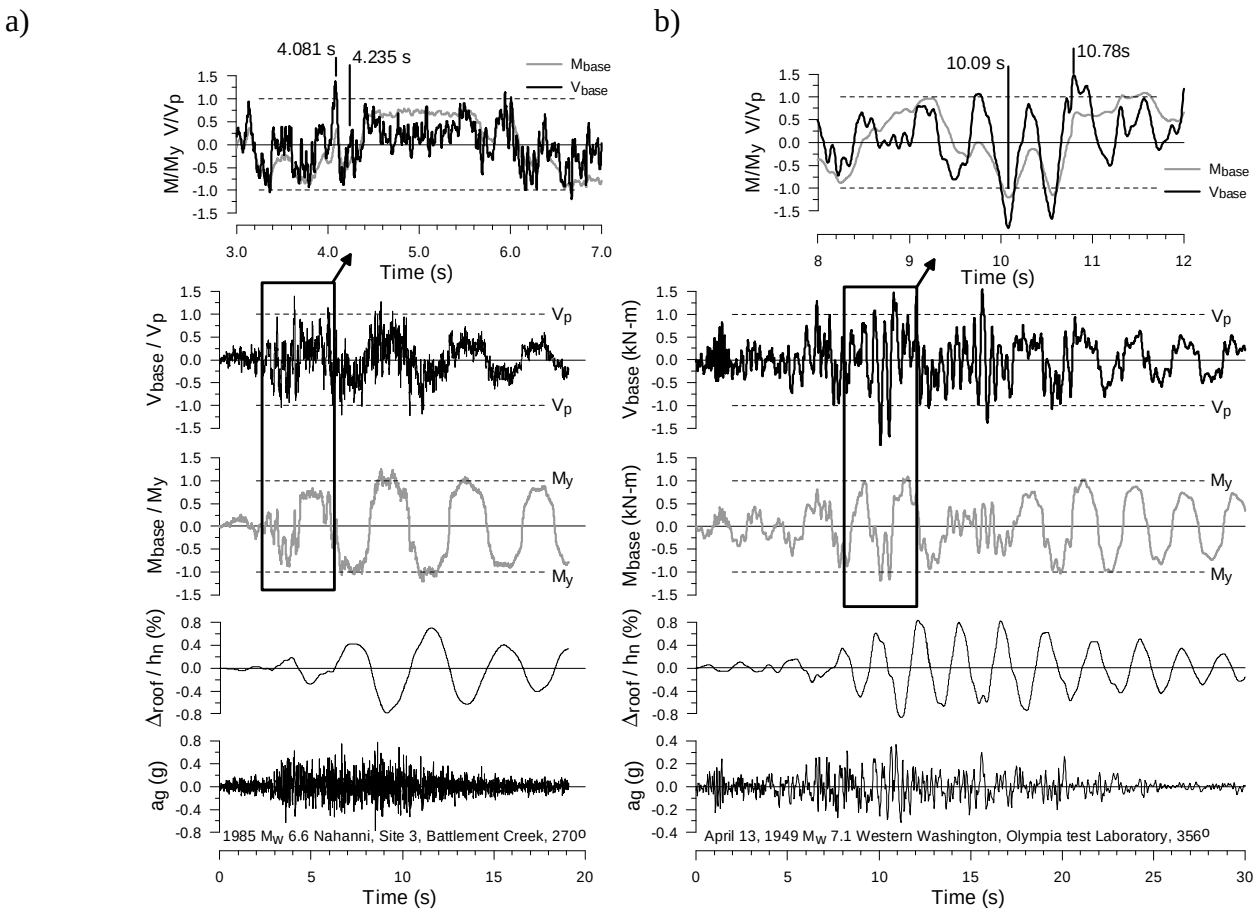

Figure 2 Time history seismic response of the 15-storey walls in: a) Vancouver; b) Montreal.

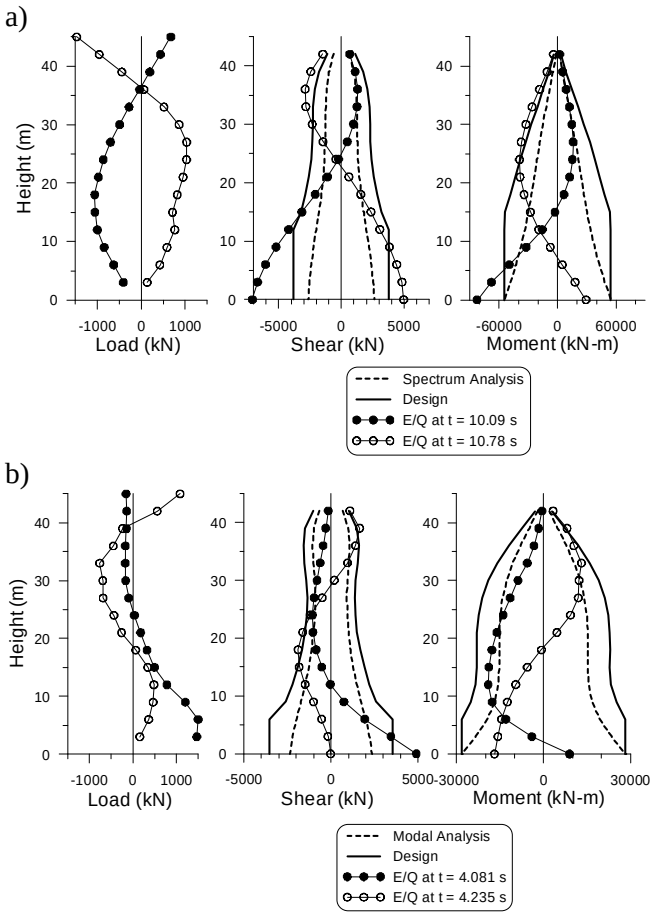

Figure 3 Vertical distributions of the inertial loads, shear forces and bending moments in the 15-storey walls in: a) Vancouver; b) Montreal.

In both cases, roof drift and base moment response are dominated by the fundamental mode. In Fig. 2a, second mode also affects the bending moment and dominates the base shear demand in the first 20 s, and the base shear from the earthquake exceeds several times the design value Vp. In the close-up view of the 8-12 s time interval, the base shear and moment are nearly in phase and Vp is reached first when the moment reaches and exceeds the yield moment, My, for the first time, at t = 10.09 s. The distribution of the lateral loads, shear forces, and bending moments along the wall height at that time are presented in Fig. 3a. As shown, the shear force significantly exceeds the design level in the first 10 m at the wall base, which could lead to a brittle shear failure. The demand from the earthquake at t = 10.78 s is also plotted in the figure. The design shear at this time is also exceeded at the base as well as above 30 m in height, and bending moments are greater than the design level in the upper floors. Inelastic rotation could then develop in a region where no ductile detailing would have been implemented. The load patterns

at these two particular times clearly indicate that this excessive demand is mainly associated to the second mode wall response. In Fig. 2b, the base shear force in Montreal is associated with high frequency motion corresponding to the second and third modes of vibrations of the wall. This time, the base shear exceeds V_p well before yielding in flexure. This wall possesses flexural overstrength due to minimum reinforcement requirements. Hence, it responded nearly elastically at the beginning of the earthquake, which contributed in attracting higher shear forces. Third mode contribution can be also observed in the inertia load and shear profiles at t = 4.235 s. At that particular time, the base shear is nearly zero but the shear forces and bending moments exceed the design values along the wall height. For this particular wall, third mode response is significant compared to that in the second mode because the ground motion contains relatively low energy near the second mode period, as shown in Fig. 1b.

The magnitude of the higher mode response during an earthquake heavily depends on the wall stiffness. Figure 2 shows that the high frequency motion tends to diminish as inelastic flexural response developed in the wall. In the numerical model used herein, the shear stiffness was assumed to remain constant. In reality, it will also degrade as cracks develop due to flexure and shear. Higher mode contributions are likely to overestimated with models that only account for inelastic flexural response. However, it is common practice to use Rayleigh damping proportional to mass and stiffness with such models, as was the case for the example presented here. Using this damping model tends to artificially attenuate the high frequency response associated to higher modes. These uncertainties in predicting higher mode effects on shear and flexural demand in shear walls were the main motivation for this research project, the main objective being to validate more accurate numerical models that could subsequently be used to better assess this phenomenon.

3. EXPERIMENTAL WORK

3.1. Preliminary Experimental and Numerical Studies

A shake table test program is being prepared to study the response of shear walls under dynamic seismic excitation. The tests will be performed on the uniaxial shake table at the Structural Engineering Laboratory of École Polytechnique of Montreal. This equipment has 15 ton payload capacity and a test height of 10 m. Preliminary studies showed that the test could be performed on a model of a 10-storey prototype building using a scaling factor on length, lr, of 0.305 to meet the physical constraints of the laboratory (Tremblay et al. 2005). Further investigations indicated that the scaling factor needed to be increased to 0.42 to easily satisfy applicable similitude requirements with available reinforcing steel bar and concrete aggregate sizes. The reference prototype structure was then changed to an 8-storey building.

Prior to initiating the shake table program, testing was carried out to verify the possibility of accurately reproduce with reduced scale models the complex inelastic flexural and shear responses anticipated in actual shear walls. Four specimens were tested: two prototype walls and two 1:2.37 scaled models. The walls were detailed according to the Canadian seismic provisions for ductile walls. Monotonic and cyclic loading protocols were considered for each group. Detail of the study can be found in Gorbanirenani et al. (2008a). Figures 4a&b show the test specimens. Excellent agreement was obtained between the prototype and model walls, as exemplified in Fig. 4c for the cyclic tests. This test program also represented an excellent opportunity to validate more refined numerical simulation tools. The Vector2 (VT2) finite element program (Wong and Vecchio 2002) is dedicated to the analysis of concrete structures. It makes use of the Disturbed Stress Field Model (Collins 2000) and its scope has recently been extended to cover cyclic and dynamic applications (Palermo and Collins 2003). The program could reproduce very well material nonlinearities under monotonic and cyclic loading, including yielding of steel, bar slippage, concrete crushing and cracking, sliding, etc. Strength and stiffness degradation in flexure and shear, as well as the failure mode, could be predicted accurately, as depicted in Fig. 4d. The VT2 program was then used in the design of the shake table specimens.

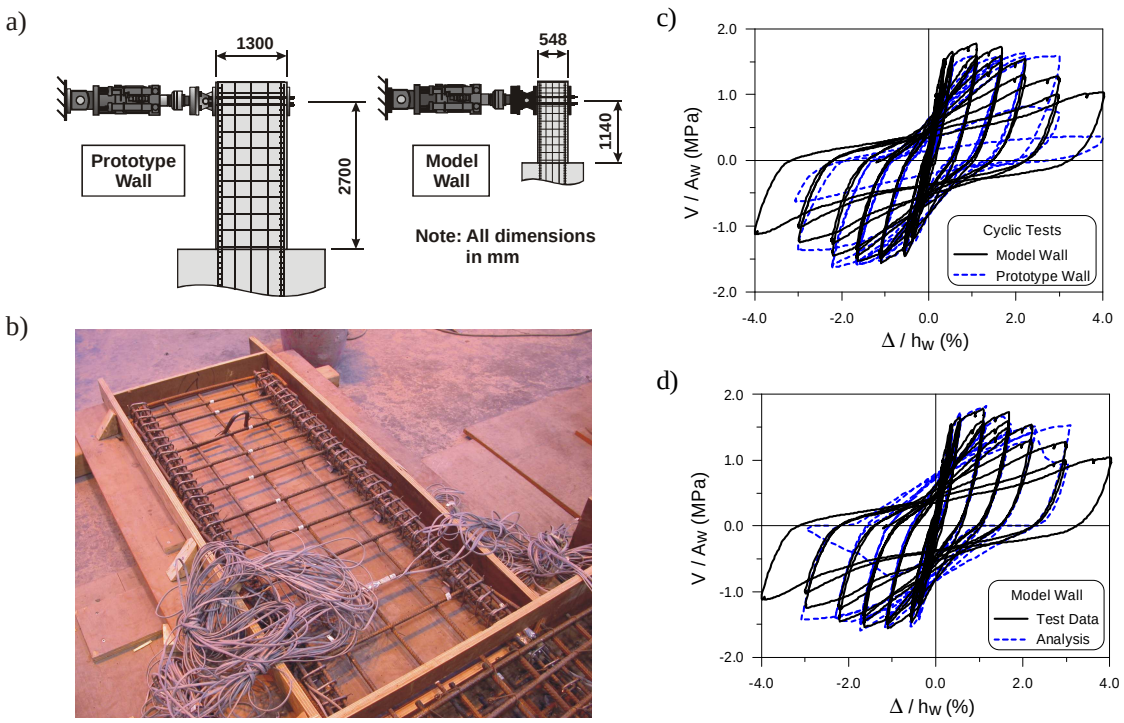

Figure 4 Preliminary testing of shear wall specimens: a) Geometry of the test walls; b) Model wall specimen under construction; c) Measured load-deformation response of the prototype and model walls under cyclic loading; and d) Analytical *vs* measured load-deformation responses of the model wall under cyclic loading.

3.2 Design and Preliminary Analysis of the Shake Table Specimens

The shake table test setup is shown in Fig. 5a. The test specimen is mounted on the earthquake simulator while the seismic weights at each level are supported on an independent structure erected on the strong floor of the laboratory, beside the shake table. The lateral stability is provided by a surrounding steel frame. The reference 8-storey prototype structure has a total height of 20.97 m (8 x 2.621 m) and a scaling factor lr = 0.429 was adopted to obtain a 9.0 m tall test structure.

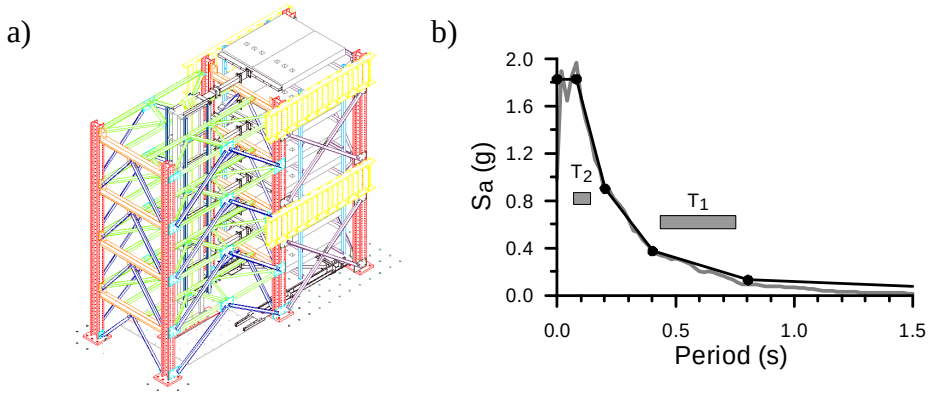

Figure 5 a) Proposed test setup; b) Design and earthquake design spectra.

The artificial mass simulation procedure was used to develop the similitude requirements. The method was modified to also introduce a scaling factor on acceleration, αr = 2.65, to keep the seismic weight per floor equal to 60 kN. This resulted in scaling factor on time, tr = 0.403. The test program is conducted for the seismic conditions prevailing in eastern North America and the fundamental period of the prototype structure was selected to fall within the 1.2-2.1 s period range estimated for a typical 8-storey residential building located in Montreal (Panneton et al. 2006). This variation in period resulted from the various assumptions that can be made in the modal analysis. At the model scale, it corresponds to approximately 0.5-0.8 s. Two possible model solutions exhibiting such period values are illustrated in Fig. 6: a simple rectangular wall and an I-shaped wall. Both structures are designed according to the Canadian seismic design provisions for moderately ductile shear walls (Rd = 2.0), assuming a site class C in Montreal. The wall with columns has a higher stiffness. The rectangular wall has a cross-section reduction at the 6th level to encourage exactly meet the required bending moment resistance at that level and examine the possibility of plastic rotation due to higher mode response. An Mw7.0 at 70 km simulated ground motion time history was selected for the test program. It was modified using a loose spectral matching technique to reproduce the design demand for the site. Fig. 5b shows the resulting spectra at the model scale: acceleration and time (period) are scaled. Response time histories obtained with the VT2 program are presented in Fig. 6. In the analysis, axial corresponding to approximately 2.5% of the Acf’c has been considered to replicate the future test conditions. As was the case for the sample 15-storey buildings, the roof drift response is governed by first mode whereas second mode dominates the base shear demand. In both cases, the design shear Vp is exceeded and inelastic strain demand (ε > 0.2%) is predicted in the

longitudinal reinforcement at the 6th level. Viscous damping was omitted in the VT2 analysis as damping in the test specimens is essentially due to concrete nonlinear behaviour. The decaying free vibration response at the end of the ground motion illustrated in Figs. 7a&b shows that this behaviour is already accounted for in the analysis.

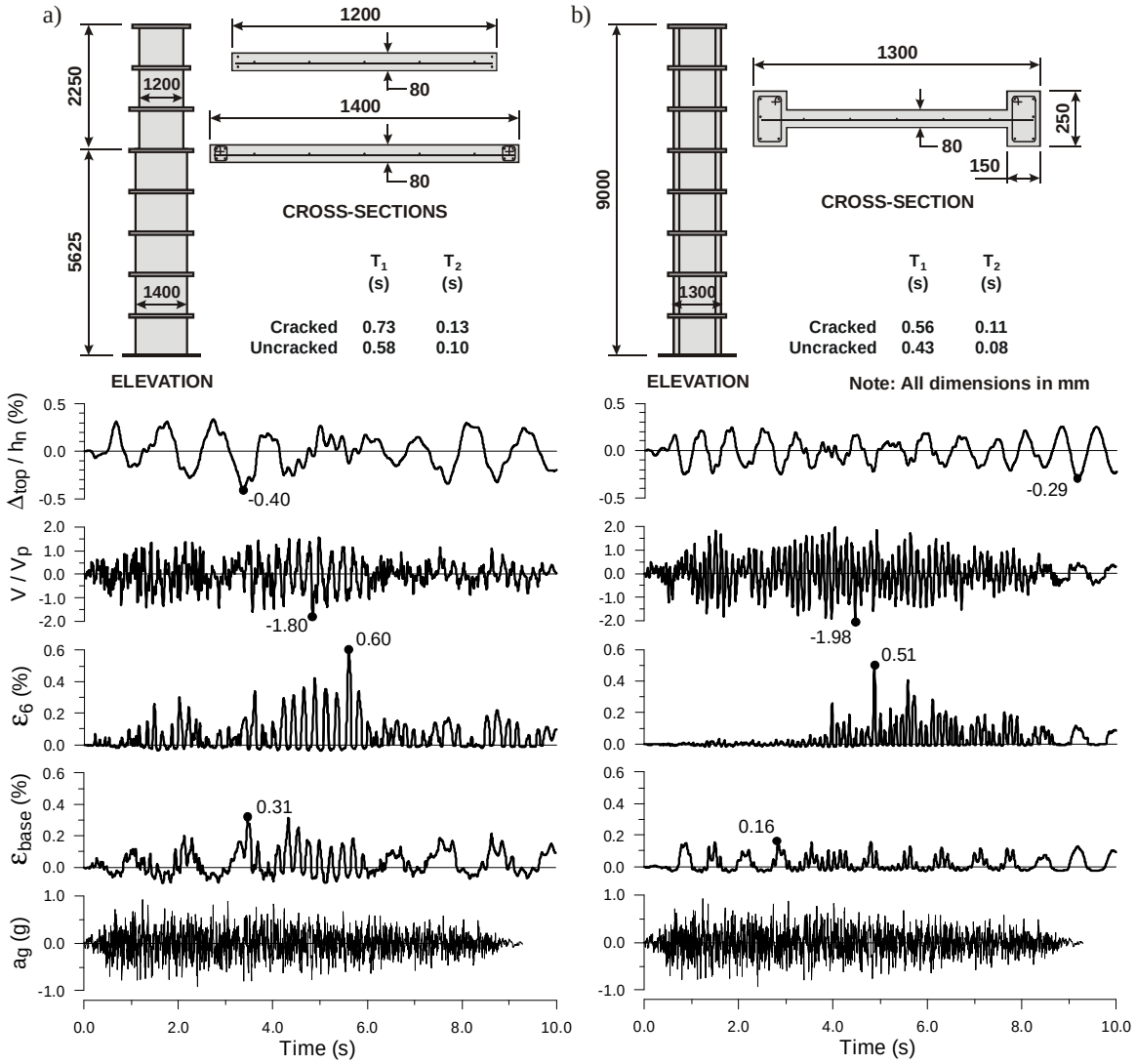

Figure 6 Properties and predicted response of test specimens studied: a) Rectangular wall; b) I-Shaped wall.

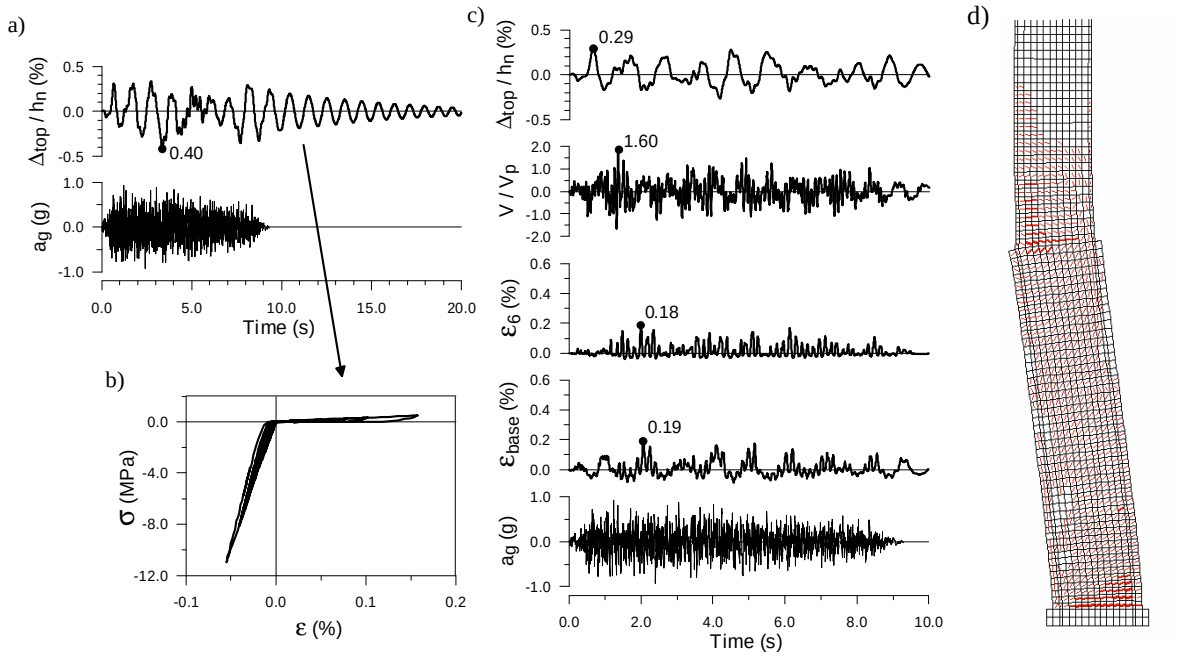

Figure 7 Additional analysis results for the rectangular wall: a) Decaying response after application of the ground motion; b) Hysteretic response of concrete under free vibration response; c) Response with 1.5% Rayleigh damping; and d) Crack pattern under the design ground motion amplified by 1.5.

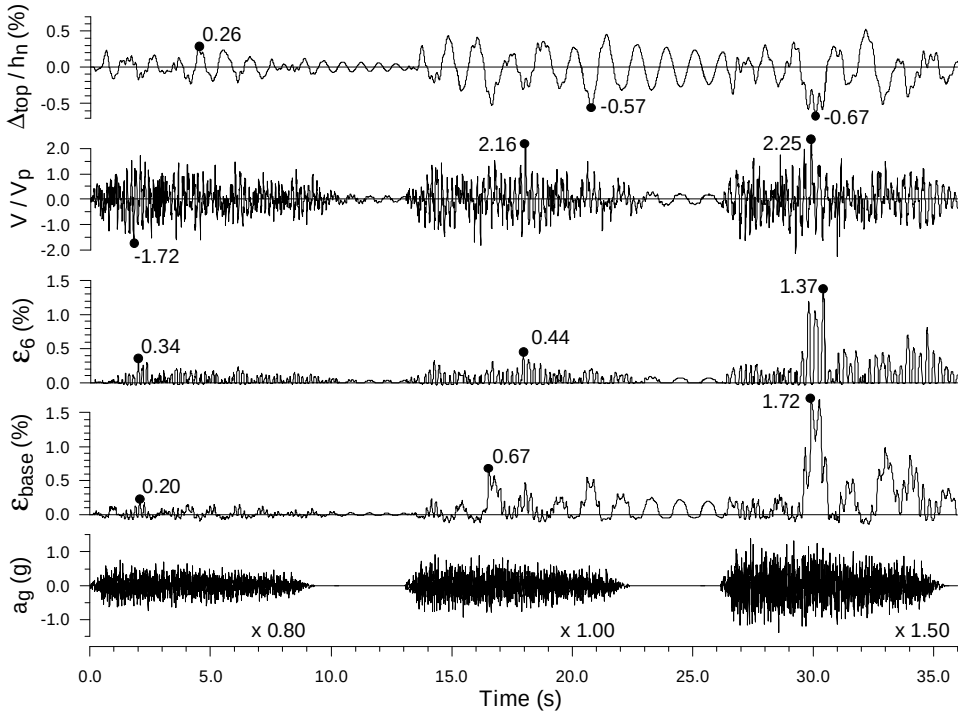

Figure 8 Predicted response of the rectangular wall specimen under successive application of ground motion amplitudes.

Figure 7c presents the response of the rectangular wall obtained when specifying 1.5% Rayleigh damping in the first two modes of vibration. The impact is significant: the roof drift and the strain demand at the 6th level reduce respectively from 0.40% and 0.60% to 0.29% and 0.18%. The base shear demand is also reduced, which illustrates the sensitivity of higher mode response to damping modelling assumptions. In the test program, it is planned to conduct successive tests at increasing amplitude of ground motions up to 150% of the design level. The crack pattern under 1.5 times the deign ground motion is shown in Fig. 7d. Significant inelastic rotation demand is expected at the base as well as at the 6th floor. Figure 8 shows the response of the rectangular wall under successive applications of the seismic excitation. When comparing the results under 1.0 times the design ground motion with the corresponding results in Fig. 6a, it is observed that the initial damage conditions can also impact significantly on the wall response.

4. CONCLUSIONS

The analysis of a 15-storey shear wall structures illustrated higher mode response on shear and flexural demand for reinforced concrete shear wall structures located at two different sites in Canada. The capability of reproducing the inelastic flexural and shear response of shear walls using reduced-scale specimens was verified experimentally. The test results could also be reproduced accurately using detailed FE simulations. Shake table test specimens were designed and were validated using FE analysis. Higher mode response is excepted in the test models but the response was found to be sensitive to the modeling of damping and the sequence of testing.

ACKNOWLEDGEMENTS

Funding for this research was provided by the Government of Quebec (FQRNT program) and the Natural Sciences and Engineering Research Council of Canada (Canada Research Chair Program).

REFERENCES

Boivin, Y. and Paultre, P. (2008). Seismic Performance of a 12-Storey Ductile Concrete Shear Wall System Designed According to the New Canadian Building Design Codes. *Proc. CSCE 2008 Annual Conf.*, Quebec, QC, Paper No. ST-442.

CSA. (2004). Design of concrete structures. Standard CAN/CSA-A23.3-04, Canadian Standard Association, Rexdale, ON.

Filiatrault, A., D'Aronco, D. and Tinawi, R. (1994). Seismic Shear Demand of Ductile Cantilever Walls: a Canadian Code Perspective, *Can. J. of Civ. Eng.*, **21:3**, 363-376.

Ghorbanirenani, I., Velev, N., Tremblay, R., Palermo, D., and Massicotte, B., and Léger, P. (2008). Modeling and Testing of Influence of loading history and scaling effects on the inelastic response of reinforced concrete shear walls. *ACI Structural J*. (submitted)

NRCC. (2005). National building code of Canada. 12th ed., National Research Council of Canada, Ottawa, ON.

Palermo, D., and Vecchio, F. J. (2003). Compression Field Modeling of Reinforced Concrete Subjected to Reversed Loading: Formulation. *ACI Struct. J.*, **100:5**, 616-625.

Panneton, M., Léger, P., and Tremblay, R. (2006). Inelastic Analysis of a Reinforced Concrete Shear Wall Building According to the NBCC 2005. *Can. J. of Civ. Eng*., **33:7**, 854-871.

Priestley, M.J.N., and Amaris, A.D. (2002). Dynamic amplification of seismic moments and shear forces in cantilever walls. *Research Report ROSE-2002/01*, Rose School, University of Pavia, Pavia, Italy.

Sullivan, T.J., Priestley, M.J.N. and Calvi, G.M. (2006). Shear Forces in RC Walls of Frame-Wall Structures.
Proc. 8th U.S. Nat. Conf. on Earthquake Eng. San Francisco, CA. Paper No. 1188.
Tremblay, R., Velev, N., Merzouq, S., Blais, C., Leclerc, M., Léger, P., Massicotte, B., and Rogers, C. (2005).

Multi-purpose earthquake simulation testing set-up for seismic force resisting systems of multi-story buildings. *Proc. First Int. Conf. on Advances in Experimental Structural Eng.*, Nagoya, Japan, Paper No. 533.

Tremblay, R., Léger, P., and Tu, J. (2001). An Evaluation of P-delta Effects on the Inelastic Seismic Response of Concrete Flexural Walls. *Can. J. of Civ. Eng.*, **28:4**, 640-655.

Vecchio, F.J. (2000). Disturbed Stress Field Model for Reinforced Concrete Formulation. ASCE J. of Struct. Eng. **126:9**, 1070-1077.

Wong, P.S., and Vecchio, F.J. (2002). VecTor2 & Formworks User's Manuals. Dept. of Civ. Eng., Univ. of Toronto, Toronto, ON, Canada.

Appendix III

Distribution of Inelastic Demand in Slender R/C Shear Walls Subjected to Eastern North America Ground Motions

I. Ghorbanirenani, A. Rallu, R. Tremblay, and P. Léger

2009 ATC&SEI Conference on Improving the Seismic Performance of Existing Buildings and Other Structures, December 9-11 2009, San Francisco, USA

ABSTRACT

This paper compares the nonlinear seismic response of an 10-story reinforced concrete shear wall building located in Montréal, Canada that was designed according to four different editions of the National Building Code of Canada: 1975, 1985, 1995 and 2005. The design seismic loads and detailing requirements used for the four designs are discussed and compared. The study focuses on the shear force demand in the wall and on the potential for inelastic flexural response in the upper levels due to higher mode response. Two different 2D models are used in the study: a plane stress finite element model using the VecTor2 software and a fibre element model using the OpenSees program.

INTRODUCTION

In Canada, the general design and loading provisions for building structures are prescribed in the National Building Code of Canada (NBCC) while the design and detailing requirements for reinforced concrete buildings are specified in the CSA A23.3 Standard. Seismic design provisions were included in the first edition of NBCC in 1941. Those provisions then evolved with significant changes taking place in the seismic design parameters and analysis methods in subsequent editions of NBCC (Tinawi 2004). Over the years, the main performance objective of NBCC still remained the safety of the building occupants under severe but rare earthquake events. The design objective under such extreme loading condition has been collapse prevention and it was in 1965 that NBCC explicitly recognized that these objectives could be achieved through ductile inelastic response. Detailing requirements and capacity design provisions aiming

at the development of stable inelastic behaviour were first introduced in the 1973 edition of CSA A23.3 (CSA 1973).

For shear wall structures, the intent of these seismic provisions has been, and still is today, that inelastic deformations concentrate in a single plastic hinging forming at the wall base. Rules have been progressively implemented in codes to ensure that ductile walls possess sufficient flexural resistance above the plastic hinge region and shear resistance over their entire height to resist the anticipated flexure and shear force demand essentially in the elastic range (Adebar et al. 2004). In multi-storey structures, that force demand is significantly influenced by the contribution of the higher modes of vibration, particularly in eastern North America where the seismic ground motions are expected to be richer in high frequencies (Tremblay and Atkinson 2001; Humar and Mahgoub 2003). Recent numerical studies on multi-storey shear walls (Filiatrault et al. 1994, Tremblay et al. 1999, Priestley and Amaris 2002; Panneton et al. 2006, Sullivan et al. 2008; Tremblay et al. 2008; Panagiotou and Restrepo 2009) indicated that the force demand can exceed the values assumed by codes, even for structures that are designed according to the most recent code provisions. Dynamic effects on shear forces were observed in shake table tests by Panagiotou et al. (2007). In this context and making use of the new information on anticipated seismic ground motions and new techniques available to examine the nonlinear response of concrete structures, a study was undertaken to identify potential deficiencies in shear wall structures designed in eastern Canada over the last decades.

In this paper, the seismic design and performance of an individual 10-storey cantilevered flexural wall designed according to four editions of NBCC, respectively 1975, 1985, 1995 and 2005, and the associated 1973, 1984, 1994 and 2004 CSA A23.3 standards. The structure is located on a firm ground site in Montréal, Quebec, which is representative of many other eastern populated cities located in moderately-active seismic zones, including cities such as Boston, New York, and Ottawa. The wall geometry is kept unchanged but the reinforcement was modified according to the respective code provisions. Nonlinear dynamic analyses were carried out using two different numerical simulation techniques: finite element modeling and fibre cross-section discretization.

The main objectives were to examine the shear force demand in the wall and the possibility of flexural yielding in the upper levels due to higher mode response.

DESIGN OF THE SHEAR WALL STUDIED

Wall Studied. The wall studied is a continuous shear wall in a regular 10-storey residential building structure with a 72 m x 48 m rectangular foot print. The storey height is 2.8 m and the wall has a 300 mm x 6000 mm uniform rectangular cross-section over the building height. The wall is located against an exterior wall and carries limited axial load. Its tributary seismic weight is 7845 kN per floor.

Seismic Loads and Analysis Methods. Table 1 summarizes the main seismic design parameters for the four designs. As shown the equation for V, the minimum earthquake lateral load varies significantly from one code to the next. In NBCC 1975, the equation was based on the peak ground horizontal acceleration, A, which was specified for a return period of 100 years. That value was equal to 0.04 for Montréal. In 1985 and 1995, the seismicity was represented by the velocity, v, determined for a period of return of 475 years. In NBCC 2005, site specific uniform hazard spectral ordinates, Sa, are specified at periods of 0.2, 0.5, 1.0, and 2.0 s for a return period of 2500 years. These Sa values are modified for the site coefficients F_a and F_v to obtain the design spectrum ordinates S, and the complete spectrum is obtained by linear interpolation between these points. In NBCC 1975, the spectrum S was a function of $T^{1/3}$ (T is the period) with a maximum value of 1.0. In 1985 and 1995, the exponent for T was changed to ½ and the plateau at short periods extended up to T = 0.25 s and was followed by a linear segment to join the $1/T^{1/2}$ curve at T = 0.5 s. Empirical expressions were given in NBCC to estimate the fundamental period of the structures. Up to 1995, Temp was function of the building height, hn, and the building length (D = 48 m) or the wall length (D_s= 6 m) parallel to the direction of loading. The expression was simplified in 2005 such that T now only depends on the building height. For the wall studied, the resulting Temp values varied from 0.36 to 1.03 s, which is significant. Values of S determined at Temp are given in the table for each code. Except for NBCC 2005, the influence of the higher modes on the structure response was indirectly accounted for by the reduced spectral decrement in the long period range ($T^{1/3}$ or $T^{1/2}$). In NBCC 2005, a factor M^v was introduced for multi-mode response. Where the ratio $S_a(0.2)/S_a(2.0)$ exceeds 8, as is the case in

eastern Canada, values greater than 1.0 are specified for T > 2.0 s and linear interpolation of the product SMv must be considered for periods between 1.0 and 2.0 s. In 1975 and 1985, the ductility was accounted by the factor K at the numerator of the equation for V. In 1995 and 2005, the ductility factors R and Rd are used at the denominator. In 2005, the structure overstrength is taken into account with the factor Ro. Importance factors (I and IE) and factors to account for local site effects (F, F_a or F_v) are all equal to 1.0 for the assumed conditions. For all four designs, the seismic loads were increased by 1.25 to account for accidental in-plane torsional effects. The design of reinforced concrete structures is performed using factored loads, with load factors also varying among the different codes. Once the calculations are performed including all these factors, the resulting factored seismic load values, V_f, vary significantly among the four codes.

All NBCC editions allow to use the dynamic (response spectrum) analysis method in lieu of the equivalent lateral force method. This option was retained herein. In the analysis, the properties of the cracked section can be used and I_{cr}/I_g ratios suggested in the 1984, 1994 and 2004 CSA A23.3 standards and shown in Table 1 were adopted in the models. In 2004, the value varies with the level of axial load, resulting in the range shown. The 1985 value was adopted for the 1975 design as no value was given in the 1973 edition of CSA A23.3. The resulting periods of vibrations are given in Table 1 and the computed fundamental periods T1 are much longer than Temp. In NBCC 1975 to 1995, elastic acceleration spectra, different from S used in the equation for V, were specified for the response spectrum analysis. These spectra are plotted in Figure 1.1a together with the 2005 NBCC S values. In NBCC 1975, the spectrum had to be modified to account for ductility assuming equal displacement principle for medium and long periods and equal energy principle for short periods. For ductile shear walls, a ductility factor of 3.0 was specified for this reduction process. Inelastic spectra are shown in Figure 1.1b. This approach, in combination with the longer fundamental periods, resulted in a much smaller seismic design load $V_{f,dyn}$ compared to the V_f value obtained previously. In NBCC 1985 and 1995, the results from the dynamic analysis are scaled such that the base shear from dynamic analysis is equal to the value of V_f. A similar approach is prescribed in NBCC 2005, except that the reference V_f value can be determined with a period of up to 2.0 times Temp, if justified by analysis, and V_f can be multiplied by 0.8 is the structure is regular. These conditions applied herein and the results were scaled with respect to Vf = 0.024W, resulting in a significant reduction compared to the value

obtained from the equation in Table 1. Figure 2 presents the distribution of the factored shear forces and bending moments from response spectrum analysis. Clearly, the 1975 and 2005 NBCC provisions resulted in much lower values than the 1985 and 1995 codes.

Table 1. Summary of NBCC seismic provisions for the 10-storey wall on a very dense soil site in Montréal, Quebec

Parameter	1975	1985	1995	2005
V	ASKIFW	vSKIFW	vSIFW(U/R) U = 0.6	$S M_v I_E W/(R_d R_0)$ $\geq S(2.0) I_E W/(R_d R_0)$ $\leq 2/3 S(0.2) I_E W/(R_d R_0)$ if $R_d > 1.5$
Return period (yrs)	100	475	475	2500
Seismic data	A = 0.04	v = 0.1	v = 0.1	S_a = 0.69, 0.34, 0.14, and 0.048 for T = 0.2, 0.5, 1.0, and 2.0 s
S	$0.5/T^{1/3}$ ≤ 1.0 S = 0.70	$0.22/T^{1/2}$ ≤ 0.62 LI[1] for T between 0.25 & 0.5 s S = 0.22	$1.5/T^{1/2}$ ≤ 4.2 LI[1] for T between 0.25 & 0.5 s S = 1.48	$F_a S_a(0.2)$ for T $\leq$ 0.2 s $\min[F_v S_a(0.5), F_a S_a(0.2)]$ for T = 0.5 s $F_v S_a(1.0)$ for T = 1.0 s $F_v S_a(2.0)$ for T = 2.0 s $F_v S_a(2.0)/2$ for T = 4.0 s LI[1] for intermediate values of T S = 0.30
T_{emp}	$0.09 h_n/D^{1/2}$ = 0.36 s	$0.09 h_n/D_s^{1/2}$ = 1.03 s	$0.09 h_n/D_s^{1/2}$ = 1.03 s	$0.05 h_n^{3/4}$ = 0.61 s
M_v Multi-mode	-	-	-	1.0 for T $\leq$ 1.0 s 2.5 for T $\geq$ 2.0 s
Ductility	K = 1.0	K = 1.0	R = 3.5	R_d = 3.5 (R_0 = 1.6)
V_f / W	0.063	0.041	0.032	0.066
Scaling wrt	-	V	V	0.8 V
I_{cr} / I_g	0.40	0.40	0.70	0.61 - 0.66 (average = 0.63)
T_1 (s) T_2 (s)	3.47 0.58	3.47 0.58	2.64 0.45	2.76 0.50
$V_{f,dyn}$ / W	0.018	0.041	0.032	0.024
$M_{f,dyn}$ / W h_n	0.0067	0.0138	0.0110	0.0063
$V_{cap.des.}$ / W	0.037	0.055	0.043	0.040

[1]LI = Linear interpolation.

Seismic Design and Detailing. A concrete strength, f'_c, of 30 MPa and a steel yield strength, f_y, of 400 MPa were assumed in all designs. The first step in the design consists in determining the

longitudinal reinforcement in the base plastic hinge region of the walls to resist the bending moment at the wall base ($M_{f,dyn}$ in Table 1). Applying CSA A23.3 requirements, the length of the plastic hinge was taken equal to 5 stories for the 1975 design, 3 stories for the 1985 and 1995 designs, and 4 stories for NBCC 2005. In that area, steel detailing rules apply to ensure ductile rotational behaviour, including minimum reinforcement concentrated near the ends of the wall.

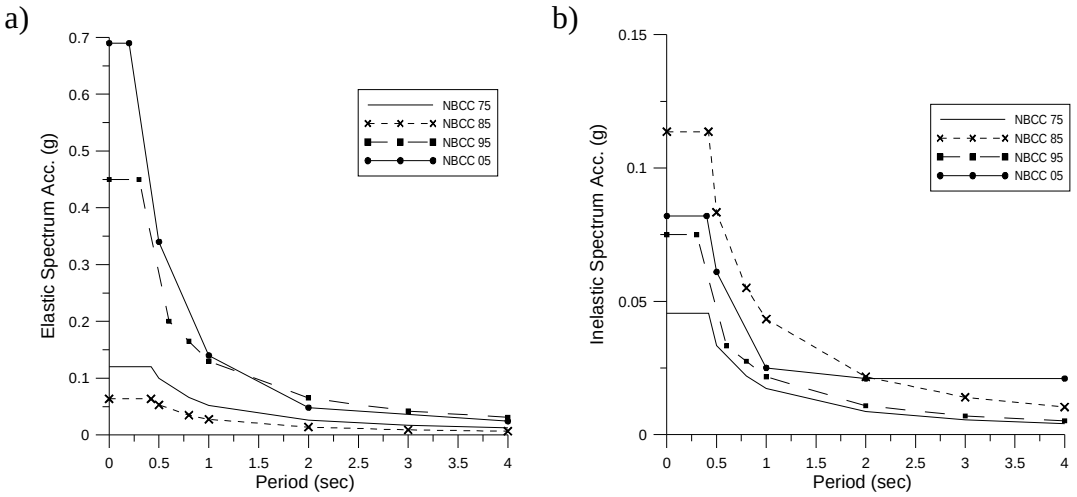

Figure 1. NBCC response spectra: a) Elastic spectra used in analysis; b) Inelastic design spectra.

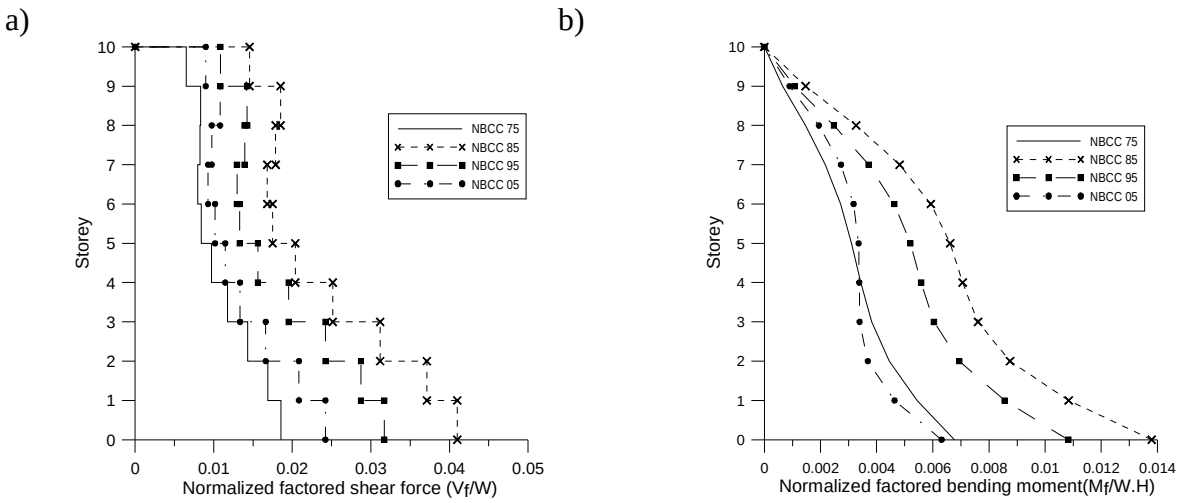

Figure 2. Factored forces from response spectrum analysis: a) Shear; b) Moment.

Once the steel is detailed, the probable flexural resistance at the base, M_p, is determined to evaluate forces that will develop upon yielding in the hinge. In the 1973 CSA A23.3, M_p is taken

equal to 1.1 the nominal moment resistance. In the other designs, M_p is obtained assuming nominal strength for the concrete and a steel yield strength of $1.25f_y$ to account for strain hardening. In the 1975 design, the shear forces are amplified by the ratio $M_p/M_{f,dyn}$ over the full building height. In the 1985 and 1995 designs, this amplification was applied only over the base hinge length. This was also the case for the 2005 design except that the shear forces above the plastic hinge were also amplified by the ratio of the wall factored moment resistance to $M_{f,dyn}$ as computed at the top of the plastic hinge. The values of the amplified design shear forces at the base, $V_{cap.des}$, are given in Table 1. In the 1973 concrete standard, no bending moment amplification was required above the plastic hinge length. In the 1984 and 1994 editions of CSA A23.3, it was suggested to assume bending moments varying linearly from M_p at the top of the plastic hinge to zero at the wall top. In the 2004 standard, the moments from response spectrum analysis above the plastic hinge are amplified by the ratio between the wall factored moment resistance and $M_{f,dyn}$ as computed at the top of the plastic hinge. The amplified design shear forces and bending moments along the wall heights are presented later for each design, together with the results of the nonlinear time history analyses. Wall reinforcement details are presented in Figure 3.

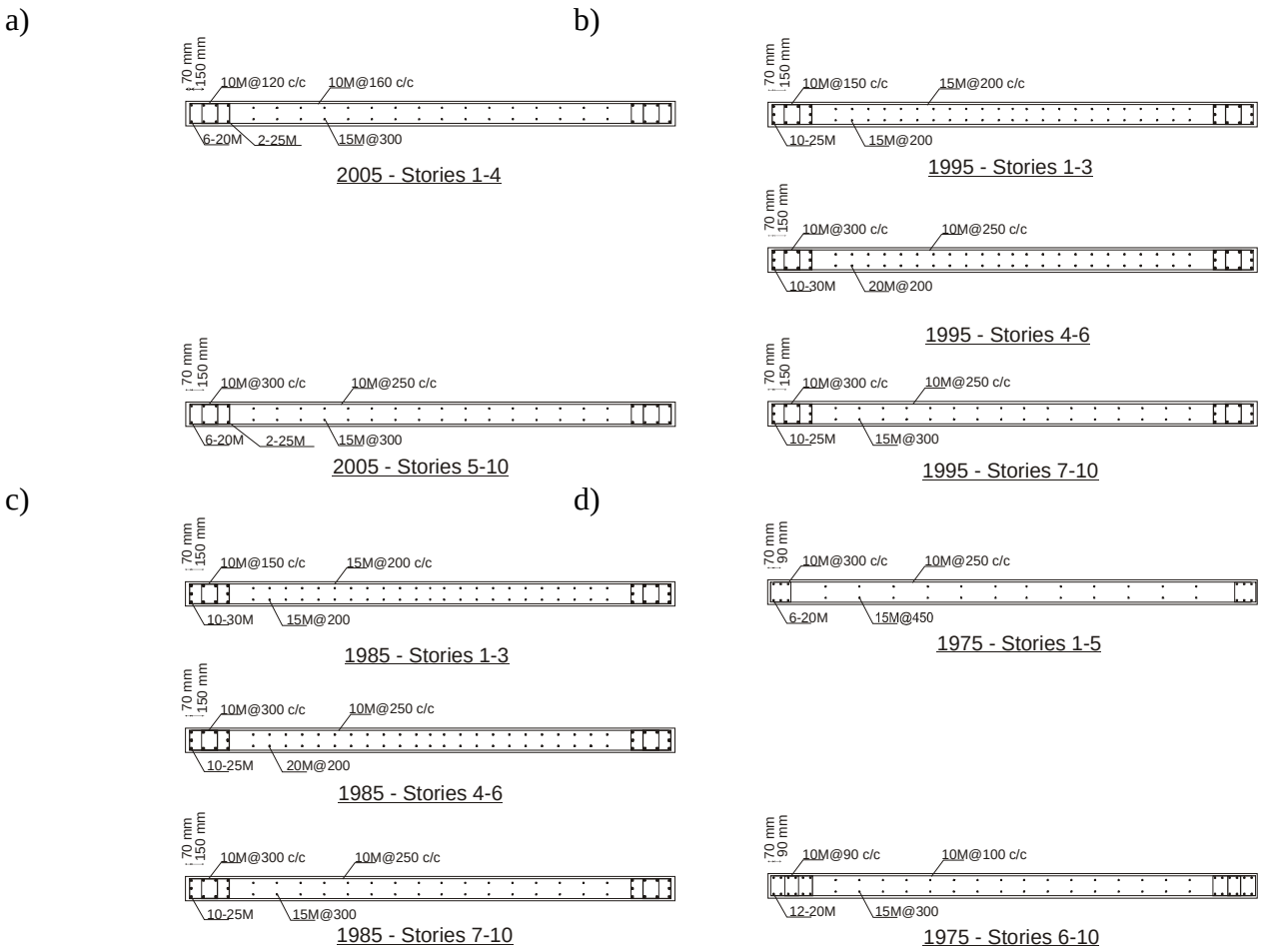

Figure 3. Reinforcement steel for NBCC: a) 2005; b) 1995; c) 1985; and d) 1975.

NONLINEAR ANALYSIS

Numerical Models. Two different models were used for the numerical simulations: a) nonlinear beam elements with fibre discretization of the cross-section using the OpenSees platform (Mazzoni et al. 2006), and b) plane stress finite element model using the VecTor2 (VT2) computer program (Wong and Vecchio 2004). The constitutive material properties for both models are shown in Figures 4 and 5, respectively. The fibre representation is simpler to use and its capability to predict the seismic inelastic dynamic response of shear walls was demonstrated by Martinelli and Filippou (2009). The VT2 program is a more comprehensive simulation tool as it is capable of reproducing the complex interaction of inelastic shear and flexural deformations in the plastic hinge region. The program has been validated against test data for shear walls subjected to cyclic loading (e.g., Ghorbanirenani et al. 2009). For both models, Rayleigh type

damping was specified in the first two modes of the structure: 1% of critical for OpenSees and half this value for VT2. Smaller damping is used with VT2 as the program more closely reproduce the damage experienced by the structure and, hence, have relatively greater hysteretic energy being dissipated.

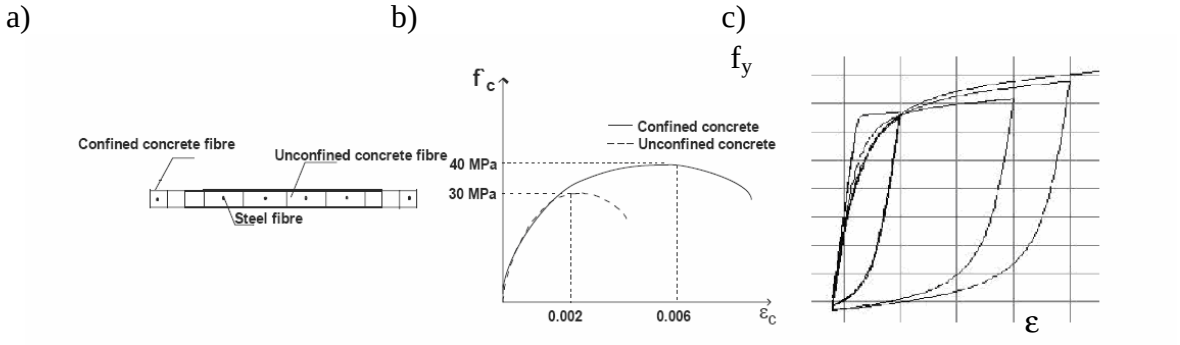

Figure 4. OpenSees model: a) Cross-section fibre discretization; b) Concrete properties; and c) Steel properties.

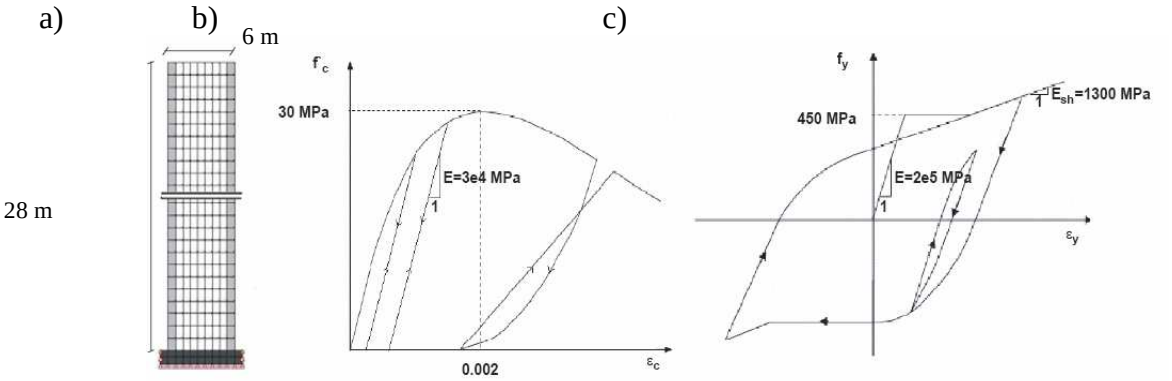

Figure 5. VT2 model: a) FE mesh of the wall; b) Unconfined concrete properties; and c) Steel properties.

Ground Motion Time Histories. Three ground motion time histories representative of eastern North America and rich in high frequency were selected for the analyses (Figure 6): two simulated motions corresponding to dominant contribution to the hazard of NBCC 2005 at the site, **M**7.0 at 70 km and **M**6.0 at 30 km (Tremblay and Atkinson 2001) and one historical motion from the 1988 Saguenay earthquake (Chicoutimi, Site 16, N124^{o}). Spectral matching with respect to the NBCC 2005 spectrum of Figure 1.1a was applied for all motions. The motions were then amplified by 1.25 for consistency with the assumption made in design for in-plane torsion.

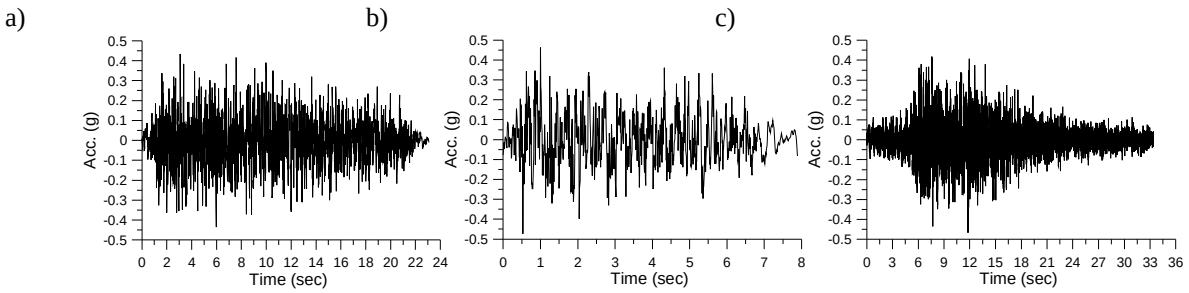

Figure 6. Spectrum matched ground motions: a) E7070; b) E6030; and c) CHI.

ANALYSIS RESULTS

Shear and Bending Moment Demand. Figures 7 and 8 give the shear forces and bending moments obtained from the nonlinear time history analyses for the four designs. The design forces that were considered after the formation of the base plastic hinge are also presented in the figure. VT2 analyses were only performed under the **M**7.0 earthquake for the 1975 and 2005 designs. Although the OpenSees (OS) fibre element models could not take in account shear cracks and shear stiffness reduction due to opening of flexural cracks, the force results from those models are in good agreement with the prediction of the VT2 software. The same observation holds true for the rotation demand described later.

In Figure 7, the shear forces computed under the selected ground motions exceed the predicted shear forces for all designs. The demand to supply ratio at the base varies between 2.0 and 2.5. This result clearly indicates that higher mode effects can lead to maximum shear forces that are much larger than those corresponding to the attainment of the yielding moment in the base hinge. In Figure 8, the 2005 code provisions predicted well the distribution and amplitude of the bending moment demand above the plastic hinge region. The flexural demand from earthquakes above the 4th level was underestimated by the 1985 and 1995 code provisions. No capacity design provisions existed in 1975 for flexure, which resulted in deficient capacity. The linear variation of the design bending moments adopted above the plastic hinge in the 1985 and 1995 codes resulted in relatively stronger walls compared to the 2005 design. Such stronger walls could resist higher seismic loads, which led to relatively larger shear force demand compared to the amplified shear values used in design.

Rotation Ductility Demand. Figure 9 shows the rotation ductility demand along the height of the walls. For the 2005 code design, significant plastic rotation is expected at the 5th and 6th floors in addition to the plastic hinge at the base (Figure 10a). The wall designed according to the NBCC 1975 can experience rotational ductility at the top that is comparable to that at the base (Figure 9d). In this design, the amplified bending moments caused significant damage just above the plastic hinge (5th level), where the reinforcement was reduced. The amplified bending moments assumed above the plastic hinge in the 1985 and 1995 codes were sufficient to prevent inelastic response in the upper part of the walls (Figures 9b and 9c).

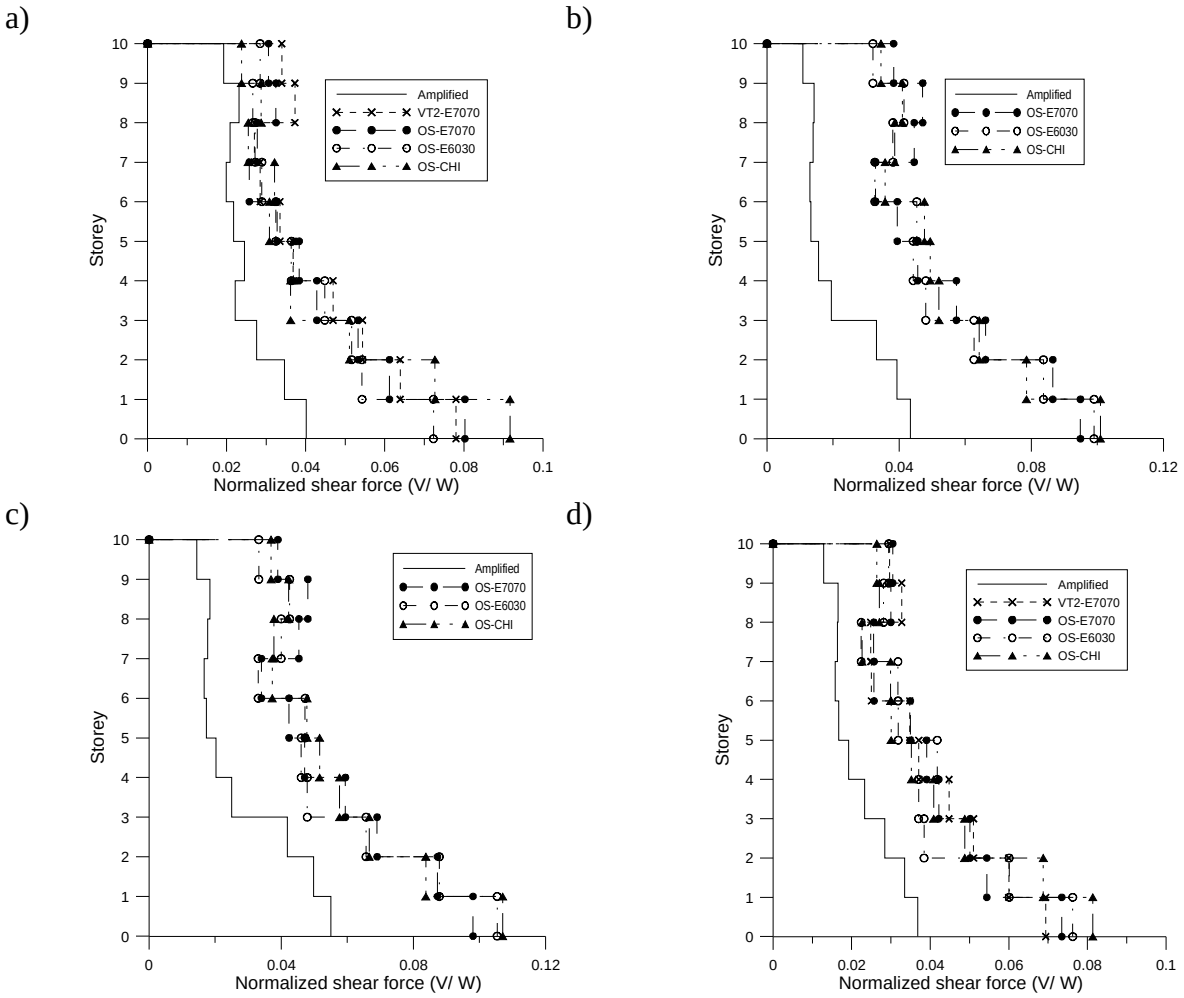

Figure 7. Design and expected shear forces: a) 2005; b) 1995; c) 1985; and d) 1975.

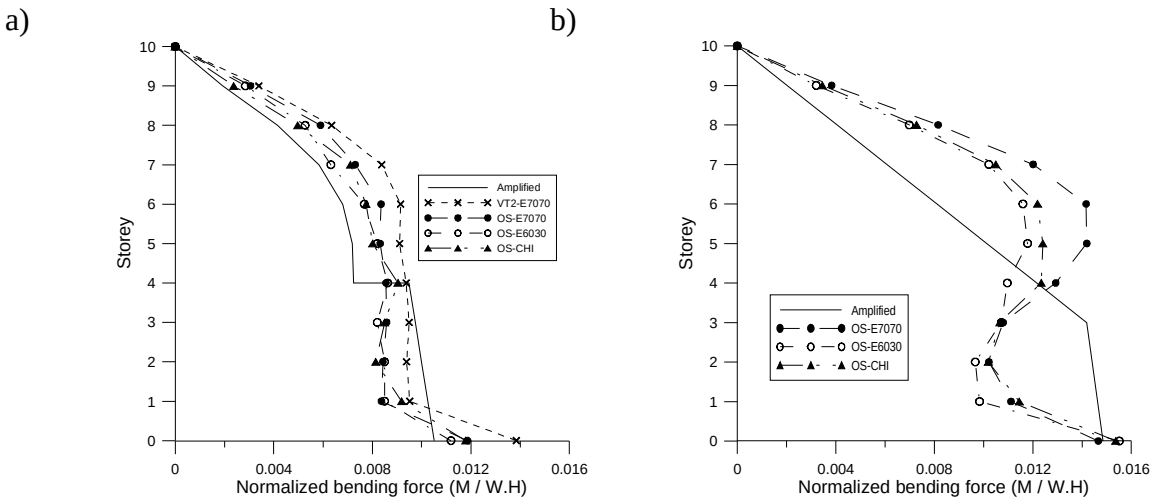

Figure 8. Design and expected bending moments: a) 2005; b) 1995.

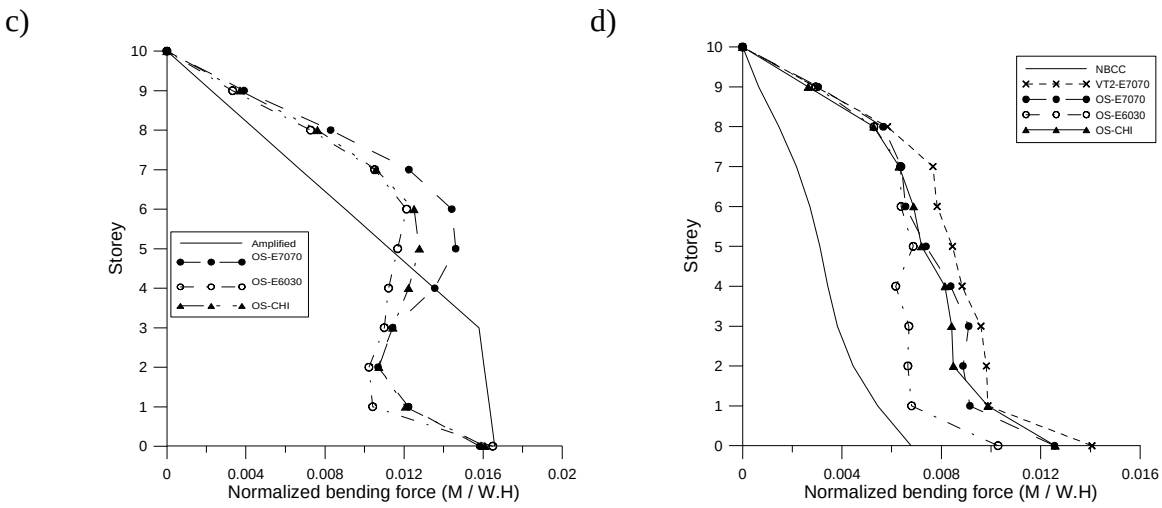

Figure 8 (cont'd). Design and expected bending moments: c) 1985; d) 1975.

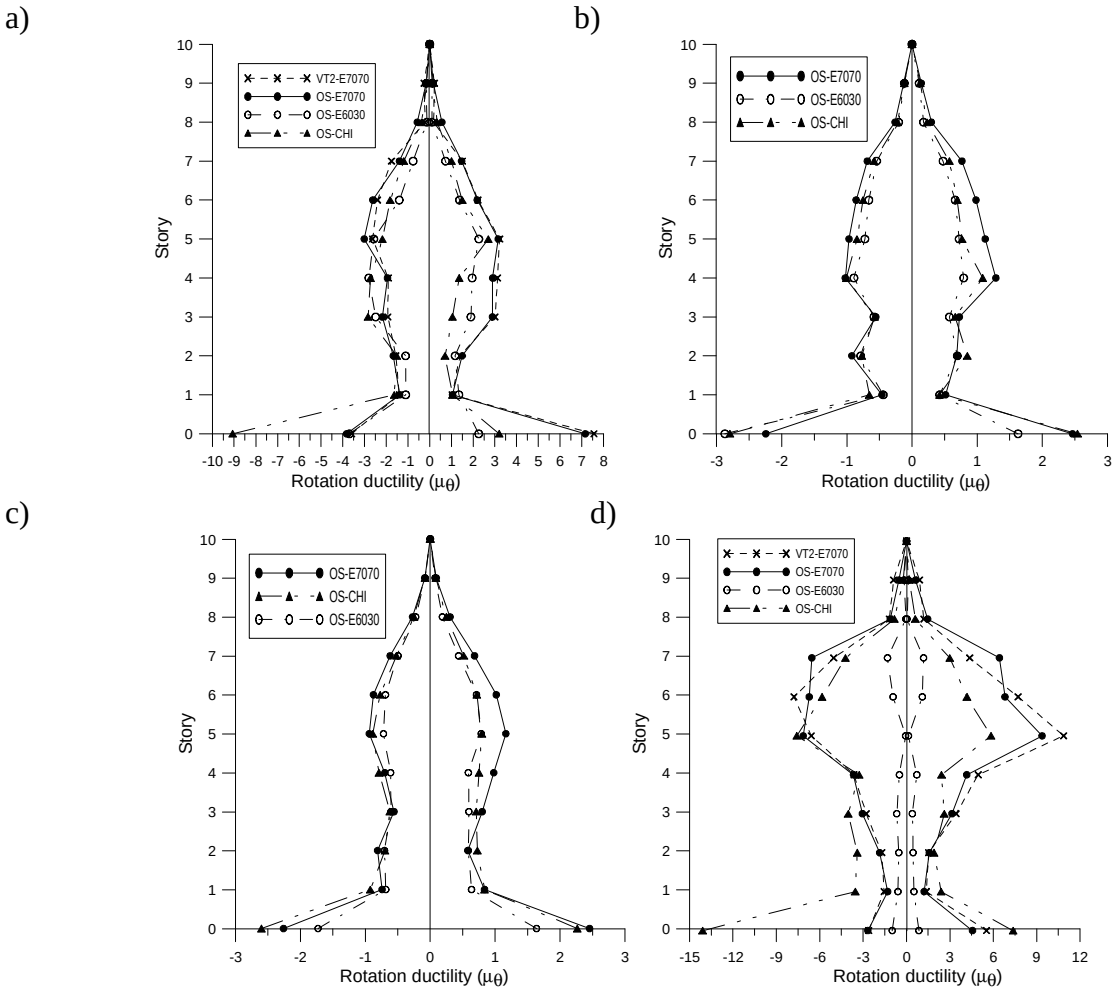

Figure 9. Rotation ductility demand: a) 2005; b) 1995; c) 1985; and d) 1975.

Performance Level. In FEMA 356 (FEMA 2007) introduces three performance levels to identify potential deficiencies in seismic designs: Immediate Occupancy (IO), Life Safety (SF) and Collapse Prevention (CP). The moment-rotation response under the **M**7.0 earthquake at the 1st and 5th levels of the walls designed according to NBCC 2005 and 1975 were examined to assess their performance. In FEMA 356, the rotation corresponding to IO performance level is equal to 0.005 rad. Figure 10 shows that the peak rotation demand from the earthquake, θ_u, is less than the IO rotation level in all cases, indicating that the observed inelastic rotations, although unexpected according to code provisions, produce limited structural damage.

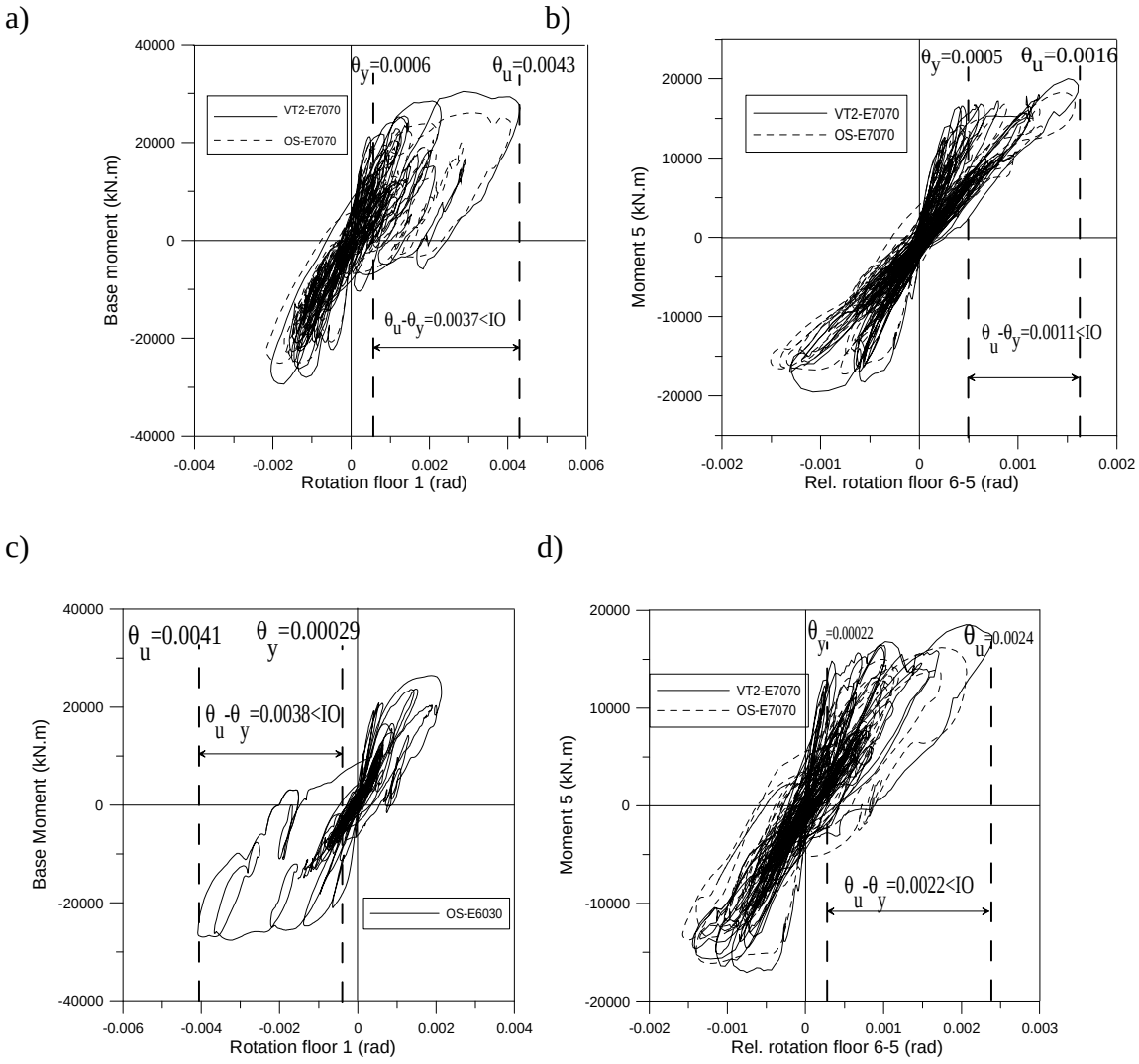

Figure 10. Moment-rotation response a) 2005-1st level; b) 2005-5th level; c) 1995-base; c) 1975-1st level; and d) 1975- 5th level.

CONCLUSIONS

The main findings of this study can be summarized as follows:

- The design seismic loads prescribed by codes between 1975 and 2005 can vary significantly. In particular, the values obtained from dynamic analysis according to the 1975 and 2005 codes are lower than the ones obtained in 1985 and 1995. Capacity design forces prescribed in the 1985 and 1995 codes were also higher.
- The predicted response from nonlinear plane section with fibre discretization modeling compared well to the results from more detailed finite element simulations, suggesting that the former can represent an effective and reliable method to assess the performance of reinforced concrete shear walls.
- The shear forces obtained from the time history analyses exceeded significantly the design shear forces prescribed by all codes. This was mainly attributed to the contribution of the higher modes of vibration of the structure.
- The distribution and amplitude of the seismic bending moment demand above the plastic hinge region was well predicted by the 2005 code provisions. The design bending moments in the other codes underestimated the flexural demand above the plastic hinge.
- Inelastic rotation was observed above the base plastic hinge of the walls designed according to the 1975 and 2005 codes. These rotations were however limited in amplitude, being less than the FEMA Immediate Occupancy performance criteria.

This study was limited to a single prototype wall and caution must be exercised when extrapolating the results and conclusions. Nevertheless, the study indicates that ductile reinforced concrete walls designed according to previous Canadian code editions are likely to lack shear force capacity over their height as well as flexural strength above the base plastic hinge. Walls designed according to NBCC 2005 can also be deficient in shear strength. Inelastic rotations are expected above the base plastic hinge region of walls designed according to 1975 and 2005 codes but they are likely to be limited to the extent that no or limited impact on the operation of the buildings. The study suggests that a better assessment of the contribution of the higher modes of vibration should be included in the capacity design verification process. It was also observed that the calibration of the results from dynamic analysis in the 1985 and subsequent codes is based on the base shear force, not the bending moment at the base. This can lead to flexural strength in the

base plastic hinge that may not be consistent with the expected demand and this aspect should be examined in future research.

ACKNOWLEDGEMENTS

This study was supported by the Fonds pour la recherche en sciences et nature of the Governement of Quebec and the Natural Sciences and Engineering Research Council of Canada. The financial support received by the second author from the Ecole Nationale de Travaux Publics de l'Etat de Lyon is also acknowledged.

REFERENCES

Adebar, P., Mutrie, J., and DeVall, R. (2004), "Ductility of concrete walls: the Canadian seismic design provisions 1984 to 2004." *Can. J. of Civ. Eng*., 32(6), 1124-1137.

Canadian Standards Association (CSA). (1973). *Code for the Design of Concrete Structures for Buildings. Standard CSA-A23.3-1973*, Mississauga, ON.

Canadian Standards Association (CSA). (1984). *Design of concrete structures for buildings. Standard CAN3-A23.3-M84*, Rexdale, ON.

Canadian Standards Association (CSA). (1994). *Design of concrete structures. Standard CSA-A23.3-94*, Rexdale, ON.

Canadian Standards Association (CSA). (2004). *Design of concrete structures. Standard CSA-A23.3-04*, Toronto, ON.

Federal Emergency Management Agency (FEMA) (1997), *NEHRP Commentary on the Guidelines for the Seismic Rehabilitation of Buildings, FEMA-356*, Washington, D.C.

Filiatrault, A., D'Aronco, D., and Tinawi, R. (1994). "Seismic shear demand of ductile cantilever walls: a Canadian code perspective." *Can. J. of Civ. Eng.*, 21(3), 363-376.

Ghorbanirenani, I., Velev, N., Tremblay, R., Palermo, D., and Massicotte, B., and Léger, P. (2009). "Modeling and Testing of Influence of loading history and scaling effects on the inelastic response of reinforced concrete shear walls," *ACI Structural J.*, 106(3), 358-367.

Humar, J.L. and Mahgoub, M.A. (2003). "Determination of seismic design forces by equivalent static load method." *Can. J. of Civ. Eng.*, 30(2), 287-307.
Martinelli, P., and Filippou, F.C. (2009). "Simulation of the shaking table test of a seven-story shear wall building." *Earthquake Eng. Struct. Dyn.*, 38(5), 587-607.

Mazzoni, S., McKenna, F., Scott, M.H., Fenves, G.L., (2006). *OpenSees Command Language Manual*, Open System for Earthquake Engineering Simulation (OpenSees),
Pacific Earthquake Engineering Research Center, University of California Berkeley, CA.

National Research Council of Canada (NRCC). (1975, 1985, 1995, 2005). *National Building Code of Canada*, Ottawa, ON.

Panagiotou, M., Restrepo, J.I., and Conte, J.P. (2007). *Shake table test of a 7-story full scale reinforced concrete structural wall building slice. Phase I: Rectangular wall section*, Report No. SSRP–07-07, Dept. Struct. Eng., Univ. of California, San Diego, CA.

Panagiotou, M., and Restrepo, J.I., (2009), "Dual-plastic hinge design concept for reducing higher-mode effects on high-rise cantilever wall buildings," *Earthquake Eng. Struct. Dyn.*, Published online www.interscience.wiley.com. DOI: 10.1002/eqe.905

Panneton, M., Léger, P., and Tremblay, R., (2006), "Inelastic Analysis of a Reinforced Concrete Shear Wall Building According to the NBCC 2005." *Can. J. Civ. Eng.*, 33(7), 854-871.

Priestley, M.J.N., and Amaris, A.D. (2002). "Dynamic amplification of seismic moments and shear forces in cantilever walls." *Research Report ROSE-2002/01*, Rose School, University of Pavia, Pavia, Italy.

Sullivan, T.J., Priestley, M.J.N and Calvi, G.M. (2008). "Estimating the Higher-Mode Response of Ductile Structures." *J. of Earthquake Eng.*, 12(3), 456-472.

Tinawi, R. (2004). "An Overview of Fifty Years of Development for the Canadian Seismic Building Code." *Egyptian Soc. for Earthquake Eng. EGYQUAKE3 Conf.,* Cairo University, Egypt Keynote address, 23 p.

Tremblay, R. and Atkinson, G.-M. (2001). "Comparative Study of the Inelastic Seismic Demand of Eastern and Western Sites." *Earthquake Spectra*, 17(2), 333-358.

Tremblay, R., Ghorbanirenani, I., Velev, N., Léger, P., Leclerc, Koboevic, S., Bouaanani, N., Galal, K., and Palermo, D. 2008. "Seismic Response of Multi-Storey Reinforced Concrete Walls Subjected to Eastern North America High Frequency Ground Motions." *Proc. 14WCEE*, Beijing, China, Paper No. 05-01-0526.

Wong, P.S., and Vecchio, F.J., (2002). *VecTor2 & Formworks User's Manuals*, Dept. Civil Eng., University of Toronto, Toronto, ON.

Appendix IV

Shake table tests and repair of ductile slender reinforced concrete shear walls

I. Ghorbanirenani, R. Tremblay, H. El-Sokkary, K. Galal ,P. Léger and M. Leclerc

9th US National and 10th Canadian Conference on Earthquake Engineering, July 25-29, 2010, Toronto, Canada

ABSTRACT

The paper describes a shake table test program on two 9m tall reinforced concrete shear wall models that are part of an 8-storey, 20.95m tall building designed in Montréal, QC according to the seismic provisions of the 2005 National Building Code of Canada and the 2004 CSA-A23.3 concrete design standard. The wall is of the moderately ductile category, as commonly built in Eastern North America (ENA). The objective of the test is to examine the contribution of the higher modes to the wall response when subjected to strong ground motions anticipated in (ENA). The focus is on the amplitude and distribution of the horizontal shear force over the building height, the inelastic rotation demand in the upper portion of the wall. It was found that significant inelastic deformations took place in the 6th storey in addition to the base plastic hinge. This dual plastic hinge response is not recognized by current codes. After testing, both walls were rehabilitated using carbon fibre-reinforced polymer (CFRP) composite sheets at the two plastic hinge locations. The walls were then retested using the same shake table loading protocol. At the wall base, uni-directional C-shaped CFRP sheets were applied horizontally on the two long sides of the wall, overlapped at the wall's boundary regions and anchored along the wall sides. On the 6th storey panel, uni-directional CFRP sheets were applied vertically and were anchored to the top and bottom slabs using CFRP anchors, above which uni-directional horizontal C-shaped CFRP sheets were applied. The rehabilitation schemes for the two walls aim to increase the flexural, shear, and ductility capacities of the wall at the 6th storey panel due to the observed increase in demand at that level, whereas the added CFRP confinement at the base panel aimed at increasing the ductility capacity at the wall base. Both rehabilitated walls performed efficiently showing

improved flexural strength at the 6th storey panel. Upon increasing the seismic ground motion intensity, the damage (cracking, plasticity) was found to spread in the other unrehabilitated stories.

INTRODUCTION

High rise reinforced concrete (RC) structural walls subjected to severe earthquakes, especially with high frequency content typical of Eastern North America (ENA), behave differently from low rise walls. The higher mode effects significantly change the seismic behaviour of these structures. Analytically, contributions of higher modes actions in slender ductile shear walls amplify the base shear and moment demand in the upper part of the walls which cause the formation of plastic hinges at those locations where they were not considered in seismic provision of CSA-A23.3-04 (Tremblay et al. 2008; Ghorbanirenani et al. 2008; Boivin et al. 2008; Panneton et al. 2006, Priestly and Amaris 2002). In complement to analytical results, experimental large scale real time tests are required to investigate the aspects of higher mode contributions.

Two identical RC walls (W1, W2) were fabricated using a prototype 8-storey building located in Montréal, QC and scaled by a length factor l_r = 0.429. The total height of the prototype building is 20.95 m and model walls were 9.0 m high. The walls were designed according to NBCC05 and CSA-A23.3-04 for moderate ductile category (ductility-related force modification factor R_d= 2.0 and overstrengh-related force modification factor R_o=1.4) and assuming a site class C in Montréal. The uniaxial seismic simulator of École Polytechnique has a payload capacity of 15 tons and 3.4 m x 3.4 m plan dimension. The 60 kN seismic masses of each floor were installed beside the table in front of each floor level on four multi-level hinged posts. The inertia loads were transferred by rigid beam that connected the wall to masses. Details of the test setup are presented in Tremblay et al. 2009 as indicated in Figure 1a, b, c.

In the test program, the two walls were subjected to several levels of a ground motion excitation spectrally matched to the NBCC 2005 design spectrum for Montréal. As it is shown in Figure 1d, 639 mm^2 to 426 mm^2 of longitudinal reinforcement bars were used along the height of the wall. As a part of the experimental program presented herein, the two wall specimens were rehabilitated after being tested and were re-subjected to the same ground motion excitations. The

objective of this second phase of the study was to evaluate the effectiveness of using FRP composites for retrofitting existing RC shear walls that are susceptible to increased demand at upper floors, compared to the designed ones, due to higher mode effects. As was observed in the tests of the original walls designed according the NBCC 2005, excessive yielding of flexural reinforcement at the 6th storey panel occurred, which resulted in wide horizontal cracking at the base of the 6th storey. This indicates that the wall seismic demand specified by the code has exceeded the wall capacity at the 6th storey level. Therefore, the rehabilitation strategy aims at increasing the flexural capacity of the wall section at the 6th storey by applying vertical CFRP sheets. As a consequent of increasing the flexural capacity at that level, an increase in the shear demand would occur. Hence, the shear capacity of the wall section at the 6th storey was increased as well by applying horizontal CFRP wraps. This rehabilitation scheme increases the wall strength and ductility capacity at the upper plastic hinge location. On the other hand, at the wall base, there is no need to increase the flexure capacity, which would result in an increased stiffness and, thereby, force demand of the wall. Thus, no vertical FRP strips were used at the base panel of the wall. Therefore, at the wall base the rehabilitation strategy was limited to increase the wall's ductility capacity without strength increase.

Selected Ground Motions

For the test program an ENA Mw7.0 at 70 km simulated ground motion time history was selected. Fig. 2 shows the ground motions, and the comparison between 5% damped acceleration spectrum and the Montréal NBCC 2005 target design spectrum. Wall 1 (W1) was tested under 40% (elastic), 100% and 120% of designed NBCC intensity. Wall (W2) was tested under 100%, 120%, 150% and 200% of designed NBCC intensity.

Test Results

Tables 1 and 2 show natural periods of the walls, ductility demand and rebar strains in the base and 6th floor of W1, W2.

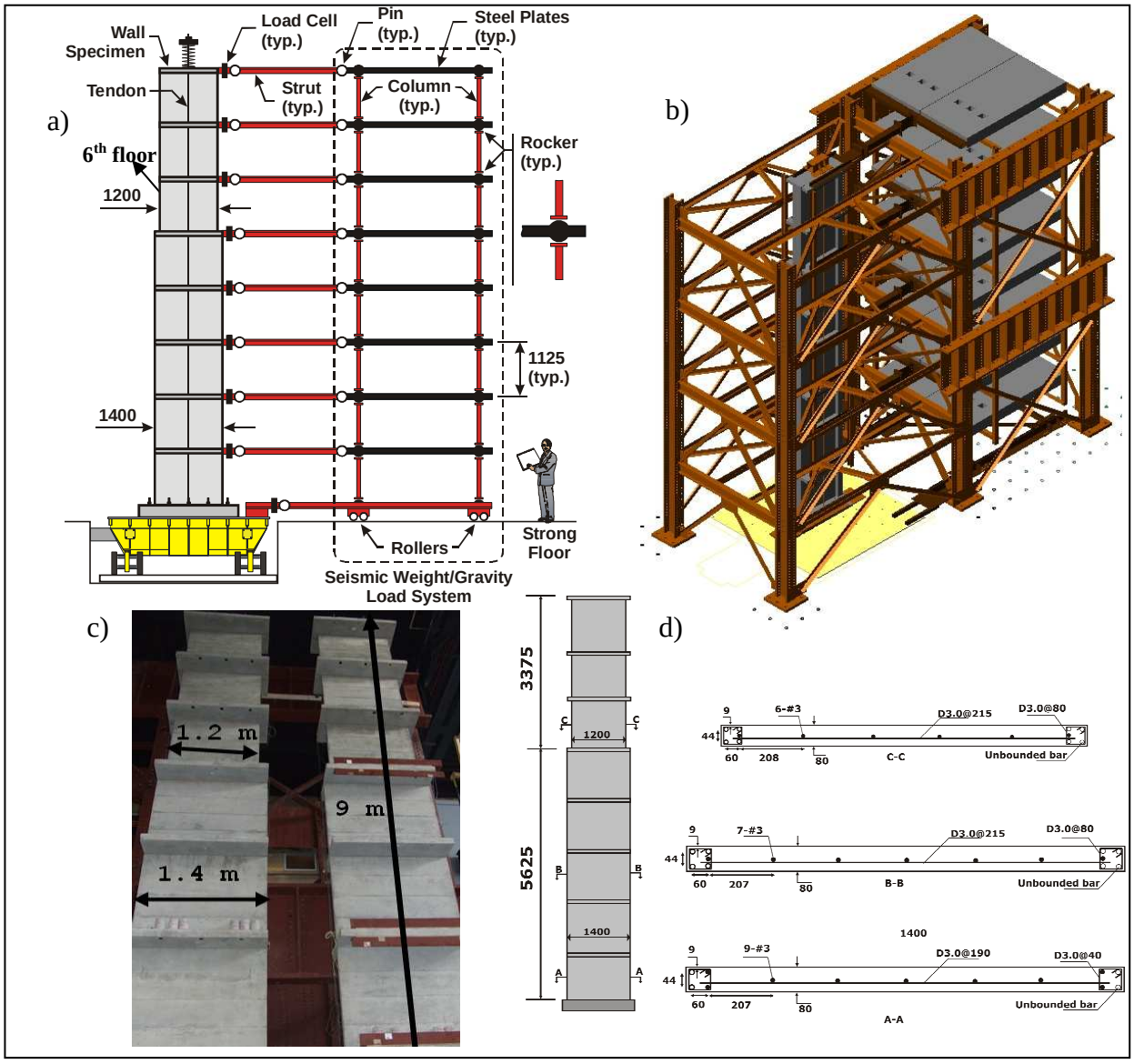

Figure 1. a) Test specimen and seismic weight/gravity load system; b) Complete test setup with stabilizing steel frame; c) model wall; and d) Cross section of model wall

The amount of rotation ductility demand at the 6th floor for W1 and W2 are approximately equal or larger than that at the base under the application of the 100% design ground motion intensity. This behaviour indicates that the walls experienced a second plastic hinge in the upper part in addition to the base hinge. The presence of the second plastic hinge is also depicted by the strain reading measured on the longitudinal rebar at the 6th floor, ε_6, which is, on average, 4 times larger than the yield strain of the bar (ε_y = 2200 με).

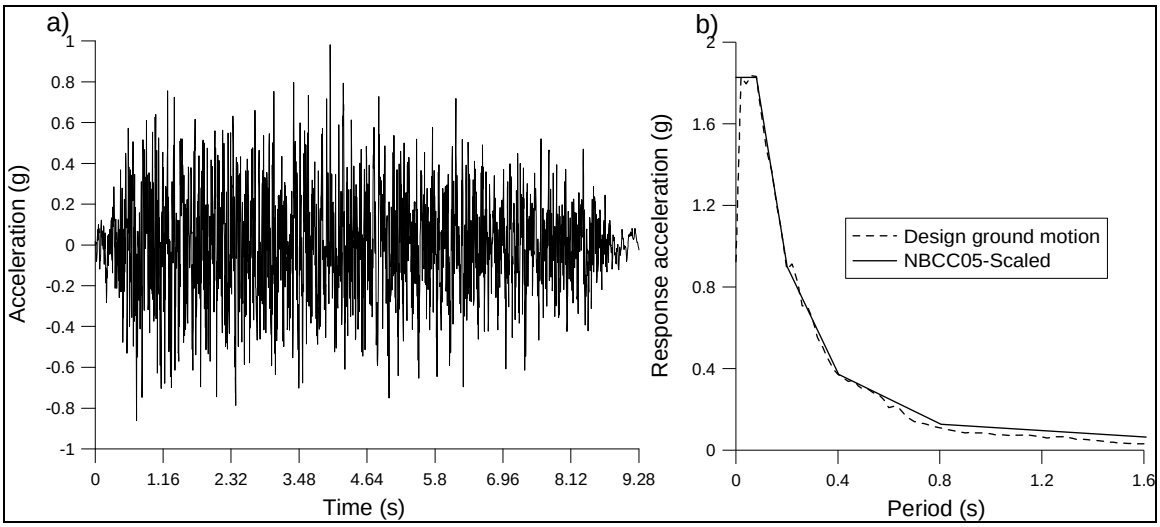

Figure 2. Selected ground acceleration: (a) time history; (b) response spectra.

Both W1 andW2 exhibited, on average, 40% elongation of their first natural period of vibration, T_1, between the initial (undamaged) condition and after the application of the designed ground motions (with 100% intensity). This represents a global damage indicator. When increasing further the ground motion intensity up to 150% for W2, no additional significant period elongation was observed and the rotation ductility demand at the base of the wall, $\mu_{\theta b}$, remained nearly unchanged. However, a significant increase in the damage and rotational ductility demand at the 6th floor was observed ($\mu_{\theta 6}$). For example, the rotational ductility demand at the base and at the 6th floor increased by 44% and 114%, respectively, when increasing the ground motion intensity from 120% to 150% for W2. Hence, damage increased at top of the wall elongating the periods associate to higher vibration modes and modifying its response accordingly.

Table 1. Key Parameters W1 – Tested first under 40% ground motion intensity (1-40%).

Test No.	**Initial**	**1 –40%**	**2- 100%**	**3 – 120%**
T1 (s)	0.67	0.72	0.90	0.960
$\mu_{\theta b}$	-	0.98	4.6	5.0
$\mu_{\theta 6}$	-	1.07	6.8	9.1
ε_b ($\mu\varepsilon$)	-	1100	2350	2360
ε_6 ($\mu\varepsilon$)	-	1440	10920	9800

Figs. 3a&b show the contribution of the concrete and the horizontal reinforcement, respectively, to the resistance of the base shear for W2 under different ground motion intensities. The shear forces contributing to the horizontal reinforcement were obtained from measured steel strain during the tests and the concrete contribution was obtained by subtracting the steel contribution from the total shear forces. The values are plotted against the total base shear. The concrete shear contribution in the first quadrant of the plot in Fig. 3a has a linear variation. There is a constant steel shear contribution in the same quadrant in Fig. 3b. This means that W2 did not experience severe damage, especially in shear, in one direction. In the third quadrant of the plots in Figs. 3a&b, a reduction of the concrete contribution and an increase of the steel contribution for different ground motion intensities can be observed. This indicates that the concrete shear strength of the wall base was reduced due to an increase of rotation ductility and shear crack width.

Table 2. Key Parameters W2 – Tested first under the design ground motion (1-100%).

Test No.	**Initial**	**1 – 100%**	**2- 120%**	**3 – 150%**	**3 – 200%**
T1 (s)	0.65	0.96	1.00	1.03	1.31
$\mu_{\theta b}$	-	5.2	4.8	6.9	7.1
$\mu_{\theta 6}$	-	5.6	6.6	14.1	20.9
ε_b (με)	-	2174	5535	11430	11368
ε_6 (με)	-	7118	15100	17880	-

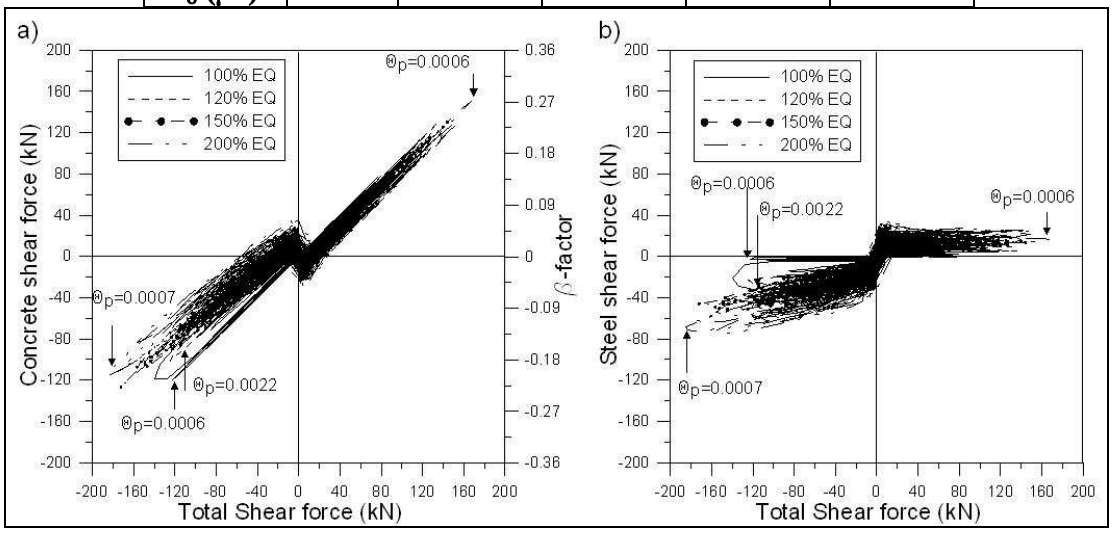

Figure 3. Shear contributions vs. total base shear (θp is the plastic rotation); (a) concrete; (b) steel.

In CSA-A23.3-04, the nominal concrete shear stress is limited to $\beta (f'_c)^{1/2}$ where β is a function of the member plastic hinge rotation (θp). Due to higher mode effects, the maximum total base shear resisted by W2 under the first test was 25% more than the nominal shear capacity predicted by the code. According to the first quadrant of the plot in Fig. 3a, this maximum total shear force occurred when the rotational ductility was limited (μ_θ=2.0). The peak value of β determined from the peak force measured in the test (0.27 in Fig.3a) is larger than the value predicted by the code (0.18), resulting in a larger contribution of the concrete to shear, which prevented yielding of the horizontal reinforcement. In the last test, where the wall experienced maximum damage, the contribution of the concrete had decreased significantly and, consequently, the stress in the horizontal steel increased up to the yield point (third quadrant in Fig. 3b). In this case the β factor, as predicted by the code, is limited to 0.18.

Seismic Strengthening of Ductile Shear Walls

FRP composite materials have been used extensively in the last few decades as a potential material for seismic retrofit of RC structures due to their high strength-to-weight ratio, high resistance to corrosion, and the ease of application. FRP laminates have been used to increase the wall flexural capacity, shear capacity, or both flexural and shear capacities by having different orientation of the laminates. Lombard et al. (2000) studied retrofitting RC shear walls using FRP composites when subjected to cyclic lateral excitations. They increased the flexural capacity, stiffness, and the shear capacity of the wall by applying one horizontal layer of CFRP sheet that is sandwiched between two vertical layers of CFRP. The vertical sheets were anchored to the foundation using steel angles. They found that FRP-retrofitted walls have better performance provided that a proper anchorage system for the sheets is used. They noted also that premature debonding of FRP sheets due to the compressive stresses in FRP vertical laminates is a critical issue in case of cyclic loading and it should be avoided. Paterson and Mitchell (2003) retrofitted RC shear walls using CFRP wraps and through-thickness headed bars. The retrofit scheme aimed to increase the wall shear strength and confinement. The retrofitted wall was able to reach displacement ductility levels that are 57% higher than those of the control wall, and was able to dissipate three times the energy absorbed by the original wall. Antoniades et al. (2003) used vertical FRP strips at the wall edges and horizontal FRP jackets to increase the wall flexural and

shear capacities, respectively. They examined different anchoring systems of the vertical FRP sheets including the use of glass FRP (GFRP) or steel anchors. Khalil and Ghobarah (2005) increased the flexural ductility of RC walls by applying FRP U-wraps horizontally at the wall end columns, and they were anchored to the wall using either steel or FRP anchors. The rehabilitated walls were able to reach high displacement ductilities compared to the control wall.

Description of FRP-rehabilitated walls (W1R, W2R)

The two original RC walls were rehabilitated and retested using the same test setup, instrumentation and under the same dynamic excitation used for the original walls. Additional strain gauges were applied on the CFRP sheets at different locations. For the first rehabilitated wall W1R, the ground motion was applied at two intensity levels; 100% and 120% of the design ground motion intensity. For the second rehabilitated wall W2R, the ground motion was applied at four intensity levels; 100, 120, 150, and 200% of the design intensity. Similar to the tests on the original walls, impact tests were carried out before each application of the ground motion level and at the end of the tests to determine the natural frequencies of the tested walls to estimate the amount of damage occurred.

As the original walls did not experience major concrete spalling, thus no concrete replacement was required. The wall surface was cleaned and grinded in several areas to achieve a smooth surface, and the wall corners were chamfered to a radius of 10 mm to avoid stress concentration upon wrapping FRP sheets. Due to the excessive yielding of the flexural reinforcement measured at the 6^{th} storey of the two original walls, the rehabilitation schemes necessitate increasing the flexure capacity at that level. For rehabilitated wall W1R, flexural capacity of the wall section at the 6^{th} floor panel was increased by applying a 200 mm wide vertical uni-directional CFRP strip at the wall boundary zones on both sides. The vertical strips were anchored to the top and bottom slab of the 6^{th} storey panel using FRP fan anchors as shown in Fig.4. The anchors were placed in previously drilled holes and then were filled with epoxy resins. The properties of the Tyfo SCH-11UP composites (Fyfe 2009) used in the rehabilitation scheme are shown in Table 3. In addition, the wall shear capacity at the 6^{th} storey was increased by applying one horizontal layer of C-shaped CFRP sheet on top of the vertical strips. The C-shaped FRP sheets were overlapped at the boundary regions of the wall in order to have a better confinement of the wall end columns as shown in Figs. 5 and 6.

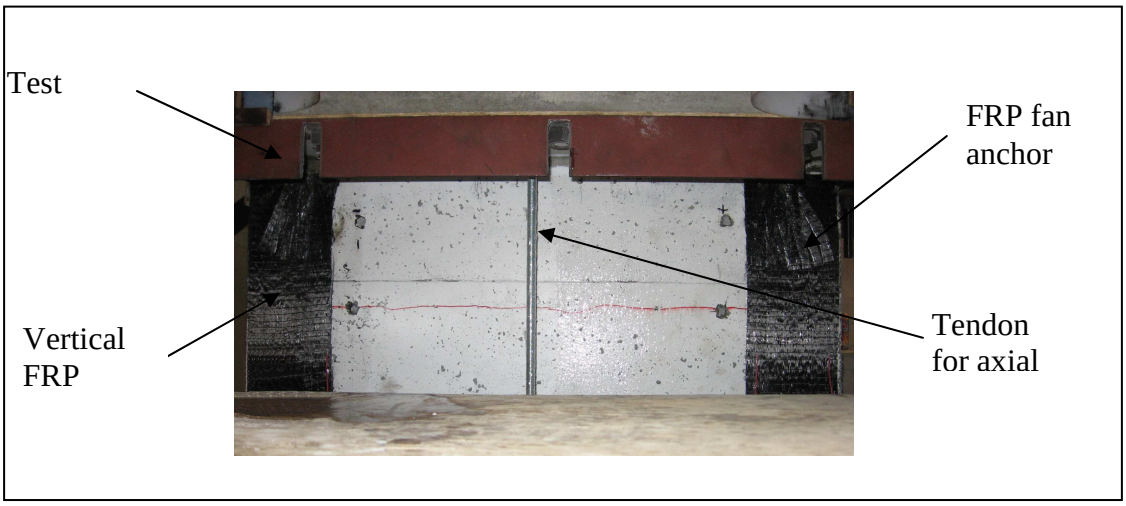

Figure 4. Vertical FRP strips and their FRP anchors at the 6th floor panel before applying the horizontal CFP sheets.

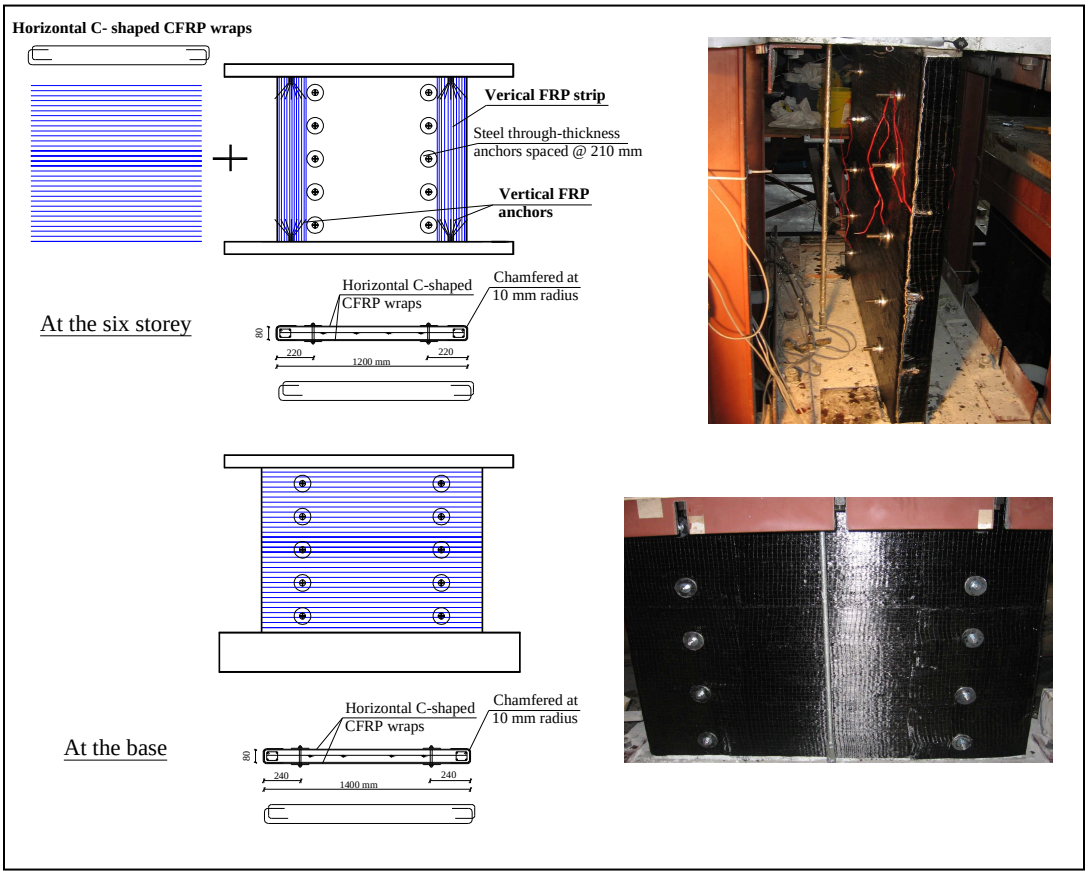

Figure 5. Details of the rehabilitation schemes for the rehabilitated walls W1R

Table 3. Properties of CFRP sheets used in the rehabilitation of the two walls (Fyfe 2009).

Properties of composite gross laminate SCH-11UP	
Composite gross laminate properties	Value
Ultimate tensile strength	903 MPa
Elongation at break	1.05%
Tensile modulus	86.9 GPa
Laminate thickness	0.27 mm

Then, the horizontal sheets were anchored along the sides of the wall using the previously drilled through-thickness steel anchors. The horizontal CFRP wraps would also prevent the premature debonding of vertical CFRP strips due to the compressive stresses. At the wall base, no increase in the flexural strength was needed. Therefore, no vertical FRP strips were used at the base storey. The panel was wrapped horizontally using the C-shaped CFRP sheets and anchored to the wall using the through-thickness steel anchors, similar to the 6^{th} storey. Such horizontal wrapping should confine the boundary regions of the wall, thus increasing its ductility and energy dissipation capacity. For the rehabilitated wall W2R, a rehabilitation scheme similar to W1R was used for both the base and 6^{th} stories, except that the through-thickness steel anchors were not used.

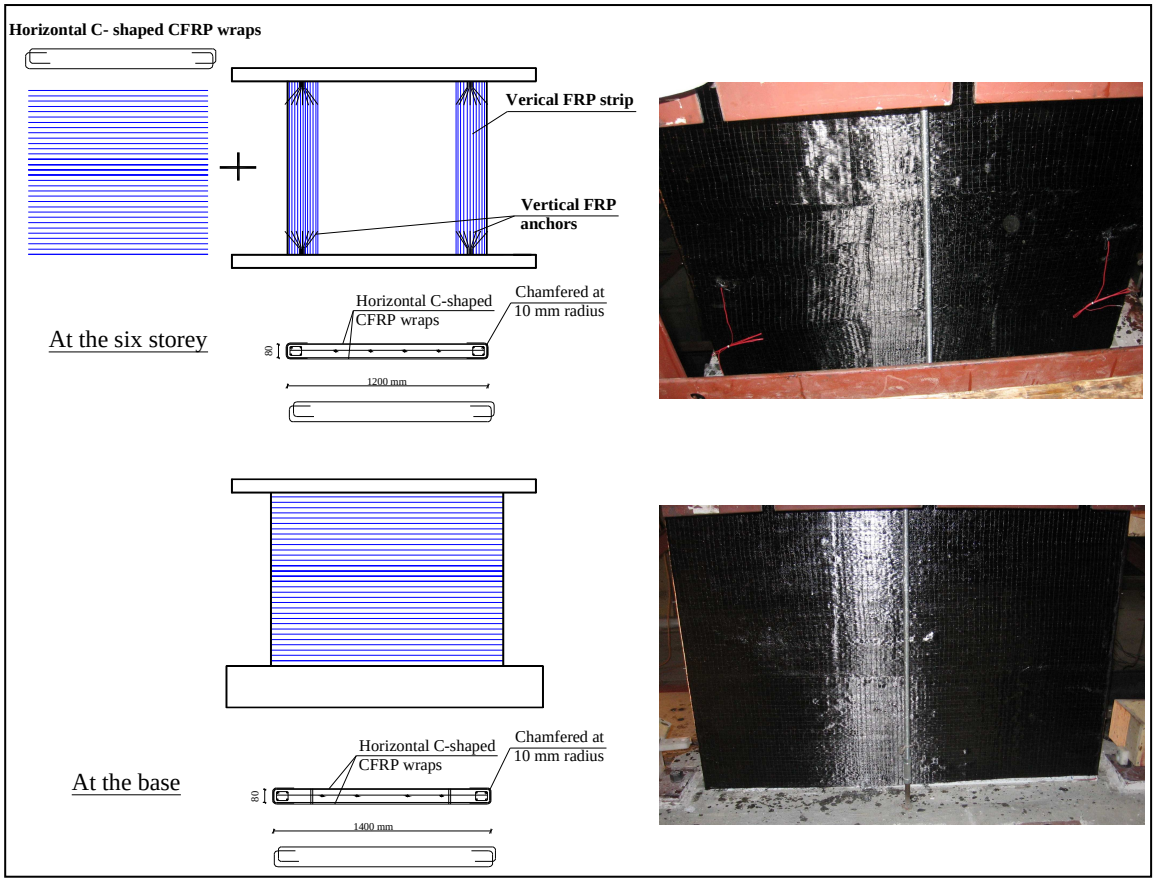

Figure 6. Details of the rehabilitation schemes for the rehabilitated walls W2R.

Test observations – Rehabilitated Walls

As was observed in the tests on the original walls, the natural frequencies of the original walls have decreased due to the accumulation of damage after each excitation. The natural frequencies of the rehabilitated walls were found to be higher than that of the original walls after being damaged, and were close to that value of the undamaged walls. The rehabilitated walls were found to perform very efficiently, no FRP debonding or anchorage failure was observed during the two tests. The vertical FRP strips applied at the 6th storey panel reduced the strains in the longitudinal steel rebars significantly at that level. In fact, the FRP was not fully utilized as the capacity of the rehabilitated walls could not be reached due to the limited capacity of the shake table. The maximum storey shear was found to be higher than that of the original walls at the same level of excitation. After applying the 120% of the design intensity on the rehabilitated wall W2R, new horizontal cracks were observed at the 2nd and 5th stories. After the 150% of the design intensity, more cracks spread in the same stories, while after the 200% of the design

intensity, the cracks spread in the 3rd and 4th stories. This could be interpreted that rehabilitating the wall base and 6th storey has led to the redistribution of demands and stresses in the other unrehabilitated parts of the wall.

Conclusions

Two series of shaking table tests on 8-storey scaled model walls designed according to NBCC 2005 and CSA-A23.3-04 were carried out to investigate the higher mode effects on multistory reinforced concrete walls. Under the design earthquake, the results of the tests showed that significant rotational ductility demand occurred at the 6th storey of the wall due to higher mode effects. That demand even exceeded the base rotational ductility. Yielding of the longitudinal reinforcement at the 6th floor confirmed the significant plastic demand at this level, which resulted to a dual hinge response not accounted for in current design codes. The damage progression due to the increase of ground motion intensity is much larger in the upper part of the wall than at the base. No shear failure was observed. However, in some instances, the contribution of the concrete to shear resistance was found to be larger than the value predicted by the code.

The two original walls were rehabilitated using two different rehabilitation schemes utilizing carbon fibre-reinforced polymer (CFRP) composite sheets at the plastic hinge locations (base panel and 6th storey). The rehabilitated walls were retested by subjecting them to the same ground motion excitation levels applied on the original walls. Both rehabilitated walls performed efficiently showing improved flexural strength at the 6th storey panel. Upon increasing the seismic ground motion intensity, the damage (cracking, plasticity) was found to spread in the other unrehabilitated stories.

Acknowledgements

The authors wish to thank the National Science and Engineering Research Council of Canada (NSERC) and the Quebec Fund for Research in Nature and Technology (FQRNT) for the financial support provided. The authors also gratefully acknowledge Fyfe Co. for donating the FRP composite materials used for this research.

References

Antoniades, K., Salonikios, T., and Kappos, A., 2003. Cyclic Tests on Seismically Damaged Reinforced Concrete Walls Strengthened using Fibre-Reinforced Polymer Reinforcement. *ACI Structural Journal*, 100 (4), 510-518.

Boivin, Y. and Paultre, P. 2008. Seismic Performance of a 12-Storey Ductile Concrete Shear Wall System Designed According to the New Canadian Building Design Codes. *Proc. CSCE 2008 Annual Conf., Quebec, QC,* Paper No. 442.

Canadian Standards Association CSA. 2004. Design of concrete structures. CSA A23.3-04, Mississauga, Ont., Canada.

Fyfe. (2009). Tyfo® SCH-11UP composite using Tyfo® S epoxy user's guide. Fyfe Company LLC, http://www.fyfeco.com.

Ghorbanirenani, I., Tremblay, R., Léger, P., and Palermo, D., 2008. Inelastic Seismic Evaluation of Slender Shear Walls Designed According to CSA-A23.3-04 and NBCC 2005. *Proc. CSCE 2008 Annual Conf., Quebec, QC,* Paper No.520.

Khalil, A., and Ghobarah, A, 2005. Behaviour of Rehabilitated Structural Walls. *Journal of Earthquake Engineering*, 9 (3), 371-391

Lombard, J., Lau, D., Humar, J., Foo, S., and Cheung, M., 2000. Seismic strengthening and repair of reinforced concrete shear walls. *Proc. 12th World Conference on Earthquake Engineering*, Auckland, NZ (CD-ROM), Paper No. 2032.

NRCC, 2005, National Building Code of Canada, 12th ed., National Research Council of Canada, Ottawa, ON.

Panneton, M., Léger, P., Tremblay, R. 2006. Inelastic analysis of a reinforced concrete shear wall building according to the national building code of Canada 2005. *Canadian Journal of Civil Engineering*, 33(7), 854-871.

Paterson, J. and Mitchell, D., 2003. Seismic Retrofit of Shear Walls with Headed Bars and Carbon Fibre Wrap. *ASCE Journal of Structural Engineering*, 129(5), 606-614.

Priestly, M.J.N, and Amaris, A. 2002. Dynamic Amplification of Seismic Moments and Shear Forces in Cantilever Walls. *Research Report ROSE – 2002-01, Rose School of Engineering,* Pavia, Italy.

Tremblay, R., Ghorbanirenani, I., Velev, N., Léger, P., Leclerc, M., Koboevic, S., Bouaanani, N., Galal, K., and Palermo, D. 2008. Seismic response of multi-story reinforced concrete walls subjected to eastern North America high frequency ground motions. *Proc. 14th World Conference on Earthquake Engineering, Beijing, China*, Paper ID: 05-01-0526.

Tremblay, R., Léger, P., Rogers, C., Bouaanani, N., Massicotte, B., Khaled, A., Lamarche, C.P., 2009. Experimental Testing of Large Scale Structural Models and Components Using Innovative Shake Table Dynamic, Real-Time Hybrid Simulation and Multi-Directional Loading Techniques. *Proc. 3rd Int. Conf. on Advances in Experimental Structural Engineering, Oct. 15-16, San-Francisco, USA, 12pp*

Appendix V
Concrete Mix Plan

FORMULAIRE DE MELANGE POUR PÂTE, MORTIER ET BETON

Paramètres

Nom du mélange : 30MPa Iman pierre 2,5/5 n05 6è étage batch2 — Préparé par : Cédric

Critères	Valeur
FS/C	0.00
E/C	0.69
E/L = E/(C+FS)	
S/C	2.48
S/G	0.70

Critères	Valeur
Sup. (ml/kg L)	6.7
(% sec L)	0.33
AEA (ml/kg L)	0.0
Visc. (ml/Leau)	0.0
Autre (ml/kg L)	2.5

Critères	Valeur
Fibre (%)	0.0
Air (%)	2.5
Pâte (%)	32.8
Vgâchée (l)	100.0

Recette de béton fibré à haute performance

Composante	Identification composante	ρ (kg/l)	Masse recette (kg/m3)	Volume recette (l/m3)	Masse gâchée (kg)	Volume gâchée (l)	
Ciment	Type GU (CSL)	3.14	300.00	95.54	30.00	9.55	
Fumée de silice	Pas de FdeS	0.00					
Eau	0	1.00	205.02	205.02	20.50	20.50	
Superplastifiant	Eucon 37	1.21	2.42	2.00	0.24	0.20	
Extrait liquide (%)	59.5	1.00	1.44	1.44	0.14	0.14	
Entraîneur d'air	Pas de AEA	0.00	0.00	0.00	0.00	0.00	
Extrait liquide (%)	100	1.00	0.00	0.00	0.00	0.00	
Agent viscosant	Visctrol	1.21	0.00	0.00	0.00	0.000	
Extrait liquide (%)	57.5	1.00	0.00	0.00	0.00	0.00	
Autre adjuvant	Eucon WR	1.21	0.91	0.75	0.09	0.08	
Extrait liquide (%)	59.5	1.00	0.54	0.54	0.05	0.05	
Eau total (adj. inclus)	0	1.00	207.00	207.00	20.70	20.70	** : Masse granulats en Msss*
Sable	Joliette	2.69	744.29	276.28	74.43	27.63	
Pierre	2.5-5 Gr. St F	2.689	1063.27	395.41	106.33	39.54	
Fibres	Pas de fibres	0.00	0.00	0.00	0.00	0.00	
Air		0.00		25.00		2.50	
Total			2315.90	1000.00	231.59	100.00	

Teneur en eau et correction des masses de granulats

Caractéristiques		Sable	Pierre	
Poids tare : PT		1313.00 g	1313.00 g	
Poids tare + granulats humides : PH		1913.00 g	2313.00 g	
Poids tare + granulats séchés : PS		1910.00 g	2311.00 g	*Total eau*
Absorption : A		0.0056 (-)	0.0061 (-)	apportée
Teneur en eau	TE = (PH - PS) / (PS - PT)	0.0050 (-)	0.0020 (-)	*par granulats :*
Eau apportée par granulats	Eau = [(TE - A) x Msss] / (1 + A)	-0.04 kg	-0.43 kg	-0.48 kg
Masse corrigée des granulats	Mhumide = [(1 + TE) x Msss] / (1 + A)	74.39 kg	105.89 kg	

Matériaux à préparer pour une gâchée de 100 litres

Composante	Masse théorique (kg) Masse	Msss	Masse au laboratoire (kg) Mcorrigée	Mpesée
Ciment	30.00 kg	------	------	30.00 kg
Fumée de silice	kg	------	------	kg
Eau	20.50 kg	------	20.98 kg	20.98 kg
Superplastifiant	242.0 g	------	------	120.00 g
Autre adjuvant	90.8 g	------	------	g
Entraîneur d'air	0.0 g	------	------	0.00 g
Agent viscosant	0.0 g	------	------	50.00 g
Sable	------	74.43 kg	74.39 kg	74.39 kg
Pierre	------	106.33 kg	105.89 kg	105.89 kg
Fibres	------	0.00 kg	------	0.00 kg

Mcorrigée d'eau correspond à la masse théorique + Total eau apportée granulats

33 % de l'eau à peser = kg
66 % de l'eau à peser = kg
⇨ Mélanger avec 33 % de l'eau
⇨ Mélanger avec 66 % de l'eau
⇨ Mélanger avec 500 ml d'eau
⇨ Ajouter seul en fin de gâchage

Caractéristiques de la gâchée

Contact E/C (date, heure) :	05/12/2008 @ 9h50	fc 7j/28j (MPa) :	
Température (°C) :	22	Masse béton airmètre (kg) :	16.1
Affaissement / Etalement (mm) :	60	Volume airmètre (l) :	7
Temps d'écoulement (s) :		Masse vol. béton exp. (kg/m3) :	2300
		Teneur en air (%) :	2.1

Remarques :

Groupe de recherche en GÉNIE DES STRUCTURES
Version 1.4 - JPC, 12 juin 2007